4-8-2014 12:00 AM

Development of an In-Vitro Passive and Active Motion Simulator for the Investigation of Shoulder Function and Kinematics

Joshua W. Giles
The University of Western Ontario

Supervisor
Prof. James A. Johnson
The University of Western Ontario

Graduate Program in Biomedical Engineering
A thesis submitted in partial fulfillment of the requirements for the degree in Doctor of Philosophy

DEVELOPMENT OF AN *IN-VITRO* PASSIVE & ACTIVE MOTION SIMULATOR FOR THE INVESTIGATION OF SHOULDER FUNCTION AND KINEMATICS

(Thesis format: Integrated Article)

by

Joshua William Giles

Graduate Program in Biomedical Engineering

A thesis submitted in partial fulfillment
of the requirements for the degree of
Doctor of Philosophy

The School of Graduate and Postdoctoral Studies
The University of Western Ontario
London, Ontario, Canada

Abstract

Injuries and degenerative diseases of the shoulder are common and may relate to the joint's complex biomechanics, which rely primarily on soft tissues to achieve stability. Despite the prevalence of these disorders, there is little information about their effects on the biomechanics of the shoulder, and a lack of evidence with which to guide clinical practice. Insight into these disorders and their treatments can be gained through *in-vitro* biomechanical experiments where the achieved physiologic accuracy and repeatability directly influence their efficacy and impact.

This work's rationale was that developing a simulator with greater physiologic accuracy and testing capabilities would improve the quantification of biomechanical parameters. This dissertation describes the development and validation of a simulator capable of performing passive assessments, which use experimenter manipulation, and active assessments – produced through muscle loading. Respectively, these allow the assessment of functional parameters such as stability, and kinematic/kinetic parameters including joint loading.

The passive functionality enables specimen motion to be precisely controlled through independent manipulation of each rotational degree of freedom (DOF). Compared to unassisted manipulation, the system improved accuracy and repeatability of positioning the specimen (by 205% & 163%, respectively), decreased variation in DOF that are to remain constant (by 6.8°), and improved achievement of predefined endpoints (by 21%). Additionally, implementing a scapular rotation mechanism improved the physiologic accuracy of simulation. This enabled the clarification of the effect of secondary musculature on shoulder function, and the comparison of two competing clinical reconstructive procedures for shoulder instability.

This was the first shoulder system to use real time kinematic feedback and PID control to produce active motion, which achieved unmatched accuracy (<1°) and repeatability (0.3°). Additionally, the controller increased the physiologic accuracy of motion simulation, compared to previous systems. Using these developments and custom

designed adjustable instrumented Reverse Total Shoulder Arthroplasty implants, the effects of implant parameters on muscle loading and joint load were assessed throughout active motion. This study provided new insights, unattainable without this research's developments.

These developments can be a powerful tool for increasing our understanding of the shoulder and also to provide information which can assist surgeons and improve patient outcomes.

Keywords

Shoulder motion, *in-vitro* simulation, biomechanics, passive simulation, active simulation.

Co-Authorship Statement

Chapter 1: Josh Giles – sole author

Chapter 2: Josh Giles – developed testing systems, study design, data collection, statistical analysis, wrote manuscript

Irfan Abdulla – data collection

James Johnson – study design, reviewed manuscript

George Athwal – study design, data collection, reviewed manuscript

Chapter 3: Josh Giles – study design, data collection, statistical analysis, wrote manuscript

Harm Boons – study design, specimen preparation, data collection, reviewed manuscript

Louis Ferreira – study design, reviewed manuscript

George Athwal – study design, data collection, reviewed manuscript

James Johnson – study design, reviewed manuscript

Chapter 4: Josh Giles – study design, data collection, statistical analysis, wrote manuscript

Ryan Degen – study design, specimen preparation, data collection, reviewed manuscript

George Athwal – posed clinical question, study design, reviewed manuscript

James Johnson – study design, reviewed manuscript

Chapter 5: Josh Giles – developed controller, study design, data collection, statistical analysis, wrote manuscript

Louis Ferreira – technical advice, study design, reviewed manuscript

George Athwal – study design, data collection, reviewed manuscript

James Johnson – study design, reviewed manuscript

Chapter 6: Josh Giles – developed implant system, study design, data collection, statistical analysis, wrote manuscript

Dan Langohr – developed implant system, study design, data collection

George Athwal – study design, specimen preparation, reviewed manuscript

James Johnson – study design, reviewed manuscript

Chapter 7: Josh Giles – sole author

Acknowledgments

I would like to begin by thanking my supervisors, Dr James Johnson and Dr George Athwal, for their continual support and advice throughout my research and training. I cannot begin to think where I would be without their help and without the lessons one can only learn from supervisors with such passion and expertise. Dr Johnson, thank you for plucking me out of your 2nd year Mechanics of Materials class and giving me the opportunity to experience research in a field that I scarcely knew existed or thought would interest me! From that time on you have always encouraged me to do the best research I can and you have always been available at just the right time to answer my questions and address my concerns. Dr Athwal, your fervor for research and your foresight in seeing how the work of this thesis could address important clinical questions allowed us to establish a line of research that I am so proud of! Thank you for always making our research a priority despite your myriad of other commitments. I feel so lucky to have worked with you over these past 5 years. I would also like to thank Dr. Graham King. Although you were not a direct supervisor of mine, you are the clinical forefather of this lab and always pushed me to achieve more with my research with your not so subtle questions, like 'got that scapula moving yet'? I can happily report that I did finally get it moving…and it was veiled encouragement like yours that helped make the shoulder simulator be all it could be during my five years.

To Louis, I always appreciated your general and technical advice and how you always made time to give it. I am not sure where I or my research would be without the knowledge you gave me. You allowed me to avoid the pitfalls you and your elbow simulator predecessors encountered, and were always there with a good idea when a problem arose during testing. For that, I cannot thank you enough.

To all of the students, surgeons, staff, and volunteers at the HULC Bioengineer lab that I have worked with over the years, thank you for always striving to produce research of such a high quality. Working with each of you on your research and your help with mine has made the past seven years unbelievably rewarding and educational. I would specifically like to thank Emily for being my closest friend in the lab throughout these years. I always enjoyed working with you, especially our LabView coding sessions,

because no matter how long it sometimes took, you always stuck it out with me! Hannah and Simon, you were great labmates and I enjoyed hanging out with you day in and day out, especially in the inevitable times when it seemed like the research just wasn't progressing. Ryan, thank you for always offering your help, especially during my long days of controller development. It never ceased to amaze me how you could always approach a problem from a different angle and produce an innovative solution! Dan, we have only started to work together more recently, but your seemingly unending energy and drive has made this period one of my most productive. I cannot wait to see the impact our studies can have! To all of the surgical residents and fellows I have worked with, without you, my research wouldn't have been nearly so clinically relevant.

I would also like to thank Brooke Thompson for creating the wonderful anatomical illustrations used throughout my first chapter. They have given this work a good foundation and great style.

To my family, thank you for all of your support and your interest in my work over the years. Mom and Dad, thank you for your continual help and encouragement throughout my schooling and in all parts of my life. I would not be where I am today without your help, especially in my early education, and wouldn't be on the verge of receiving my Doctorate.

Finally, and most importantly, to my better half and long suffering editor, Jasmine, you have been by my side since before I started in the lab seven years ago. In that time many things have changed, I have flown on my first plane (transpacific no less), we have moved in together, bought a house (sold a house), and gotten married, but the one constant was that you were always there to listen, encourage, and help me with my research. I love you so much and will never be able to repay you for your patience, effort, and investment of time but I can promise that there are fewer work nights ahead and I know that we will fill them with conversation and new experiences as we always have!

Table of Contents

List of Tables

List of Figures

List of Equations

List of Appendices

Abbreviations, Symbols And Nomenclature

Add ..... Adduction

Abd ..... Abduction

ANOVA ..... Analysis of Variance statistical method

ASD ..... Average Standard Deviation

BMI ..... Body Mass Index

PID ..... Proportional Integral Derivative

CS ..... Coordinate System

DC ..... Direct Electrical Current

DOF ..... Degree(s)-Of-Freedom

ER ..... External Rotation

$F_{x,y,z}$ ..... Force along the x, y, or z axis

GSA ..... Dr George S. Athwal

GMD ..... Geometric Motion Decomposition

HH ..... Humeral Head

HULC ..... Hand and Upper Limb Centre

INA ..... Dr. Irfan N. Abdullah

IE ..... Internal-External

IR ..... Internal Rotation

ISB ..... International Society of Biomechanics

JCS ..... Joint Coordinate System

K_u ..... Proportional gain causing oscillation in a proportional only controller

K_p ..... Proportional gain in proportional only controller causing a Quarter Amplitude Decay Response

$M_{x,y,z}$ ..... Moment about the x, y, or z axis

MRI ..... Magnetic Resonance Imaging

N ..... Force in Newtons

Nm ..... Moment in Newton Meters

NR ..... Neutral IE Rotation

N/mm ..... Stiffness in Newtons per Millimeter

p ..... Statistical significance p-value

pCSA ..... physiologic Cross Sectional Area

${}^{B_x}p_A$ ..... position element of CS A wrt x axis of CS B

${}^{B}\hat{P}_A$ ..... position vector of point A wrt CS B

${}^{B_x}r_{A_x}$ ..... rotation element of CS A wrt CS B – example shown is for x axis in each CS

ROM ..... Range Of Motion

RM ..... Repeated Measures

RMSE ..... Root Mean Squared Error

RSA ..... Radio-Stereometric Analysis

RTSA ..... Reverse Total Shoulder Arthroplasty

SD ..... Standard Deviation

SDA ..... Screw Displacement Axis

SH&C ..... Short Head of the Biceps & Coracobrachialis

${}^{B}_{A}T$ ..... Transformation matrix of A wrt CS B

T_d ..... Initial derivative time value

T_i ..... Initial integral time value

T_u ..... Estimated oscillation period

wrt ..... with respect to

${}^{B}_{A}\hat{X}, {}^{B}_{A}\hat{Y}, {}^{B}_{A}\hat{Z}$ ..... Axes column vectors of CS A wrt CS B

%BW ..... Percent Body Weight

Δθ ..... Change in angle Theta (θ)

^ ..... over a vector label denotes a unit vector

° ..... degrees (unit of rotation)

± ..... plus or minus; prefixes magnitude of one standard deviation

Δ ..... (delta) indicating change

→ ..... between items; denotes sequence of execution in direction of arrow

CHAPTER 1 – Introduction

OVERVIEW

This chapter explores the gross anatomy of the shoulder joint complex, its stabilizing mechanisms, and its physiologic function. A review is also provided of previous and current testing methodologies used for the assessment of static, passive, and active shoulder biomechanics, and of the technologies and techniques underlying this research. In concluding, the chapter addresses the biomechanical and clinical questions to be addressed, and the hypotheses of this work.

1.1 The Shoulder Complex

The "shoulder joint," as it is commonly (mis)termed, is in fact composed of three bones, three joints, a gliding articulation, and an array of muscles, tendons and ligaments all functioning together to produce arm motion with the goal of positioning the hand in space (Jobe et al., 2009). The combined effect of these components is a joint complex capable of achieving the largest range of motion, greater than a hemisphere, of any in the human body (Culham & Peat, 1993; Peat, 1986). However, optimal joint function and kinematics are readily disturbed if any of these components are affected by injury or disease (Neer, 1990).

1.2 Anatomy

In order to understand the function and biomechanics of the shoulder complex, it is first necessary to examine each component composing the joint. These components can be categorized as osseous constructs, passive soft tissues including joint capsule and ligamentous structures, and active soft tissues composed of muscle-tendon units. These groups are described below.

1.2.1 Osseous Constructs

The shoulder complex is composed of three bones – the clavicle, the scapula, and the humerus, which articulate with each other and the torso through three joints – the sternoclavicular joint, the acromioclavicular joint, and the glenohumeral joint (Figure 1.1). Additionally, the complex includes the scapulothoracic joint, a gliding articulation between the scapula and the chest wall, and the subacromial articulation, composed of the scapula and humerus (Culham & Peat, 1993).

1.2.1.1 Bones

The scapula is a triangular bone which forms the primary link between the upper limb and the axial skeleton (Figure 1.2), and serves as the main attachment site for many muscles involved in shoulder motion. These muscles originate on the torso and insert on the scapula to cause scapular motion, or originate on the scapular body and insert on one of the bones of arm to produce arm motion. The scapula's primary role is two-fold: to support the mass of the upper limb during motion, and to expand the hand's functional range of motion by acting as a movable platform for the arm (Rockwood, 2009). Despite its function, the scapula is a very thin bone, to the point of translucency in many cases, and requires support from attaching muscles and articulating structures to prevent it from buckling (von Schroeder, Kuiper, & Botte, 2001).

Three processes originate from the scapula: the spine, acromion, and coracoid process (Figure 1.2). The spine, or spinous process, originates at the medial border of the scapula and projects progressively more posterior to the scapular body as it moves lateral and superior. This process acts as an insertion for the trapezius, which originates on the torso, and as an origin for the posterior deltoid, which attaches on the humerus. It also creates a boundary to separate the supra and infra-spinatus fossae. The acromion is an extension of the spine at its lateral aspect that continues anterosuperior to create an arc of bone superior to the humeral head and which articulates with the lateral portion of the clavicle.

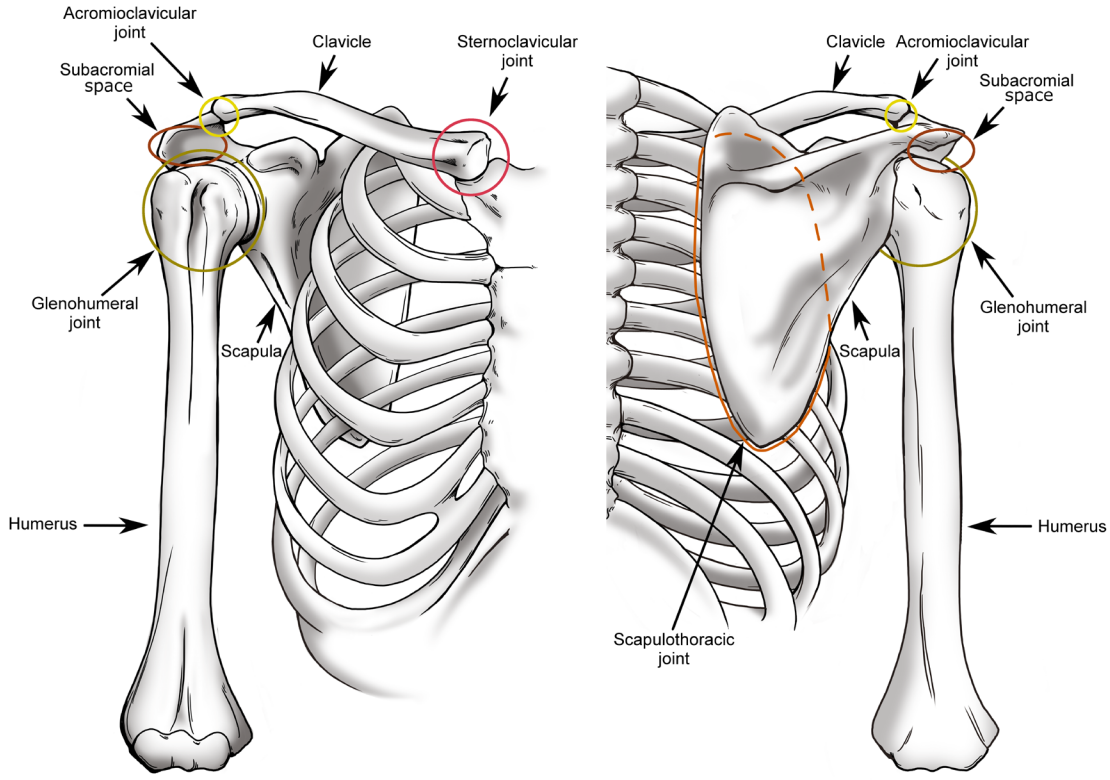

Figure 1.1: The shoulder complex
Pictured is an illustration of the bones and joints of the shoulder complex. Anterior (left) and posterior (right) views of the right side of the body.

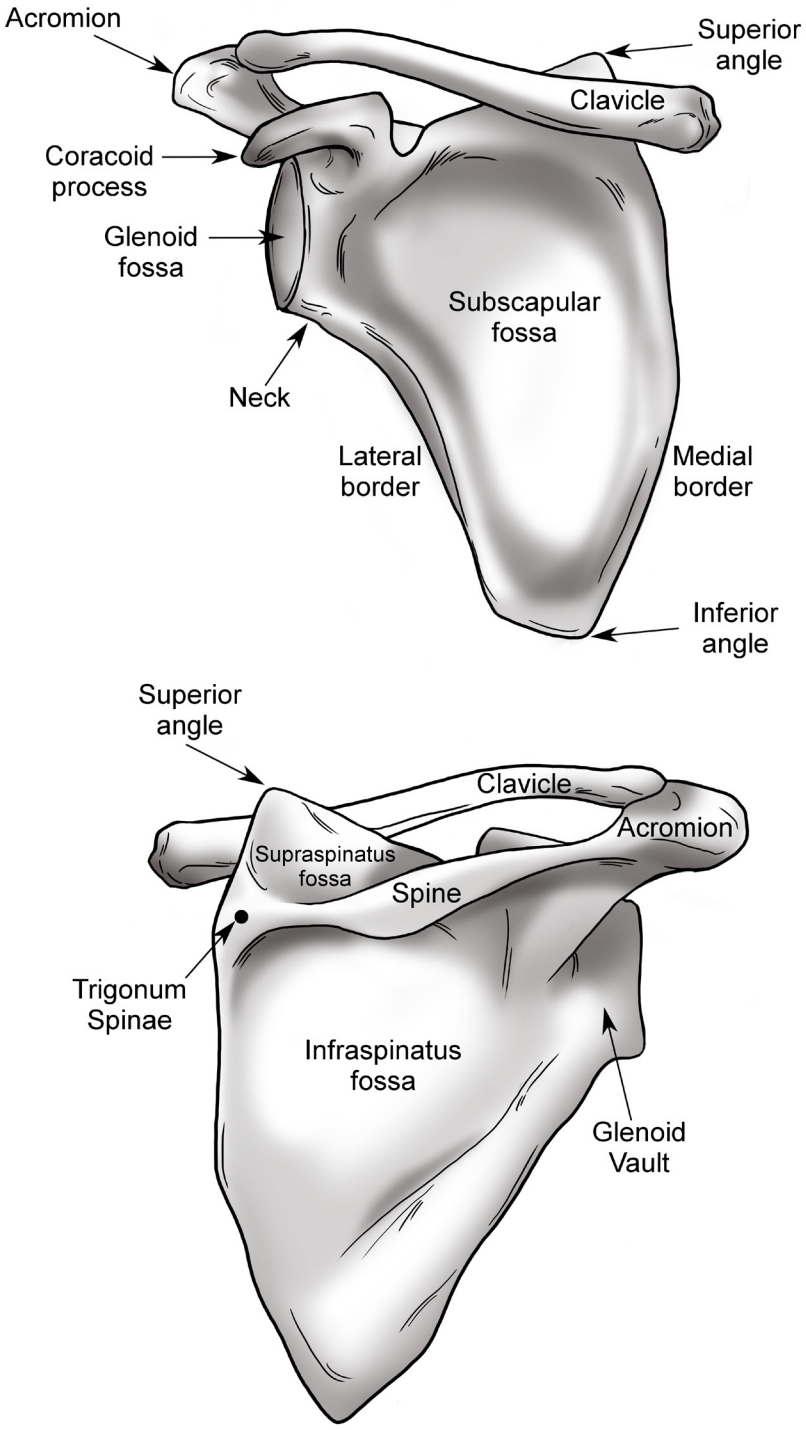

Figure 1.2: The osseous anatomy of the scapula and clavicle.
Anterior (top) and posterior (bottom) views of a right scapula and clavicle.

It functions as an attachment for the deltoid and trapezius muscles and increases the middle deltoid's moment arm (*i.e.* mechanical advantage) (Goss & Owens, 2009; Jobe et al., 2009). It is also the attachment site for one end of the coracoacromial ligament whose other end attaches to the coracoid process. The coracoid process is also the insertion site of the pectoralis minor muscle which runs from the torso, as well as the origin site of the conjoint tendon, which crosses the shoulder. O'Brien, Voos, Neviaser, and Drakos (2009) suggested that the coracoid may also act as an anterior humeral head stabilizer with the arm in 90° of abduction.

Since the scapula's role is to function as a platform for arm motion, its most important osseous anatomical feature is the shallow pear-shaped fossa located at the lateral aspect of the scapular body known as the glenoid (Figure 1.3). The glenoid surface is covered in hyaline cartilage, which has been found to have increasing thickness at the periphery in order to deepen the fossa and increase conformity with the head of the humerus (Soslowsky, Flatow, Bigliani, & Mow, 1992). Additionally, the fossa's depth is further increased by a fibrocartilaginous ring of tissue at the rim of the glenoid termed the glenoid labrum. The labrum also broadens the articular surface, thus increasing the available contact area with the humeral head, and also serves as an attachment site for various glenohumeral ligaments (Culham & Peat, 1993; O'Brien et al., 2009). The advantage of this stabilizing soft tissue structure lies in the increased range of motion it permits compared to a more conforming osseous cup, as with the acetabulum of the hip (Itoi, Morrey, & An, 2009; Moseley & Overgaard, 1962). Glenoid fossa size and orientation has been assessed by a number of groups with significantly variable findings; however, glenoid surface area is generally accepted to be approximately 1/3 that of the humeral head with the labrum attached and 1/4 without, and is oriented upward by ~5° and between 7° retroverted and 2° anteverted (Itoi et al., 2009).

The clavicle (Figure 1.2) is an S shaped bone (when viewed in the axial plane) that extends laterally from its articulation with the sternum in a predominantly horizontal manner when the scapula is in the neutral position. Its lateral end similarly articulates with the anteromedial aspect of the acromion. The role of the clavicle is to connect the scapula to the torso, to act as a strut to support arm loading, and to maintain separation

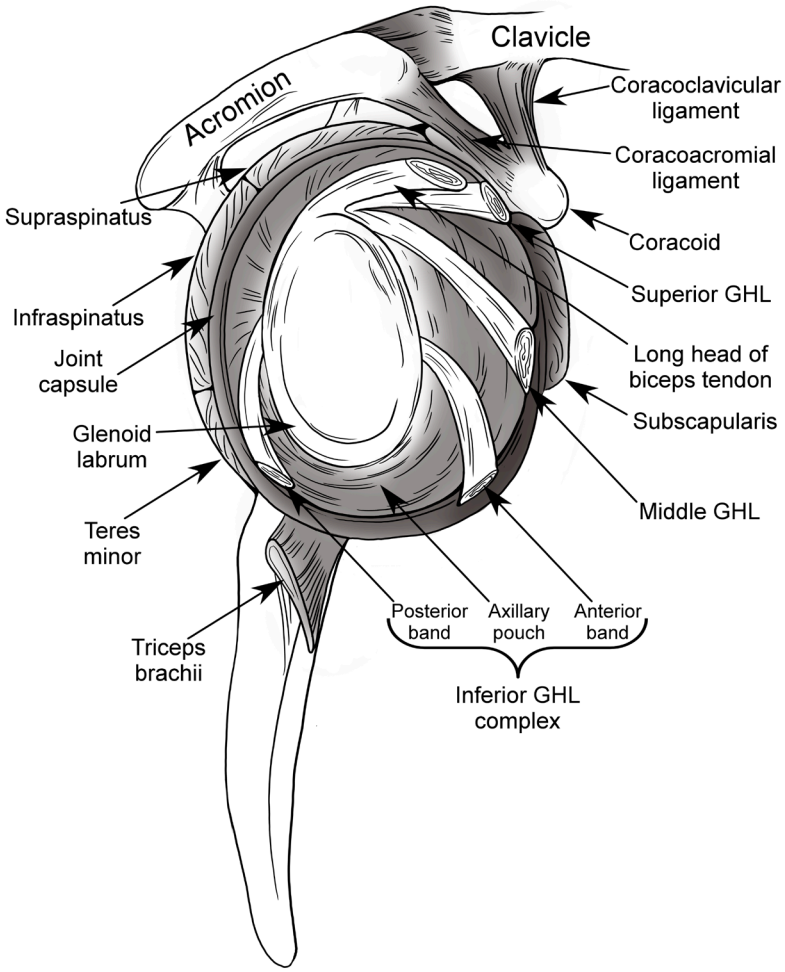

Figure 1.3: Soft tissue structures of scapula viewed from lateral.
This figure illustrates the joint capsule, ligaments, musculotendinous junctions of the rotator cuff, triceps brachii, and long head of the biceps tendon.

between the scapula and torso which would be otherwise compromised by scapulothoracic and humerothoracic muscle loading. The clavicle also serves as an attachment site for many muscle groups and influences scapular rotation during arm motion (Ludewig et al., 2009; McClure, Michener, Sennett, & Karduna, 2001; Van der Helm & Pronk, 1995).

The humerus (Figure 1.4) forms the proximal portion of the upper extremity. Its proximal end terminates as the humeral head, whose articular surface forms a third of a sphere and faces superior, medial, and posterior (O'Brien et al., 2009). The orientation of this articular surface is intended to facilitate load transmission from the arm to the torso while permitting maximum motion and maintaining joint stability (Itoi et al., 2009). As with the glenoid fossa, the humeral articular surface is coated in cartilage to disperse the transmitted load over a larger surface and thus decrease contact stresses on the bone; however, in this case, cartilage thickness is nearly constant (Soslowsky et al., 1992).

The humeral head possesses a number of other important anatomical features including the lesser and greater tuberosities, and bicipital groove. Both the lesser and greater tuberosities originate just lateral to the articular margin of the humeral head, with the lesser tuberosity lying anterolateral and the greater tuberosity lying posterolateral. The lesser tuberosity serves as the insertion site for the subscapularis muscle of the rotator cuff, and the greater tuberosity serves as an attachment for the supraspinatus superiorly, infraspinatus posteriorly, and teres minor posteroinferiorly. The moment which can be applied by the supraspinatus and deltoid muscle groups about the glenohumeral joint is enhanced by the structure of the greater tuberosity which elevates the supraspinatus above 30° of abduction and causes deltoid wrapping below 60° (Ackland, Pak, Richardson, & Pandy, 2008; Jobe et al., 2009). The bicipital groove is located between the two tuberosities and acts as a pathway that allows the long head of the biceps, which originates on the supraglenoid tubercle, to exit the glenohumeral joint. The groove also helps to transform the force in the biceps into a secondary stabilizer of the glenohumeral joint (Itoi, Newman, Kuechle, Morrey, & An, 1994). Distal to the humeral head, important features include the deltoid tuberosity, and medial and lateral epicondyles of the elbow. The deltoid tuberosity is located on the lateral surface of the humerus at

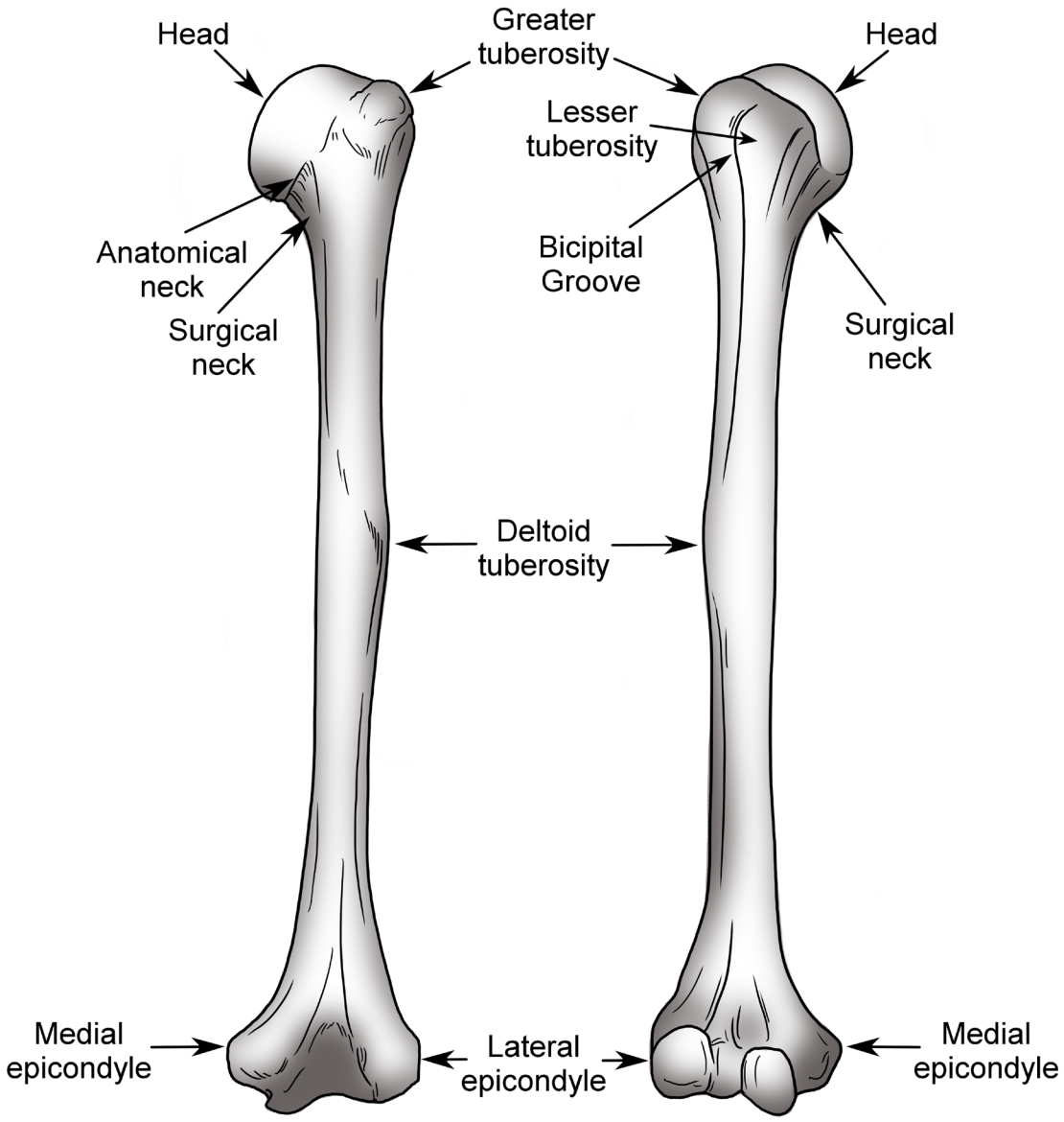

Figure 1.4: The osseous anatomy of the humerus.
Posterior (left) and anterior (right) views of a right humerus.

approximately mid-shaft, and serves as a common insertion for the three subgroups of the deltoid muscle. The medial and lateral epicondyles are located within the elbow anatomy and serve no shoulder function but are an important landmark for physiologically describing shoulder motion.

1.2.1.2 Joints

The joints that form the shoulder complex serve two primary functions: to achieve maximal range of motion and to maintain sufficient stability to prevent dysfunction and/or injury (Jobe et al., 2009).

The majority of the motion produced by the shoulder joint complex can be attributed to the glenohumeral joint which has the largest range of motion, about all three axes, of any diarthrodial joint in the body (An, Browne, Korinek, Tanaka, & Morrey, 1991; Halder et al., 2001; Howell, Galinat, Renzi, & Marone, 1988; Karduna, Williams, Williams, & Iannotti, 1996; Lippitt & Matsen, 1993; P. M. Ludewig et al., 2009). The articulating surfaces of this joint are the shallow pear shaped glenoid fossa, and the humeral head. The shallow structure of the glenoid effectively increases the humerus' impingement free arc and thus the overall range of motion of the joint. Abduction, however, is limited by impingement of the prominent greater tuberosity and the acromion on the scapula (Culham & Peat, 1993). The surface area of the humeral head is approximately three times larger than the glenoid (Itoi et al., 2009; Neer, 1990) and thus only a small and ever changing portion of it is in contact with the glenoid throughout motion, while the glenoid contact patch remains relatively constant (Bey, Kline, Zauel, Kolowich, & Lock, 2010; Kelkar et al., 2001; Soslowsky et al., 1992; Warner et al., 1998). The radius of curvature of the glenoid has also been found to be slightly greater than that of the humeral head (Soslowsky et al., 1992) and thus it is theoretically possible that the kinematics of the glenohumeral joint could be characterized by both rotations and translations (Bey et al., 2010; Itoi et al., 2009; Sahara, Sugamoto, Murai, Tanaka, & Yoshikawa, 2007). However, it has been shown that when the glenoid labrum, joint capsule, and glenohumeral ligaments are intact, sufficient stability is provided to eliminate all meaningful humeral head translation (Harryman et al., 1990; Howell et al., 1988; Poppen & Walker, 1976;

Veeger, 2000). With this in mind, the glenohumeral joint is thus typically considered a true three rotation ball-in-socket joint (Culham & Peat, 1993; Howell et al., 1988; Poppen & Walker, 1976; Veeger, 2000); however, translations of the humeral head have been shown to be relevant in pathological and reconstructed joint conditions, such as following dislocation (Apreleva et al., 1998; Burkart, Debski, Musahl, & McMahon, 2003; McMahon, Burkart, Musahl, & Debski, 2004).

The acromioclavicular and sternoclavicular joints are the articulations between the lateral clavicle and the acromion on the scapula, and the medial clavicle and the sternum, respectively. Both of these joints are characterized by the fibrocartilaginous coverings on each bone surface and a fibrocartilaginous disc interposed between them (Culham & Peat, 1993; Peat, 1986). Although these joints can be anatomically defined as plane synovial joints, the sternoclavicular joint functions similarly to a ball-in-socket joint, allowing the clavicle to move in a cone of motion which in turn permits scapular elevation and pro-retraction (Culham & Peat, 1993). In contrast, the acromioclavicular joint permits minimal motion typically composed of inferomedial translation during excessive load application. The role of these two joints is to support and stabilize the scapula while transmitting loads axially to the torso (Culham & Peat, 1993).

The subacromial space is formed by the rotator cuff inferiorly, the acromion superiorly, and the coracoid, and coracoacromial ligament anteriorly (Culham & Peat, 1993). This space's primary role is to aid smooth humeral motion under the acromion, and its anterior structures (coracoid and coracoacromial ligament) act to stabilize the joint superiorly.

The scapulothoracic joint is an articulation between the scapular body and the torso separated by the subscapularis muscle belly. The role of this articulation is to increase arm motion by delaying acromial impingement of the greater tuberosity during abduction and increasing horizontal flexion through pro-retraction (Culham & Peat, 1993). These motions are also critical in maintaining joint stability by ensuring that the joint loading direction remains within the glenoid's articular surface, thus limiting load and potential damage on the soft tissue stabilizers (Lippitt & Matsen, 1993).

1.2.2 Joint Capsule and Ligaments

The joint capsule and ligaments (Figure 1.3 & Figure 1.5) compose the portion of soft tissues in the shoulder complex responsible for providing passive stability as will be discussed in Section 1.5.2.

A joint's capsule is a thin membrane surrounding the articulating surfaces of a synovial joint that excretes nutrients and lubricating synovial fluid. In the glenohumeral joint, the capsule is relatively loose but becomes tensioned at extreme joint configurations (Peat, 1986). Medially, the glenohumeral joint capsule blends into the glenoid labrum and rim, while, laterally, it attaches to the articular margin of the humeral head.

The joint capsule is reinforced posteriorly by the infraspinatus and teres minor tendons, and anteriorly by both the subscapularis tendon and the glenohumeral ligaments (Clark & Harryman, 1992; Hess, 2000). The morphology of the glenohumeral ligaments varies but they are most commonly characterized as broad thickenings of the capsule superiorly, anteriorly, and inferiorly that may or may not blend into each other (Clark & Harryman, 1992; Neer, 1990). This structure is believed to exist in place of the discrete ligamentous bands seen in other joints as a result of the need to support both tensile and shear loads present in the highly mobile glenohumeral joint (Debski et al. 1999b). Additionally, unlike other ligaments, the glenohumeral ligaments can become taut in the mid-range of motion, typically as a result of internal or external rotation (Burkart & Debski, 2002).

The superior and middle glenohumeral ligaments originate at the superior glenoid between the biceps tubercle and the base of the coracoid (Figure 1.5). The superior ligament inserts on the humerus between the upper lesser tuberosity and the anatomical neck, and acts to limit inferior humeral head translation with the arm adducted (Burkart & Debski, 2002; Culham & Peat, 1993; Kask et al., 2010). The middle ligament inserts on the anterior aspect of the anatomical humeral neck and limits anterior translation and external rotation in mid-abduction (Burkart & Debski, 2002; Culham & Peat, 1993). The inferior glenohumeral ligament attaches to the anterior, inferior, and posterior aspects of the glenoid labrum, and inserts on the inferior anatomic and surgical neck of the humerus. This ligament is further sub-divided into an anterior band and axillary pouch, and

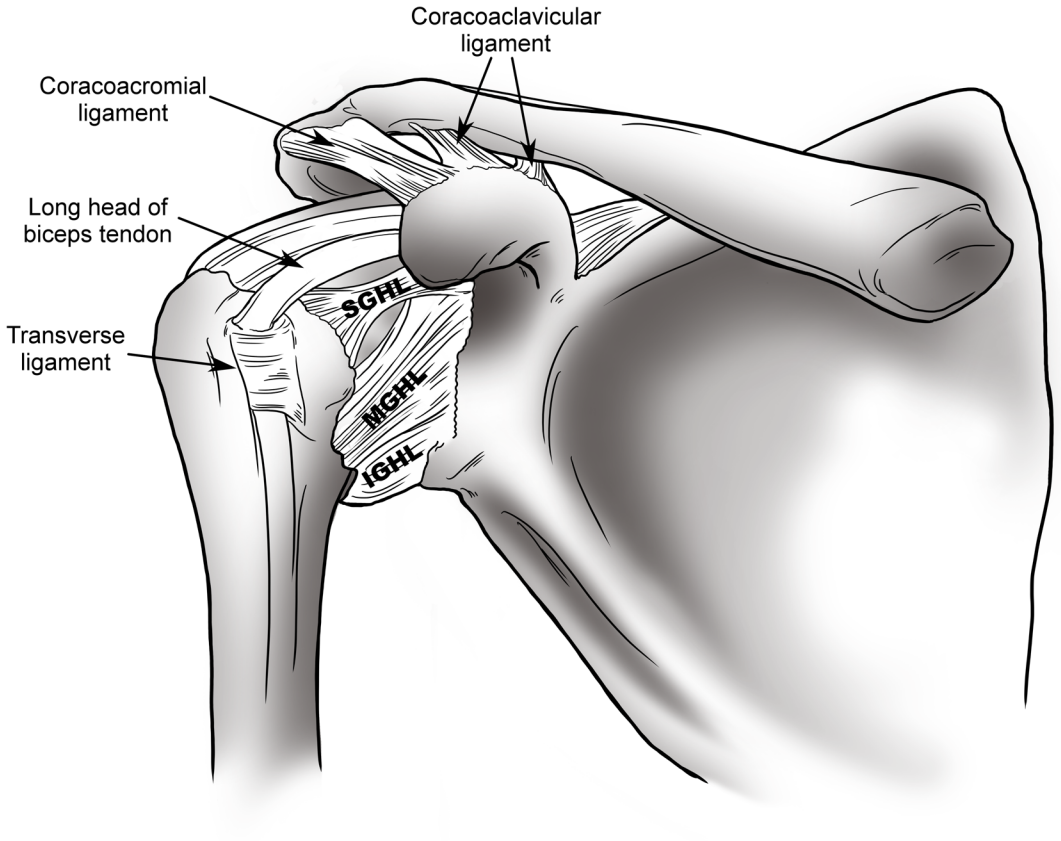

Figure 1.5: Anterolateral view of the joint capsule and ligaments.
In this isometric view of a right shoulder, in addition to the other structures, note that the three bands of the glenohumeral ligaments blend together and with the joint capsule.

posterior band. The former has been found to limit external rotation and anterior translation during abduction while the latter limits internal rotation and posterior translation in abduction (Burkart & Debski, 2002; Culham & Peat, 1993).

The transverse humeral ligament runs from the lesser to the greater tuberosity, thus covering the bicipital groove and creating a tunnel for the biceps tendon, helping to maintain the muscle's line-of-action throughout motion (Jobe et al., 2009).

The coracoacromial ligament runs from the horizontal pillar of the coracoid to the anterior aspect of the acromion, and together, these three structures form what is known as the coracoacromial arch. The role of the arch is to articulate with the humerus and prevent it from migrating superiorly due to external or muscle loading (Itoi et al., 2009). The coracoclavicular ligament runs from the vertical pillar and angle of the coracoid to the clavicle and helps to support the scapula while also preventing the clavicle from translating posteriorly (Neer, 1990). The acromioclavicular ligament forms a portion of the acromioclavicular joint and provides it with horizontal stability.

1.2.3 Muscles

The large number of muscles that enable motion and provide stability in the shoulder complex are commonly grouped based on their combined origin and insertion sites as the scapulohumeral, humerothoracic, scapulothoracic, and multi-joint muscles. Each of the muscles in these groups are described below and illustrated in Figure 1.6, Figure 1.7, and Figure 1.8.

1.2.3.1 Scapulohumeral Muscles

The scapulohumeral muscles are those muscles that originate on the scapula and insert on the humerus and consequently play the largest role in achieving glenohumeral motion and stability. These muscles are the deltoid, supraspinatus, subscapularis, infraspinatus, teres minor, teres major, and coracobrachialis.

The primary function of the deltoid is abduction of the humerus and has been found to provide approximately 50% of the total required glenohumeral abduction moment

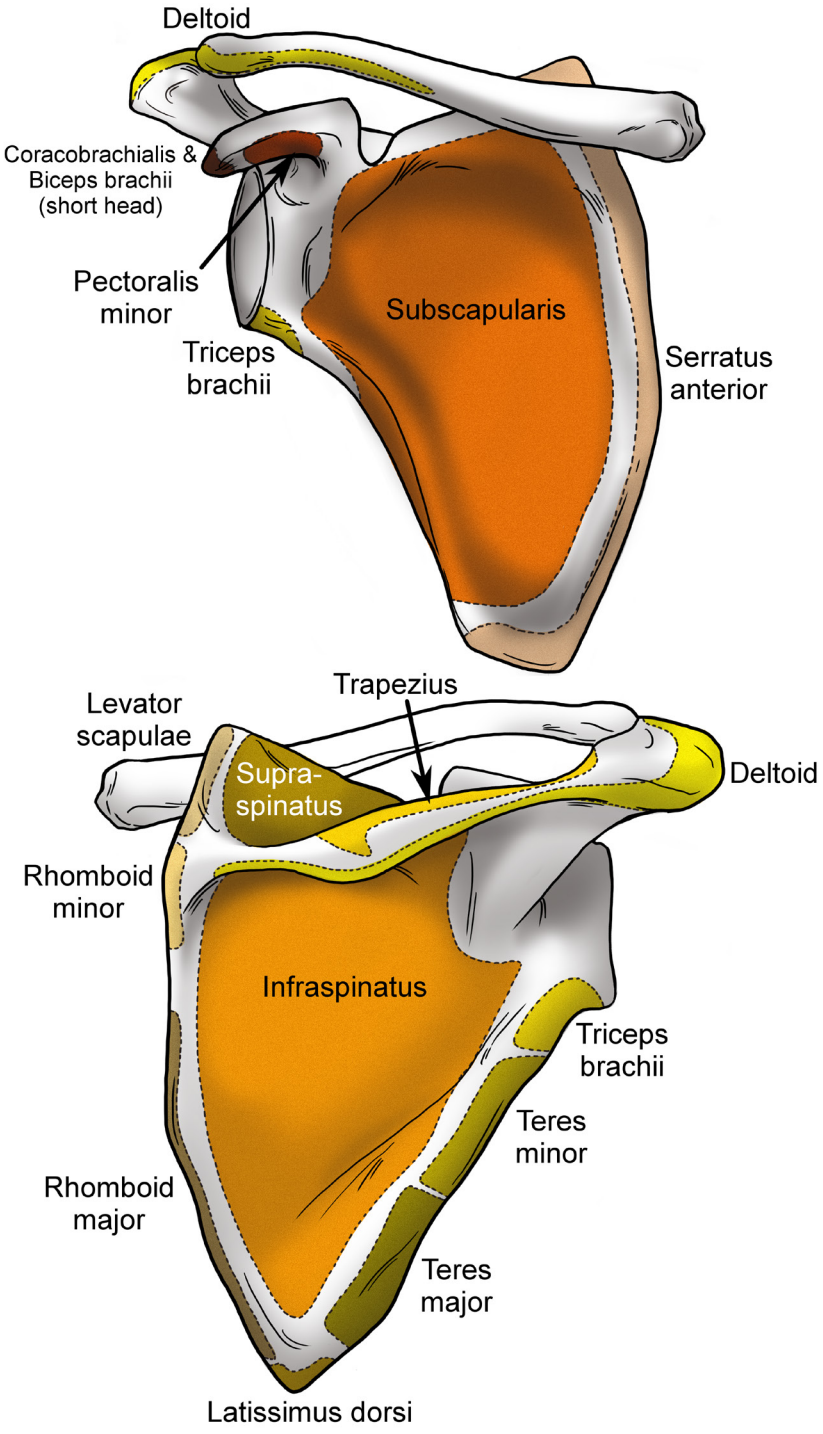

Figure 1.6: The muscular origins and insertions on the scapula.
Anterior (top) and posterior (bottom) view of a right scapula.

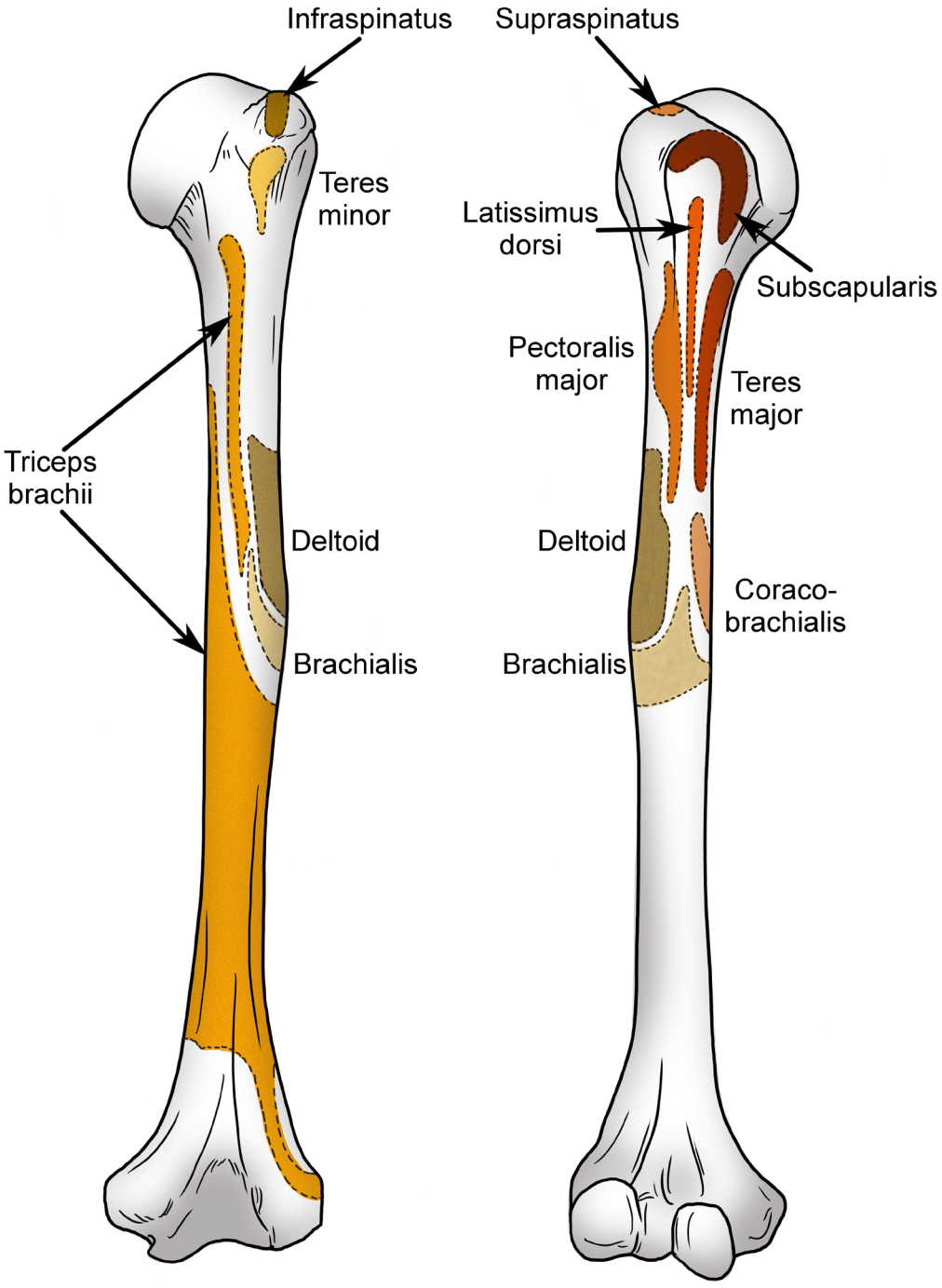

Figure 1.7: The muscular origins and insertions on the humerus.
Posterior (left) and anterior (right) view of a right humerus.

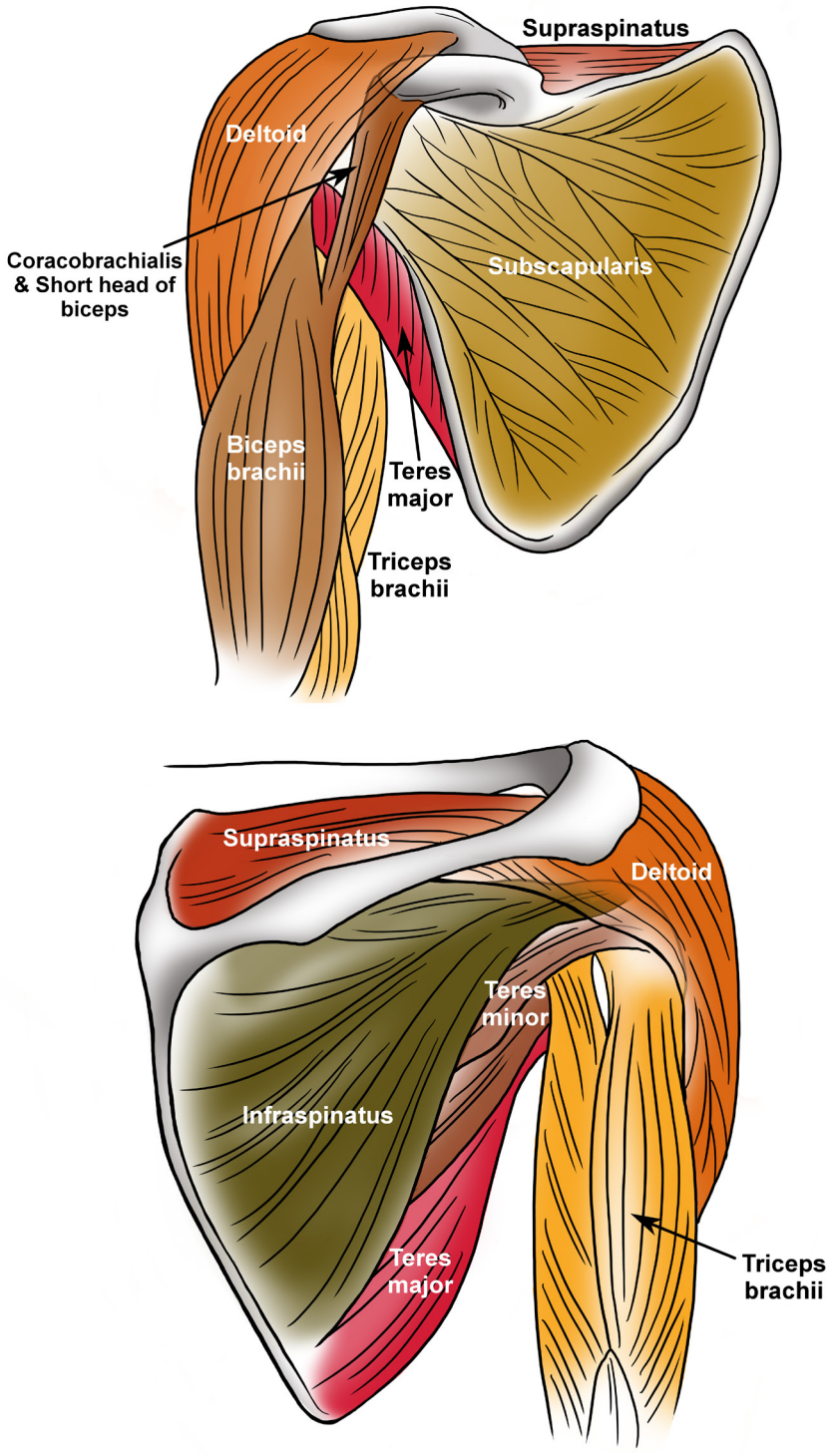

Figure 1.8: The muscles of the shoulder complex.
Anterior (top) and posterior (bottom) views of a right shoulder.

(Hess, 2000). The deltoid muscle can be divided into three independently functioning sub-regions: anterior, middle, and posterior. The largest proportion of the total moment produced by the deltoid is a result of anterior and middle deltoid loading, with the posterior deltoid contributing a much smaller portion (Ackland et al., 2008). Controversy exists with respect to the posterior deltoid's precise function, with some investigators showing that it possesses an adduction instead of an abduction moment arm when the arm is in its resting position (Ackland et al., 2008). In addition to their role in abduction, the anterior and posterior deltoids contribute to flexion and internal rotation, and extension and external rotation, respectively (Ackland & Pandy, 2011).

The rotator cuff is composed of four muscle bellies (supraspinatus, subscapularis, infraspinatus, and teres minor) and associated tendons, as well as the joint capsule, and glenohumeral ligaments. This blended structure surrounds the glenohumeral joint anteriorly, superiorly, and posteriorly. It is believed that the primary function of the rotator cuff is to provide stability to the joint during motion (Culham & Peat, 1993), but it has also been identified as a source of both abduction and axial rotation moments (Neer, 1990). It has also been noted that although each of the rotator cuff muscles can be activated independently, the high level of interconnection of these groups through their musculotendinous junctions and the joint capsule may cause loading of one muscle to influence the passive tension of another (Soslowsky, Carpenter, Bucchieri, & Flatow, 1997).

The supraspinatus originates on the supraspinous fossa of the scapula, between its spine and superior edge, and inserts on the humeral greater tuberosity. This muscle is activated during elevation motions (Howell et al., 1988; Kedgley et al., 2008; Wuelker, Plitz, Roetman, & Wirth, 1994; Wuelker, Schmotzer, Thren, & Korell, 1994). The role of the supraspinatus in elevation is especially prominent during the initiation of abduction (Ackland et al., 2008; Kedgley et al., 2007).

The subscapular fossa, the entire anterior face of the scapula, serves as the origin of the subscapularis, which in turn inserts on the humeral head at the lesser tuberosity. Ackland et al. (2008) have demonstrated that the subscapularis is composed of a superior and

inferior portion that can be loaded separately. The inferior portion's role is primarily stabilization, since it has a relatively smaller ability to apply moments compared to the superior portion, which itself provides joint stability while also being capable of applying forward flexion moments. The primary moment applied by each of these sub-regions is internal rotation (Ackland & Pandy, 2011; Escamilla, Yamashiro, Paulos, & Andrews, 2009; Jenp, Malanga, Growney, & An, 1996).

The infraspinatus originates on the infraspinatus fossa, which lies inferior to the scapular spine, and inserts on the posterior aspect of the greater tuberosity. Similar to the subscapularis, the infraspinatus is composed of a superior and inferior portion. The infraspinatus possesses an abduction moment arm (Ackland et al., 2008), but it is much smaller than the flexion moment arm of the subscapularis. Therefore, the role of the infraspinatus is more predominantly stabilization than motion production. As with the subscapularis, the primary moment applied by each of these sub-regions produces axial rotation, which in this case, is external (Ackland & Pandy, 2011; Escamilla et al., 2009; Jenp et al., 1996).

The teres minor and major both originate on the lateral border of the scapula with the minor located superior to the major. The teres minor blends with the infraspinatus and inserts on the greater tuberosity while the teres major inserts on anterior humeral shaft. The role of each of these muscles is primarily joint stabilization and humeral adduction (Neer, 1990) with the teres minor also producing external rotation and the teres major producing internal rotation (Ackland & Pandy, 2011).

The coracobrachialis originates on the tip of the coracoid process and inserts on the anteromedial aspect of the humeral shaft. The role of this muscle is to adduct and flex (Ackland et al., 2008), but electromyography studies have shown that it is only active during resisted adduction (Jonsson, Olofsson, & Steffner, 1972).

1.2.3.2 Humerothoracic Muscles

The humerothoracic muscles – those muscles which originate on the thoracic cage and insert on the humerus – are the pectoralis major and the latissimus dorsi. The pectoralis

major originates on anterior surface of the medial half of the clavicle and the sternum and inserts on the lateral lip of the bicipital groove. The role of this muscle is to adduct, flex, and internally rotate (Ackland & Pandy, 2011; Ackland et al., 2008). The latissimus dorsi has broad origins on the lower thoracic and upper lumbar vertebrae, the iliac crest of the pelvis, the inferior three ribs, and the inferior angle of the scapula, and it inserts on the floor of the bicipital groove. The function of this muscle is to adduct, extend, and internally rotate the humerus (Ackland & Pandy, 2011; Ackland et al., 2008).

1.2.3.3 Scapulothoracic Muscles

The scapulothoracic muscles – those muscles which originate on the thoracic cage and insert on the scapula – are the serratus anterior, levator scapulae, rhomboids, trapezius, and pectoralis minor. The serratus anterior inserts on the anterior side of the scapula along the entire length of the medial scapular border. Conversely, the levator scapulae and rhomboids insert on the posterior surface of this medial border. The trapezius inserts on the superior edge of the scapular spine, and the pectoralis minor inserts on the anterior aspect of the horizontal pillar of the coracoid process. Each of these muscles is responsible for a different movement of the scapula relative to the torso including scapular elevation, tilting, and version.

1.2.3.4 Biarticular Muscles

In the shoulder, there are three biarticular muscles, or muscles which cross more than one joint from origin to insertion. These muscles are the triceps brachii and the short and long heads of the biceps brachii. Each of these muscles primarily affects elbow motion; however, their paths across the glenohumeral joint influence shoulder joint function and kinematics. The long head of the triceps originates on the lateral scapular border just inferior to the glenoid rim, crosses the glenohumeral and elbow joints, and inserts on the ulna. The role of the triceps with respect to shoulder function is limited, but has been shown to resist inferior shear forces induced by the primary adductor muscles during resisted adduction activities (Jobe et al., 2009). The biceps brachii originates as two distinct heads, the short head from the tip of the coracoid process and the long head from

the supraglenoid tuberacle, exiting through the bicipital groove. These two heads converge at the level of the deltoid tuberosity and cross the elbow before inserting on the radius. The long head of the biceps depresses the humeral head due to the pulley effect of it wrapping over the humeral head, and has been shown to stabilize the joint anteriorly (Itoi, Newman et al., 1994; Itoi, Newman et al., 1994). The role of the short head of the biceps remains unclear but some have proposed that it provides resistance to anterior translation of the humeral head primarily by providing a barrier when taut (Itoi et al., 2009).

1.3 Function

The functional purpose of the shoulder complex is to allow the placement of the hand in space across the largest possible range of motion while maintaining joint stability (Itoi et al., 2009). The degree of mobility of the joint, number of degrees of freedom (DOF), and possible interplay between scapulothoracic and glenohumeral motion, mean that placement of the hand can be achieved using multiple pathways. Each of these pathways will use a unique combination of independent joint rotations and thus the same hand position may result in significantly differing joint contact patterns and kinetics.

1.4 Humerothoracic Motions

Humeral movement with reference to the thorax is commonly described in terms of four motions: elevation, forward flexion, horizontal flexion-extension, and axial rotation (Figure 1.9). These motions result from motion of both the humerus and the scapula and can be more precisely described using three independent rotations of each bone. The rotations of the humerus relative to the scapula can be described as the rotation which defines the plane in which the humerus elevates (plane of elevation), the rotation which moves the humerus away from the body (elevation), and the rotation about the long axis of the humerus (axial rotation). The scapula's rotations relative to the thorax are in turn rotation of the scapula across the chest and away from the mid-line (elevation), rotation about a superior axis which changes the direction of the glenoid (internal-external rotations), and rotation about a lateral axis tilts the glenoid (anterior-posterior tilting) (Figure 1.10).

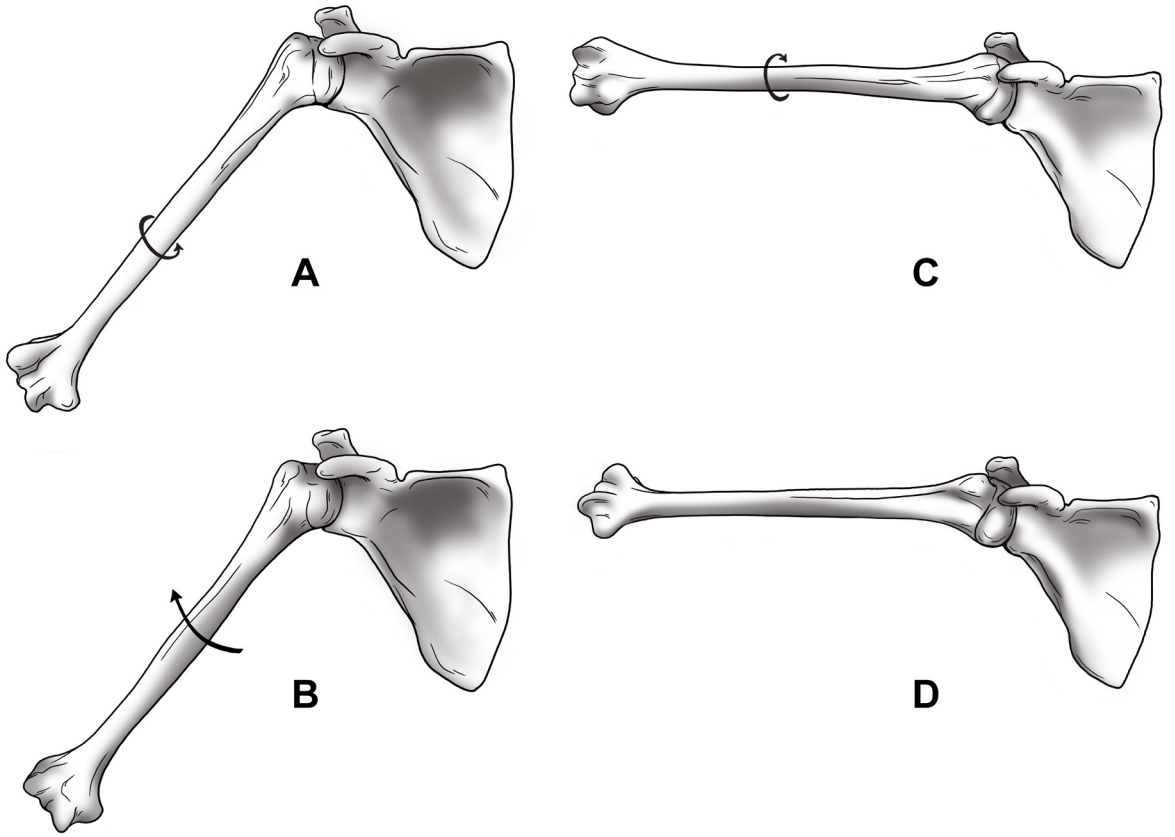

Figure 1.9: Humeral rotations used to describe motion.
Sequence of rotations used to describe humeral orientation relative to the scapula. (A) Humerus at rest with epicondyles in coronal plane; (B) humerus with epicondyles in scapular plane following 'plane of elevation' rotation indicated in (A); (C) humerus parallel to ground following 'abduction' rotation indicated in (B); (D) humerus 'externally' rotated following rotation indicated in (C).

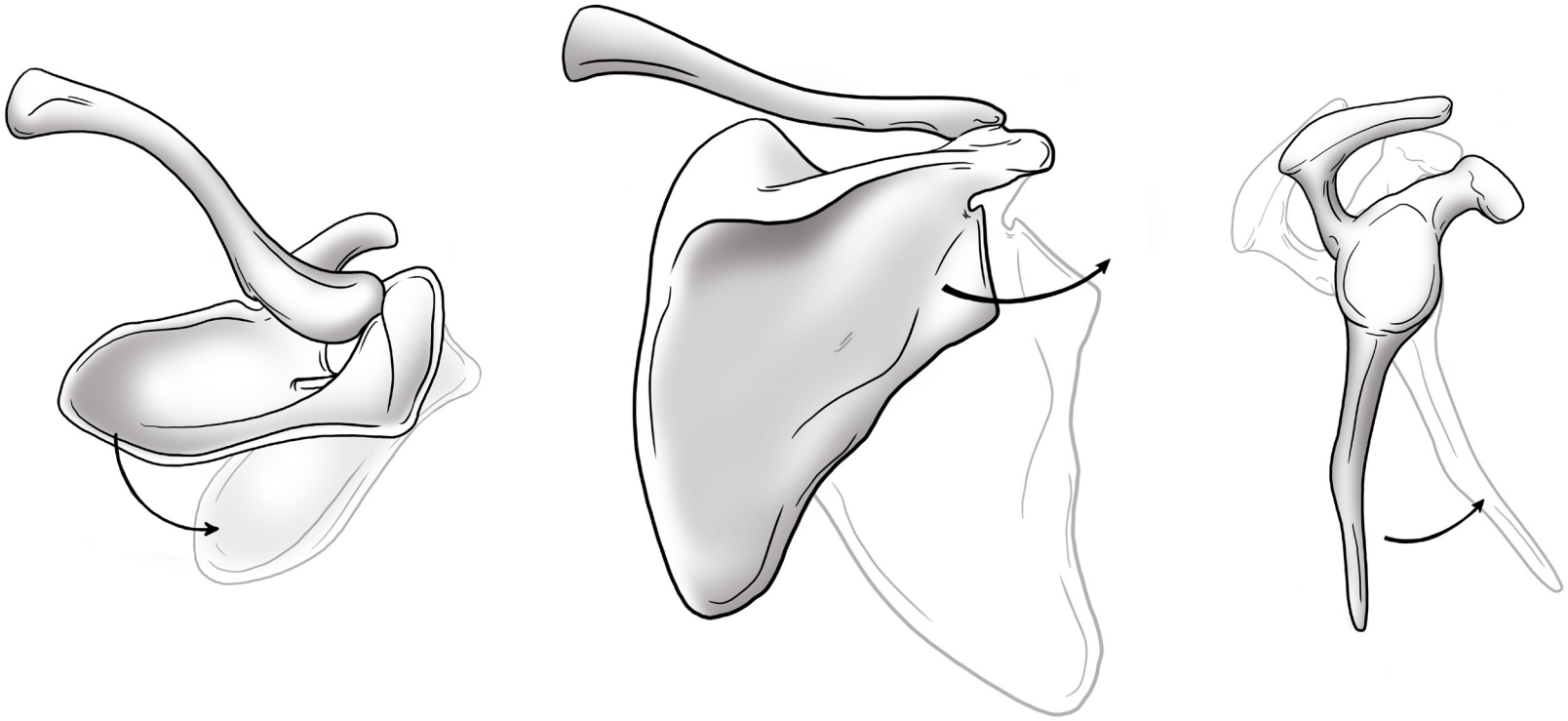

Figure 1.10: Scapular rotations used to describe motion.
Displayed are rotations about the axes most commonly used to describe scapular orientation relative to the thorax. Version rotation (left) showing scapula moving into anteversion; elevation rotation (middle) showing scapula upwardly rotating; tilting rotation (right) showing scapula moving into a posterior tilt.

‘Elevation’ is the common term used to describe the motion of the arm away from the body in the lateral direction. Although this motion may be thought of as movement in the coronal plane, it is more common for this motion to occur in the scapular plane – which lies ~30° anterior – in which the deltoid and supraspinatus are optimally aligned for elevation. (Itoi et al., 2009; Poppen & Walker, 1976). This motion may exceed 180° of rotation but on average is limited to 171° for women and 167° for men (Itoi et al., 2009). This range of motion, however, is influenced by individual anatomy and laxity, and decreases with age due to joint stiffening and degenerative muscle changes (Barnes, Van Steyn, & Fischer, 2001). In order to achieve optimal joint function, stability, and kinematics, this large range of motion is divided between glenohumeral elevation and scapulothoracic elevation. Combining these two motions optimizes function in three ways. First, it enables an arm range of motion unattainable through glenohumeral joint only, because a 180° rotation at this joint would trap the muscles within the articulation, rendering them non-functional (Van der Helm & Pronk, 1995). Second, the decreased ROM of each joint allows the muscles crossing the joint to function within the optimal region of their length-tension curve (Itoi et al., 2009). Third, the presence of scapular rotation moves the glenoid beneath the humeral head, providing support against the weight of the arm, and thus maintaining optimal joint kinetics, kinematics, and stability (Itoi et al., 2009).

The manner in which the arm’s motion is divided between the glenohumeral and scapulothoracic joints during elevation is termed the ‘scapulohumeral rhythm.’ In 1944, Inman and Abbott, described that when averaging the rhythm over a full range of motion, its ratio is 2:1 (glenohumeral:scapulothoracic). Plane of abduction, direction of motion (raising vs. lowering), shoulder dominance, gender, level of resistance, and level of muscle fatigue have been widely studied in relation to this rhythm since then (see Crosbie, Kilbreath, Hollmann, & York, 2008; Crosbie, Kilbreath, & Dylke, 2010; Dayanidhi, Orlin, Kozin, Duff, & Karduna, 2005; Ebaugh, McClure, & Karduna, 2005; Fayad et al., 2006; Forte, de Castro, de Toledo, Ribeiro, & Loss, 2009; Graichen et al., 2000; Inman & Abbott, 1944; Ludewig et al., 2009; Ludewig, Cook, & Nawoczenski,

1996; Matsuki et al., 2010; McClure et al., 2001; McClure, Michener, & Karduna, 2006; McQuade & Smidt, 1998; Nagai et al., 2013; Poppen & Walker, 1976; Prinold, Villette, & Bull, 2013; Scibek & Carcia, 2012; Yano et al., 2010). While these investigations have resulted in varying and often contradictory conclusions, some supporting one constant ratio, and others, a variable ratio across motion, the commonly accepted ratio remains Inman & Abbott's (1944) 2:1 (glenohumeral:scapulothoracic) for a full range of abduction.

In addition to elevating during humeral elevation, the scapula has also been shown to undergo internal-rotation and tilting. Reports of the initial direction and magnitude of movement of these two rotations vary; however, it has been shown that across a full range of abduction, the scapula tends to externally rotate and tilt posteriorly relative to its initial resting posture, with the majority of this motion occurring beyond 90° of humerothoracic elevation (Itoi et al., 2009; McClure et al., 2001). The function of these rotations is not well understood, but McClure et al. (2001) posit that they allow the humeral head and rotator cuff tendons to more easily pass beneath the acromion as the humerus elevates beyond 90°. The ability of the humeral head and rotator cuff to clear beneath the acromion is also aided by external rotation of the humerus, which occurs during elevation in any plane anterior to the scapula. Browne, Hoffmeyer, Tanaka, An, and Morrey (1990) demonstrated that maximal elevation occurs 23° anterior to the scapular plane and is facilitated by 35° of external rotation. This external rotation has the additional effect of relaxing the inferior capsuloligamentous tissues, thus permitting further motion. In contrast, maximal elevation in planes posterior to the scapula requires internal rotation and peaks at 115° in a plane ~20-30° posterior to the scapula (Browne et al., 1990).

The term ‘forward flexion’ is commonly used to describe motion of the arm away from the body in the anterior direction. This motion can be considered a special case of elevation in a plane anterior to the scapula; however, this is only the case if the humerus is internally rotated prior to elevation. If the humerus is instead left in neutral rotation, the glenohumeral kinematics and contact mechanics would be significantly different. It is the latter case which is commonly termed ‘forward flexion.’ Despite this motion’s unique

glenohumeral kinematics, the scapula's motion is remarkably similar to that observed during elevation in the scapular plane (McClure et al., 2001).

Horizontal flexion-extension is a common motion – especially in throwing sports – which involves changes in the humeral plane of elevation while the elevation level is maintained parallel to the ground, and for which internal-external rotation can be constant or variable. The boundary between flexion and extension is commonly considered to be the scapular plane. Itoi et al. (2009) have found that when the arm is placed in this plane and externally rotated, the glenohumeral joint achieves maximum stability. However, in patients with anterior shoulder instability, orientation in this plane, as well as planes posterior to the scapular plane, have been described as the most unstable (Speer, Hannafin, Altchek, & Warren, 1994). Scapular kinematics for horizontal flexion-extension have not been evaluated during independent rotation about this one axis, but rather only during throwing motions. However, results from throwing motions have shown that scapular upward rotation is decreased to approximately 20° with the arm in full humeral horizontal extension from approximately 40° with the arm in the scapular plane (Ludewig et al., 2009). Additionally, the scapula progressively internally rotates from approximately 20° in maximal horizontal extension to its resting posture of 30° when the humerus is in the scapular plane.

For the remainder of this thesis, glenohumeral elevation in the scapular plane will be termed 'abduction,' while the rotation defining this plane will be termed 'plane of elevation,' and rotation about the humeral longitudinal axis will be termed 'internal-external rotation'.

1.5 Joint Stabilizers

Stability of the glenohumeral joint is provided by a combination of a number of different types of stabilizing structures. These can be classified as static or dynamic (Itoi et al., 2009). Static stabilizing structures include the joint's bony anatomy, as well as the following passive soft tissues: joint capsule, ligaments, and labrum. Dynamic stability is provided by activation of various muscle groups. The work of Burkhart and Debski has

demonstrated that no single structure is primarily responsible for stability across the shoulder's large range of motion, but that instead, stability is produced through a combination of factors (Burkart & Debski, 2002; Debski, Sakane, Wong, Fu, & Warner, 1999; Debski et al., 1999b). This combination of factors is critical in enabling shoulder motion, but this dependence on an array of stabilizers – especially soft tissue stabilizers – results in the shoulder being the most unstable joint in the body (Itoi et al., 2009; Jobe et al., 2009). Specifically, the shoulder is most unstable anteriorly but patients also commonly experience instability inferiorly and posteriorly (Peat, 1986; Speer et al., 1994).

1.5.1 Bony Anatomy

The bony anatomy of the glenohumeral joint is significantly less conforming than that of other major joints in the body and as a result, its primary stabilizing effect is restricted to resisting joint subluxation due to the arm's gravitational loading. This role is especially relevant in abducted arm positions where the scapula rotates such that the glenoid sits more directly beneath the humeral head (Itoi et al., 2009). Additionally, the bony structures' stabilizing role in relation to shear forces resulting from muscle loading has been shown to be minimal (Halder, Kuhl, Zobitz, Larson, & An, 2001; Lippitt & Matsen, 1993; Lippitt et al., 1993). This can be attributed to the low conformity and small contact area between the glenoid and humeral head (Soslowsky, Flatow, Bigliani, & Mow, 1992; Soslowsky et al., 1992). In fact, it is only with the addition of the glenoid labrum that meaningful stabilization is achieved by the glenoid (Itoi et al., 2009; Peat, 1986). Two of the scapula's other bony processes are also thought to play a limited role in joint stability. In extreme motions, the acromion is believed to prevent excessive superior migration of the humeral head (Itoi et al., 2009) while the coracoid limits anterior translation (O'Brien et al., 2009).

1.5.2 Soft Tissue Passive Stabilizers

The joint capsule, glenoid labrum, and ligaments greatly increase the stability of the glenohumeral joint by directly augmenting the effect of the bony anatomy and by restraining against forces and motions which cannot be resisted by the osseous structures.

1.5.2.1 Joint Capsule

The soft tissues composing the glenohumeral joint capsule have been shown to have little direct mechanical stabilizing ability especially in the mid-range of motion. Debski et al. (1999b) found that with the humerus in neutral rotation and the humeral head well centered, the joint capsule in fact carries no load. It does, however, mechanically stabilize the joint when it is placed in extreme positions such as maximal abduction (Burkart & Debski, 2002; Debski et al., 1999). Some investigators have found that disruption of the anteroinferior capsule has minimal effect on joint translation during abduction in external rotation (Apreleva et al., 1998) while others have shown that anterior capsular disruption increases humeral translations at maximal abduction while posterior disruption increases posterior translations between 60 and 90° of abduction (Ovesen & Nielsen, 1986). These differing findings may be explained by the effect of externally rotating the humerus which could tighten the remaining anterior soft tissues and prevent humeral translations.

Perhaps the most important stabilizing effect of the joint capsule does not relate to direct mechanical stabilization, but instead is a result of the fluid filled cavity created by the capsule that causes negative intra-articular pressure (Itoi et al., 2009). Although this pressure is small, it has been shown to be a significant contributor to joint stability especially when the joint is subject to minimal muscle and joint loading (Alexander, Southgate, Bull, & Wallace, 2013; Habermeyer, Schuller, & Wiedemann, 1992; Hurschler, Wülker, & Mendila, 2000).

1.5.2.2 Glenoid Labrum

Although the joint capsule is an important stabilizer to the minimally loaded joint, its effect is far outweighed by that of the glenoid labrum, especially when the joint is loaded (Itoi et al., 2009). The labrum increases the contact area with the humeral head and deepens the glenoid socket by approximately double the depth of the bony anatomy alone (Itoi, Hsu, & An, 1996; Soslowsky et al., 1992). These anatomical changes increase the concavity compression effect of the glenoid (Lippitt et al., 1993) which has been shown to improve the stability ratio – the ratio of dislocating force to compression force – in all directions. It has also been shown that surgical removal results in marked decreases in the stability ratio (Halder et al., 2001; Lippitt & Matsen, 1993; Lippitt et al., 1993).

1.5.2.3 Ligaments

The three bands of the glenohumeral ligaments are the most important stabilizer when the arm is placed in extreme positions since they act to maintain the humeral head centered on the glenoid (Burkart & Debski, 2002; Clark & Harryman, 1992; Debskiet al., 1999b; Itoi et al., 2009; Jobe et al., 2009; Karduna et al., 1996); however, these ligaments have little effect on stability with the arm in the mid-range of motion since they, along with the joint capsule, are lax in this position (Itoi et al., 2009).

1.5.3 Soft Tissue Active Stabilizers – Muscles

As described above, the glenohumeral joint is largely unconstrained and the bony anatomy and soft tissue passive stabilizers are insufficient to maintain stability across large arcs of motion. Thus, the muscles crossing the glenohumeral joint, in addition to producing motion, play an uncommonly important role in stabilizing the joint. The contribution of muscle activity to glenohumeral stability can be achieved through a combination of five different stabilizing mechanisms:

1. **Passive Muscle Tension –** it is thought that the natural resting length of the shoulder muscles plays some role in maintaining joint stability by providing joint compression as the tissues are stressed (Itoi et al., 2009; Ovesen & Nielsen, 1986);

however, observation of this effect has been inconsistent and, as with passive soft tissues, the effect is likely minimal in the mid-range of motion (Motzkin, Itoi, Morrey, & An, 1994).

2. **Compression of the Articular Surface –** the joint load resulting from muscle activity causes compression of the two articular surfaces and induces concavity compression (Itoi et al., 2009) which is enhanced by the glenoid labrum as discussed in 1.5.2.2. The role of this stabilizing phenomenon has been widely studied for an array of healthy and dysfunctional joint conditions (Howell & Kraft, 1991; Karduna et al., 1996; Kedgley et al., 2007; Kedgley et al., 2008; Lippitt & Matsen, 1993; Lippitt et al., 1993; McMahon et al., 1995).
3. **Muscle Induced Motion Causing Secondary Tightening of Passive Stabilizers –** the muscles move the shoulder to an extreme position which causes the passive stabilizers to provide additional stabilization (Itoi et al., 2009).
4. **Barrier Effect of Active Muscles –** when a muscle is active, it shortens and becomes taut. This in turn creates a semi-rigid barrier which is capable of resisting humeral head translation (Itoi et al., 2009). The barrier effect is most pronounced when a muscle that wraps over a bony structure is tensioned. Application of this tension causes the muscle to apply a force to the bone it is wrapping over which is normal to its line of action. This force can effectively increase joint stability especially when balanced by forces from other wrapped muscles.
5. **Centralization of Joint Reaction Force –** in order to maintain joint stability, it is essential that the joint reaction force is directed within the articular surface of the glenoid (Lippitt & Matsen, 1993). This can be achieved through activity of muscles which are not primarily responsible for motion, such as the anterior and posterior rotator cuff during abduction.

As the largest single muscle group crossing the glenohumeral joint, many have proposed that the deltoid is an important dynamic stabilizer; however, little research has been performed to demonstrate its role. Motzkin et al. (1994) demonstrated that the deltoid in fact has little passive effect on inferior stability in adduction or abduction. Others have demonstrated that activity of some sub-groups of the deltoid provide stability during

abduction in the scapular plane but not in the coronal plane (Lee & An, 2002; Michiels & Bodem, 1992). Kido et al. (2003) found that the stabilizing function of the deltoid is enhanced in abduction and external rotation when the joint becomes increasingly unbalanced. Still others have argued that the morphology of the acromion is an important factor in whether the deltoid acts as a stabilizer or destabilizer; in people with large lateral extension of the acromion, the deltoids are forced to originate more lateral and thus have a more vertical line-of-action which may destabilize the joint superiorly (Nyffeler, Werner, Sukthankar, Schmid, & Gerber, 2006).

Although the rotator cuff muscles play an important role in producing arm motion, they are often largely considered as stabilizers of the shoulder. In comparison to the deltoid, the physiological lines of action of the rotator cuffs are nearly concentric and thus, in a healthy shoulder, activity within these groups effectively compresses the humeral head into the glenoid concavity creating stability and ball-in-socket kinematics (Itoi et al., 2009). This effect persists throughout motion but is the most critical to joint stability when the arm is in the mid-range of motion where passive stabilizers are ineffective (Harryman et al., 1990; Itoi et al., 2009; Lippitt & Matsen, 1993). In addition to compressing the articular surfaces, the inferior angulation of the subscapularis, infraspinatus, and teres minor are able to produce a force couple with the superior deltoids which can help to medialize the joint reaction force. Were they not activated, the joint reaction force would be directed superiorly (Sharkey & Marder, 1995). The stabilizing role of the supraspinatus in both the inferior and superior directions has been studied but remains unclear. Traditionally, the supraspinatus has been viewed as a superior stabilizer due to its location (Sharkey & Marder, 1995; Thompson et al., 1996); however, more recent research has disputed this claim (Halder, Zhao, O'driscoll, Morrey, & An, 2001). Similarly, it is often thought that the supraspinatus tethers the humeral head and prevents inferior instability (Soslowsky, Malicky, & Blasier, 1997); however, research has shown that intact force couples in the horizontal and frontal planes are a more important stabilizing factor (Halder et al., 2001; Sharkey & Marder, 1995; Thompson et al., 1996).

The long head of the biceps has also been shown to be a joint stabilizer in all directions. As a result of its wrapped path over the humeral head, the biceps' primary stabilizing effect is to resist superior movement by depressing the humeral head. The stabilizing effect is most pronounced in the anterior direction with the arm in external rotation (Itoi, Kuechle, Morrey, & An, 1993; Itoi, Newman et al., 1994; Itoi et al., 2009).

1.6 Techniques in the Study of Glenohumeral Joint Biomechanics

In the field of biomechanics, there are three broad techniques that can be used to assess outcome measures of interest: *in-vivo*, *in-silico*, and *in-vitro*. Each of these models has strengths but also suffers from limitations.

In-vivo biomechanical research encompasses any study which seeks to answer a question through the use of live subjects. Many researchers have used this model to assess normal shoulder biomechanics, pathological changes, and repaired function. These investigations have used an array of technologies including goniometers and potentiometers to measure static osseous rotations (Doody, Freedman, & Waterland, 1970; Ludewig et al., 1996; Van der Helm & Pronk, 1995), single plane radiography to assess 2D static joint kinematics (Chopp, O'Neill, Hurley, & Dickerson, 2010; Keener, Wei, Kim, Steger-May, & Yamaguchi, 2009; Mercer et al., 2011; Poppen & Walker, 1976), optical and electromagnetic tracking devices to measure continuous joint kinematics (Harryman et al., 1990; Karduna et al., 1996; McClure et al., 2001; McClure et al., 2006; McQuade & Smidt, 1998), magnetic resonance imaging (MRI) to assess 2D and 3D joint mechanics (Graichen et al., 2000; Graichen et al., 1998; Graichen et al., 2005; Pierrart et al., 2013; Sahara et al., 2007), and bi-plane radiography to continuously assess 3D joint kinematics and contact mechanics (Bey, Zauel, Brock, & Tashman, 2006; Bey et al., 2007; Bey et al., 2010; Giphart, van der Meijden, Olivier, & Millett, 2012; Matsuki et al., 2010). This type of study is the most externally valid as data can be measured under completely accurate environmental and loading conditions on a subject group that can be chosen to match a desired populations of interest. However, *in-vivo* research is limited in its ability to assess competing treatment options due to ethical constraints and to achieve high repeatability

with respect to specific parameters of interest such as injury type, size, position, etc. and repair technique.

The *in-silico* approach to biomechanical research is the newest, and involves the development of computer models and computational methods to replicate the anatomy of the joint and simulate the loading and motion it experiences. *In-silico* modelling can include Finite Element Analysis (FEA) techniques which consider material properties, applied forces, and contact mechanics to assess the stresses and deformation in a system (Harrysson, Hosni, & Nayfeh, 2007; Sharma, Debski, McMahon, & Robertson, 2010; Terrier, Brighenti, Pioletti, & Farron, 2012; Terrier, Buchler, & Farron, 2005; Terrier, Buchler, & Farron, 2006; Terrier, Ramondetti, Merlini, Pioletti, & Farron, 2010; Virani et al., 2008; Walia, Miniaci, Jones, & Fening, 2013; Yongpravat et al., 2013; Zhang et al., 2013), rigid body dynamic musculoskeletal modelling which accounts for bony anatomy as well as muscle lines of action and loading in order to evaluate joint kinetics and kinematics (Bolsterlee, Veeger, & Chadwick, 2013; Nikooyan et al., 2010; Veeger, Van der Helm, Van der Woude, Pronk, & Rozendal, 1991), and statistical shape modelling which can evaluate osseous anatomy across a population in order to better understand implant design considerations (Blanc, Syrkina, & Székely, 2009; Querol, Büchler, Rueckert, Nolte, & Ballester, 2006; Yang, Rueckert, & Bull, 2008). These types of investigations have proven useful as they are highly adaptable, and, compared to *in-vivo* or *in-vitro* studies, allow many more conditions to be tested and compared, and allow variables to be assessed in a more systematic manner. However, in many cases, these approaches have lower external validity in comparison to *in-vivo* and *in-vitro* research, primarily due to the assumptions which must be made in order for the model to approximate the living condition. Specifically, whereas *in-vivo* research allows testing in the native environment and *in-vitro* research (described subsequently) uses the native anatomy but must replicate the environment, *in-silico* research must replicate both of these factors.

In-vitro research methods make use of samples drawn from the native anatomy of living or deceased donors and can range from small tissue samples to whole joint/limb cadaveric

specimens. The testing systems used with these methods vary in complexity, from very simple systems used to replicate a specific parameter on a discrete tissue sample to very complex systems which aim to replicate the *in-vivo* environment experienced by a joint as much as possible. *In-vitro* investigations of the shoulder regularly involve the use of benchtop testing apparatuses which apply prescribed loads or displacements to a sample ranging from a single tissue band to a full joint; however, muscle loading and joint motion are not considered (Panossian et al., 2005; Sano et al., 1997). More complex devices use full joint specimens and may or may not involve muscle loading but do quantify overall joint motion and stability (Itoi et al., 1993, Itoi, Newman et al., 1994; McMahon, Chow, Sciaroni, Yang, & Lee, 2003). The most complex testing protocols use muscle forces in order to produce joint motion and thus they allow the most accurate replication of *in-vivo* joint function (Debski et al., 1995; Kedgley et al., 2007; Wuelker et al., 1994). *In-vitro* investigations integrate the strengths of both *in-vivo* and *in-silico* research by using the native anatomy as used in *in-vivo* testing, while also enabling the evaluation of a range of testing conditions as assessed using *in-silico* methods. The limitations of this technique, however, lie in its inability to truly replicate the *in-vivo* environment of the shoulder and in the potential for the specimen's properties to change during testing.

The study of shoulder biomechanics through *in-vitro* testing requires the use of a wide array of technologies and processes in order to acquire meaningful data. This is especially the case for whole joint experimental protocols, where the environmental conditions to be replicated are particularly complex. In these cases, relevant biomechanical outcomes commonly require the measurement of joint motion and various types of loading data, and the subsequent manipulation of these data streams into a physiologically meaningful form. To replicate the desired environment and acquire these data streams, it is necessary to implement relevant technologies. These include actuation methods such as pneumatic and/or servomotor devices to produce loading and motion, a spatial tracking system to record position data for real-time and *post-hoc* use, and application specific load sensors to assess the relevant kinetics. In order for these data to be meaningful, it is also necessary to implement coordinate transformations of both bone and testing components, to

construct bone fixed coordinate systems from surface digitizations, and to perform a rotation sequence analysis such as Euler Angle decomposition.

1.6.1 The Technologies of *In-Vitro* Biomechanical Research

1.6.1.1 Actuation Methods

Replication of the loading environment represents the most important goal when designing a whole joint experimental protocol, and can be achieved through the selection of appropriate actuation technologies. The primary means of actuation used for *in-vitro* biomechanical experimentation are pneumatic cylinders and computer controlled DC servo-motors. These two technologies are equally valuable in applying loads to cadaveric specimens; however, each exhibits unique strengths and limitations which lend them to different applications.

Pneumatic actuation is inexpensive, does not require large amounts of equipment, and is simple to implement, and thus, has traditionally been the more common means for applying loads in the field of *in-vitro* biomechanics (Dunning, Duck, King, & Johnson, 2001; Kedgley et al., 2007). A typical pneumatic system is composed of an air compress to supply a constant pressure source, a computer controlled proportional pressure controller, and a pneumatic cylinder to apply the force. This type of actuation is always dictated by the applied load and cannot easily be controlled with respect to variables such as position or velocity of the piston. This limitation, therefore, precludes pneumatic actuators from being used in *in-vitro* applications where its role would be to maintain a structure at a given position or to move it at a desired velocity. Instead, pneumatics are most often used to apply constant loads or loads which vary in a predefined way. Additionally, in the context of applying forces to a muscle group, pneumatics can be limited by the length of their stroke and in some cases this precludes their use with muscles which experience large amounts of shortening during motion. A final limitation of pneumatics is the compressibility of the working fluid (air) which causes the performance of the actuator to suffer as higher, rapidly changing pressure levels are required.

In some situations, one or more of these limitations may preclude the use of pneumatics. In such cases, DC servo-motor driven actuators are a useful alternative method for the application of force and motion in a whole joint experimental protocol (Debski et al., 1995; Ferreira, Johnson, & King, 2010). In comparison to a pneumatic system, a DC servo-motor system has less required infrastructure; however, the control of this type of actuator and integration of it into an experimental computer control system can be far more challenging. This type of system is composed of a DC electrical power supply, a DC servo-motor and appropriate gearhead, a load/motion application mechanism, and a proprietary coding language to send commands to the motor. Load and position sensing abilities can be implemented and, unlike with pneumatics, this additional feedback can be used to provide improved control of the system because the function of the motor can be dictated based on position, speed and acceleration. As well, a motor and pulley configuration is not limited by a maximum stroke and thus can apply loads to any muscle group.

1.6.1.2 Spatial Tracking Methods

Spatial tracking is an integral component to *in-vitro* biomechanical investigations both as an outcome variable and process variable during testing. Tracking of the osseous structures and testing components – for instance, joint replacement components – can be achieved through a number of means including direct mechanical measurement, indirect medical imaging, and a variety of tracking technologies which use physical phenomena (*i.e.* sound, light, magnetic fields, accelerations, etc.) to record the poses of manually placed fiducial markers.

The first tools to be used in biomechanical investigations were direct mechanical measurement tools, such as manual goniometers, which linked to two structures of interest, allowing the measurement of joint rotation in static poses. This progressed to the use of electrical resistance transducers which provided greater precision and reliability, and permitted motion, rather than static poses, to be recorded (Doody et al., 1970). These systems eventually became capable of measuring all six degrees of freedom between two

mechanically linked structures (Siegler, Lapointe, Nobilinit, & Berman, 1996) but were exceedingly complex and were likely to affect, rather than just measure, joint function. An additional limitation of these systems is the difficulty associated with precisely aligning the linkage with the desired anatomical axes. Failure to achieve this precise alignment would result in misleading rotational crosstalk between the three DOF and as such, the use of these mechanical linkages has decreased.

Medical imaging, such as plane radiographs, fluoroscopy, radiostereometric analysis (RSA), 3D model based biplane x-ray, and magnetic resonance imaging can also be used to assess joint kinematics during biomechanical investigations. Plane radiography has been used for many years to assess the 2D translations and rotations of joints and, in some cases, to infer knowledge of the 3D pose (Poppen & Walker, 1976). Fluoroscopy has been used similarly but with the added advantage of allowing the assessment of motion. RSA has been used to increase the accuracy of both of these techniques through the placement of clearly defined radiopaque beads. More recently, 3D model-based (or beadless) biplane x-ray (Bey et al., 2006) and MRI (Graichen et al., 2000) techniques have allowed the assessment of 3D translation and rotations of a joint, but MRI is frequently limited by its low acquisition rate. Despite the accuracy and non-invasive nature of these last two techniques, the associated costs, size, and radiation exposure (during biplane x-ray, for the experimenter) have reduced their widespread application.

Six DOF tracking technologies, which use specimen affixed markers that transmit or receive a signal from a central unit, have been develop using a number of concepts from physics. The common element in each of these systems is the use of three independent sensors rigid relative to one another which enable all six DOF to be calculated.

Electromagnetic tracking is a widely used technique that uses a central transmitter and a set of receivers attached to relevant anatomy and testing components. By using these three measures for each of the three transmitter coils (nine total measurements) it is possible to determine the 3D position and orientation of the receivers. Electromagnetic systems can achieve accuracies of ±0.5mm and ±0.5° which are sufficient for use in most biomechanical investigations. Despite this level of accuracy, the use of these systems is

somewhat limited by their sensing range (2 meters) and the inability to use any metal in the design of the experiment.

Optical tracking, which measures the position of optical markers using infrared light, is another widely used technique. Similar to electromagnetic tracking, optical tracking uses a central camera with multiple light sensors as well as a minimum of three markers on each bone that either act as light reflectors or sources. In one case, light is emitted from a central source and reflected by the bone markers, with the light sensors then recording the light reflected by each maker simultaneously. In the other, each bone marker emits light when signaled to do so, and the light sensors record simultaneously. In each of these scenarios, the accuracy of the recordings is heavily dependent on the ability of the recorded light in each camera to uniquely define each rigid body. When properly defined, the accuracy of these systems can reach as high as 0.1mm and 0.1°, which is the highest of any current tracking technique. Although this technology does permit the use of metal in the experimental protocol – which is particularly useful in the setting of orthopaedic research involving implants – the requirement for continuous line of sight in these systems can be limiting. Light emitting systems such as the Optotrak Certus (Northern Digital Inc., Waterloo, ON) are especially effective at overcoming this issue because the sequence of marker firing is predefined and thus redundant marker sets are permissible and do not require an asymmetric marker structure to be accurately tracked.

More recently, the use of systems which combine the data provided by gyroscopes, accelerometers, and magnetometers to determine position and orientation of a body has become more prevalent. These systems, however, have a number of limitations in comparison to those discussed above. First, the determination of a body's position is dependent on the double integration of accelerometer readings to obtain translations. Previous research has shown that error in these acceleration measurements rapidly leads to unreliable and inaccurate position values following integration (Giansanti, Macellari, Maccioni, & Cappozzo, 2003). Second, the readings from the magnetometers can experience interference from magnetic fields in the testing environment which will also affect accuracy. Third, orientation data which is produced through a combination of the

three discrete sensors currently has an accuracy of at best one order of magnitude poorer than the systems discussed above. As a result of these limitations, these systems are more commonly used in studies interested in general motion pathways and/or recording of motion for animation purposes and not in cases where measurement of precise joint mechanics are required.

1.6.1.3 Load Sensing

In addition to tracking the motion of the joint, it is often important to monitor the externally applied loads and loads within the joint itself. The technique used to measure these loads depends heavily on the application at hand and the associated constraints, but these include pressure sensitive films, application specific custom strain gauge based load sensors, and commercially available load cells with varying DOF. For this thesis, the most relevant technique is the use of commercially available load cells and thus this is the only technology to be discussed below.

Commercially available load cells are the most widely used tool for measuring applied and internal loads; they are produced in an array of sizes and designs, with varying load limits, and the capability of measuring one to six DOF. Single DOF – or uni-axial – load cells are frequently used in the measurement of applied muscle loads, and two DOF – or thrust-torque – load cells can measure the applied force and rotational moment applied to a limb. Six DOF load cells provide a full description of the loading environment and thus are the most useful in complex loading environments such as between the articulating surfaces of a joint; however, these sensors are typically larger than lower DOF systems and can be quite expensive.

Unlike simpler load cells, six DOF sensors report their load measurements with respect to a well-defined coordinate system that typically coincides with the center of its ‘tool plate,’ and thus, can be replicated through the identification of landmarks on the load cell (Figure 1.11). With this coordinate system defined, it is possible to report the three components of force acting on the sensor relative to their respective axes, and to determine the moments acting on the sensor about each axis. Load data acquired using

this method are of great value, as they can be transformed into any physiologically meaningful coordinate system, thus increasing interpretability and decreasing the need to precisely position the load cell.

1.6.2 The Processes of *In-Vitro* Biomechanical Research

1.6.2.1 Coordinate Descriptions & Transformations

A coordinate system is composed of three mutually orthogonal vectors of unit magnitude which allow the description of a body's 3D position and orientation. These coordinate systems are classified either as global – typically permanently fixed –, or local – specific to the object and free to move. By using a combination of global and local coordinate systems, it is possible to describe any object's coordinate system relative to another's. These coordinate systems are constructed by selecting two vectors on the object of interest that are oriented in a useful/meaningful way, such as along a long axis or in an important plane. The cross product of these two vectors can then be calculated in order to determine a mutually orthogonal third vector. As the coordinate system must contain three mutual orthogonal vectors, only one of the two initial vectors can be retained. Once this choice is made, the chosen vector and the resultant of the cross product can be crossed to create a final vector. Normalization of these three vectors produces an orthonormal coordinate system which enables the description of the 3D relative displacements of an object; however, in order to define the object's absolute position, it is necessary to define an origin. This origin is typically (0, 0, 0) for a global coordinate system but can be any arbitrary point. To simplify the description and transformation of an object's motion, a matrix descriptor known as a Transformation Matrix is typically used (Equation 1.1A). This format allows the easy calculation of a point's 3D location in space relative to the new coordinate system. In the case of a rigid body with a defined coordinate system, this format also allows the description of this rigid body's 3D orientation with respect to the coordinate system using a rotation about each axis. A rigid body is fully defined in all six degrees of freedom when its 3D translational and 3D rotational descriptions are combined. Further, it is possible to multiply a chain of these

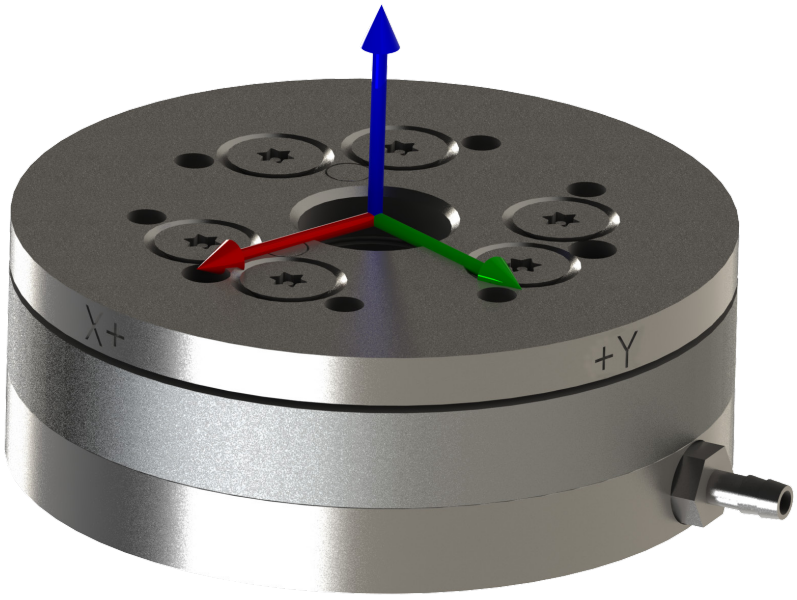

Figure 1.11: Six DOF load cell coordinate system.
The coordinate system shown is coincident with the sensing system of the load cell and can be accurately reproduced using landmarks on the tool (top) plate. Shown is a Mini45 (ATI-IA, Apex, NC) six DOF load cell which has a 45mm diameter and 15.7mm height.

matrices, transforming the description of an object's six DOF pose from one coordinate system to another (Equation 1.1B).

$$ {}^{B}_{A}T = \begin{bmatrix} {}^{B}_{A}\hat{X} & {}^{B}_{A}\hat{Y} & {}^{B}_{A}\hat{Z} & {}^{B}\hat{P}_{A} \\ 0 & 0 & 0 & 1 \end{bmatrix} = \begin{bmatrix} {}^{B_x}r_{A_x} & {}^{B_x}r_{A_y} & {}^{B_x}r_{A_z} & {}^{B_x}p_A \\ {}^{B_y}r_{A_x} & {}^{B_y}r_{A_y} & {}^{B_y}r_{A_z} & {}^{B_y}p_A \\ {}^{B_z}r_{A_x} & {}^{B_z}r_{A_y} & {}^{B_z}r_{A_z} & {}^{B_z}p_A \\ 0 & 0 & 0 & 1 \end{bmatrix} \quad \text{Eq. 1.1A} $$

$$ {}^{ScapCS}_{HumCS}T = {}^{ScapCS}_{\cancel{SMarker}}T * {}^{\cancel{SMarker}}_{\cancel{Camera}}T * {}^{\cancel{Camera}}_{\cancel{HMarker}}T * {}^{\cancel{HMarker}}_{HumCS}T \quad \text{Eq. 1.1B} $$

Equation 1.1: Transformation matrix definition and chain multiplication rule.
(A) Middle term indicates column vectors which define transformation matrix where X, Y, Z are the axes of A projected onto the axes of B, and P is the position of A with respect to B. Right term shows individual elements of transformation where subscript x, y, z correspond to the axes in question. (B) Example of common use of chain rule to transform humeral and scapular coordinate systems known with respect to optical tracking markers, to be with respect to each other. Note that strikethroughs indicate cancellation of corresponding coordinate systems.

1.6.2.2 Local Bone Coordinate Systems

In order for the six DOF descriptors produced from coordinate transformations to be meaningful and useful in the context of biomechanical research, it is necessary to define Local Bone Fixed coordinate systems for all bones of interest (Figure 1.12). These coordinate systems are defined relative to a rigidly fixed tracking marker using the bone's anatomy and/or functionality, and, once created, are constant irrespective of changes in time, position, or orientation of the bone.

Bone fixed coordinate systems are created using the process outlined in the previous section, and the two initial vectors are obtained by measuring the location of at least three points of physiological importance. For many bones, form reflects function, and thus osseous landmarks can be chosen to define these vectors. The most common method for measuring these points is through point digitizations, where a calibrated pointer (or stylus) is used to localize an anatomical feature while a tracker records the location of the stylus tip relative to the bone affixed marker. When the point of interest is not easily identified on the bone (unlike, for instance, the apex of the epicondyles in the elbow), multiple points may be recorded, and their location data can be mathematically analyzed

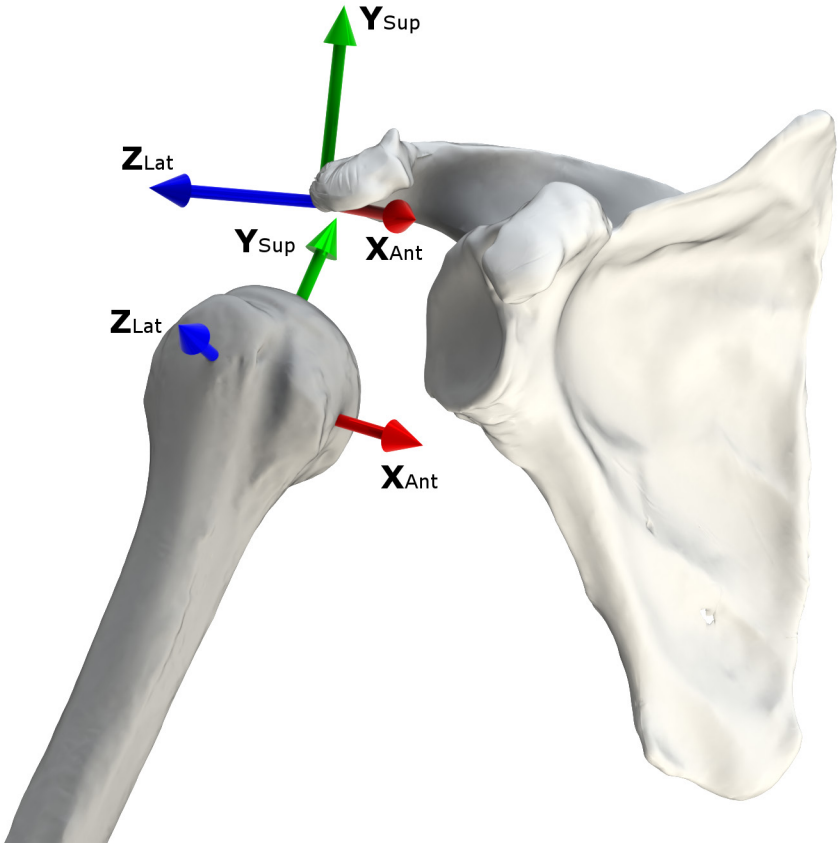

Figure 1.12: Local Bone Fixed coordinate systems in the shoulder complex.
A right shoulder is shown here illustrating the scapular and humeral coordinate systems used in this thesis. 'Ant', 'Sup', 'Lat' correspond to the anterior, superior, and lateral directions. Note that the red X-axes for both bones point posterior on a left shoulder.

to define a single point (for instance, a sequence of points with a circle fit algorithm can define a geometric center).

Point digitizations are a simple and accurate method for creating bone fixed coordinate systems but in some joints, the structure of the osseous anatomy is not necessarily the optimal physiologic descriptor of joint motion. Instead, the most physiologically meaningful coordinate system is defined relative to a functional joint center (*e.g.* center of the hip or shoulder) or natural axis of rotation (*e.g.* long axis of the forearm). In these cases, the point or axis is defined by recording the motion of the marker fixed to the bone while it is moved through a set of physiologically meaningful motions. Various methods exist to analyse these data but the most common ones use the motion descriptor known as the Screw Displacement Axis (SDA). SDAs describe the instantaneous axis of rotation experienced by a body and thus, in a joint with a well-defined axis of motion, the average of a series of SDAs across a motion can be used to define the physiologic axis (Ferreira, King, & Johnson, 2011). Conversely, in joints with varying rotation axes but a common rotation center, the construction of a coordinate system can make use of the point where all SDAs are closest to intersecting (Woltring, 1990).

1.6.2.3 Rotation Sequence Decomposition

Through the use of bone fixed coordinate systems and coordinate transformations, it is possible to describe the orientation of one bone with respect to another using a nine element rotation matrix. This matrix is difficult to interpret in a precise physiological manner, so rotation sequence decomposition methods have been developed. The most widely used decomposition in biomechanics is the Euler angle sequence. Using this method, the 3D orientation of an object is defined using a rotation about each axis in a predefined order, and the calculation of each rotation is based on the preceding orientation of the object (Figure 1.13).

Differing sequences of rotation about the three axes will yield different magnitudes of rotation for each axis and thus consistent standards are required in order to permit comparison of results between investigators. It is also important to choose a sequence

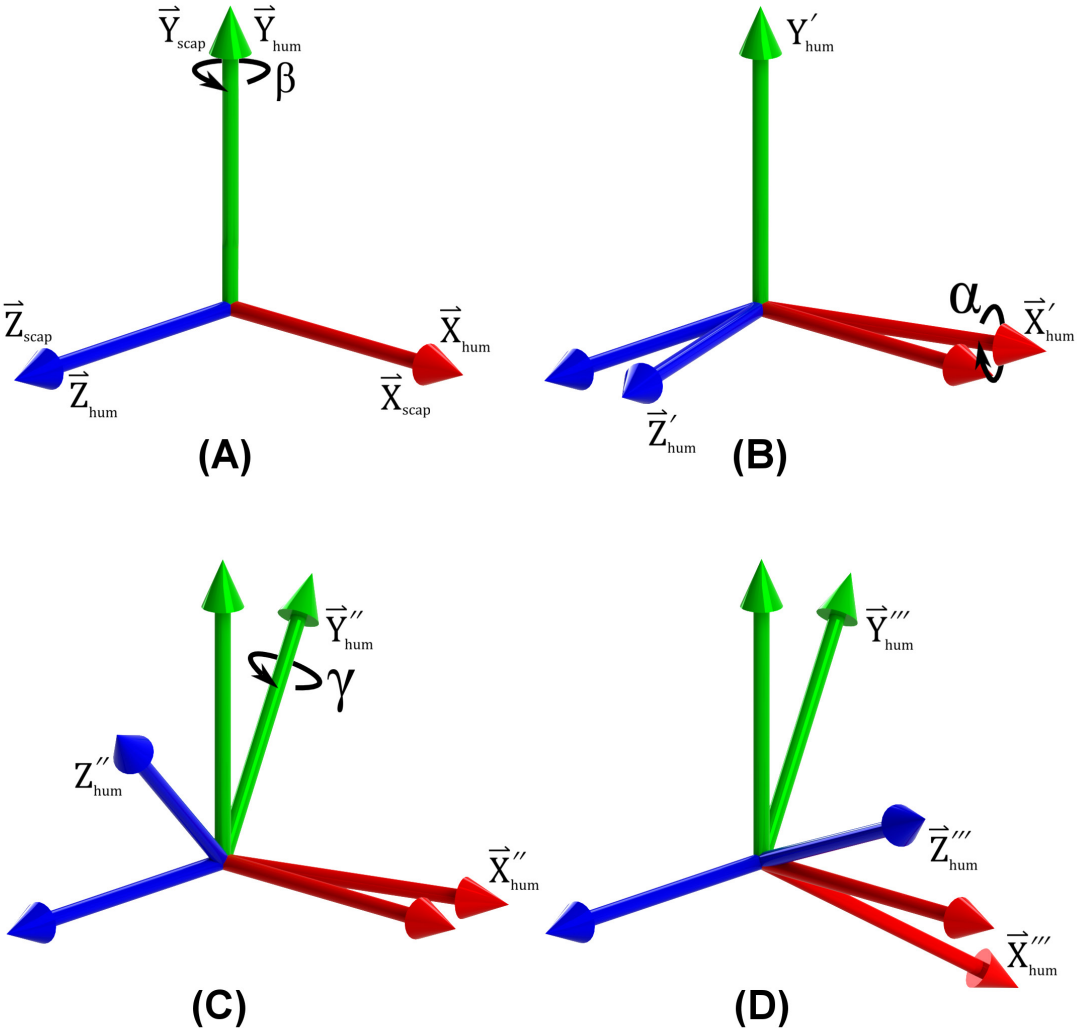

Figure 1.13: Y-X-Y Euler angle decomposition method.
This figure demonstrates how Euler angles are used to describe orientation and how this description is sequence dependent. (A) Rotation about the coincident Y axes of the humeral and scapular coordinate systems; (B) rotation about the newly oriented humeral X axis; (C) rotation about the humeral Y axis following rotation about the new X axis; (D) final orientation of humeral coordinate system.

which results in the magnitude of rotation most consistent with the physiological case. In the case of scapulothoracic motion, Karduna, McClure, and Michener (2000) have shown that choice of rotation sequence can alter kinematics outcomes by as much as 50° and in some cases result in different directions of rotation (*e.g.* posterior rotation for one sequence and anterior for another). The most widely used sequence in biomechanics is rotation about Z→Y→X because it permits the description of a rotation about each axis, which corresponds well to the physical situation in the body. However, other sequences of the three axes are permissible, as are rotation sequences that incorporate rotation about the same axis in the first and third step of the process such as Y→X→Y. Sequences with repeated rotations are commonly used in joints with a large range of motion where rotation about one axis can produce motion of different physiologic meaning when an intermediate rotation occurs. For example, a Y→X→Y rotation sequence in the shoulder – where Y is rotation about the humerus' long axis and X is rotation about the humerus' anterior axis – is meaningful because the first Y rotation defines the plane in which the second rotation (abduction of the humerus) occurs, while the second Y rotation defines the humerus' degree of axial rotation.

A further consideration which influences the choice of sequence and use of a repeated sequence is the possibility of encountering "gimbal lock" – a special case whereby the first and third rotations become mathematically undefined as a result of the magnitude of the second rotation. In non-repeating rotation sequences this singularity occurs when the second rotation is equal to 90°. In this case, it is mathematically unclear as to whether the first or third rotation caused the calculated motion. In the case of a repeated sequence, this singularity occurs at 0° and 180° because these are the rotations in which the first and third axes align. Selection of an optimal sequence should therefore be based on pre-existing biomechanical understanding of a joint's function and the joint positions which are of clinical interest. Ideally, to avoid gimbal lock, a non-repeating sequence should be chosen in which the second rotation never reaches 90°. However, 90° of shoulder abduction is clinically meaningful, thus a repeating sequence is commonly used.

Unfortunately, this makes interpretation of results with the arm in 0° of abduction difficult. Grood and Suntay (1983) proposed a method to decompose joint rotations while avoiding gimbal lock. Amadi and Bull (2010) adapted this method for use in the shoulder; however, this has not been used experimentally. In this method, basic knowledge about the primary rotation being analyzed enables the rotations to be determined using a stepwise decomposition method.

1.7 *In-Vitro* Shoulder Simulators

Dowson and Jobbins (1988) defined a simulator as "any device or system that simulates specific conditions or the characteristics of a real process for the purpose of research or operator training" (p.111). Applied to *in-vitro* biomechanical research, a simulator is a system which replicates the physiologic conditions, such as loading and motion, experienced by a joint complex and the environment it functions in. Previous investigators have employed *in-vitro* simulators using full cadaveric shoulder specimens as a means to increase the efficacy and accuracy of their biomechanical research; however, their level of accuracy and the types of testing employed have varied widely.

These simulators can be classified as (1) static, or (2) 'dynamic'[1], where dynamic can be sub-classified into passive or active motion simulators. The majority of research has focused on the assessment of static biomechanical outcomes, and passive, investigator driven functional assessments. A far smaller group of simulators have addressed the replication of *in-vivo* active muscle driven motion. Each of these methods represents an important opportunity for broadening our understanding of basic shoulder biomechanics and the biomechanics of clinically relevant questions related to orthopaedic injury, dysfunction, and reconstruction.

[1] where this simply denotes motion and not the traditional definition of 'dynamic'

1.7.1 Static Shoulder Simulators

The purpose of a static joint simulator is to replicate the conditions of a joint in one discrete joint configuration. As a result, these systems cannot assess how outcomes change as the joint configuration changes, but are well suited to describing discrete biomechanical variables which exist at a given joint pose such as muscle lines of action or moment arms. These systems have been widely used in shoulder research (Ackland et al., 2008; Alexander et al., 2013; Karduna et al., 1996; Kelkar et al., 2001; L. J. Soslowsky et al., 1992) and typically employ loading of appropriate muscle groups or direct loading of the bones in order to articulate the joint.

1.7.2 Dynamic Shoulder Simulators

Dynamic simulators differ from static simulators in that they seek to replicate the motion of the joint in addition to its loading and environmental conditions. Thus, these simulators are capable of evaluating outcome variables continuously across a given motion. Previous simulators have replicated this motion both passively and actively as outlined below.

1.7.2.1 Passive Shoulder Motion Simulators

Passive simulation of the shoulder involves the assessment of the joint's motion and function through a series of tests performed by the investigator. These tests are carried out using a minimally dissected shoulder joint complex on a simulator designed to replicate a predefined set of environmental conditions drawn from the *in-vivo* state. Passive assessments commonly involve the evaluation of the joint's ranges of motion, articular contact mechanics, and stability. Although not as physiologically accurate as the active motion simulation discussed in the following section, passive simulation is a very important part of fully assessing the shoulder as it enables investigators to perform tests similar to those used clinically in the evaluation of this joint.

Passive *in-vitro* shoulder simulators expanded beyond simple bench top studies in the early 1990s when investigators instrumented shoulder specimens with motion tracking

and load cell hardware (Harryman et al., 1990; Itoi, Motzkin, Morrey, & An, 1994) which permitted the recording of loads and joint kinematics during passive motion. These early devices, however, relied entirely on the experimenter's ability to consistently manipulate the humerus relative to the scapula and thus resulted in large variability in their results. The following years saw the emergence of systems that enabled greater control over the load applied to individual degrees of freedom during the monitoring of joint translations (Warner, Deng, Warren, & Torzilli, 1992); however, these did not accurately model physiologic bone configurations and did not dynamically load the muscles of the shoulder complex. Further developments by Itoi et al. (1994) resulted in a simulator capable of properly orienting the constituent bones of the shoulder relative to gravity while also loading relevant rotator cuff muscle groups in physiologic patterns. More recently, these types of systems have allowed an increasing number of muscle groups to be loaded and a greater range of outcome variables to be assessed (Ackland & Pandy, 2011; D. C. Ackland et al., 2008; Alexander et al., 2013; Yu, McGarry, Lee, Duong, & Lee, 2005). Subsequently, other groups began to acquire the ability to perform objective assessments of joint motion by recording loads while pneumatic and robotic systems moved the shoulder through predefined motion pathways (Debski, Wong, Woo, Sakane, Fu, & Warner, 1999a; McMahon et al., 2003). Despite the widespread development and use of these simulators, no one simulator has been developed which possesses all of the key design features required to improve the accuracy of the replicated environment (*i.e.* simulated muscle loading, scapular motion, etc…) and permit objective evaluations of physiologically meaningful outcome variables (*i.e.* develop a mechanism to permit isolation of individual DOF, implement a continuous tracking system, etc…).

1.7.2.2 Active Shoulder Motion Simulators

Although passive shoulder motion simulators can provide important information regarding joint function and stability, the external validity of these results are limited because the motions are not driven by muscle loading as is the case *in-vivo*. Therefore, a number of groups have focused on the development of active motion simulators which rely entirely on muscle loading to produce glenohumeral motion. Kedgley et al. (2007)

have additionally shown that the implementation of a simulator which uses continually variable muscle forces to drive shoulder motion can produce motions with higher repeatability than those performed passively. This higher repeatability in turn increases the statistical power of the findings and their physiologic validity, because the kinetics of the joint are more closely replicated.

Active motion can be produced through one of three control methods: (1) muscle load control, (2) position control, (3) computational model driven muscle loading. Muscle load control has been the most widely implemented technique, whereby the muscle primarily responsible for the motion of interest, termed the 'prime mover,' is used to define a set of muscle loading ratios. Despite its widespread use, muscle load control is of limited value as it has difficulty producing slow, smooth, and repeatable motion (Dunning et al., 2001). Position control has the potential to produce much more repeatable motion than load control, but traditionally has produced loads that are less representative of the true *in-vivo* loading environment (Dunning et al., 2001). At the time of writing, there are no reports in the literature of the third method being implemented in a manner which can produce smooth motion. This may relate to the computational complexity of implementing a system that can use a computational model while also adjusting appropriately given real time feedback.

Cain et al. and Soslowsky et al. were the first to develop active simulators; however, they used these to place the joint in discrete positions and record outcomes rather than produce continuous motions (Cain, Mutschler, Fu, & Lee, 1987; L. Soslowsky et al., 1992). Debski et al. (1995) and Wuelker et al. (1994) concurrently developed the first simulators capable of achieving dynamic joint motions by using an open loop muscle load controller in which the muscle length of the 'prime mover' was shortened at a constant rate, and the secondary muscle loads were apportioned based on this muscle's measured load. These systems, however, did not adjust scapular orientation, attempt to maintain a constant rotational velocity, or, in the case of Desbki et al., use physiologic muscle loading ratios, all of which affected the accuracy and repeatability of the reported kinematic outcomes relative to the *in-vivo* condition. Other simulators have used physiologically accurate

muscle loading ratios but have continued to depend on a constant prime mover velocity to achieve repeatable motions (Halder, Zhao et al., 2001; Halder et al., 2001; Malicky, Soslowsky, Blasier, & Shyr, 1996; McMahon et al., 1995).

Muscle loading ratios were initially chosen as constant values across an entire motion, thus neglecting variations observed in *in-vivo* electromyographic (EMG) studies; however, Kedgley et al. (2007) demonstrated that the use of continuously varying loading ratios produces a more physiologically accurate loading model. Despite these developments, these simulators continue to depend on muscle loading ratios drawn from the literature and as a result, the ability of these systems to control all three rotational DOF of the shoulder is limited, since population average ratios are unlikely to produce exactly the desired motion in any given specimen. As well, the data used to construct muscle loading ratios is limited to a very small set of motions which have been investigated *in-vivo* and thus these systems are somewhat limited to simulating these motions. There remains to be a simulator described in the literature which uses motion control through real time kinematic feedback to achieve improved repeatability and control of all three of the shoulder's rotations.

1.8 Rationale

In-vitro experimentation is a critical tool in increasing our understanding of shoulder kinematics, function, and stability in healthy and dysfunctional joint conditions. Additionally, this testing can elucidate the effects of various treatment options prior to their application in patients. Moreover, while *in-vivo* investigations cannot directly compare different joint conditions and repair techniques within individual subjects, and thus require the recruitment of large patient populations, *in-vitro* investigations have the statistical advantage of using within subject methods of comparison of joint conditions. Simulators that use complete shoulder complexes are the most efficacious tools for performing *in-vitro* assessments; however, to date, the development of these simulators has lagged behind those of other joints, especially in the area of active motion simulation. Thus, our understanding of shoulder biomechanics and the effects of various

repairs/reconstructions and implant designs remains limited, and in some cases potentially incorrect.

Our understanding of the biomechanics of shoulder function, stability and kinematics can be improved through the use of static, passive and active simulators; however, each of these types of systems remains underdeveloped in their own way. The ability to concurrently assess these biomechanical variables using a system capable of all three types of simulation would greatly enhance the power and interpretability of the findings by producing complementary data sets. As well, by combining these testing methods within one system, it will be possible to understand and weigh a joint condition's effects on the shoulder's overall biomechanics. Developments in each of these simulation areas are presented in this work.

1.9 Objectives and Hypotheses

The overall goal of this dissertation was to develop a shoulder simulator capable of static, passive, and active simulation and to investigate areas of basic biomechanical interest and clinically relevant questions.

Specific Objectives:

1. To further develop an existing *in-vitro* shoulder simulator such that it could:
    a. Accurately replicate the scapular rotations observed *in-vivo* that are most relevant to proper shoulder function and stability.
    b. Load the traditionally simulated muscle groups along physiologically accurate lines of action while accounting for scapular motion produced by developments in Objective 1a.
    c. Accurately load the multi-articular short and long heads of the biceps.
2. To develop a static/passive glenohumeral joint positioning and constraint mechanism that allows the joint to be repeatably positioned throughout its range of motion, and locked globally while leaving the articular kinematics unaffected. This mechanism must also enable individual DOF to be manipulated. As well, to

develop a load sensing device for the objective quantification of passive outcome variables of interest such as range of motion.

3. To assess the static and passive effects of the short head of the biceps and coracobrachialis on shoulder biomechanics.
4. To compare the static and passive effects of two competing coracoid transfer reconstructions used to treat anterior glenoid bone loss.
5. To develop a motion based controller that would allow the production of unconstrained active glenohumeral rotation entirely through muscle loading, and that could effectively control all three rotational DOF.
6. To assess the static, passive, and active biomechanics of the reverse total shoulder replacement across a range of component configurations encompassing both commercially available and previously unstudied implant arrangements.

Hypotheses:

1. The simulator will allow the repeatable assessment of static and passive shoulder biomechanics.
2. The simulator will enable clarification of the biomechanical role of elements of shoulder anatomy on joint stabilization and passive motion.
3. The simulator will enable the assessment of the effects of clinical disorders and treatment options on joint stabilization and passive motion.
4. The simulator, when equipped with the new motion based controller, will increase the repeatability of experimental simulations of glenohumeral motion in comparison to previous simulators, and will also provide control over the two rotational DOF not involved in the primary simulated motion.
5. The static, passive, and active *in-vitro* simulation capabilities of the simulator will enable a previously unexplored range of outcome variables to be assessed in order to provide more complete evaluations of biomechanical and clinical questions

1.10 Thesis Overview

Chapter 2 describes the development of the static and passive *in-vitro* simulator as described in Objectives 1 and 2 of Section 1.9. Chapter 3 describes the application of these developments to evaluate the basic biomechanical effect of the short head of the biceps on shoulder function. Chapter 4 addresses a clinical question of current interest in the orthopaedic community by comparing two competing coracoid transfer procedures on the basis of their static and passive effects on the shoulder. Chapter 5 describes the development and validation of the active motion functionality outlined in Objective 5 of Section 1.9. Chapter 6 describes how this new control system was used, along with the developments in the previous chapters, to assess a novel set of reverse total shoulder implant configurations. Chapter 7 provides a discussion of this dissertation's work, and provides conclusions and future directions for this research.

1.11 References

Ackland, D. C., & Pandy, M. G. (2011). Moment arms of the shoulder muscles during axial rotation. *Journal of Orthopaedic Research, 29*(5), 658-667.

Ackland, D. C., Pak, P., Richardson, M., & Pandy, M. G. (2008). Moment arms of the muscles crossing the anatomical shoulder. *Journal of Anatomy, 213*(4), 383-390. doi:10.1111/j.1469-7580.2008.00965.x

Alexander, S., Southgate, D. F., Bull, A. M., & Wallace, A. L. (2013). The role of negative intraarticular pressure and the long head of biceps tendon on passive stability of the glenohumeral joint. *Journal of Shoulder and Elbow Surgery / American Shoulder and Elbow Surgeons ...[Et Al.], 22*(1), 94-101. doi:10.1016/j.jse.2012.01.007; 10.1016/j.jse.2012.01.007

Amadi, H. O., & Bull, A. M. (2010). A motion-decomposition approach to address gimbal lock in the 3-cylinder open chain mechanism description of a joint coordinate system at the glenohumeral joint. *Journal of Biomechanics, 43*(16), 3232-3236. doi:10.1016/j.jbiomech.2010.07.034

An, K. N., Browne, A. O., Korinek, S., Tanaka, S., & Morrey, B. F. (1991). Three-dimensional kinematics of glenohumeral elevation. *Journal of Orthopaedic Research : Official Publication of the Orthopaedic Research Society, 9*(1), 143-149. doi:10.1002/jor.1100090117

Apreleva, M., Hasselman, C., Debski, R., Fu, F., Woo, S. L., & Warner, J. (1998). A dynamic analysis of glenohumeral motion after simulated capsulolabral injury. A cadaver model*. *The Journal of Bone & Joint Surgery, 80*(4), 474-480.

Barnes, C. J., Van Steyn, S. J., & Fischer, R. A. (2001). The effects of age, sex, and shoulder dominance on range of motion of the shoulder. *Journal of Shoulder and Elbow Surgery, 10*(3), 242-246.

Bey, M. J., Brock, S. K., Beierwaltes, W. N., Zauel, R., Kolowich, P. A., & Lock, T. R. (2007). In vivo measurement of subacromial space width during shoulder elevation: Technique and preliminary results in patients following unilateral rotator cuff repair. *Clinical Biomechanics, 22*(7), 767-773.

Bey, M. J., Kline, S. K., Zauel, R., Kolowich, P. A., & Lock, T. R. (2010). In vivo measurement of glenohumeral joint contact patterns. *EURASIP Journal on Advances in Signal Processing, 2010*, 5.

Bey, M. J., Zauel, R., Brock, S. K., & Tashman, S. (2006). Validation of a new model-based tracking technique for measuring three-dimensional, in vivo glenohumeral joint kinematics. *Journal of Biomechanical Engineering, 128*(4), 604.

Blanc, R., Syrkina, E., & Székely, G. (2009). Estimating the confidence of statistical model based shape prediction. Paper presented at the *Information Processing in Medical Imaging,* 602-613.

Bolsterlee, B., Veeger, D. H., & Chadwick, E. K. (2013). Clinical applications of musculoskeletal modelling for the shoulder and upper limb. *Medical & Biological Engineering & Computing, 51*(9), 953-963. doi:10.1007/s11517-013-1099-5; 10.1007/s11517-013-1099-5

Browne, A. O., Hoffmeyer, P., Tanaka, S., An, K. N., & Morrey, B. F. (1990). Glenohumeral elevation studied in three dimensions. *The Journal of Bone and Joint Surgery.British Volume, 72*(5), 843-845.

Buis, A., & Convery, P. (1997). Calibration problems encountered while monitoring stump/socket interface pressures with force sensing resistors: Techniques adopted to minimise inaccuracies. *Prosthetics and Orthotics International, 21*(3), 179-182.

Burkart, A. C., & Debski, R. E. (2002). Anatomy and function of the glenohumeral ligaments in anterior shoulder instability. *Clinical Orthopaedics and Related Research, 400*, 32-39.

Burkart, A., Debski, R. E., Musahl, V., & McMahon, P. J. (2003). Glenohumeral translations are only partially restored after repair of a simulated type II superior labral lesion. *The American Journal of Sports Medicine, 31*(1), 56-63.

Cain, P. R., Mutschler, T. A., Fu, F. H., & Lee, S. K. (1987). Anterior stability of the glenohumeral joint A dynamic model. *The American Journal of Sports Medicine, 15*(2), 144-148.

Chopp, J. N., O'Neill, J. M., Hurley, K., & Dickerson, C. R. (2010). Superior humeral head migration occurs after a protocol designed to fatigue the rotator cuff: A radiographic analysis. *Journal of Shoulder and Elbow Surgery, 19*(8), 1137-1144.

Clark, J. M., & Harryman, D. T.,2nd. (1992). Tendons, ligaments, and capsule of the rotator cuff. gross and microscopic anatomy. *The Journal of Bone and Joint Surgery.American Volume, 74*(5), 713-725.

Crosbie, J., Kilbreath, S. L., Hollmann, L., & York, S. (2008). Scapulohumeral rhythm and associated spinal motion. *Clinical Biomechanics, 23*(2), 184-192.

Crosbie, J., Kilbreath, S. L., & Dylke, E. (2010). The kinematics of the scapulae and spine during a lifting task. *Journal of Biomechanics, 43*(7), 1302-1309. doi:10.1016/j.jbiomech.2010.01.024

Culham, E., & Peat, M. (1993). Functional anatomy of the shoulder complex. *The Journal of Orthopaedic and Sports Physical Therapy, 18*(1), 342-350.

Dayanidhi, S., Orlin, M., Kozin, S., Duff, S., & Karduna, A. (2005). Scapular kinematics during humeral elevation in adults and children. *Clinical Biomechanics, 20*(6), 600-606.

Debski, R. E., Sakane, M., Wong, E. K., Fu, F. H., & Warner, J. J. (1999). Contribution of the passive properties of the rotator cuff to glenohumeral stability during anterior-posterior loading. *Journal of Shoulder and Elbow Surgery, 8*(4), 324-329.

Debski, R. E., McMahon, P. J., Thompson, W. O., Woo, S. L., Warner, J. J., & Fu, F. H. (1995). A new dynamic testing apparatus to study glenohumeral joint motion. *Journal of Biomechanics, 28*(7), 869-874.

Debski, R. E., Wong, E. K., Woo, S. L., Sakane, M., Fu, F. H., & Warner, J. J. (1999a). In situ force distribution in the glenohumeral joint capsule during anterior-posterior loading. *Journal of Orthopaedic Research : Official Publication of the Orthopaedic Research Society, 17*(5), 769-776. doi:10.1002/jor.1100170523

Debski, R. E., Wong, E. K., Woo, S. L., Sakane, M., Fu, F. H., & Warner, J. J. (1999b). In situ force distribution in the glenohumeral joint capsule during anterior-posterior loading. *Journal of Orthopaedic Research : Official Publication of the Orthopaedic Research Society, 17*(5), 769-776. doi:10.1002/jor.1100170523

Doody, S. G., Freedman, L., & Waterland, J. C. (1970). Shoulder movements during abduction in the scapular plane. *Archives of Physical Medicine and Rehabilitation, 51*(10), 595-604.

Dowson, D., & Jobbins, B. (1988). Design and development of a versatile hip joint simulator and a preliminary assessment of wear and creep in charnley total replacement hip joints. *Engineering in Medicine, 17*(3), 111-117.

Dunning, C. E., Duck, T. R., King, G. J., & Johnson, J. A. (2001). Simulated active control produces repeatable motion pathways of the elbow in an in vitro testing system. *Journal of Biomechanics, 34*(8), 1039-1048.

Ebaugh, D. D., McClure, P. W., & Karduna, A. R. (2005). Three-dimensional scapulothoracic motion during active and passive arm elevation. *Clinical Biomechanics, 20*(7), 700-709.

Escamilla, R. F., Yamashiro, K., Paulos, L., & Andrews, J. R. (2009). Shoulder muscle activity and function in common shoulder rehabilitation exercises. *Sports Medicine, 39*(8), 663-685.

Fayad, F., Hoffmann, G., Hanneton, S., Yazbeck, C., Lefevre-Colau, M., Poiraudeau, S., . . . Roby-Brami, A. (2006). 3-D scapular kinematics during arm elevation: Effect of motion velocity. *Clinical Biomechanics, 21*(9), 932-941.

Ferreira, L. M., King, G. J., & Johnson, J. A. (2011). Motion-derived coordinate systems reduce inter-subject variability of elbow flexion kinematics. *Journal of Orthopaedic Research, 29*(4), 596-601.

Ferreira, L. M., Johnson, J. A., & King, G. J. (2010). Development of an active elbow flexion simulator to evaluate joint kinematics with the humerus in the horizontal position. *Journal of Biomechanics, 43*(11), 2114-2119. doi:10.1016/j.jbiomech.2010.04.007

Forte, F. C., de Castro, M. P., de Toledo, J. M., Ribeiro, D. C., & Loss, J. F. (2009). Scapular kinematics and scapulohumeral rhythm during resisted shoulder abduction--implications for clinical practice. *Physical Therapy in Sport : Official Journal of the Association of Chartered Physiotherapists in Sports Medicine, 10*(3), 105-111. doi:10.1016/j.ptsp.2009.05.005; 10.1016/j.ptsp.2009.05.005

Giansanti, D., Macellari, V., Maccioni, G., & Cappozzo, A. (2003). Is it feasible to reconstruct body segment 3-D position and orientation using accelerometric data? *Biomedical Engineering, IEEE Transactions on, 50*(4), 476-483.

Giphart, J. E., van der Meijden, Olivier AJ, & Millett, P. J. (2012). The effects of arm elevation on the 3-dimensional acromiohumeral distance: A biplane fluoroscopy study with normative data. *Journal of Shoulder and Elbow Surgery, 21*(11), 1593-1600.

Goss, T. P., & Owens, B. D. (2009). Fractures of the scapula. In C. A. J. Rockwood, F. A. Matsen 3rd, C. J. Wirth & S. B. Lippitt (Eds.), *The shoulder* (4th ed., pp. 333-380). Philadelphia: Saunders Elsevier.

Graichen, H., Stammberger, T., Bonel, H., Haubner, M., Englmeier, K., Reiser, M., & Eckstein, F. (2000). Magnetic resonance based motion analysis of the shoulder during elevation. *Clinical Orthopaedics and Related Research, 370*, 154-163.

Graichen, H., Bonel, H., Stammberger, T., Heuck, A., Englmeier, K. H., Reiser, M., & Eckstein, F. (1998). A technique for determining the spatial relationship between the rotator cuff and the subacromial space in arm abduction using MRI and 3D image processing. *Magnetic Resonance in Medicine : Official Journal of the Society of Magnetic Resonance in Medicine / Society of Magnetic Resonance in Medicine, 40*(4), 640-643.

Graichen, H., Hinterwimmer, S., von Eisenhart-Rothe, R., Vogl, T., Englmeier, K. H., & Eckstein, F. (2005). Effect of abducting and adducting muscle activity on glenohumeral translation, scapular kinematics and subacromial space width in vivo. *Journal of Biomechanics, 38*(4), 755-760. doi:10.1016/j.jbiomech.2004.05.020

Grood, E. S., & Suntay, W. J. (1983). A joint coordinate system for the clinical description of three-dimensional motions: Application to the knee. *Journal of Biomechanical Engineering, 105*(2), 136-144.

Habermeyer, P., Schuller, U., & Wiedemann, E. (1992). The intra-articular pressure of the shoulder: An experimental study on the role of the glenoid labrum in stabilizing the joint. *Arthroscopy: The Journal of Arthroscopic & Related Surgery, 8*(2), 166-172.

Halder, A., Kuhl, S., Zobitz, M., Larson, D., & An, K. (2001). Effects of the glenoid labrum and glenohumeral abduction on stability of the shoulder joint through concavity-compression an in vitro study. *The Journal of Bone & Joint Surgery, 83*(7), 1062-1069.

Halder, A., Zhao, K., O'driscoll, S., Morrey, B., & An, K. (2001). Dynamic contributions to superior shoulder stability. *Journal of Orthopaedic Research, 19*(2), 206-212.

Halder, A. M., Halder, C. G., Zhao, K. D., O'Driscoll, S. W., Morrey, B. F., & An, K. N. (2001). Dynamic inferior stabilizers of the shoulder joint. *Clinical Biomechanics (Bristol, Avon), 16*(2), 138-143.

Harryman, D. T.,2nd, Sidles, J. A., Clark, J. M., McQuade, K. J., Gibb, T. D., & Matsen, F. A.,3rd. (1990). Translation of the humeral head on the glenoid with passive glenohumeral motion. *The Journal of Bone and Joint Surgery.American Volume, 72*(9), 1334-1343.

Harrysson, O. L., Hosni, Y. A., & Nayfeh, J. F. (2007). Custom-designed orthopedic implants evaluated using finite element analysis of patient-specific computed tomography data: Femoral-component case study. *BMC Musculoskeletal Disorders, 8*, 91. doi:10.1186/1471-2474-8-91

Hess, S. A. (2000). Functional stability of the glenohumeral joint. *Manual Therapy, 5*(2), 63-71. doi:10.1054/math.2000.0241

Howell, S., Galinat, B., Renzi, A., & Marone, P. (1988). Normal and abnormal mechanics of the glenohumeral joint in the horizontal plane. *The Journal of Bone and Joint Surgery.American Volume, 70*(2), 227-232.

Howell, S. M., & Kraft, T. A. (1991). The role of the supraspinatus and infraspinatus muscles in glenohumeral kinematics of anterior shoulder instability. *Clinical Orthopaedics and Related Research, 263*, 128-134.

Hurschler, C., Wülker, N., & Mendila, M. (2000). The effect of negative intraarticular pressure and rotator cuff force on glenohumeral translation during simulated active elevation. *Clinical Biomechanics, 15*(5), 306-314.

Inman, V. T., & Abbott, L. C. (1944). Observations on the function of the shoulder joint. *The Journal of Bone & Joint Surgery, 26*(1), 1-30.

Itoi, E., Hsu, H., & An, K. (1996). Biomechanical investigation of the glenohumeral joint. *Journal of Shoulder and Elbow Surgery, 5*(5), 407-424.

Itoi, E., Kuechle, D. K., Morrey, B., & An, K. (1993). Stabilizing function of the biceps in stable and unstable shoulders. *Journal of Bone & Joint Surgery, British Volume, 75*(4), 546-550.

Itoi, E., Motzkin, N. E., Morrey, B. F., & An, K. N. (1994). Contribution of axial arm rotation to humeral head translation. *The American Journal of Sports Medicine, 22*(4), 499-503.

Itoi, E., Newman, S. R., Kuechle, D. K., Morrey, B. F., & An, K. N. (1994). Dynamic anterior stabilizers of the shoulder with the arm in abduction. *The Journal of Bone and Joint Surgery.British Volume, 76*(5), 834-836.

Itoi, E., Morrey, B. F., & An, K. (2009). Biomechanics of the shoulder. In C. A. J. Rockwood, F. A. Matsen 3rd, C. J. Wirth & S. B. Lippitt (Eds.), *The shoulder* (4th ed., pp. 213-266). Philadelphia: Saunders Elsevier.

Jenp, Y., Malanga, G. A., Growney, E. S., & An, K. (1996). Activation of the rotator cuff in generating isometric shoulder rotation torque. *The American Journal of Sports Medicine, 24*(4), 477-485.

Jobe, C. M., Phipatanakul, W. P., & Coen, M. J. (2009). Gross anatomy of the shoulder. In C. A. Rockwood, F. A. Matsen 3rd, C. J. Wirth & S. B. Lippitt (Eds.), *The shoulder* (4th ed., pp. 33-100). Philadelphia: Saunders Elsevier.

Jonsson, B., Olofsson, B. M., & Steffner, L. C. (1972). Function of the teres major, latissimus dorsi and pectoralis major muscles. A preliminary study. *Acta Morphologica Neerlando-Scandinavica, 9*(4), 275-280.

Karduna, A. R., McClure, P. W., & Michener, L. A. (2000). Scapular kinematics: Effects of altering the euler angle sequence of rotations. *Journal of Biomechanics, 33*(9), 1063-1068.

Karduna, A. R., Williams, G. R., Williams, J. L., & Iannotti, J. P. (1996). Kinematics of the glenohumeral joint: Influences of muscle forces, ligamentous constraints, and articular geometry. *Journal of Orthopaedic Research : Official Publication of the Orthopaedic Research Society, 14*(6), 986-993. doi:10.1002/jor.1100140620

Kask, K., Poldoja, E., Lont, T., Norit, R., Merila, M., Busch, L. C., & Kolts, I. (2010). Anatomy of the superior glenohumeral ligament. *Journal of Shoulder and Elbow Surgery / American Shoulder and Elbow Surgeons ...[Et Al.], 19*(6), 908-916. doi:10.1016/j.jse.2010.01.019

Kedgley, A. E., Mackenzie, G. A., Ferreira, L. M., Drosdowech, D. S., King, G. J., Faber, K. J., & Johnson, J. A. (2007). The effect of muscle loading on the kinematics of in vitro glenohumeral abduction. *Journal of Biomechanics, 40*(13), 2953-2960. doi:10.1016/j.jbiomech.2007.02.008

Kedgley, A. E., Mackenzie, G. A., Ferreira, L. M., Drosdowech, D. S., King, G. J., Faber, K. J., & Johnson, J. A. (2008). Humeral head translation decreases with muscle loading. *Journal of Shoulder and Elbow Surgery / American Shoulder and Elbow Surgeons ...[Et Al.], 17*(1), 132-138. doi:10.1016/j.jse.2007.03.021

Keener, J. D., Wei, A. S., Kim, H. M., Steger-May, K., & Yamaguchi, K. (2009). Proximal humeral migration in shoulders with symptomatic and asymptomatic rotator cuff tears. *The Journal of Bone & Joint Surgery, 91*(6), 1405-1413.

Kelkar, R., Wang, V. M., Flatow, E. L., Newton, P. M., Ateshian, G. A., Bigliani, L. U., . . . Mow, V. C. (2001). Glenohumeral mechanics: A study of articular geometry, contact, and kinematics. *Journal of Shoulder and Elbow Surgery / American Shoulder and Elbow Surgeons ...[Et Al.], 10*(1), 73-84. doi:10.1067/mse.2001.111959

Kido, T., Itoi, E., Lee, S., Neale, P. G., & An, K. (2003). Dynamic stabilizing function of the deltoid muscle in shoulders with anterior instability. *The American Journal of Sports Medicine, 31*(3), 399-403.

Lanting, B. A., Ferreira, L. M., Johnson, J. A., Athwal, G. S., & King, G. J. (2013). The effect of excision of the radial head and metallic radial head replacement on the tension in the interosseous membrane. *The Bone & Joint Journal, 95-B*(10), 1383-1387. doi:10.1302/0301-620X.95B10.31844; 10.1302/0301-620X.95B10.31844

Lee, S., & An, K. (2002). Dynamic glenohumeral stability provided by three heads of the deltoid muscle. *Clinical Orthopaedics and Related Research, 400*, 40-47.

Lippitt, S., & Matsen, F. (1993). Mechanisms of glenohumeral joint stability. *Clinical Orthopaedics and Related Research, (291)*(291), 20-28.

Lippitt, S. B., Vanderhooft, J. E., Harris, S. L., Sidles, J. A., Harryman, D. T.,2nd, & Matsen, F. A.,3rd. (1993). Glenohumeral stability from concavity-compression: A quantitative analysis. *Journal of Shoulder and Elbow Surgery / American Shoulder and Elbow Surgeons ...[Et Al.], 2*(1), 27-35. doi:10.1016/S1058-2746(09)80134-1; 10.1016/S1058-2746(09)80134-1

Ludewig, P. M., Phadke, V., Braman, J. P., Hassett, D. R., Cieminski, C. J., & LaPrade, R. F. (2009). Motion of the shoulder complex during multiplanar humeral elevation. *The Journal of Bone & Joint Surgery, 91*(2), 378-389.

Ludewig, P. M., Cook, T. M., & Nawoczenski, D. A. (1996). Three-dimensional scapular orientation and muscle activity at selected positions of humeral elevation. *The Journal of Orthopaedic and Sports Physical Therapy, 24*(2), 57-65.

Malicky, D. M., Soslowsky, L. J., Blasier, R. B., & Shyr, Y. (1996). Anterior glenohumeral stabilization factors: Progressive effects in a biomechanical model. *Journal of Orthopaedic Research, 14*(2), 282-288.

Matsuki, K., Matsuki, K. O., Mu, S., Yamaguchi, S., Ochiai, N., Sasho, T., . . . Banks, S. A. (2010). In vivo 3-dimensional analysis of scapular kinematics: Comparison of dominant and nondominant shoulders. *Journal of Shoulder and Elbow Surgery / American Shoulder and Elbow Surgeons ...[Et Al.],* doi:10.1016/j.jse.2010.09.012

McClure, P. W., Michener, L. A., Sennett, B. J., & Karduna, A. R. (2001). Direct 3-dimensional measurement of scapular kinematics during dynamic movements in vivo. *Journal of Shoulder and Elbow Surgery, 10*(3), 269-277.

McClure, P. W., Michener, L. A., & Karduna, A. R. (2006). Shoulder function and 3-dimensional scapular kinematics in people with and without shoulder impingement syndrome. *Physical Therapy, 86*(8), 1075-1090.

McMahon, P. J., Burkart, A., Musahl, V., & Debski, R. E. (2004). Glenohumeral translations are increased after a type II superior labrum anterior-posterior lesion: A cadaveric study of severity of passive stabilizer injury. *Journal of Shoulder and Elbow Surgery, 13*(1), 39-44.

McMahon, P. J., Chow, S., Sciaroni, L., Yang, B. Y., & Lee, T. Q. (2003). A novel cadaveric model for anterior-inferior shoulder dislocation using forcible apprehension positioning. *Journal of Rehabilitation Research and Development, 40*(4), 349-359.

McMahon, P. J., Debski, R. E., Thompson, W. O., Warner, J. J., Fu, F. H., & Woo, S. L. (1995). Shoulder muscle forces and tendon excursions during glenohumeral abduction in the scapular plane. *Journal of Shoulder and Elbow Surgery / American Shoulder and Elbow Surgeons ...[Et Al.], 4*(3), 199-208.

McQuade, K. J., & Smidt, G. L. (1998). Dynamic scapulohumeral rhythm: The effects of external resistance during elevation of the arm in the scapular plane. *The Journal of Orthopaedic and Sports Physical Therapy, 27*(2), 125-133.

Mercer, D., Saltzman, M. D., Neradilek, M. B., Gilmer, B. B., Warme, W. J., & Matsen III, F. A. (2011). A reproducible and practical method for documenting the position of the humeral head center relative to the scapula on standardized plain radiographs. *Journal of Shoulder and Elbow Surgery, 20*(3), 363-371.

Michiels, I., & Bodem, F. (1992). The deltoid muscle: An electromyographical analysis of its activity in arm abduction in various body postures. *International Orthopaedics, 16*(3), 268-271.

Moseley, H., & Overgaard, B. (1962). The anterior capsular mechanism in recurrent anterior dislocation of the shoulder. *J Bone Joint Surg Br, 44*(4), 913-927.

Motzkin, N. E., Itoi, E., Morrey, B. F., & An, K. (1994). Contribution of passive bulk tissues and deltoid to static inferior glenohumeral stability. *Journal of Shoulder and Elbow Surgery, 3*(5), 313-319.

Nagai, K., Tateuchi, H., Takashima, S., Miyasaka, J., Hasegawa, S., Arai, R., . . . Ichihashi, N. (2013). Effects of trunk rotation on scapular kinematics and muscle activity during humeral elevation. *Journal of Electromyography and Kinesiology,*

Neer, C. S. (1990). *Shoulder reconstruction*. Philadelphia ;; Toronto: Saunders.

Nikooyan, A. A., Veeger, H. E., Westerhoff, P., Graichen, F., Bergmann, G., & van der Helm, F. C. (2010). Validation of the delft shoulder and elbow model using in-vivo glenohumeral joint contact forces. *Journal of Biomechanics, 43*(15), 3007-3014. doi:10.1016/j.jbiomech.2010.06.015; 10.1016/j.jbiomech.2010.06.015

Nyffeler, R. W., Werner, C. M., Sukthankar, A., Schmid, M. R., & Gerber, C. (2006). Association of a large lateral extension of the acromion with rotator cuff tears. *The Journal of Bone & Joint Surgery, 88*(4), 800-805.

O'Brien, S. J., Voos, J. E., Neviaser, A. S., & Drakos, M. C. (2009). Developmental anatomy of the shoulder and anatomy of the glenohumeral joint. In C. A. J. Rockwood, F. A. Matsen 3rd, C. J. Wirth & S. B. Lippitt (Eds.), *The shoulder* (4th ed., pp. 1-32). Philadelphia: Saunders Elsevier.

Ovesen, J., & Nielsen, S. (1986). Anterior and posterior shoulder instability: A cadaver study. *Acta Orthopaedica, 57*(4), 324-327.

Panossian, V. R., Mihata, T., Tibone, J. E., Fitzpatrick, M. J., McGarry, M. H., & Lee, T. Q. (2005). Biomechanical analysis of isolated type II SLAP lesions and repair. *Journal of Shoulder and Elbow Surgery, 14*(5), 529-534.

Peat, M. (1986). Functional anatomy of the shoulder complex. *Physical Therapy, 66*(12), 1855-1865.

Pierrart, J., Lefevre-Colau, M. M., Skalli, W., Vuillemin, V., Masmejean, E. H., Cuenod, C. A., & Gregory, T. M. (2013). New dynamic three-dimensional MRI technique for shoulder kinematic analysis. *Journal of Magnetic Resonance Imaging : JMRI,* doi:10.1002/jmri.24204; 10.1002/jmri.24204

Poppen, N. K., & Walker, P. S. (1976). Normal and abnormal motion of the shoulder. *The Journal of Bone and Joint Surgery.American Volume, 58*(2), 195-201.

Prinold, J. A., Villette, C. C., & Bull, A. M. (2013). The influence of extreme speeds on scapula kinematics and the importance of controlling the plane of elevation. *Clinical Biomechanics,*

Querol, L. B., Büchler, P., Rueckert, D., Nolte, L. P., & Ballester, M. Á. G. (2006). Statistical finite element model for bone shape and biomechanical properties. *Medical image computing and computer-assisted Intervention–MICCAI 2006* (pp. 405-411) Springer.

Rockwood, C. A. (2009). *The shoulder* (4th ed.). Philadelphia, PA: Saunders/Elsevier.

Sahara, W., Sugamoto, K., Murai, M., Tanaka, H., & Yoshikawa, H. (2007). The three-dimensional motions of glenohumeral joint under semi-loaded condition during arm abduction using vertically open MRI. *Clinical Biomechanics, 22*(3), 304-312.

Sano, H., Ishii, H., Yeadon, A., Backman, D. S., Brunet, J. A., & Uhthoff, H. K. (1997). Degeneration at the insertion weakens the tensile strength of the supraspinatus tendon: A comparative mechanical and histologic study of the bone-tendon complex. *Journal of Orthopaedic Research, 15*(5), 719-726.

Scibek, J. S., & Carcia, C. R. (2012). Assessment of scapulohumeral rhythm for scapular plane shoulder elevation using a modified digital inclinometer. *World Journal of Orthopedics, 3*(6), 87.

Sharkey, N. A., & Marder, R. A. (1995). The rotator cuff opposes superior translation of the humeral head. *The American Journal of Sports Medicine, 23*(3), 270-275.

Sharma, G. B., Debski, R. E., McMahon, P. J., & Robertson, D. D. (2010). Effect of glenoid prosthesis design on glenoid bone remodeling: Adaptive finite element based simulation. *Journal of Biomechanics, 43*(9), 1653-1659. doi:10.1016/j.jbiomech.2010.03.004

Siegler, S., Lapointe, S., Nobilinit, R., & Berman, A. T. (1996). A six-degrees-of-freedom instrumented linkage for measuring the flexibility characteristics of the ankle joint complex. *Journal of Biomechanics, 29*(7), 943-947.

Soslowsky, L., Flatow, E., Bigliani, L., Pawluk, R., Ateshian, G., & Mow, V. (1992). Quantitation of in situ contact areas at the glenohumeral joint: A biomechanical study. *Journal of Orthopaedic Research, 10*(4), 524-534.

Soslowsky, L. J., Carpenter, J. E., Bucchieri, J. S., & Flatow, E. L. (1997). Biomechanics of the rotator cuff. *Orthopedic Clinics of North America, 28*(1), 17-30.

Soslowsky, L. J., Malicky, D. M., & Blasier, R. B. (1997). Active and passive factors in inferior glenohumeral stabilization: A biomechanical model. *Journal of Shoulder and Elbow Surgery, 6*(4), 371-379.

Soslowsky, L. J., Flatow, E. L., Bigliani, L. U., & Mow, V. C. (1992). Articular geometry of the glenohumeral joint. *Clinical Orthopaedics and Related Research, (285)*(285), 181-190.

Speer, K. P., Hannafin, J. A., Altchek, D. W., & Warren, R. F. (1994). An evaluation of the shoulder relocation test. *The American Journal of Sports Medicine, 22*(2), 177-183.

Terrier, A., Brighenti, V., Pioletti, D. P., & Farron, A. (2012). Importance of polyethylene thickness in total shoulder arthroplasty: A finite element analysis. *Clinical Biomechanics, 27*(5), 443-448.

Terrier, A., Buchler, P., & Farron, A. (2005). Bone-cement interface of the glenoid component: Stress analysis for varying cement thickness. *Clinical Biomechanics (Bristol, Avon), 20*(7), 710-717. doi:10.1016/j.clinbiomech.2005.03.010

Terrier, A., Buchler, P., & Farron, A. (2006). Influence of glenohumeral conformity on glenoid stresses after total shoulder arthroplasty. *Journal of Shoulder and Elbow Surgery / American Shoulder and Elbow Surgeons ...[Et Al.], 15*(4), 515-520. doi:10.1016/j.jse.2005.09.021

Terrier, A., Ramondetti, S., Merlini, F., Pioletti, D. D., & Farron, A. (2010). Biomechanical consequences of humeral component malpositioning after anatomical total shoulder arthroplasty. *Journal of Shoulder and Elbow Surgery / American Shoulder and Elbow Surgeons ...[Et Al.], 19*(8), 1184-1190. doi:10.1016/j.jse.2010.06.006; 10.1016/j.jse.2010.06.006

Thompson, W. O., Debski, R. E., Boardman, N. D., Taskiran, E., Warner, J. J., Fu, F. H., & Woo, S. L. (1996). A biomechanical analysis of rotator cuff deficiency in a cadaveric model. *The American Journal of Sports Medicine, 24*(3), 286-292.

Van der Helm, F., & Pronk, G. M. (1995). Three-dimensional recording and description of motions of the shoulder mechanism. *Journal of Biomechanical Engineering, 117*(1), 27-40.

Veeger, H. E. (2000). The position of the rotation center of the glenohumeral joint. *Journal of Biomechanics, 33*(12), 1711-1715.

Veeger, H. E., Van der Helm, F. C., Van der Woude, L. H., Pronk, G. M., & Rozendal, R. H. (1991). Inertia and muscle contraction parameters for musculoskeletal modelling of the shoulder mechanism. *Journal of Biomechanics, 24*(7), 615-629.

Virani, N. A., Harman, M., Li, K., Levy, J., Pupello, D. R., & Frankle, M. A. (2008). In vitro and finite element analysis of glenoid bone/baseplate interaction in the reverse shoulder design. *Journal of Shoulder and Elbow Surgery / American Shoulder and Elbow Surgeons ...[Et Al.], 17*(3), 509-521. doi:10.1016/j.jse.2007.11.003; 10.1016/j.jse.2007.11.003

von Schroeder, H. P., Kuiper, S. D., & Botte, M. J. (2001). Osseous anatomy of the scapula. *Clinical Orthopaedics and Related Research, (383)*(383), 131-139.

Walia, P., Miniaci, A., Jones, M. H., & Fening, S. D. (2013). Theoretical model of the effect of combined glenohumeral bone defects on anterior shoulder instability: A finite element approach. *Journal of Orthopaedic Research : Official Publication of the Orthopaedic Research Society, 31*(4), 601-607. doi:10.1002/jor.22267; 10.1002/jor.22267

Warner, J. J., Bowen, M. K., Deng, X., Hannafin, J. A., Arnoczky, S. P., & Warren, R. F. (1998). Articular contact patterns of the normal glenohumeral joint. *Journal of Shoulder and Elbow Surgery, 7*(4), 381-388.

Warner, J. J., Deng, X. H., Warren, R. F., & Torzilli, P. A. (1992). Static capsuloligamentous restraints to superior-inferior translation of the glenohumeral joint. *The American Journal of Sports Medicine, 20*(6), 675-685.

Westerhoff, P., Graichen, F., Bender, A., Rohlmann, A., & Bergmann, G. (2009). An instrumented implant for in vivo measurement of contact forces and contact moments in the shoulder joint. *Medical Engineering & Physics, 31*(2), 207-213. doi:10.1016/j.medengphy.2008.07.011

Woltring, H. (1990). Data processing and error analysis. In P. Berne, & A. Capozzo (Eds.), *Biomechanics of human movement, applications in rehabilitation, sport and ergonomics*. (pp. 203-237). Worthington, OH: Berlec Corporation.

Wuelker, N., Plitz, W., Roetman, B., & Wirth, C. J. (1994). Function of the supraspinatus muscle: Abduction of the humerus studied in cadavers. *Acta Orthopaedica, 65*(4), 442-446.

Wuelker, N., Schmotzer, H., Thren, K., & Korell, M. (1994). Translation of the glenohumeral joint with simulated active elevation. *Clinical Orthopaedics and Related Research, 309*, 193-200.

Yang, Y. M., Rueckert, D., & Bull, A. M. (2008). Predicting the shapes of bones at a joint: Application to the shoulder. *Computer Methods in Biomechanics and Biomedical Engineering, 11*(1), 19-30.

Yano, Y., Hamada, J., Tamai, K., Yoshizaki, K., Sahara, R., Fujiwara, T., & Nohara, Y. (2010). Different scapular kinematics in healthy subjects during arm elevation and

lowering: Glenohumeral and scapulothoracic patterns. *Journal of Shoulder and Elbow Surgery, 19*(2), 209-215.

Yongpravat, C., Kim, H. M., Gardner, T. R., Bigliani, L. U., Levine, W. N., & Ahmad, C. S. (2013). Glenoid implant orientation and cement failure in total shoulder arthroplasty: A finite element analysis. *Journal of Shoulder and Elbow Surgery,*

Yu, J., McGarry, M. H., Lee, Y. S., Duong, L. V., & Lee, T. Q. (2005). Biomechanical effects of supraspinatus repair on the glenohumeral joint. *Journal of Shoulder and Elbow Surgery / American Shoulder and Elbow Surgeons ...[Et Al.], 14*(1 Suppl S), 65S-71S. doi:10.1016/j.jse.2004.09.019

Zhang, J., Yongpravat, C., Kim, H. M., Levine, W. N., Bigliani, L. U., Gardner, T. R., & Ahmad, C. S. (2013). Glenoid articular conformity affects stress distributions in total shoulder arthroplasty. *Journal of Shoulder and Elbow Surgery / American Shoulder and Elbow Surgeons ...[Et Al.], 22*(3), 350-356. doi:10.1016/j.jse.2012.08.025; 10.1016/j.jse.2012.08.025

CHAPTER 2 – Development, Augmentation, and Validation of a Static and Passive Glenohumeral-Scapulothoracic Shoulder Simulator

OVERVIEW

Static and passive in-vitro simulation is an important tool in characterizing the ranges of motion and function of the shoulder joint complex. Previous simulators have assessed these outcomes but each has had limitations that have affected their ability to perform objective assessments based on quantifiable criteria, assess outcomes in multiple joint positions, or replicate physiologically accurate conditions. This chapter describes the design and validation of a series of apparatuses that address these areas. These apparatuses are: a humeral positioning apparatus to improve the accuracy and repeatability of positioning the humerus by decomposing the glenohumeral joint's three rotational DOF; a scapula rotation mechanism to maintain the proper osseous relationship with the humerus throughout its range of motion; a muscle loading and cable guide system to improve load transmission to the muscles and the physiologic accuracy of the replicated lines-of-action; and a instrumented humeral rod with integrated load sensing and spatial tracking capabilities to aid in the objective assessment of biomechanical outcome variables. The results indicated that joint positioning with the humeral guide was significantly more accurate than unaided positioning ($p<0.008$). The muscle loading system produced total losses of no greater than 3.8 N and the instrumented humeral rod allowed for accurate functional assessments. Therefore, these systems are likely to improve the validity of biomechanical and clinical assessments performed on this simulator and thus the value of the results obtained.

2.1 Introduction

The shoulder possesses the largest range of motion of any joint in the body due, in part, to its largely unconstrained structure. This trade-off between greater motion and decreased constraint predisposes the shoulder to various forms of instability and dysfunction. As a result, when testing various joint conditions using an *in-vitro* simulator, it is important not only to assess how the shoulder moves, but also how differing joint conditions influence its range of motion and stability in various joint positions. These assessments take the form of static or passive motion evaluations of the joint's function in various, clinically relevant positions. However, in order to obtain experimentally valid data, it is necessary to assess these outcomes in repeatable, objective, and quantifiable ways. This requires the development of a static-passive simulator that can repeatably orient the joint, isolate individual DOF of interest, and permit outcomes to be quantified using objective end points.

Past investigators have developed static-passive shoulder simulators to enable the evaluation of range of motion and joint stability (Ackland, Pak, Richardson, & Pandy, 2008; Harryman et al., 1990; Huffman et al., 2006; Itoi, Motzkin, Morrey, & An, 1994; Warner, Deng, Warren, & Torzilli, 1992); however, each of these systems have been limited in their ability to perform objective assessments based on quantifiable criteria, assess outcomes in multiple joint positions, or replicate physiologically accurate conditions. Harryman et al. (1990) were the first to develop a passive whole joint shoulder simulator that could record continuous kinematic and kinetic data, but this system relied on unguided investigator manipulation of the humerus and thus the repeatability and objectivity of the outcomes was limited. Itoi et al. (1994) and Warner et al. (1992) developed systems with greater abilities to objectively assess and quantify outcome variables of interest; however, neither apparatus simulated muscle loading, thus decreasing the physiological accuracy of the experimental model, and limiting the clinical relevance of the findings. Lee and colleagues have more recently developed a simulator that loads both glenohumeral and humerothoracic muscles and that has the ability to perform objective assessments with quantitative outcomes (Yu, McGarry, Lee, Duong, &

Lee, 2005); unfortunately, this system is limited to testing with the arm in 90° of abduction which prevents the full characterization a joint condition's effect on should motion and function. Finally, Ackland and Pandy have designed a simulator that is advanced in its ability to replicate physiologic loading and osseous configurations across a range of joint positions, but they have not implemented a means to objectively define the end point of outcomes, such as range of motion (Ackland et al., 2008). Instead, their simulator focuses on the assessment of intrinsic joint parameters, such as moment arms, in predefined joint configurations. Each of these simulators has advanced the field of *in-vitro* shoulder static-passive experimentation; however, none of these simulators possesses all of the design features required to improve the accuracy of the replicated environment and to permit objective evaluations of physiologically meaningful outcome variables.

Therefore, the purpose of this work was to develop a novel simulator that can accurately and repeatably orient both the scapula and the humerus while also allowing individual DOF of the glenohumeral joint to be manipulated. Additionally, a mechanism was developed that would allow physiologically accurate muscle loads to be applied with the joint in any configuration. Finally, a device with integrated capabilities for load sensing and spatial tracking was developed to enable the objective, quantifiable assessment of functional shoulder outcomes, such as joint stability and range of motion. It was hypothesized that implementation of these mechanisms would improve the accuracy and repeatability in performing tests and achieving predefined end points when compared to an experimenter acting alone. Additionally, it was hypothesized that while the devices would aid in the repeatability of orienting the specimen, they would not unduly constrain joint articular kinematics.

2.2 Methods

The following sections will outline the design, development and validation of the components required to achieve the goals outlined above.

2.2.1 Design Requirements & Constraints

The design was guided by a number of requirements and constraints. The requirements were: (1) all components must be able to interface with the lab's existing first generation, load driven shoulder active motion simulator as described by Kedgley et al. (2007); (2) the humeral positioning apparatus must be able to mate to a shoulder specimen that is transected at mid-humerus, and to accurately and repeatably orient it throughout a clinically meaningful range of motion (~130° of abduction); (3) the humeral positioning apparatus must also be able to independently control/constrain each rotational shoulder DOF in a way that corresponds to clinical descriptions of shoulder motion, thus facilitating the replication of clinical assessments; (4) the scapular rotation apparatus must allow a scapula to be potted in a physiologic orientation and produce rotations in rhythm with the humerus; (5) an augmented cable guide system must ensure that physiologic muscle lines-of-action are maintained irrespective of scapular orientation; (6) the design of the load sensing and spatial tracking device must permit it to interface with the humerus and humeral positioning apparatus while providing real time data to be used as objective endpoints.

The primary constraints in this design process were: (1) the design of the humeral positioning system and its method for mating to the specimen must not rigidly fix the glenohumeral joint or otherwise influence its articular kinematics (*i.e.* translations); and (2) the design of the scapular rotation mechanism could not alter glenohumeral kinematics.

2.2.2 Humeral Positioning Apparatus

In designing the humeral positioning apparatus, a number of options were considered. Debski et al. (1999) designed an industrial robot based system, and Walker and Dickey

(2007) designed a custom hexapod robot system for spinal testing; however, neither type of system can decompose the glenohumeral joint's motion into interpretable DOF during testing, and both would unduly complicate the replication of clinical assessments. Additionally, the hexapod concept could not accommodate the full range of motion of the shoulder.

With these options eliminated, a mechanical rather than mechatronic concept was pursued. Therefore, in order to satisfy the requirement of decomposing the shoulder's motion into individual DOF, an apparatus with three distinct mechanisms (Figure 2.1) was developed to isolate each of the three rotations: axial rotation, abduction, and plane of abduction. The axial rotation DOF of the glenohumeral joint was isolated by implementing a mechanism which could mate to an intramedullary humeral rod – used in the previous version of the simulator (Kedgley, 2004) – and permit rotation about its long axis, which is coincident with the humeral axial rotation axis. A spherical bearing was selected for this component as it permitted axial rotation of the rod within the bearing and of the bearing within its casing (Figure 2.2). This bearing was also selected because it allowed the humeral rod to slide through it and incorporated two additional rotational DOF. Combining these three DOF at the rod-bearing interface enabled the humeral head – at the opposite end of the humeral rod – to freely translate in all three directions, and thus prevented the humeral positioning apparatus from having an undesirable influence on glenohumeral kinematics. This is particularly important in the event that a misalignment is present between the shoulder specimen and the apparatus as discussed below.

A mechanism to control the abduction DOF was then designed by connecting the spherical bearing to a slider mechanism that moved along a hemispherical arc connected to the existing simulator base (Figure 2.3). The slider mechanism was designed to allow the center of the spherical bearing to reach full adduction (axis of the bearing directed vertically) while also enabling it to move to a position which would simulate 130° of humeral abduction (Figure 2.4). The slider was also designed with a clamping mechanism

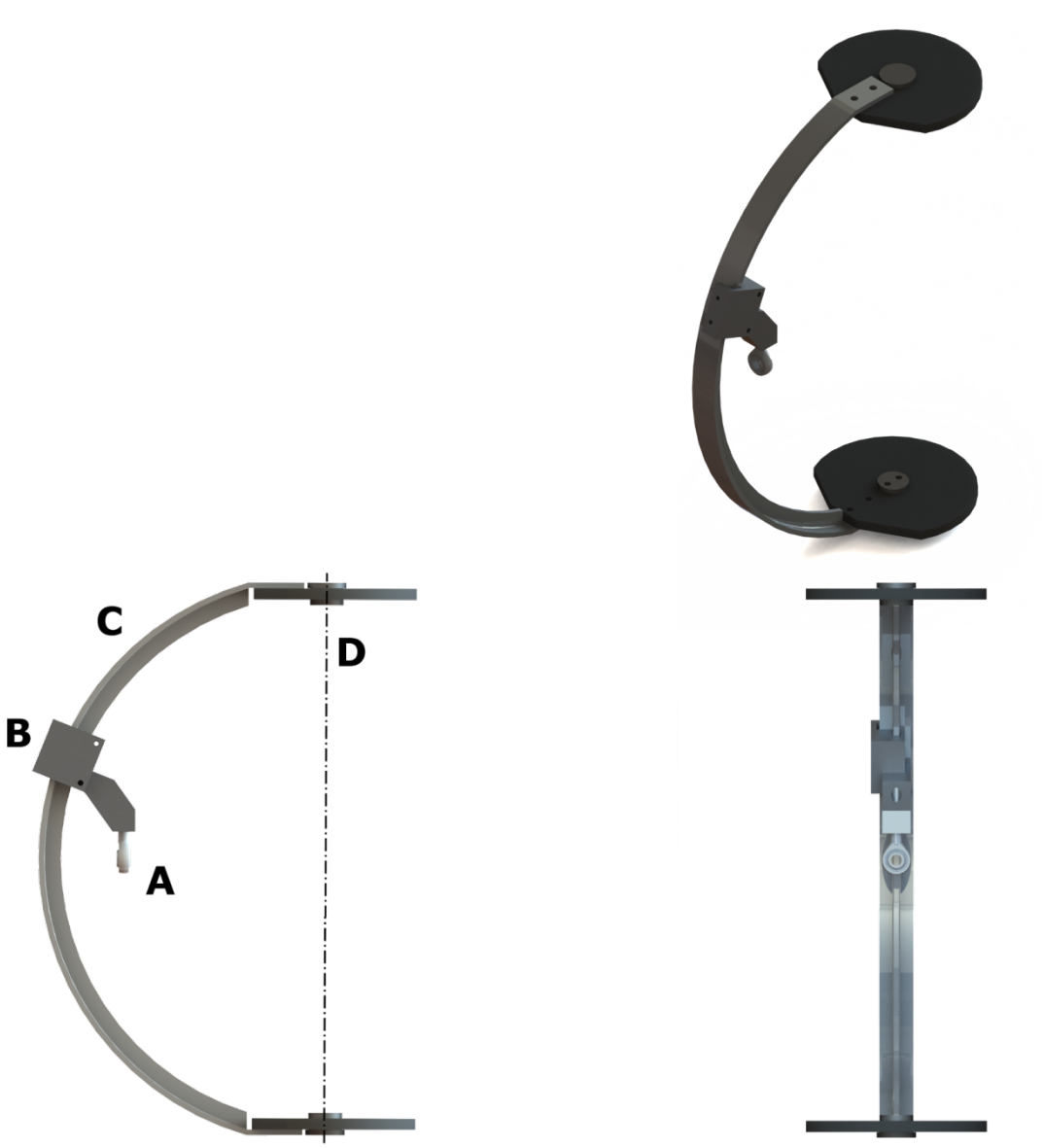

Figure 2.1: The humeral guide arc.
Note the slider mechanism with attached spherical bearing positioned for 90° of humerothoracic abduction. In the bottom left image, also note the dashed line indicating the vertical hinge which controls the plane of abduction. (A) Spherical bearing, (B) slider mechanism, (C) humeral abduction guide arc, (D) vertical hinge for plane of elevation control.

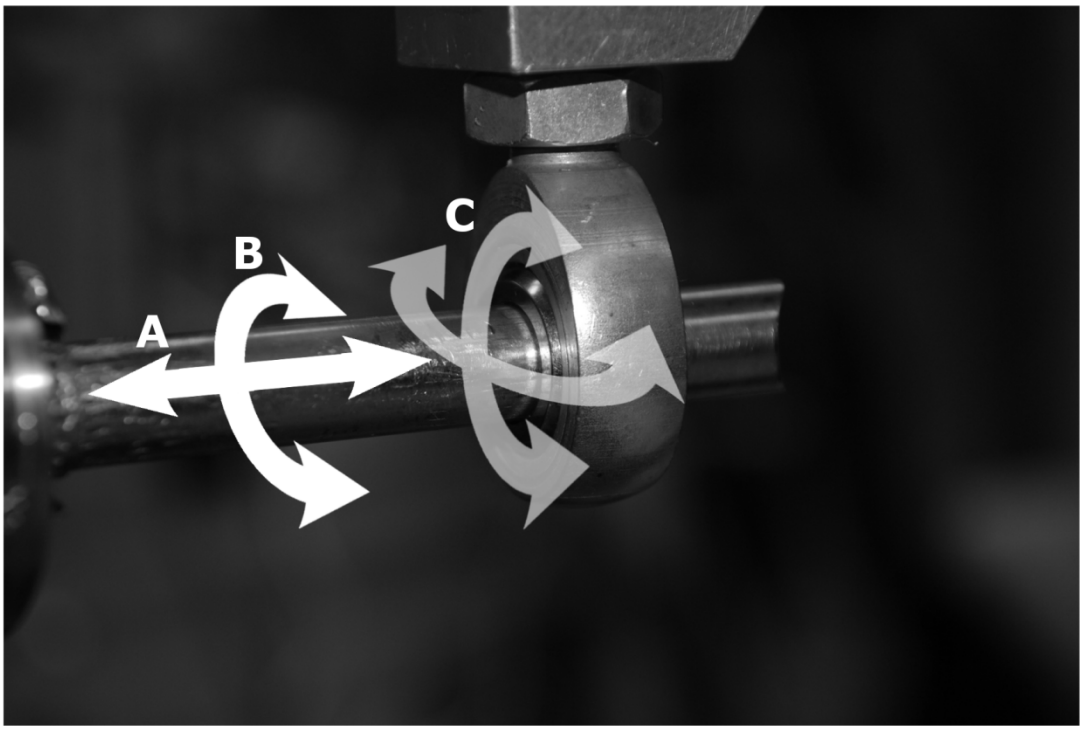

Figure 2.2: Spherical bearing used to mate humeral rod to guide arc.
The degrees of freedom permitted by the bearing are (A) axial translation, (B) axial rotation, (C) two transverse rotations.

to enable the slider, bearing, and humerus to be locked at any level of abduction without influencing/constraining glenohumeral articular kinematics.

The final rotational DOF of the shoulder, plane of elevation, was also controlled through the slider and arc mechanisms by connecting the arc to the simulator base using a vertical hinge construct instead of a rigid connection. The design of the hinge mechanism enabled the humerus to be rotated by greater than 130° anterior and 45° posterior to the scapular plane, thus enabling the entire range of glenohumeral horizontal flexion-extension to be assessed (Figure 2.5) (Itoi, Morrey, & An, 2009). Therefore, in the same way that the Euler angle sequence for the glenohumeral joint defines the plane of elevation, and then abduction occurs about an axis perpendicular to that plane, rotation of the arc about the vertical hinge defines the abduction plane, and the level of abduction is defined by the slider's position. This hinge mechanism was also designed to lock in place once the correct plane was achieved, or be left free to vary depending on the assessment being performed. To ensure the center of the glenohumeral joint could be properly aligned with the vertical hinge, the components which mate the arc to the base were designed so that the axis of the hinge lay at a distance off the simulator base that was approximately equal to half the distance between the posterior acromion and the anterior coracoid. Additionally, as discussed above, the spherical bearing permits three DOF between the humeral guide arc apparatus and the intramedullary humeral rod, thus mitigating any effects of misalignment of the vertical hinge.

Each of these mechanisms serves two roles, first to aid in the accurate orienting of the joint in its associated DOF, and second to physically resist motion in that DOF once the experimenter has specified its desired value. By combining the effect of these three components, it is possible to position the glenohumeral joint in any configuration while also allowing any individual rotational DOF to vary independently. Thus, this design enables the assessment of any conceivable position or motion and allows these assessments to be carried out in a clinically interpretable manner because the DOF of the apparatus coincide with the shoulder's physiologic rotations.

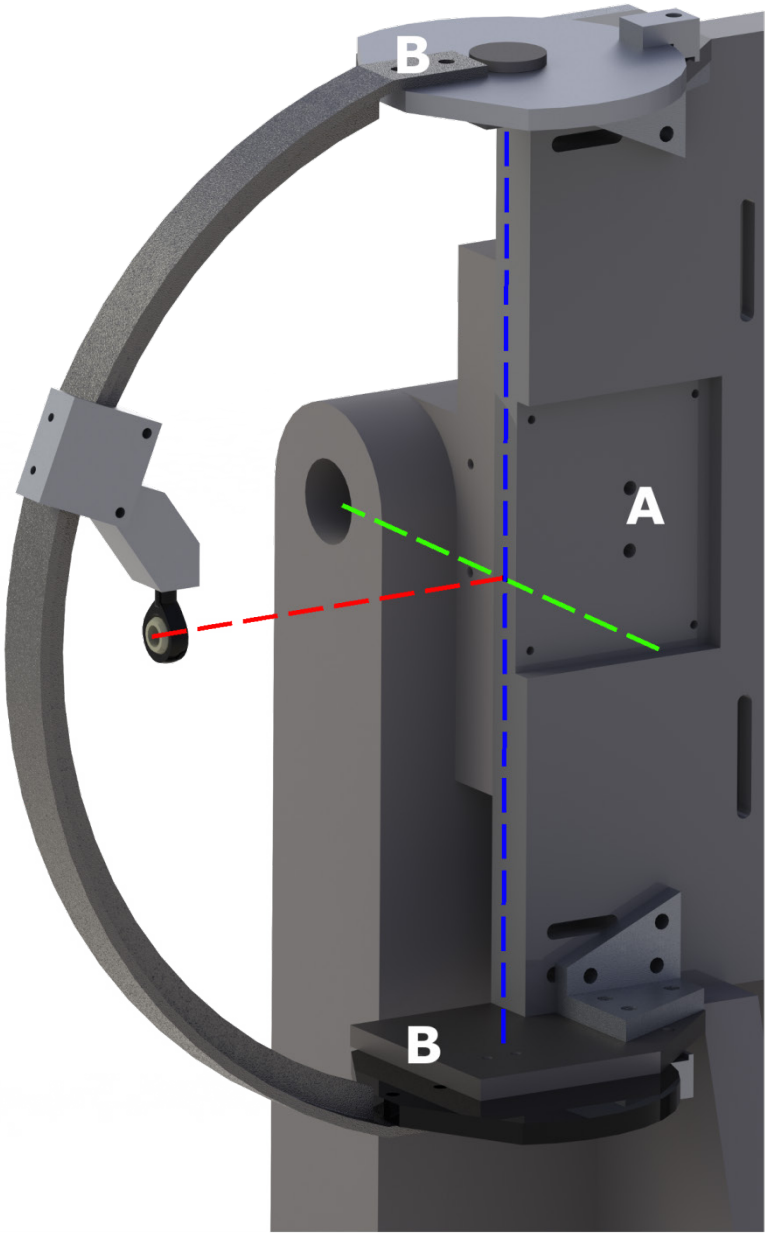

Figure 2.3: Humeral guide arc mounted to existing simulator base
(A) Existing simulator base, (B) hinged connecting plates to mate the guide arc to existing simulator. The coloured lines: (red) the internal-external rotation DOF controlled by the bearing, (green) the abduction DOF controlled by the slider, and (blue) the plane of elevation DOF by the vertical hinge plates.

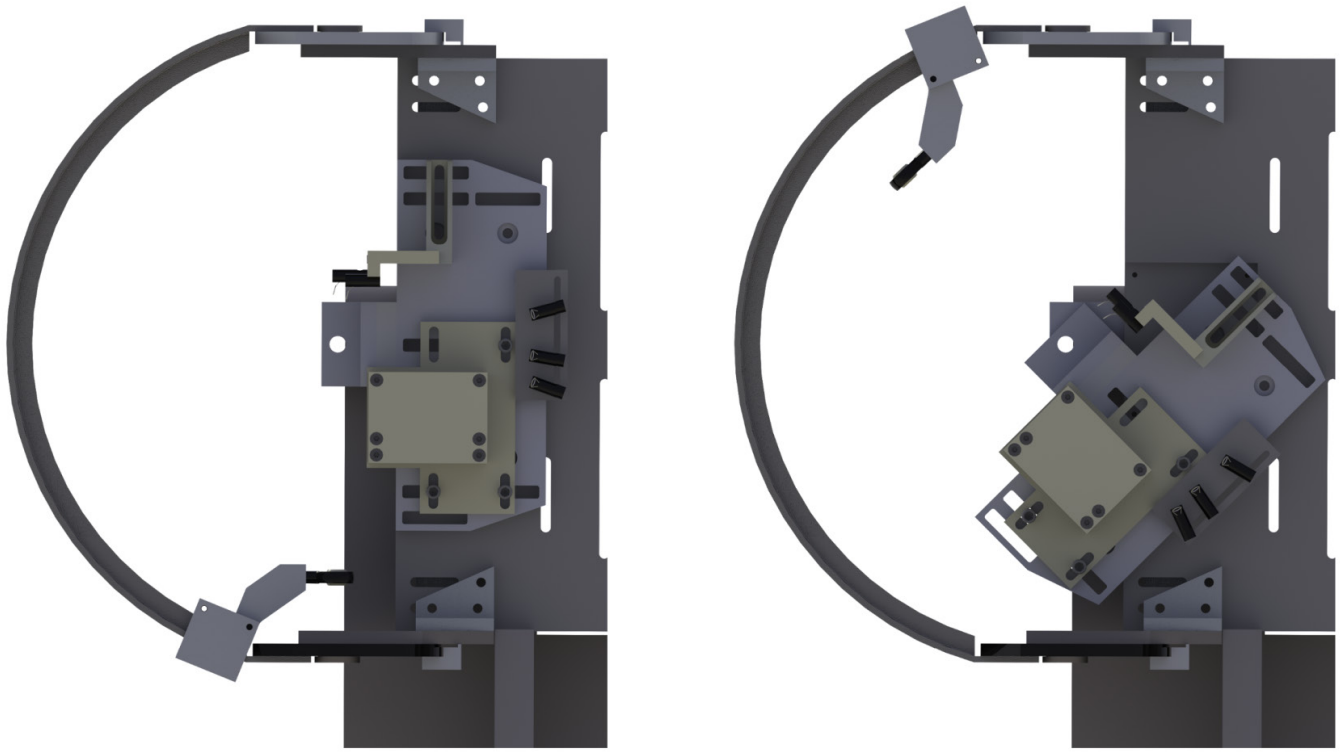

Figure 2.4: Simulator with humeral guide arc and scapular potting and rotation mechanism
In the left image, the two mechanisms are oriented for 0° of abduction while the right image shows them in their maximal abduction orientation which produces a 2:1 glenohumeral-to-scapulothoracic rhythm.

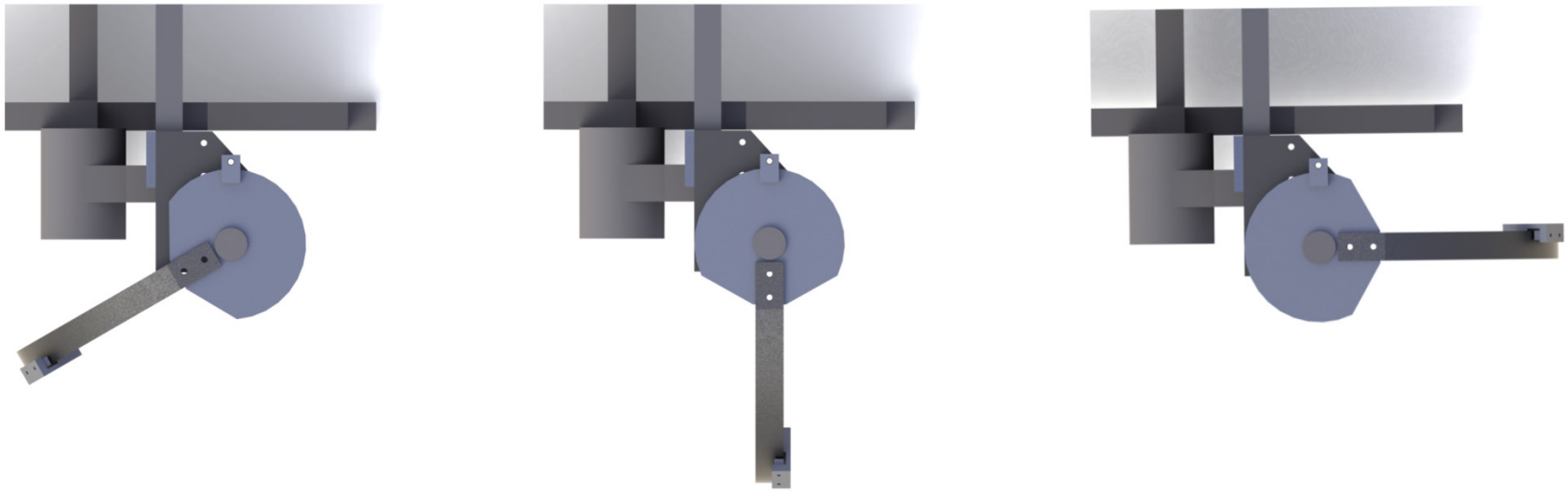

Figure 2.5: The humeral guide arc viewed from above
The range of horizontal flexion-extension permitted by the apparatus is shown. Top, maximal horizontal extension position; middle, position corresponding to humerus in scapular plane; bottom, maximal horizontal flexion position.

2.2.3 Scapular Rotation Apparatus

The scapular rotation apparatus was designed to fulfill two objectives: (1) replicate the orientation of the scapula relative to the rotation of the humerus; and (2) facilitate proper alignment between the glenohumeral joint center and the center of the arc positioning apparatus describe in Section 2.2.2. During the development of this apparatus, the relevance and importance of each rotational DOF of the scapula was evaluated with respect to its effect on glenohumeral function, stability, and kinematics. From these evaluations, it was clear that scapular elevation played a critical role in stabilizing the glenohumeral joint during abduction by supporting the weight of the arm. Similarly, scapular anterior-posterior tilting influenced the stability of the humeral head by dictating which portion of the inferior glenoid would resist inferior subluxation. Protraction-retraction, on the other hand, was considered to be of minimal importance, as this rotation occurred about an axis coincident with the gravity vector (*i.e.* a vertical axis), and thus changes in its value did not alter the portion of the glenoid which supported the humerus. Therefore, if changes in protraction-retraction were required, they could be simulated by altering the glenohumeral plane of elevation using the humeral positioning apparatus. Although scapular tilting was determined to influence joint stability, this rotation was omitted in this design process because there is currently no agreed upon description in the literature of how this rotation changes during glenohumeral motion. Conversely, scapular elevation has been well described and thus the design of the scapular rotation apparatus focused on replicating this motion.

Since the humeral positioning apparatus was specifically designed to ensure that its mechanical center of rotation could be aligned with the glenohumeral joint center, it was critical that the scapular rotation apparatus did not move the joint center out of alignment when the scapula was rotated. To meet this requirement, the scapular rotation mechanism was composed of an adjustable scapula pot and a baseplate that rotated about a lockable horizontal hinge connected to the existing simulator (Figure 2.6). When mounted to the existing simulator, the axis of rotation of the hinge was designed to intersect the center of the humeral positioning arc. Once the scapula was potted in rough alignment with the

hinge, it was possible to use the two translational and one rotational degree of adjustability of the scapula pot to fine tune the position of the glenohumeral joint center. The rotational mechanism was designed to allow scapular orientations from neutral to >60° elevation, which would more than cover the scapular rotation required to achieve the desired maximum humerothoracic rotation of 130° when using the 2:1 glenohumeral-to-scpaulothoracic rhythm commonly described in the literature (Inman & Abbott, 1944) (Figure 2.4).

2.2.4 Muscle Loading & Guide System

The implementation of a muscle loading and guide system is critical to the physiologically accurate replication of the *in-vivo* loading environment during *in-vitro* simulation. The primary factors in the design of an effective system are the minimization of load losses in the system, and the accurate replication of the muscle lines-of-action. The existing simulator was equipped with a muscle loading and guide system that loaded three rotator cuff muscles and three deltoid heads using cables routed through a custom guide system, with each cable connecting to an independently controlled pneumatic actuator. Despite the successful use of the existing system, a number of changes were required to accommodate the added functionality described above and to improve the system's overall performance.

To reduce the magnitude of losses incurred by the guide system for each muscle, a number of modifications were made to the existing system. This system used traditional pneumatic cylinders whose pistons were fitted with rubber o-rings. These pistons, however, incurred up to 6 N of static frictional loss, which was deemed excessive in the case of static/passive testing where the commanded load may be as low as 7.5 N. Therefore, air-bearing style cylinders – which use a borosilicate glass cylinder and graphite piston machined to extremely tight tolerances – were used to improve the system's performance, since they permit a small amount of air leakage but produce

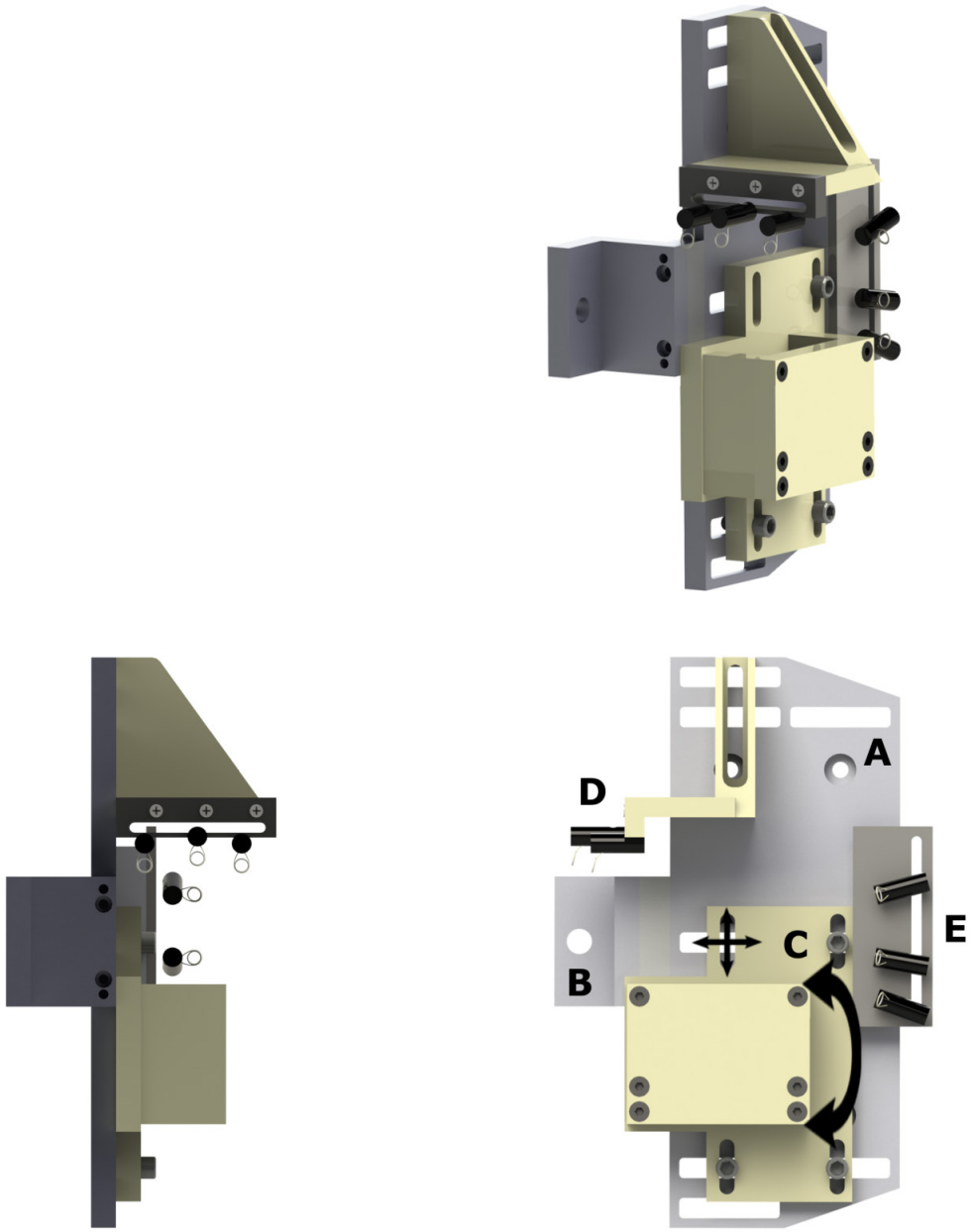

Figure 2.6: The scapular potting and rotation mechanism
Note the horizontal hinge that the pot rotates about, the scapula pot with 3 DOF of adjustability, and the muscle cable guides. (A) Scapular rotation base plate, (B) scapular elevation hinge, (C) adjustable scapula pot, (D) deltoid guides, (E) rotator cuff guides. Note that black arrows indicate the three DOF that the scapula pot can be moved in.

frictional loses of less than 0.1 N and eliminate stiction[2] (Airpel Anti-Stiction Air Cylinders, Airpot Co., Norwalk, CT). Additionally, the previous cabling system, which relied on a complex set of guides with moving components and bushings, was replaced with a fixed construct design that provided predictable frictional losses for any entrance and exit cable angle. This guide was composed of an ultra-low friction Silicon Carbide ring-shaped fishing rod guide (Fuji Fishing Tackle, Ballina, New South Wales, AU) paired with a manufacturer recommended low friction braided Spectra line (PowerPro Super 8 Slick, Shimano Inc., Peterborough, ON) (Figure 2.7).

For each muscle group, we ensured that: (1) the guide placement facilitated minimization of actuator load losses; and (2) the final cable direction, when routing the cable to the muscle, was coincident with the physiologic line-of-action (Figure 2.8). Despite the low friction design of the pneumatic cylinders used in this system, significant losses would occur if the cylinder experienced off-axis loading. Therefore, a guide was placed collinear to the piston of each cylinder, just beyond the maximum stroke, in order to ensure any off-axis loading was carried by the guide and not the cylinder.

As a result of the addition of scapular rotation as described in Section 2.2.3, the routing of each cable to its respective muscle was significantly altered in comparison to the design for the existing simulator. Similar to the existing system, a mounting system was designed for each guide, which allowed its position to be translated in two directions in order to account for specimen-to-specimen variation in muscle lines-of-action. However, unlike the previous system, each guide was fixated to the scapula rotation mechanism rather than the simulator base so that the line-of-action was maintained in any testing configuration.

This design resulted in the use of two guides for each muscle group: one on the scapula rotation mechanism, and another on the simulator base, meant to align the cable to the actuator. In the case of the three deltoid heads, however, it was found that the physiologic

---

[2] Stiction - the frictional force to be overcome to set one object in motion when it is in contact with another. In air cylinders, it is the phenomenon which causes inconsistent break away loads at the start of a cylinders stroke.

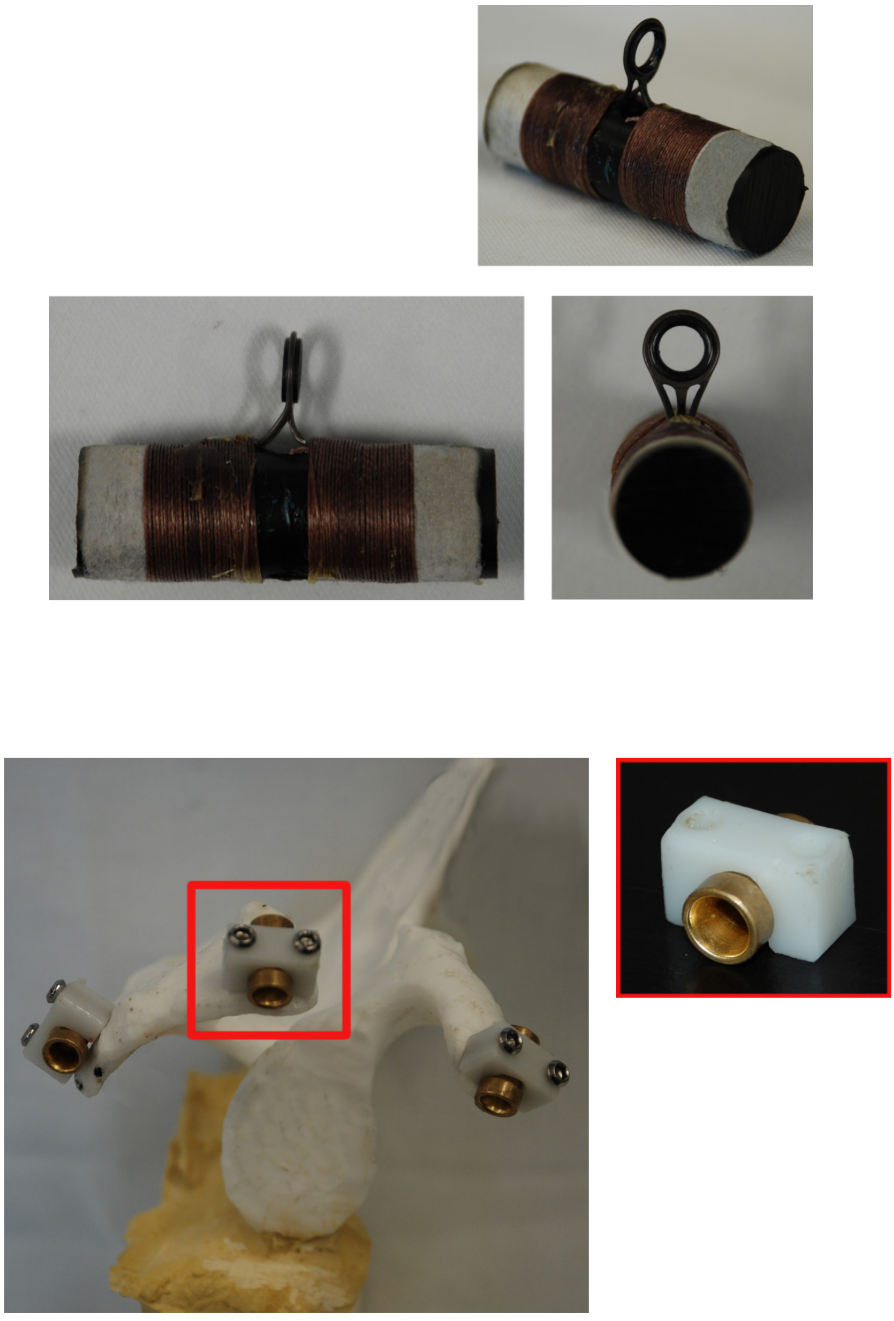

Figure 2.7: The two muscle cable guides.

Top, cable guides used for all muscle groups; bottom, acromion and clavicle affixed deltoid cable guides. Note that in bottom image, anterior deltoid guide is placed on coracoid rather than clavicle as saw bones model in image did not include the clavicle.

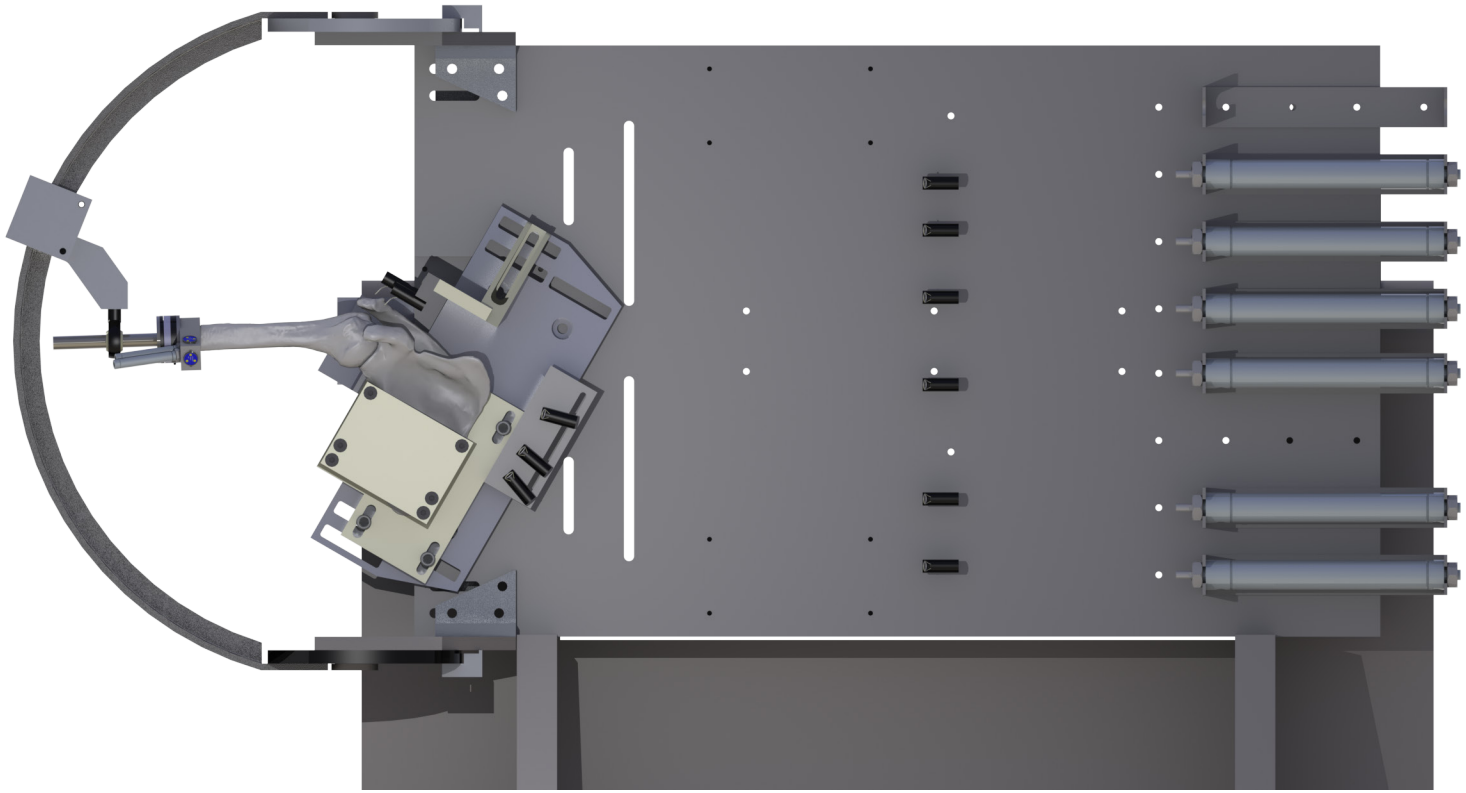

Figure 2.8: The entire shoulder simulator with specimen mounted.
Note that soft tissues of specimen are omitted for clarity.

line-of-action could not be accurately replicated using these two guides because the muscles' origins are located at the very lateral edge of the acromion. Therefore, a custom set of bone affixed guides was created for the three heads of the deltoid that were placed on the lateral acromion and the clavicle. These guides were composed of a polished brass double sided funnel, in the shape of the center of a torus[3], which was secured to the bone using a plastic clamp and two cortical bone screws (Figure 2.7). Use of these guides improved replication of the deltoid lines-of-action but were used in combination with the existing guides in order to ensure the deltoid cables were not obstructed by the medial scapula in any rotational configuration.

2.2.5 Multi-Articular Muscle Loading

Loading multi-articular muscles presents a unique challenge in whole joint simulation, since the experimenter often does not have access to both the insertion and origin of the muscles. In the shoulder, the short and long heads of the biceps muscle run from the scapula to the bones of the forearm; however, the forearm is not present during testing and thus load application from a proximal cable onto the insertion site is not possible. The proximal origin must therefore be loaded from a distal location; however, this is difficult due to the limited space available, and because the humerus is not fully constrained during testing. As a result of these obstacles, and the relative lack of importance of these muscles during active shoulder motion, loading of these muscles had not been implemented on the existing active motion simulator. These muscles do, however, influence the motion and stability outcomes assessed by a static/passive simulator, and thus design of a method to simulate these muscles was undertaken as part of this research.

Previous static/passive simulators have simulated loading of these muscles by simply hanging weights from a cable that is connected to the muscle and routed in a physiologic manner (Itoi, Kuechle, Morrey, & An, 1993; Lin et al., 2013). However, depending on the specific design, the use of weights may either apply unrealistic inferior subluxation forces

---

[3] Torus-a surface or solid formed by rotating a closed curve, esp. a circle, around a line that lies in the same plane but does not intersect it (*e.g.*, like a ring-shaped doughnut).

to the glenohumeral joint or, if routed to a separate structure, may restrict the passive assessments which can be performed. To avoid these limitations, a miniature pneumatic actuator system (5/16” bore, Original Line, Bimba Manufacturing Co., University Park, IL) was implemented to independently load each of the two muscle groups (Figure 2.9). By mounting the actuators to the intramedullary humeral rod, the force of each actuator was internal to the humerus and glenohumeral joint. The cable between the actuator and the muscle was then routed using a bone affixed eyelet screw in order to achieve a physiologically accurate line-of-action. This configuration thus allowed any load level to be applied without applying the external loads associated with hanging masses that negatively affecting joint kinematics.

2.2.6 Integrated Load Sensing and Spatial Tracking Device

An integrated load sensing and spatial tracking device was designed with the goal of continuously quantifying various static and passive outcome variables, while also providing the experimenter with a means to set objective end point criteria for these variables. The device was attached to the humerus, because the majority of outcome variables of interest to a static/passive simulator involve some form of experimenter manipulation of the humerus. With this in mind, the existing intramedullary humeral rod was redesigned to accommodate a commercially available load cell and an array of optical trackers, while also permitting the rod to properly mate to the humeral guide arc (Figure 2.9). A six DOF load cell (Mini 45, ATI – Industrial Automation, Apex, NC) was selected for use in this device and was interposed between the two halves of a custom designed stainless steel humeral rod, thus permitting any test to be performed while fully describing the applied loading. The proximal half of the humeral rod consisted of a disk machined with a bolt pattern matching that of the tool side of the Mini 45 load cell and with a 4” long, ¼” diameter rod attached, to permit insertion into the humeral canal while leaving sufficient space for an appropriate cement mantle. The distal half had a similar disk and matching bolt pattern, along with a 5” long, ½” diameter rod machined to a polished finish, in order to facilitate smooth motion with the spherical bearing on the humeral guide arc.

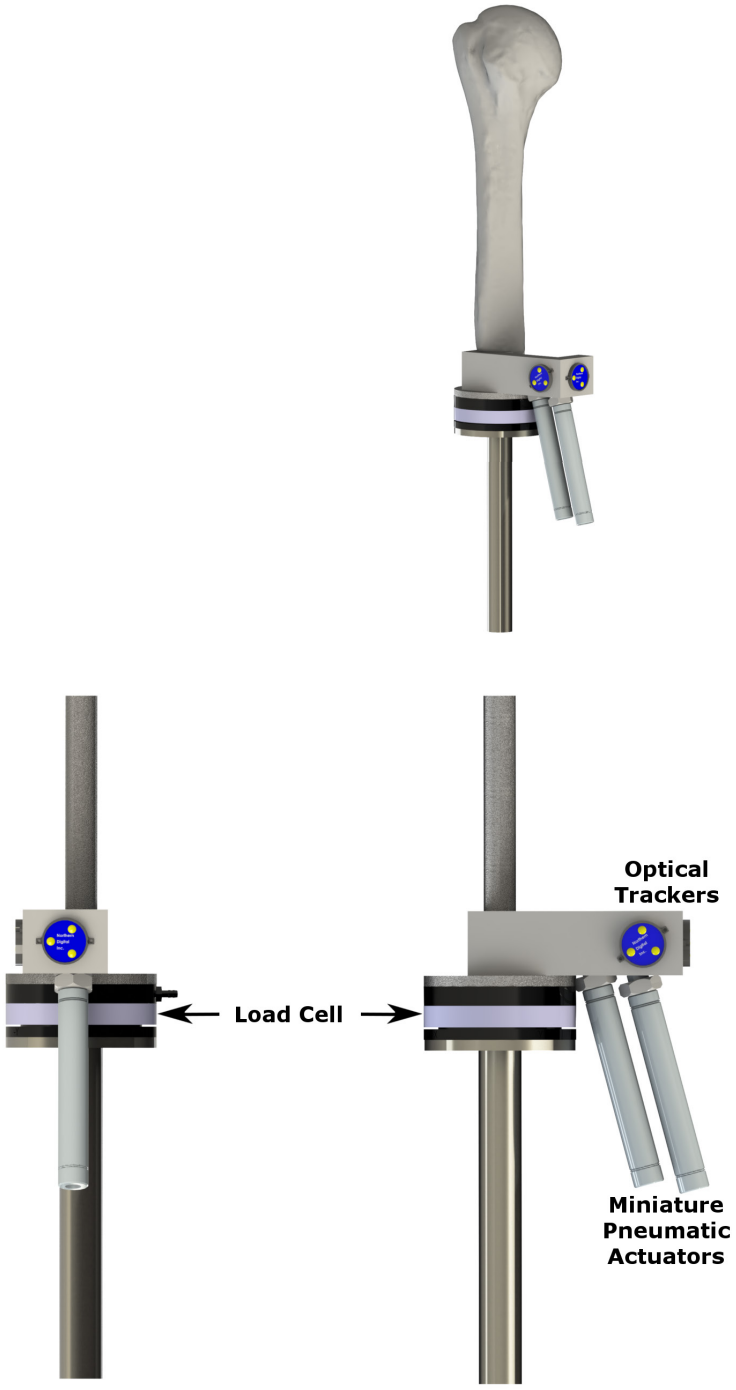

Figure 2.9: The instrumented intramedullary humeral rod.

In order to ensure that the humerus could be tracked throughout its full range of motion, a custom optical tracking rigid body was created, composed of two standard Optotrak Certus rigid body markers – each with three infrared LEDs – mounted perpendicular to each other (Figure 2.9). The most difficult humeral motion to track is internal-external rotation; however, the geometry of this rigid body allowed it to be tracked over a total arc of 210°, which far exceeds the physiologic range of motion. This custom rigid body was defined so that any three of the six LEDs could be used to track the 6 DOF motion of the humerus.

By creating a device which integrates these two data streams, it is possible to use one as an objective end point in real time, while the other is recorded as an outcome variable. For instance, the internal-external rotation range of motion of the glenohumeral joint can be assessed using this device by defining an applied axial torque as an end point and monitoring how much internal and external rotation exists when this criterion is met.

2.2.7 Validation

Once each of the new components which compose this static/passive shoulder simulator were implemented, it was necessary to assess their overall performance. Therefore, the humeral rotation mechanism, the muscle loading and guide system, and the load sensing and spatial tracking device were each assessed using outcome variables relevant to their respective function. The humeral rotation mechanism was assessed for its ability to help improve the accuracy and repeatability in positioning the specimen, and its ability to constrain DOF, which are intended to be constant during certain tests. These tests were performed by two experimenters: an orthopaedic resident (INA) and an experienced, fellowship trained shoulder specialist (GSA)[4]. To assess this first measure, the experimenter was instructed to position the specimen in various clinically relevant positions (45° & 90° abduction, and 30° external rotation in 90° abduction) five separate times. This was first done without use of the humeral guide arc, and blinded to real time tracking, then done again using the guide with tracking feedback. The second measure,

[4] INA – Dr Irfan Abdulla & GSA – Dr George Athwal.

the guide's ability to constrain individual DOF, was compared to manual experimenter positioning by measuring the degree to which the level of humeral abduction changed during an external rotation motion both in and outside of the guide. For the unguided external rotation tasks, the experimenter was instructed to maintain the level of abduction to the best of their ability. Finally, to assess the humeral guide's validity as a means to isolate and constrain rotational DOF but leave the associated glenohumeral articular kinematics unaffected, the humeral head translations associated with the external rotation task were compared for trials in and outside of the humeral guide arc.

The muscle loading and guide system was assessed for the amount of load loss present when the cable was oriented in various experimentally relevant directions. Specifically, the humerus was abducted from 0° to 90° in 15° increments, with scapular rotation simulated using a 2:1 ratio. This range of rotation produced a corresponding angle of 90° to 30° between the cable and the most lateral guide. Load loss may result from frictional losses or losses in the actuator system; therefore, the loss was quantified as the measured load at the insertion site compared to the actuator load command (10, 20, 30, 40 N). Repeatability of the loss was assessed using five repeated trials at 0° and 90° of abduction.

The load sensing and spatial tracking device was also evaluated. Since the end point criterion for tests involving this device would primarily be based on load data, the device was assessed for its ability to increase the accuracy and repeatability of tests that depend on a load based endpoint. Specifically, the ability to meet a predefined torque end point was assessed for an external rotation test first with the experimenter blinded, and subsequently with the experimenter able to see the torque they were applying in real time. The torque endpoint for this test (0.8 Nm) was chosen by recording the self-selected endpoint of an experienced shoulder surgeon (GSA) instructed to perform their standard clinical assessment of external rotation without real time feedback. Prior to the blinded trials, the experimenter was given as much time as required to practice the test while observing the real time feedback, in order to allow them an opportunity to assess the level of resistance corresponding to the desired endpoint.

During the validation tests of the humeral guide and the instrumented humeral rod, the muscles of the shoulder were loaded using ratios previously defined by Wellmann et al. (2009), and with the minimum magnitude required to reduce the joint. Tests performed with this level of muscle loading were considered to be a 'standard load' while tests were also performed with no muscle load and two times the standard load. In the cases where real time feedback was used to achieve a desired endpoint, the largest value of overshoot recorded in the trial was selected as the achieved endpoint because in many experimental protocols, surpassing the target may cause some form of damage. Thus, it was important to assess this overshoot value rather than simply selecting the point in the data stream which most closely matched the endpoint. The differences between the tests performed using the guide and the unconstrained trials were compared using Paired Samples T-tests with significance set a $p<0.05$. Note that p-values are only present for the outcomes where sufficient statistical power (80%) was achieved with the five repeated trials.

2.3 Results

2.3.1 Humeral Guide

Placing the humerus in 45° and 90° of abduction was found to be significantly more accurate ($p<0.008$) and repeatable when using the humeral guide arc and real time feedback; it achieved average values of 45.0±0.2° and 90.2±0.2° while manual positioning produced values of 50.0±1.7° and 94.1±1.5°, respectively. The accuracy of orienting the humerus in a predefined external rotation value of 30° was not markedly improved by the humeral guide (31.4±0.7°) versus manual positioning (31.7±1.5°) for the primary experimenter (INA). However, both accuracy and repeatability were noticeably increased for the secondary experimenter (GSA) (30.8±0.7° vs 34.2±3.1°) but this comparison did not reach significance ($p=0.122$).

During an external rotation range of motion test with the humerus initially held in 90° of abduction, the variation in abduction angle was found to be significantly smaller ($p=0.01$) with the humerus constrained by the humeral guide arc (0.5±0.03°) in comparison to the experimenter manually maintaining abduction (7.3±3.4°). However, this difference was

less pronounced in the results of the secondary experimenter (GSA) (0.4±0.1° vs 1.0±0.3°). Comparison of the variation in abduction between the two experimenters out of the arc and in the arc demonstrated that their ability to maintain abduction significantly differed during unconstrained positioning (6.3±4.0°, $p=0.024$) but not when using the humeral guide arc (0.1±0.1°, $p=0.094$). Variations in humeral abduction for tests both in and outside of the arc were found to increase when no muscle loading was applied and decrease when 2x muscle loading was applied (Figure 2.10). However, the largest amount of variation, when using the guide, remained less than half that of the smallest variation during unconstrained testing (0.5±0.1° vs 1.8±0.1°), and comparisons between these two methods at both load levels were found to be significant ($p<0.04$).

Evaluation of the glenohumeral kinematics associated with the external rotation task demonstrated that, during standard and 2x standard muscle loading, humeral head translations were similar for trials performed in and outside of the arc (average resultant translation: 2.2±0.8mm vs 2.1±0.6mm, $p>0.451$) (Figure 2.10). However, with no muscle load applied, humeral head translations were markedly smaller when using the humeral guide arc compared to unconstrained positioning (average resultant translation: 16.6±0.4mm vs 21.9±0.5mm, $p<0.001$).

2.3.2 Muscle Loading & Guide System

Across abduction, the load lost due to the actuator and cable guide system ranged from an average of 2.2±1.3 N at 0° abduction to 0.6±0.3 N at 90° abduction when averaged over the four load levels (Figure 2.11). Additionally, on average, the measured load loss increased by 0.7 N for each 10 N increment in actuator load. The repeatability of these loss measurements were found to range from ±0.03-0.08 N across the four load levels with the humerus in 0° abduction and ±0.02-0.05 N in 90° abduction.

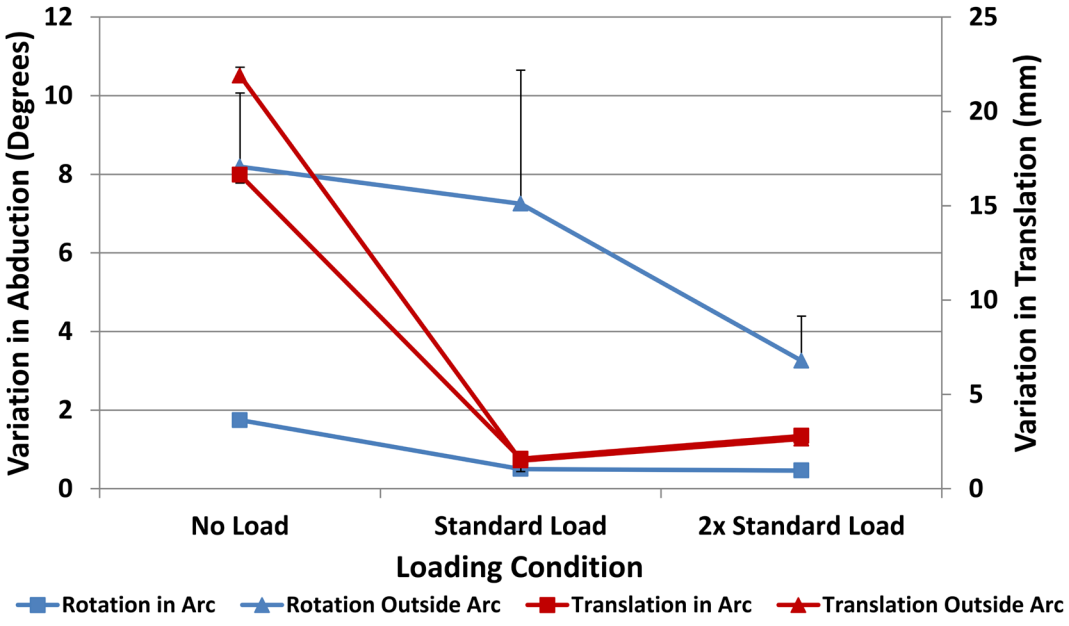

Figure 2.10: Variation in abduction.
Variations were monitored during an external rotation motion performed with and without assistance of humeral guide.

2.3.4 Integrated Load Sensing and Spatial Tracking Device

The accuracy and repeatability of meeting a predefined torque endpoint was markedly higher when using the humeral guide arc and instrumented humeral rod (0.01±0.01 Nm) in comparison to attempting to achieve the same value using only clinical experience while blinded to real time feedback (0.2±0.1 Nm). Trials performed by the secondary, more experienced experimenter (GSA), produced similar accuracy results (0.02 Nm vs 0.1 Nm); however, this experimenter's repeatability was not decreased to the extent of the first experimenter when performing the task outside of the guide (±0.01 Nm vs ±0.04 Nm). Using the humeral guide arc, performing tests with no load produced greater accuracy and repeatability (0.01±0.003 Nm) than performing tests with 2x standard loading (0.03±0.02 Nm) (Figure 2.12). In contrast, when manually positioning the humerus, results did not change when load was removed (0.2±0.1 Nm) but accuracy and repeatability did improve with 2x load applied (0.06±0.04 Nm); however, these results did not reach the levels achieved using the humeral guide arc.

2.4 Discussion

Previously developed *in-vitro* shoulder simulators have focused on the assessment of static and passive outcome variables; however, in many cases these systems have relied on the experimenter's ability to accurately and repeatably orient the joint during testing. Additionally, these systems have used only minimal levels of real time data to ensure that testing end points are based on objective criteria rather than experimenter experience and 'feel'. As well, many of these systems have neglected critical aspects of shoulder function, thus limiting the clinical relevance of their findings. The simulator described above, therefore, was intended to address the limitations encountered in previously reported simulators in order to achieve higher levels of physiologic accuracy, assessment repeatability, and endpoint objectivity. By achieving these goals, data produced in future biomechanical investigations will be able to effectively investigate phenomenon with smaller effect sizes (*i.e.* smaller differences between conditions and greater variance in the data) while also decreasing the sample sizes required to obtain sufficient power to address questions of interest.

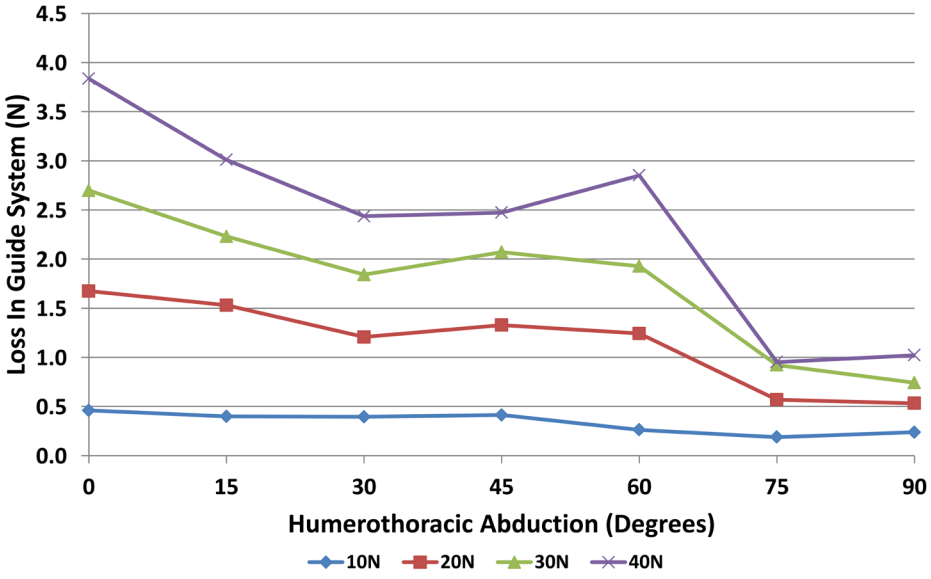

Figure 2.11: Load loss in actuator and guide system.
Losses were recorded as a function of applied load and abduction angle.

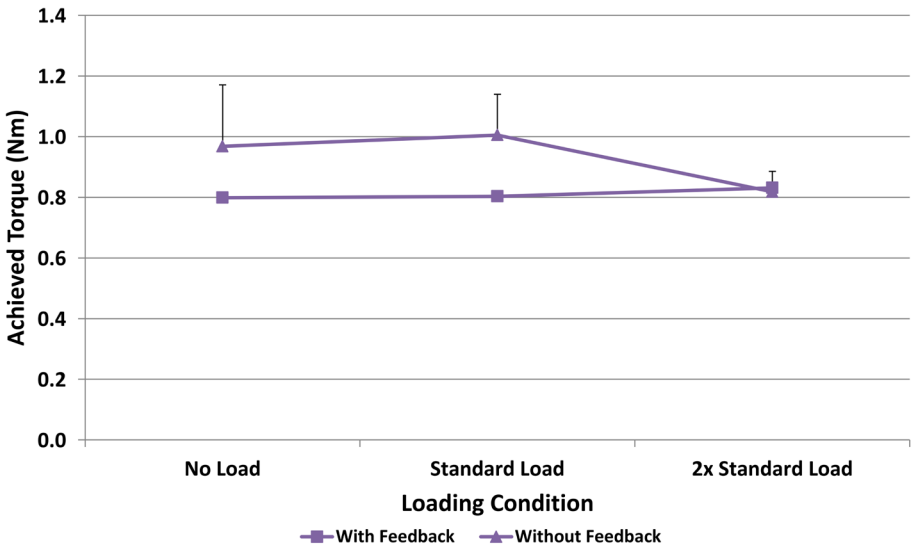

Figure 2.12: Ability to meet a predefined torque value.
The torque achieved during external rotation test with and without real time feedback.

The systems developed to augment the existing simulator were each intended to improve one or more of the above goals; however, it was necessary to validate each of these in terms of their ability to achieve the desired goal (*i.e.* improve physiological accuracy, etc.) and to confirm that they did not unduly alter or influence shoulder function. The effect of the humeral guide arc was first assessed, and it was found to significantly improve the accuracy and repeatability of specimen placement in predefined levels of abduction. In the case of orienting the joint in axial rotation, use of the arc improved the repeatability of achieving a desired target but only improved the accuracy in one experimenter. This, however, can be attributed to the high accuracy achieved manually by one experimenter rather than inaccuracy when using the guide.

Beyond aiding in the positioning of the glenohumeral joint, the guide arc was intended improve the experimenter's ability to perform passive motion assessments by isolating each of the three rotational DOF so that they could be independently constrained or manipulated. Together, the positioning capability and ability to isolate rotations ensures that desired rotations can be maintained while others are independently varied thus increasing the accuracy and repeatability of assessments. The success of the arc in achieving isolation of rotations was assessed during an external rotation task, with the arm in 90° abduction, by measuring the degree to which the humerus' abduction angle varied during the motion. During standard muscle loading, the humeral guide permitted significantly less variation in abduction as compared to the variation seen without the guide. Variation was found to decrease for the unconstrained tasks when double the muscle load was applied; however, these variations never decreased to the level achieved by the humeral guide. It was additionally found that abduction variation differed between experimenters without use of the humeral guide, but not when the guide was employed. Therefore, we can say that the humeral guide arc is effective at eliminating the variability associated with inter-experimenter positioning, thus increasing the validity of these assessments. Overall, these findings demonstrate that the arc is effective at isolating the abduction DOF which is important for a number of clinically relevant tests in which performing a functional test in a very specific joint orientation is critical to correctly assessing the effect of an injury and/or reconstruction.

Another important assessment of the influence of the humeral guide system is the evaluation of how it affects the articular translations of the glenohumeral joint. Evaluation of this outcome gives an indication of whether the apparatus constrains or alters normal translational kinematics. With this in mind, data from the external rotation trials demonstrated that translations of the humeral head do not statistically differ between motions in and outside of the arc when standard and 2x standard muscle loading are applied. Therefore, the humeral arc can be considered to not significantly influence or constrain articular kinematics despite it locking the joint in a set level of abduction. Articular kinematics did, however, differ between tests in and outside of the arc when no muscle load was applied. In this case, translations in the arc were increased compared to when load was applied, but these were still significantly smaller than the translations accompanying tests outside of the arc. However, this difference is most likely attributable to the larger variation in abduction associated with performing this test outside of the humeral arc rather than to any undue constraint caused by the arc. It should be noted that a limitation of this evaluation was that the magnitude of misalignment between the glenohumeral joint center and the humeral guide was not varied and thus it was not possible to characterize the sensitivity of changes in glenohumeral kinematics to changes in alignment. However, it is believe that the degrees of freedom permitted between the guide and the humeral rod decreases the level of sensitivity to misalignments which are of a reasonable magnitude.

Despite the positive results produced by the humeral guide in terms of reducing variation in humeral orientation during testing and its lack of effect on joint translations, the use of this system to control humeral orientation does have an associated limitation. Namely, it precluded the replication of the arms true mass and inertial properties. Additionally, the manner in which the mass of the arm was supported by the arc may not have accurately replicated the way in which this was achieved by the experimenter during testing outside of the arc. With that said, because no differences were seen between the glenohumeral kinematics with and without the guide, it is believed that these limitations had minimal effects on the physiologic accuracy of the conditions produced by the simulator.

Evaluation of the muscle loading and guide system demonstrated that the total load loss in the system, due to both actuator losses and friction in the guides, never exceeded 3.8 N. Additionally, this loss level was only observed in the case where the highest load (40 N) was applied in 0° of abduction, corresponding to an ~90° angle of wrapping of the cable around the guide. Beyond this configuration, all losses fell below 3 N, and for the majority of the abduction range of motion (30°-90°), only one configuration was above 2.5 N. Although the data have an overall decreasing trend across abduction, some non-linearity exists between 30° and 75°. This non-linearity can be attributed to the effect of simulating scapular motion during these tests, which caused the angle of the cable with respect to the actuator alignment guide to vary in an irregular fashion. The load losses observed with this system, therefore, can be considered small in relation to the loads applied during testing. Also, in cases where precise application of a desired load is critical, this data can be used to adjust the commanded actuator load. Therefore, the system implemented here has minimal effect on the accurate application of a desired muscle load, and thus enables loading scenarios with greater physiologic accuracy to be implemented.

The instrumented humeral rod improved accuracy by ~21% and repeatability by ~24% in meeting torque endpoints, relative to the target value of 0.8 Nm. However, these improvements were not statistically significant, which can be attributed to the relatively small target value and the signal noise associated with the measurements. The data also indicated that the ability to meet a torque endpoint criterion, both with and without feedback, did not change when no muscle loading was applied. However, the experimenter's ability to accurately achieve the desired endpoint was improved when twice the standard muscle load was applied. It is probable that this improvement in accuracy resulted from the greater joint stability due to muscle loading, which allowed the experimenter to concentrate more closely on achieving the desired target, and less on maintaining joint reduction in the desired level of abduction. Although these findings were not able to demonstrate a significant difference between manual and feedback aided assessments, use of the instrumented humeral rod had no negative effects on achieving

predefined load endpoints and thus may represent a useful tool in improving the consistency of biomechanical assessments.

Evaluation of each of the major improvements to the existing simulator system was undertaken to assess their performance and perhaps more importantly, to ensure that their function did not unduly affect joint function and kinematics. The results of this evaluation process, taken together, have shown that the systems achieved improved accuracy and repeatability in comparison to existing systems and methodologies, which rely on the experience of the experimenter. As well, the systems developed herein were not found to have undesirable effects on shoulder function nor, most importantly, on the articular kinematics of the glenohumeral joint when it is positioned and constrained by the humeral guide system. Therefore, these systems are likely to improve the validity of biomechanical and clinical assessments performed on this simulator and thus the value of the results obtained. These new systems will also improve the simulator's overall ability to detect differences between various testing conditions and reduce the sample size required to address questions of interest.

2.5 References

Ackland, D. C., Pak, P., Richardson, M., & Pandy, M. G. (2008). Moment arms of the muscles crossing the anatomical shoulder. *Journal of Anatomy, 213*(4), 383-390. doi:10.1111/j.1469-7580.2008.00965.x

Debski, R. E., Wong, E. K., Woo, S. L., Sakane, M., Fu, F. H., & Warner, J. J. (1999). In situ force distribution in the glenohumeral joint capsule during anterior-posterior loading. *Journal of Orthopaedic Research : Official Publication of the Orthopaedic Research Society, 17*(5), 769-776. doi:10.1002/jor.1100170523

Harryman, D. T.,2nd, Sidles, J. A., Clark, J. M., McQuade, K. J., Gibb, T. D., & Matsen, F. A.,3rd. (1990). Translation of the humeral head on the glenoid with passive glenohumeral motion. *The Journal of Bone and Joint Surgery. American Volume, 72*(9), 1334-1343.

Huffman, G. R., Tibone, J. E., McGarry, M. H., Phipps, B. M., Lee, Y. S., & Lee, T. Q. (2006). Path of glenohumeral articulation throughout the rotational range of motion in a thrower's shoulder model. *The American Journal of Sports Medicine, 34*(10), 1662-1669.

Inman, V. T., & Abbott, L. C. (1944). Observations on the function of the shoulder joint. *The Journal of Bone & Joint Surgery, 26*(1), 1-30.

Itoi, E., Kuechle, D. K., Morrey, B., & An, K. (1993). Stabilising function of the biceps in stable and unstable shoulders. *Journal of Bone & Joint Surgery, British Volume, 75*(4), 546-550.

Itoi, E., Motzkin, N. E., Morrey, B. F., & An, K. N. (1994). Contribution of axial arm rotation to humeral head translation. *The American Journal of Sports Medicine, 22*(4), 499-503.

Itoi, E., Morrey, B. F., & An, K. (2009). Biomechanics of the shoulder. In C. A. J. Rockwood, F. A. Matsen 3rd, C. J. Wirth & S. B. Lippitt (Eds.), *The shoulder* (4th ed., pp. 213-266). Philadelphia: Saunders Elsevier.

Kedgley, A., E. (2004). *Design and development of a shoulder testing simulator.* London, Ont.: Faculty of Graduate Studies, University of Western Ontario.

Kedgley, A. E., Mackenzie, G. A., Ferreira, L. M., Drosdowech, D. S., King, G. J., Faber, K. J., & Johnson, J. A. (2007). The effect of muscle loading on the kinematics of in vitro glenohumeral abduction. *Journal of Biomechanics, 40*(13), 2953-2960. doi:10.1016/j.jbiomech.2007.02.008

Lin, T., Javidan, P., McGarry, M. H., Gonzalez-Lomas, G., Limpisvasti, O., & Lee, T. Q. (2013). Glenohumeral contact pressure in a simulated active compression test using cadaveric shoulders. *Journal of Shoulder and Elbow Surgery, 22*(3), 365-374.

Walker, M. R., & Dickey, J. P. (2007). New methodology for multi-dimensional spinal joint testing with a parallel robot. *Medical & Biological Engineering & Computing, 45*(3), 297-304.

Warner, J. J., Deng, X. H., Warren, R. F., & Torzilli, P. A. (1992). Static capsuloligamentous restraints to superior-inferior translation of the glenohumeral joint. *The American Journal of Sports Medicine, 20*(6), 675-685.

Wellmann, M., Petersen, W., Zantop, T., Herbort, M., Kobbe, P., Raschke, M. J., & Hurschler, C. (2009). Open shoulder repair of osseous glenoid defects: Biomechanical effectiveness of the latarjet procedure versus a contoured structural bone graft. *The American Journal of Sports Medicine, 37*(1), 87-94. doi:10.1177/0363546508326714

Yu, J., McGarry, M. H., Lee, Y. S., Duong, L. V., & Lee, T. Q. (2005). Biomechanical effects of supraspinatus repair on the glenohumeral joint. *Journal of Shoulder and Elbow Surgery / American Shoulder and Elbow Surgeons ...[Et Al.], 14*(1 Suppl S), 65S-71S. doi:10.1016/j.jse.2004.09.019

CHAPTER 3 – The Effect of the Conjoined Tendon of the Short Head of the Biceps and Coracobrachialis on Shoulder Stability & Kinematics during *In-Vitro* Simulation

OVERVIEW

This chapter demonstrates the passive capabilities of the simulator to evaluate basic biomechanical phenomenon. Specifically, this study investigates the biomechanical effects of a secondary shoulder muscle. Existing simulators have actuated the rotator cuff and deltoid, however, the effects of secondary muscles, such as the short head of the biceps and coracobrachialis (SH&C) are not well understood. This study investigated the effect of SH&C tension at four loading levels: 0, 5, 10, 15 N. Outcomes included glenohumeral stiffness for anterior loading and extension range of motion (ROMs). Four joint configurations were tested: adduction and 90^{o} abduction, each in neutral and external rotation. Increasing SH&C load resulted in a significant trend of increased stiffness across all joint configurations (p=0.008). However, only loading in neutral rotation produced significant comparisons (10 & 15 N compared to 0 N: p=0.038 & p=0.043). An insignificant trend was observed between increases in SH&C load and decreased extension ROM (p=0.065). Thus, the SH&C provides a stabilizing barrier effect, but only in configurations when it wraps directly anterior to the humeral head. Thus, SH&C may be important to improving the physiologic accuracy of in-vitro simulation. These results also illustrate the simulator's ability to elucidate the effects of basic biomechanical phenomena.[5]

---

[5] A version of this work has been published: Giles, J. W., Boons, H. W., Ferreira, L. M., Johnson, J. A., & Athwal, G. S. (2011). The effect of the conjoined tendon of the short head of the biceps and coracobrachialis on shoulder stability and kinematics during in-vitro simulation. *Journal of Biomechanics, 44*(6), 1192-1195. doi:10.1016/j.jbiomech.2011.02.012

3.1 Introduction

The use of complex simulators for the measurement of *in-vitro* glenohumeral joint stability and kinematics under active loading is increasingly prevalent. Existing simulators have commonly actuated major muscle groups such as the rotator cuff and deltoids. However, there is no agreed upon set of secondary muscles, that are critical for accurate replication of joint mechanics, such as the biceps brachii, coracobrachialis, pectoralis major, and latissimus dorsi (Wellmann et al., 2009; Schamblin et al., 2009; McMahon et al., 2003; Kedgley et al., 2007). Before a definitive set can be defined, the biomechanical effects and importance of each of these secondary muscles must be assessed.

As discussed in Section 1.2.3.1, the conjoined tendon of the short head of the biceps and coracobrachialis (SH&C) crosses the glenohumeral joint anterior to the humeral head (HH), providing a barrier effect, that increases joint stiffness, with the joint in abduction (Itoi et al., 1993). Although the SH&C has gained surgical importance in treating complex instability (Armitage et al., 2010; Wellmann et al., 2009), its role during *in-vitro* replication of *in-vivo* conditions has not been studied. Hence, we investigated the effect of SH&C loading on glenohumeral joint stiffness and kinematics in various joint positions. We hypothesized that the passive capabilities described in Chapter 2 would enable studies performed on the simulator to identify the conditions in which the SH&C has a significant effect on shoulder biomechanics. More specifically, we hypothesized that SH&C loading contributes a significant stiffening effect to the glenohumeral joint, and that loading of this muscle group during extension will decrease anterior humeral head translations to levels similar to those of the *in-vivo* physiologic state, without unduly limiting shoulder range of motion (ROM).

3.2 Methods

3.2.1 Simulator Configuration

Six specimens (average age: 76.7 yrs) were tested following visual and radiographic examination for any evidence of joint degeneration, injury, or prior surgery. The

specimens were sectioned at the mid-humerus and the skin and subcutaneous tissues were dissected away. The intra-medullary humeral rod – described in Section 2.2.6 – instrumented with a six degree-of-freedom load cell (Mini45, ATI-IA, NC) and optical trackers (Optotrak Certus, NDI, ON), was cemented into the sectioned humeral shaft, while the distal portion was left free to mate with the simulator. To provide a reference for rotation, a transverse axis on the humeral rod was aligned with the anatomic transepicondylar axis of the elbow using the relationship between the transepicondylar axis and the biceps groove at the level of the surgical neck as described by Balg et al. (Balg, Boulianne, & Boileau, 2006).

Humeral and scapular digitizations were taken with respect to the bone-affixed optical markers to create an International Society of Biomechanics (ISB) Euler rotation sequence (Wu et al., 2005). The functional glenohumeral joint center was determined from kinematic recordings using Woltring's algorithm (Ehrig, Taylor, Duda, & Heller, 2006; Monnet, Desailly, Begon, Vallee, & Lacouture, 2007; Woltring, 1990). The scapula was then cemented to the simulator – described in Section 2.2.3 and seen in Figure 3.1– in 10° of anterior tilt as measured between the superior axis of the ISB scapular coordinate system and the vertical surface of the simulator's main plate. Ten degrees of anterior tilt was drawn from the literature as an average value of scapular tilt with the arm in adduction, and this was maintained during abducted testing as the literature also indicates that scapular tilt is minimal up to 90° of humerothoracic rotation (Forte, de Castro, de Toledo, Ribeiro, & Loss, 2009; McClure, Michener, & Karduna, 2006). At the completion of testing, the joint was further dissected to gain access to the joint surfaces, and digitizations at the superior, inferior, anterior and posterior aspects of the glenoid rim were recorded and used to create a separate glenoid coordinate system coincident with the intact glenohumeral joint center. This coordinate system was used in *post-hoc* analyses to determine glenohumeral joint translations.

As discussed in Section 2.4, the simulator achieved highly repeatable joint configurations without affecting the true unconstrained motion of the natural glenohumeral joint by positioning the humeral rod using a spherical bearing, which allowed free glenohumeral translation and rotation. As well, nine muscle groups were loaded along physiologically

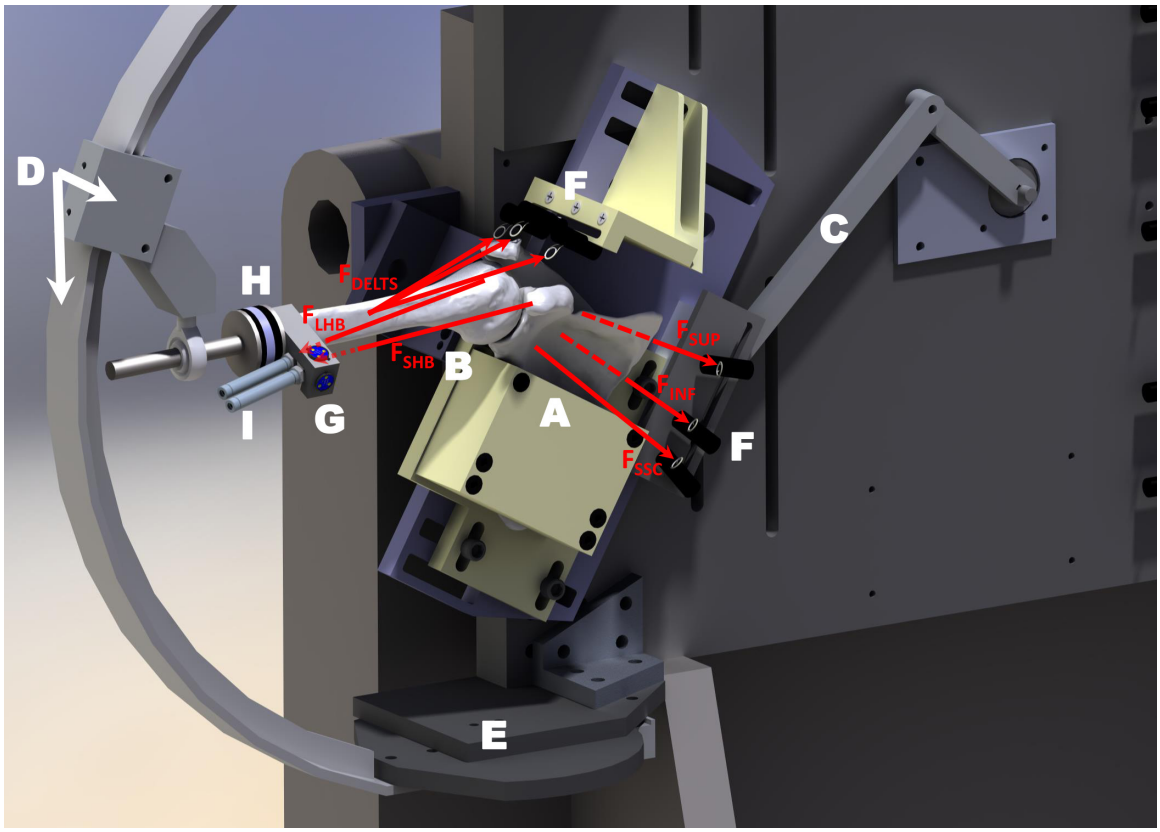

Figure 3.1: Rendering of the *in-vitro* shoulder simulator.
Note that mounted specimen has soft tissues removed for clarity. The overlaid red arrows indicate the loading vectors for each of the muscle groups (F_{DELTS} – three Deltoid heads, F_{SUP} – Supraspinatus, F_{INF} – Infraspinatus & Teres Minor, F_{SSC} – Subscapularis, F_{LHB} – Long Head of Biceps, F_{SHB} – Conjoint tendon of the Short Head of Biceps). The simulator is capable of physiologically orienting the scapula and glenohumeral joint in 4 degrees of freedom (DOF). (A) Potted scapula specimen (with soft tissues omitted for clarity); (B) humerus (with soft tissues omitted for clarity); (C) computer controlled scapular elevation mechanism which achieves repeatable positioning (added during development described in Chapter 5 which occurred concurrently with testing in Chapter 4); (D) glenohumeral abduction guide arc and slider; (E) glenohumeral plane of elevation adjustment plate; (F) low friction deltoid and rotator cuff guide system which routes cables to pneumatic actuators; (G), 6 DOF tracking markers; (H) cemented humeral rod with interposed 6 DOF load cell; and (I) miniature pneumatic actuators used to separately load the long head of the biceps and the conjoint group.

accurate lines-of-action using the simulator's low friction guide system and low friction computer controlled pneumatic actuators (Airpel E16, Airpot Co., Norwalk, CT). Sutures in each of the primary muscle groups were loaded as follows: the supraspinatus, infraspinatus and teres minor, and subscapularis (7.5 N); anterior, middle, and posterior deltoids (5 N) (Wellmann et al., 2009). The ratios between these loads and their specific magnitudes were drawn from previous literature which utilized similar protocols (Wellmann et al., 2009) as well as literature which investigated the effect of joint load magnitude on glenohumeral joint stability (Lippitt et al., 1993). Although the precise glenohumeral-to-scapulothoracic rhythm – and how it varies across abduction – remains controversial, the traditional 2:1 ratio described by McQuade *et al.* was used in this study (McQuade & Smidt, 1998).

This simulator enables loads to be applied to the long head of the biceps and SH&C which are considered secondary to the muscles traditionally loaded during *in-vitro* simulation (*i.e.* supraspinatus, infraspinatus, teres minor, subscapularis, three deltoid heads). Although the long head of the biceps is described as a secondary muscle, it is well reported as an important shoulder stabilizer (Burkart et al., 2003; Pagnani et al., 1996). Therefore, the long head of biceps was loaded (10 N) in order to ensure that its normal stabilizing role was not transferred to the SH&C (Figure 3.2). To assess the effect of the SH&C at various levels of tension, the suture was loaded to 0, 5, 10 and 15 N (Wellmann et al., 2009).

3.2.2 Stiffness & Kinematics

Two glenohumeral joint configurations were used to assess stability and ROM: (1) adduction (Add: 0° abduction in the scapular plane), and (2) abduction (Abd: 60° glenohumeral abduction in the scapular plane with 30° scapulothoracic elevation). Stability was quantified using glenohumeral joint stiffness (N/mm). Stiffness was calculated by passively applying an anteroinferiorly quasi-static load – which was directed through the center of the humeral head to limit the application of an associated moment – and dividing it by the magnitude of humeral translation relative to the glenoid (Figure 3.3). This produced a linear measure of the overall joint stiffness which was

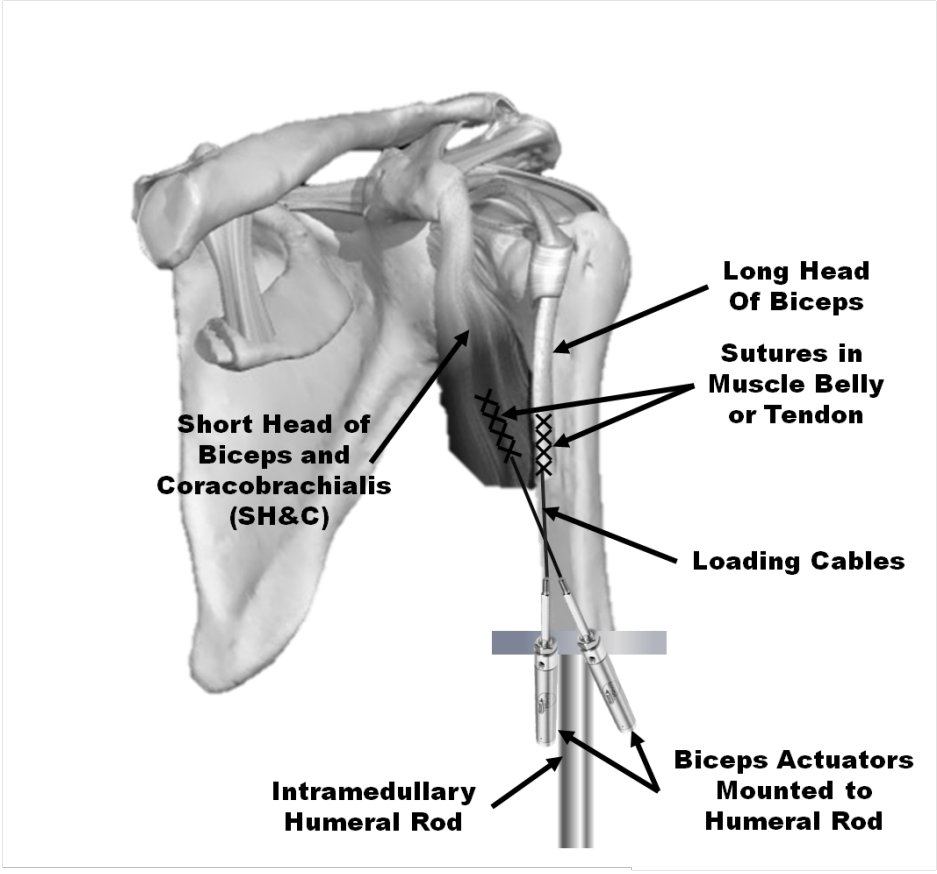

Figure 3.2: Schematic of shoulder specimen testing configuration.
Specimen's humerus is resected midshaft and a steel intramedullary rod is inserted. This rod allows for the mounting of two miniature pneumatic actuators used to load the SH&C and Long Head of the Biceps, with physiologic lines of action, as indicated. Each muscle was loaded by a single actuator connected via a suture which was passed through the musculotendinous junction using a running locking stitch. Image of shoulder anatomy provided by Primal Pictures (ww.primalpictures.com).

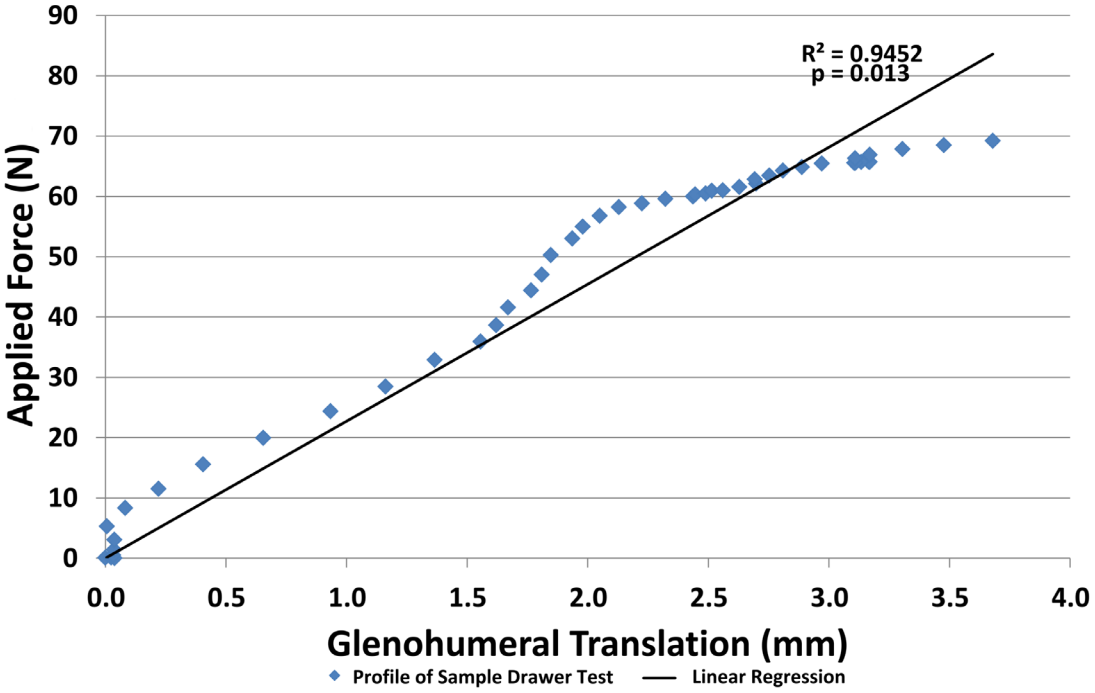

Figure 3.3: Sample load versus displacement profile for drawer test.
Also note the linear regression line which exhibits the high linearity (R^2=0.95, p=0.013) of the joint's response to the application of a quasi-static external load.

roughly linear across the trial but did exhibit some degree of non-linearity as applied load increased. Seventy (70) N was chosen as the maximum load during this test by first consulting the literature and then through pilot testing. *In-vitro* studies previously described in the literature used applied loads of between 20 and 150 N (Alberta et al., 2006; Burkart et al., 2003; Itoi et al., 2000; Itoi et al., 1994; Lee et al., 2001; Wellmann et al., 2009) and *in-vivo* testing which used 100 N loading (McQuade and Murthi, 2004; McQuade et al., 1999). Due to this wide range of values, pilot testing was performed in which a load cell was used to determine the average maximum force, over multiple trials, applied by an experienced shoulder surgeon (GSA[6]) performing a standard drawer test. Maximum humeral translation was defined as the magnitude of displacement at the time of maximum force application.

Stiffness was evaluated in both neutral rotation (defined as epicondylar axis parallel to the coronal body plane) and maximal external rotation. Maximal external rotation was defined as the rotation accompanying application of a predefined axial torque (±0.8 Nm). This torque was determined, as the average of repeated trials, by the same experienced shoulder surgeon (GSA) rotating the humerus until reaching a resistance consistent with clinical evaluation.

Real-time feedback of the load applied to the glenohumeral joint was achieved using an uni-axial load cell (Model 34, Honeywell, Golden Valley, MN) while glenohumeral kinematics and forces were monitored during testing using the optical tracking markers and intra-medullary load cell described above.

Internal-external rotation ROM was quantified as the magnitude of rotation permitted by the glenohumeral joint when an external axial rotation torque of 0.8 Nm was applied. This torque criterion was selected as it represented the load recorded during repeated blinded trials of a standard clinical assessment of axial rotation as performed by an experienced shoulder surgeon (GSA). The extension ROM was recorded in abduction and 60° of external rotation while tracking HH translation. The end range of extension was

---

[6] GSA- Dr. George S. Athwal MD FRCSC

determined by an experienced shoulder surgeon (GSA), as the point at which soft tissue tension limited extension, as in clinical evaluations.

3.2.3 Outcome Variables & Statistical Methods

Stability was quantified in terms of glenohumeral joint stiffness (N/mm), while ROM was reported in degrees. For internal-external rotation, this value was taken as the rotation from the maximum internal to the maximal external rotation position, while horizontal extension ROM was quantified as the magnitude of humeral rotation about the scapula's superior axis posterior to the scapular plane**.** A three-way ANOVA was performed for anterior translation tests across all configurations using SPSS 17.0 (SPSS Inc., Chicago, IL). The factors were: abduction (0° or 90°), humeral rotation (neutral or external), and SH&C load (0, 5, 10, 15 N). One-way ANOVAs and pair-wise comparison procedures were performed for all outcome variables at each tested shoulder configuration. The dependent variables were internal/external rotation ROM, extension ROM, HH translation and joint stiffness.

3.3 Results

Increasing SH&C load resulted in a significant trend of increased glenohumeral stiffness across the average of all joint configurations ($p=0.008$) (Figure 3.4). With the arm abducted and neutrally rotated, 0 N SH&C loading resulted in a stiffness of 10.4±5.3 N/mm, which was less than the 5, 10 and 15 N cases by 8.9±6.1 N/mm, 10.8±5.9 N/mm and 11.2±6.2 N/mm, respectively. However, the difference at 5 N was not statistically significant ($p=0.093$, $p=0.038$ and, $p=0.043$, respectively) (Figure 3.5). There was no significant difference between 10 and 15 N cases ($p=1.000$). There were no significant differences between the 0 N SH&C loading case and the 5-15 N cases for all remaining joint configurations ($p\geq0.228$) (Figure 3.5).

Internal/external rotation ROM for both abduction levels (0°&90°), exhibited a nearly significant trend of decreasing motion with increasing SH&C loading ($N=5$, $p=0.069$). One-way ANOVA of each abduction level revealed no significant trends ($N=5$, $p\geq0.176$) (Figure 3.6). Internal/external rotation kinematics were not measured in one specimen due

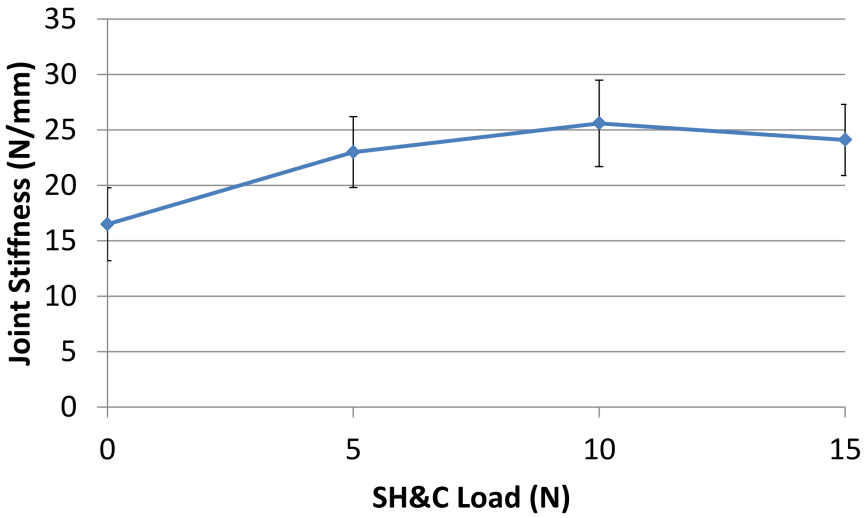

Figure 3.4: Joint stiffness for varying SH&C load.
Effect of conjoined tendon loading on glenohumeral joint stiffness (mean ± 1 standard deviation) for applied anterior load across all joint configurations. Joint stiffness showed a significant, increasing trend (p=0.008) in abducted and adducted loading cases with the humerus in neutral or external rotation; however, no pairwise comparison was significantly different.

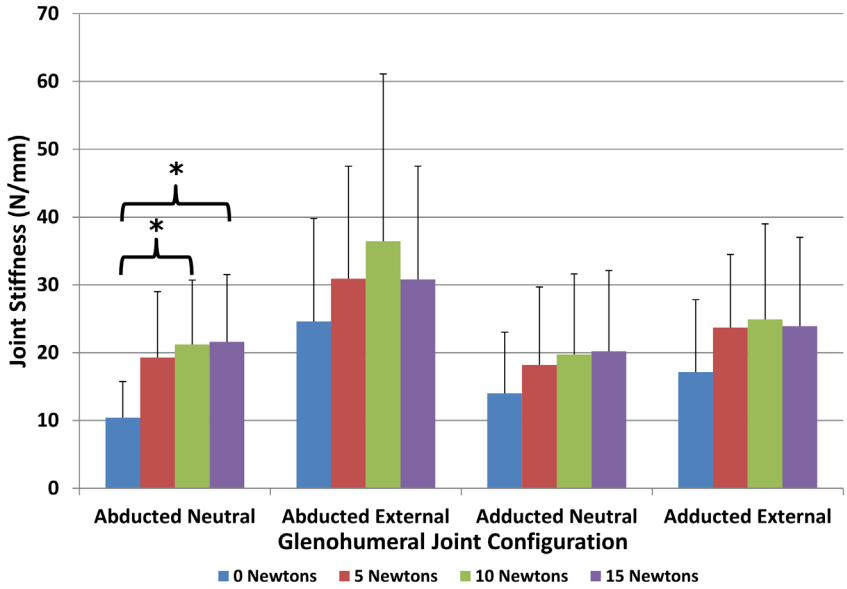

Figure 3.5: Joint stiffness for varying SH&C load and joint configuration.
Effect of conjoined tendon loading on glenohumeral joint stiffness (mean + 1 standard deviation) for an applied anterior load with the joint in four different configurations.

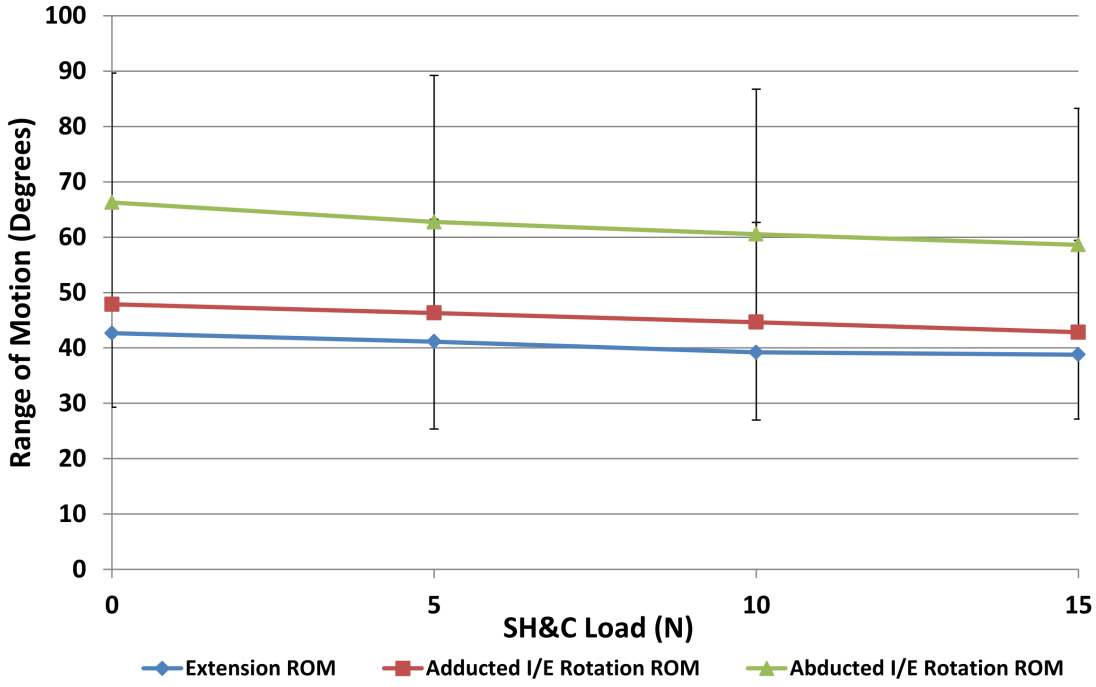

Figure 3.6: Ranges of motion for varying SH&C load.
The relationship between the magnitude of conjoined tendon load and range of motion (mean and 1 standard deviation) is displayed. This is shown for extension (diamond marker) and internal/external rotation for two test configurations (triangle marker: abducted ROM, square marker: adducted ROM). In all configurations, the ROM tended to decrease with increased SH&C load, with the trend in extension approaching significance ($p=0.065$) but not in internal/external rotation ($p \geq 0.176$). Note that for clarity each data series is shown with only a plus or minus error bar.

to an equipment failure. There was a nearly significant trend of decreased extension with increasing SH&C load ($p=0.065$) (Figure 3.6). However, no comparisons between SH&C loading cases approached significance (0.2-4.1°, $p=0.158$-1.000). There was no effect of SH&C load on maximal anterior-posterior HH translation during extension ($p=0.110$). No SH&C load permitted significantly different translations from any other case, and all translations were <1.5 mm.

3.4 Discussion

The importance of particular muscles in accurate replication of *in-vivo* conditions during *in-vitro* shoulder testing using complex simulators is not fully understood. Increasing SH&C load was found to increase joint stiffness across all test configurations. This trend indicates that the SH&C plays a role in providing glenohumeral stability against externally applied anterior loads. This agrees with Itoi et al. (1993), who found that increasing short head load permitted decreased anterior HH translations.

Additionally, abducted neutrally rotated translation results for 0 N of SH&C loading agree with those of McQuade et al. (1999), who assessed *in-vivo* translations using a clinical anterior drawer test with the subject's shoulder relaxed. McQuade observed translations of ~8 mm with the application of a 70 N load, corresponding to a stiffness of ~8.8 N/mm using our quantification method. McQuade and Murthi (2004) observed increased joint stiffness accompanying isometric muscle contraction, which agrees with our findings. However, quantitative comparison with these results is difficult due to the unknown amount of muscle contraction caused by this *in-vivo* study's loading protocol.

Translations during abduction, neutral rotation indicate a minimum SH&C load required to achieve a significant increase in stiffness and a maximum after which stiffness will not increase significantly further. A 5 N load was not sufficient to bring the tissues fully taut and achieve the expected barrier effect, but 10 N did cause a significant increase in stiffness. However, increasing SH&C load to 15 N did not provide a further increase in stiffness; indicating that the tendon is fully tensioned beginning at 10 N. This agrees with McQuade and Murthi (2004), who found that increased *in-vivo*, isometric muscle contraction did not have a greater stiffening effect than mild contraction. This suggests

that the SH&C be loaded with 10 N in biomechanical simulations, as this was the first loading value to have a significant stiffening effect. This load is greater than those applied to the rotator cuff muscles in this study, which may seem to contradict its secondary classification; however, the rotator cuff loads were chosen solely to achieve joint reduction and replicate resting tone. Dynamic motion of the shoulder through rotator cuff and deltoid loading would require much higher loads than the 10 N SH&C force required to initiate its stabilizing effect.

Comparisons can be drawn between our results for the adducted, neutrally rotated and 0 N SH&C loading case and those of Harryman, who recorded *in-vivo* glenohumeral translations while performing the clinical anterior drawer test on subject's adducted shoulder (Harryman et al., 1992). This comparison revealed levels of end-state translation similar to our own.

The adducted, neutrally and externally rotated, as well as the abducted, externally rotated configurations, showed no significant differences in joint stiffness. This lack of effect was due to the position of the SH&C relative to the HH, which agrees with previous observations by Itoi et al. (1993). In both adducted configurations, the SH&C was observed to be positioned medial to the center of the glenohumeral joint and thus could not provide a barrier effect. Similarly, the abducted, externally rotated configuration caused the SH&C to sit primarily on the lateral aspect of the HH.

The biomechanical hypothesis to be investigated in this study was that SH&C loading would affect shoulder kinematics by decreasing anterior HH translations during extension. However, no loading level significantly affected HH translations, which were consistently less than 1.5 mm. This agrees with Harryman et al. (1992) who recorded 0±3 mm of *in-vivo* HH translation during a clinical apprehension test with the shoulder relaxed. The labrum and rotator cuff were intact throughout our testing protocol. We believe that these structures alone provided effective joint reduction during extension (Hess, 2000). Despite this, we expect SH&C to have a significant stabilizing effect during extension in joints with anterior instability because it wraps directly across the anterior

HH. As hypothesized, SH&C loading did not limit extension or internal/external rotation, similar to the SH&C's expected effect *in-vivo*.

Some simplifying assumptions were utilized and can be counted as limitations of this study. One weakness is our modeling of each muscle with a single line-of-action which would not completely replicate the physiologic state. Additionally, in the case of the three deltoid groups, the muscle bellies were not loaded as this would have required suturing the tissues proximally resulting in impingement with the deltoid guides on the acromion. Instead, sutures were inserted directly into the tendinous insertion on the deltoid tuberosity. Thus, we did not replicate any barrier effects resulting from deltoid tensioning which must be viewed as a limitation of this testing setup. Some variability in the translational loading rate, which would affect the stiffness properties of soft tissues, did exist and was a weakness of this study; however, this was minimized by the experimenter's clinical evaluation experience. Related to this, the joint stiffness was expressed as a single value intimating that it is a constant value across load application; however, as demonstrated in Figure 3.3 a joint's stiffness does exhibit some non-linearity. Therefore, the values presented here can only be used as an overall measure while further data would be required to fully understand a joint's stiffness profile. A final weakness was the use of only six specimens despite some secondary outcomes continuing to increasingly approach significance; however, their changes were not physiologically meaningful.

Our findings demonstrate that the SH&C does cause an anterior stabilizing effect by providing a soft tissue barrier which stiffens the glenohumeral joint, but only in configurations when it wraps directly anterior to the HH. However, this effect did not reduce the already small HH translations which accompany extension. Additionally, in no case did SH&C loading cause limitation of the joint's ROM in extension or internal/external rotation. Thus, SH&C loading does play a role in the intact stability of the glenohumeral joint and may be an important means to increase the physiological accuracy of *in-vitro* simulation. Additionally, we suspect the importance of replicating this structure will be increased when studying shoulder instability conditions such as labral tears and glenoid fractures. Finally, the data presented here demonstrates that the

simulator approximates physiologic conditions and experimental tests whose repeatability are sufficient to clarify the biomechanical effects of discrete structures such as the SH&C.

3.5 References

Alberta, F. G., ElAttrache, N. S., Mihata, T., McGarry, M. H., Tibone, J. E., & Lee, T. Q. (2006). Arthroscopic anteroinferior suture plication resulting in decreased glenohumeral translation and external rotation: Study of a cadaver model. *The Journal of Bone & Joint Surgery, 88*(1), 179-187.

Armitage, M. S., Faber, K. J., Drosdowech, D. S., Litchfield, R. B., & Athwal, G. S. (2010). Humeral head bone defects: Remplissage, allograft, and arthroplasty. *Orthopedic Clinics of North America, 41*(3), 417-425.

Balg, F., Boulianne, M., & Boileau, P. (2006). Bicipital groove orientation: Considerations for the retroversion of a prosthesis in fractures of the proximal humerus. *Journal of Shoulder and Elbow Surgery / American Shoulder and Elbow Surgeons ...[Et Al.], 15*(2), 195-198. doi:10.1016/j.jse.2005.08.014

Burkart, A., Debski, R. E., Musahl, V., & McMahon, P. J. (2003). Glenohumeral translations are only partially restored after repair of a simulated type II superior labral lesion. *The American Journal of Sports Medicine, 31*(1), 56-63.

Ehrig, R. M., Taylor, W. R., Duda, G. N., & Heller, M. O. (2006). A survey of formal methods for determining the centre of rotation of ball joints. *Journal of Biomechanics, 39*(15), 2798-2809. doi:10.1016/j.jbiomech.2005.10.002

Forte, F. C., de Castro, M. P., de Toledo, J. M., Ribeiro, D. C., & Loss, J. F. (2009). Scapular kinematics and scapulohumeral rhythm during resisted shoulder abduction--implications for clinical practice. *Physical Therapy in Sport : Official Journal of the Association of Chartered Physiotherapists in Sports Medicine, 10*(3), 105-111. doi:10.1016/j.ptsp.2009.05.005; 10.1016/j.ptsp.2009.05.005

Harryman II, D. T., Sidles, J. A., Harris, S. L., & Matsen III, F. A. (1992). Laxity of the normal glenohumeral joint: A quantitative in vivo assessment. *Journal of Shoulder and Elbow Surgery, 1*(2), 66-76.

Hess, S. (2000). Functional stability of the glenohumeral joint. *Manual Therapy, 5*(2), 63-71.

Itoi, E., Lee, S., Berglund, L. J., Berge, L. L., & An, K. (2000). The effect of a glenoid defect on anteroinferior stability of the shoulder after bankart repair: A cadaveric study*. *The Journal of Bone & Joint Surgery, 82*(1), 35-46.

Itoi, E., Kuechle, D. K., Newman, S. R., Morrey, B. F., & An, K. N. (1993). Stabilising function of the biceps in stable and unstable shoulders. *The Journal of Bone and Joint Surgery. British Volume, 75*(4), 546-550.

Itoi, E., Newman, S. R., Kuechle, D. K., Morrey, B. F., & An, K. N. (1994). Dynamic anterior stabilisers of the shoulder with the arm in abduction. *The Journal of Bone and Joint Surgery. British Volume, 76*(5), 834-836.

Kedgley, A. E., Mackenzie, G. A., Ferreira, L. M., Drosdowech, D. S., King, G. J., Faber, K. J., & Johnson, J. A. (2007). The effect of muscle loading on the kinematics of in vitro glenohumeral abduction. *Journal of Biomechanics, 40*(13), 2953-2960.

Lee, T. Q., Black, A. D., Tibone, J. E., & McMahon, P. J. (2001). Release of the coracoacromial ligament can lead to glenohumeral laxity: A biomechanical study. *Journal of Shoulder and Elbow Surgery, 10*(1), 68-72.

Lippitt, S. B., Vanderhooft, J. E., Harris, S. L., Sidles, J. A., Harryman, D. T.,2nd, & Matsen, F. A.,3rd. (1993). Glenohumeral stability from concavity-compression: A quantitative analysis. *Journal of Shoulder and Elbow Surgery / American Shoulder and Elbow Surgeons ...[Et Al.], 2*(1), 27-35. doi:10.1016/S1058-2746(09)80134-1; 10.1016/S1058-2746(09)80134-1

McClure, P. W., Michener, L. A., & Karduna, A. R. (2006). Shoulder function and 3-dimensional scapular kinematics in people with and without shoulder impingement syndrome. *Physical Therapy, 86*(8), 1075-1090.

McMahon, P. J., Chow, S., Sciaroni, L., Yang, B. Y., & Lee, T. Q. (2003). A novel cadaveric model for anterior-inferior shoulder dislocation using forcible apprehension positioning. *Journal of Rehabilitation Research and Development, 40*(4), 349-360.

McQuade, K. J., & Murthi, A. M. (2004). Anterior glenohumeral force/translation behavior with and without rotator cuff contraction during clinical stability testing. *Clinical Biomechanics, 19*(1), 10-15.

McQuade, K. J., Shelley, I., & Cvitkovic, J. (1999). Patterns of stiffness during clinical examination of the glenohumeral joint. *Clinical Biomechanics, 14*(9), 620-627.

McQuade, K. J., & Smidt, G. L. (1998). Dynamic scapulohumeral rhythm: The effects of external resistance during elevation of the arm in the scapular plane. *The Journal of Orthopaedic and Sports Physical Therapy, 27*(2), 125-133

Monnet, T., Desailly, E., Begon, M., Vallee, C., & Lacouture, P. (2007). Comparison of the SCoRE and HA methods for locating in vivo the glenohumeral joint centre. *Journal of Biomechanics, 40*(15), 3487-3492. doi:10.1016/j.jbiomech.2007.05.030

Pagnani, M. J., Deng, X., Warren, R. F., Torzilli, P. A., & O'Brien, S. J. (1996). Role of the long head of the biceps brachii in glenohumeral stability: A biomechanical study in cadavera. *Journal of Shoulder and Elbow Surgery, 5*(4), 255-262.

Schamblin, M., Gupta, R., Yang, B. Y., McGarry, M. H., McMaster, W. C., & Lee, T. Q. (2009). In vitro quantitative assessment of total and bipolar shoulder arthroplasties:

A biomechanical study using human cadaver shoulders. *Clinical Biomechanics, 24*(8), 626-631.

Wellmann, M., Petersen, W., Zantop, T., Herbort, M., Kobbe, P., Raschke, M. J., & Hurschler, C. (2009). Open shoulder repair of osseous glenoid defects: Biomechanical effectiveness of the latarjet procedure versus a contoured structural bone graft. *The American Journal of Sports Medicine, 37*(1), 87-94. doi:10.1177/0363546508326714; 10.1177/0363546508326714

Woltring, H. (1990). Data processing and error analysis. In P. Berne, & A. Capozzo (Eds.), *Biomechanics of human movement, applications in rehabilitation, sport and ergonomics.* (pp. 203-237). Worthington, OH: Berlec Corporation.

Wu, G., Van der Helm, Frans CT, Veeger, H., Makhsous, M., Van Roy, P., Anglin, C., . . . Wang, X. (2005). ISB recommendation on definitions of joint coordinate systems of various joints for the reporting of human joint motion—Part II: Shoulder, elbow, wrist and hand. *Journal of Biomechanics, 38*(5), 981-992.

CHAPTER 4 – The Bristow-Latarjet: Why These Techniques Should Not Be Considered Synonymous

OVERVIEW

This chapter presents the application of the shoulder simulator to the investigation of a clinical question of interest. Recurrent shoulder instability is commonly associated with glenoid bone defects. As such, coracoid transfer procedures, like the Bristow and Latarjet, are frequently used to address these bone deficiencies. Despite the frequent synonymous labeling of these transfers as the 'Bristow-Latarjet', their true equivalence has not been demonstrated; therefore, our purpose was to compare the biomechanical effects of these two procedures. Eight cadaveric specimens were tested in their intact state, and following both Bristow and Latarjet reconstructions for three bone deficiency levels. At each condition, anterior joint stiffness and dislocation were assessed in adduction (Add) and abduction (Abd) with neutral (NR) and external rotation (ER). Substantially greater joint stiffness/stability occurred following the Latarjet, as compared to the Bristow, for 15 and 30% glenoid bone loss conditions. During instability testing, 3 more specimens dislocated following Bristow reconstruction of a 15% defect and 5 more with a 30% defect as compared with the Latarjet. The Bristow and Latarjet procedures are not equivalent in terms of their effects on glenohumeral joint stiffness and stability in cases of glenoid bony deficiency. These findings have also helped to demonstrate the simulator's ability to address clinical questions such as the purported equivalence of two structurally similar procedures[7].

---

[7] A version of this work has been accepted for journal publication: Giles, J.W., Degen, R.M., Johnson, J.A., & Athwal, G.S. (Accepted Feb 2014). The Bristow-Latarjet: Why these techniques should not be considered synonymous. Journal of Bone and Joint Surgery.

4.1 Introduction

Patients with recurrent anterior shoulder instability and associated glenoid bone deficiency pose a complex problem for orthopedic surgeons attempting to select the optimal surgical treatment. This is especially true when this deficiency comprises a substantial portion of the glenoid width, making selection of the optimal surgical treatment particularly difficult as isolated soft-tissue repairs have exhibited failure rates as high as 56%-67% (Burkhart & De Beer, 2000; Tauber, Resch, Forstner, Raffl, & Schauer, 2004). Itoi *et al.* found that defects as small as 21% of the glenoid width require significantly less translational force to produce humeral head subluxation (Itoi, Lee, Berglund, Berge, & An, 2000) and consequently recommended osseous reconstruction. Various techniques have been proposed for osseous reconstruction, including iliac crest autograft (Montgomery et al., 2005; Warner, Gill, O'hollerhan, Pathare, & Millett, 2006), allograft reconstruction, and coracoid transfer. Biomechanical investigations by Wellmann *et al.* (Wellmann et al., 2009) and Giles *et al.* (Giles et al., 2013), however, have shown that coracoid transfer procedures outperform other reconstructive options due to the additive dynamic stabilizing 'sling' effect produced by the repositioned conjoint tendon. These findings support the thought that coracoid transfer represents a favorable option for instability-related glenoid defects, with some even proposing its use in the treatment of isolated capsulolabral tears (Helfet, 1958; Latarjet, 1954).

Coracoid transfer has been described using multiple techniques, with the most common being the Bristow procedure and the Latarjet procedure, but with little consensus on which is optimal. While the Bristow procedure transfers only the tip of the coracoid such that the resected surface contacts the glenoid vault (Helfet, 1958), the Latarjet procedure transfers the entire horizontal pillar such that the inferior surface of the coracoid contacts the vault (Figure 4.1) (Latarjet, 1954). Despite the frequent synonymous labeling of these coracoid transfers as the Bristow-Latarjet coracoid transfer (Boileau, Mercier, & Old, 2010; Boileau, Mercier, Roussanne, Thelu, & Old, 2010; Emami, Solooki, Meshksari, & Vosoughi, 2011; Griesser, Harris, McCoy, Hussain, Jones, Bishop, & Miniaci, 2013a; Griesser, Harris, McCoy, Hussain, Jones, Bishop, & Miniaci, 2013b; Hovelius, Vikerfors,

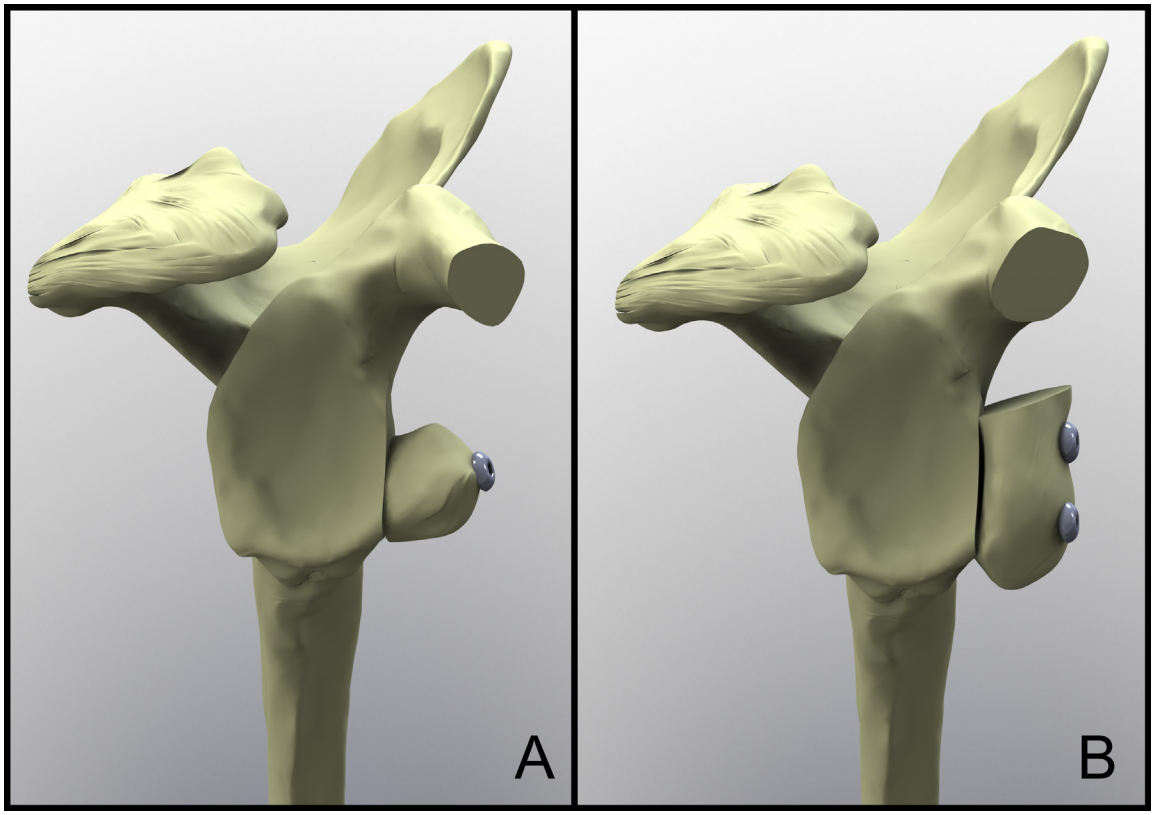

Figure 4.1: Renderings of the Bristow (A) and Latarjet (B) coracoid transfers.
Note that these renderings illustrate reconstruction of a 15% anterior glenoid bone defect; however, the graft size and orientation for both repairs is consistent across the three tested defect sizes (0%-isolated capsulolabral injury, and 15% and 30% glenoid defects).

Olofsson, Svensson, & Rahme, 2011; Hovelius, Sandstrom, Olofsson, Svensson, & Rahme, 2012; Omidi-Kashani, Sadri-Mahvelati, Mazlumi, & Makhmalbaf, 2008; Paladini, Merolla, De Santis, Campi, & Porcellini, 2012), they represent different reconstructive procedures and their true equivalence has not been demonstrated. As such, the purpose of this comparative study was to investigate the effects of the Bristow and the Latarjet procedures in order to define which technique is biomechanically superior, providing clarity to the orthopedic community. This was achieved by comparing shoulder stability and motion when treating progressive levels of anterior instability (isolated capsulolabral injury, 15 and 30% glenoid deficiency). We hypothesized that the smaller coracoid fragment transferred during the Bristow procedure would result in inferior stabilization of the glenohumeral joint, in comparison to the Latarjet reconstruction, which would become more notable with increasing glenoid defects.

4.2 Materials & Methods

4.2.1 Specimen Preparation and Shoulder Simulator

Eight (8) fresh-frozen cadaveric shoulders (74±11years) were tested after being screened for rotator cuff deficiency, osteoarthritis, or prior surgery. Following transection at the mid-humerus, shoulder dissection was performed to identify the deltoid muscle, rotator cuff muscles, short and long heads of the biceps, and glenohumeral joint capsule. Specimen preparation then proceeded as described in Section 3.2.1 including the suturing of the same muscles, creation of coordinate systems, and potting of the specimen into the simulator seen in Figure 3.1. As well, testing parameters such as muscle loads and testing positions followed those described in Chapter 3 (Section 3.2.1). Some small modifications to the setup and procedure described in Chapter 3 (Section 3.2.1), were made for the purposes of this study. First, digitization of the glenoid was performed following intact testing rather than at the completion of testing because the anterior glenoid is compromised during the testing protocol. As before, these digitizations included the superior, inferior, anterior and posterior aspects of the glenoid rim and were used to create a separate glenoid coordinate system coincident with the intact glenohumeral joint center. This coordinate system was again used in *post-hoc* analyses to determine glenohumeral joint translations. Second, using the results obtained in Chapter

3, a constant load of 10 N was applied to the conjoint tendon of the short head of the biceps and coracobrachialis.

4.2.2 Experimental Testing Protocol

The protocol was designed to compare the effects of the Bristow and Latarjet procedures on joint stiffness, stability and ROM when treating isolated capsulolabral injuries, as well as 15% and 30% bony glenoid defects. In order to achieve repeated joint access, required in this repeated-measures study, an extended lesser tuberosity osteotomy was utilized. A microsagittal saw cut the osteotomy, which was then fixated using two 1/8" bicortical nut-and-bolt constructs. Previous investigations demonstrated that the osteotomy has no effect on biomechanical outcomes (Giles et al., 2011).

Seven conditions were tested: Intact, Bristow and Latarjet coracoid transfers with an isolated capsulolabral injury (intact glenoid), followed by Bristow and Latarjet with 15 and 30% anterior glenoid bone defects. The anterior capsulolabral injury was created by releasing the anteroinferior glenoid labrum away from the glenoid rim and sectioning the capsule from the humeral neck to the inferior glenoid pole. Glenohumeral instability was ensured by propagating the injury through forcible dislocation in the anteroinferior direction.

The 15 and 30% bone defects were created as per the description of Saito *et al.* who found that the average defect is located close to the 3:00 o'clock position (Saito et al., 2005). Yamamoto's technique for creating simulated glenoid defects was also utilized (Yamamoto et al., 2009). Using digital calipers, the maximum anteroposterior glenoid width was measured, while a microsagittal saw then created the defects by cutting along a line perpendicular to the anteroposterior direction at 15 and 30% of the glenoid width (Figure 4.2).

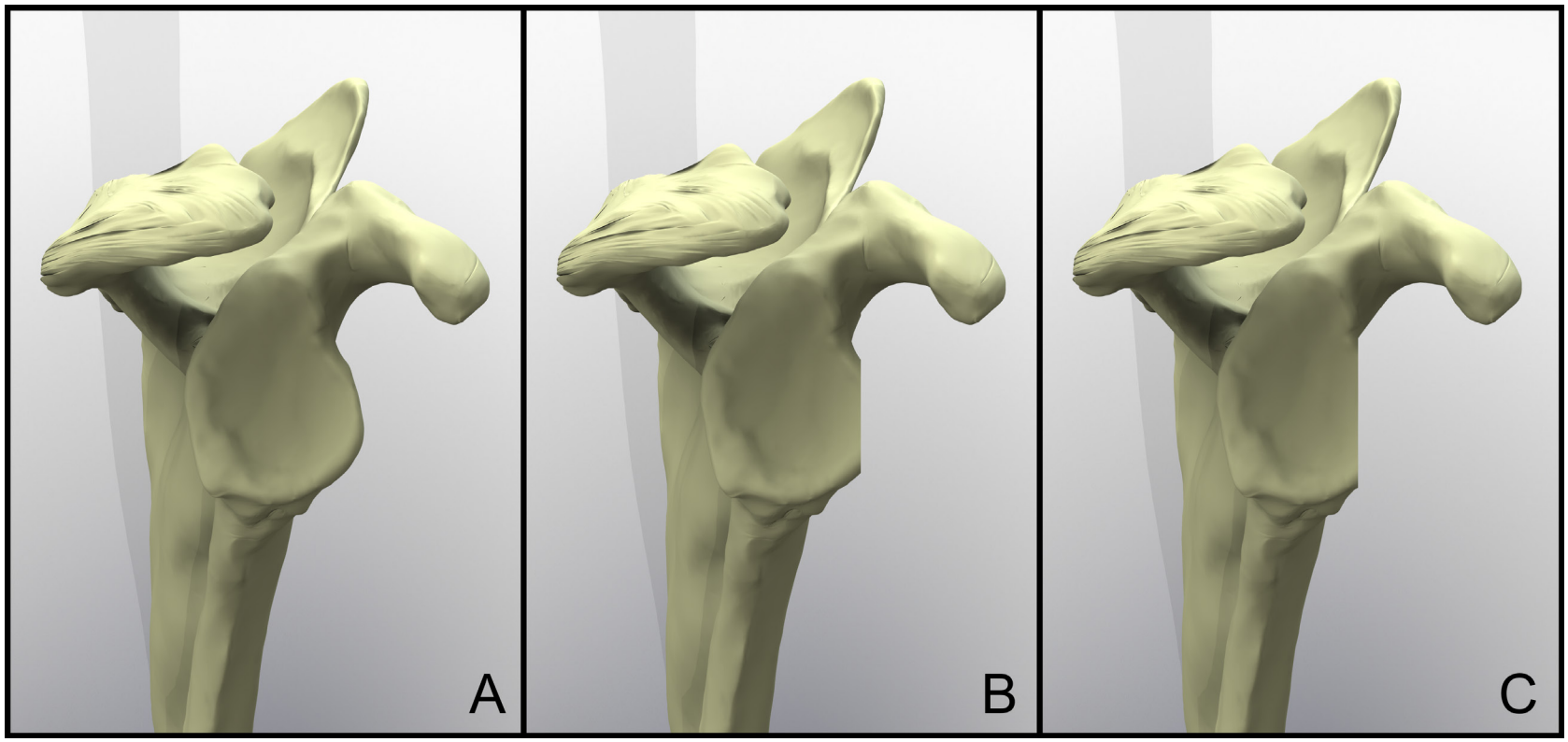

Figure 4.2: Renderings of the scapula showing the three levels of bony deficiency.
All renderings are viewed perpendicular to the glenoid plane. (A) Isolated capsulolabral tear with intact glenoid bony anatomy, (B) capsulolabral tear with associated glenoid deficiency equivalent to 15% of the glenoid width, and (C) capsulolabral tear with associated 30% glenoid deficiency.

Following creation of the isolated capsulolabral tear and the subsequent 15 and 30% bone defects, a coracoid transfer was performed and tested. The initial reconstruction was then removed and the second transfer was performed. Reconstruction order was randomized and balanced between the two procedures. The Bristow reconstruction was performed as originally described (Helfet, 1958) while the Latarjet was performed as described by Walch & Boileau (Walch & Boileau, 2000). Both reconstructions required the transfer of a segment of the coracoid with an attached conjoint tendon; however, differing graft sizes were required. Therefore, in order to test both reconstructions in random order and at multiple defect levels, a size-matched coracoid with attached conjoint tendon was harvested from a fresh-frozen donor for each specimen tested. The reconstruction that employed this harvested coracoid was selected using a balanced randomization procedure to ensure that equal numbers of Bristow and Latarjet reconstructions were performed using the donor. For the Bristow reconstruction, the coracoid tip was osteotomized 10mm from its end and, along with the attached conjoint tendon, was transferred through a horizontal subscapularis split to the anterior glenoid. The subscapularis split was conducted between the upper 2/3rd and lower 1/3rd of the tendon. The osteotomized surface of the coracoid tip was then rigidly fixed to the glenoid vault using one 3.75mm bicortical screw inserted along the graft's long axis (Figure 4.1). For the Latarjet reconstruction, the coracoid process was osteotomized at its angle or elbow and transferred with the conjoint tendon to the anterior glenoid through the same subscapularis split. The inferior surface of the coracoid was decorticated and fixed to the anterior glenoid using two 3.75mm bicortical screws (Figure 4.1). For each of these reconstructions, the coracoid was removed following testing in order to allow the other reconstruction to be fixated and tested or in order to create the next defect level. Because repeated fixation to the glenoid vault was required, care was taken to utilize the same holes for each reconstruction, obtaining bicortical purchase through the posterior cortex of the glenoid neck (no loss of coracoid fixation was observed at any point during testing).

During testing, the conjoint tendon was loaded in order to replicate the dynamic 'sling' effect (Burkhart et al., 2007). Although the location of its origin (the coracoid) was shifted, the tendon was loaded in the same manner as in Sections 2.2.5 & 3.2.1, by suturing the proximal musculotendinous junction and replicating its natural line-of-action before connecting it to a miniature pneumatic actuator (Bimba, University Park, IL) mounted to the humerus (Figure 3.1 & Figure 3.2). Despite this change in position, the tendon was able to be accurately tensioned, throughout the tested ROM, to a magnitude of 10 N.

4.2.3 Stability and Range of Motion

Two glenohumeral joint configurations were used to assess stability and ROM: (1) adduction (Add: 0° abduction in the scapular plane); and (2) abduction (Abd: 60° glenohumeral abduction in the scapular plane with 30° scapulothoracic elevation). Stability was quantified using glenohumeral joint stiffness (N/mm) and the occurrence of humeral head dislocation. As in Chapter 3 (Section 3.2.2), stiffness was calculated by passively applying a 70 N anteroinferiorly directed quasi-static load and dividing it by the magnitude of humeral translation relative to the glenoid (Figure 3.3). Maximum humeral translation was defined as the magnitude of displacement at the time of glenohumeral dislocation, or during maximum force application if dislocation did not occur. Dislocation, which was considered to have occurred when the apex of the humeral head passed the intact/reconstructed glenoid rim, was assessed visually during testing and confirmed using optical tracking data. Stiffness was evaluated in both neutral rotation (NR) (defined as epicondylar axis parallel to the coronal body plane) and 60° of external rotation (ER). Real-time feedback of the load applied to the glenohumeral joint was achieved using an uni-axial load cell (Model 34, Honeywell, Golden Valley, MN) while glenohumeral kinematics and forces were monitored during testing using the optical tracking markers and intra-medullary load cell as described in Chapter 3.

Two modes of dislocation were assessed. The first mode of dislocation involved passively extending the shoulder in a manner consistent with clinical evaluation until a soft-tissue end-point was reached or dislocation occurred. This test was performed with the shoulder in 60° of external rotation and 90° of composite abduction, commonly termed the

'position of anterior apprehension.' Results from this test provided a qualitative assessment of the incidence of dislocation and a quantitative measure of horizontal extension ROM. The second assessment involved identifying dislocation during the above described joint stiffness test with the shoulder in abduction and external rotation. This assessment replicated dislocation during a clinical drawer test.

The internal-external rotation ROM test procedure of Chatper 3 was repeated here. Briefly, ROM was quantified as the magnitude of rotation permitted by the glenohumeral joint when an external axial rotation torque of 0.8 Nm was applied.

4.2.4 Outcome Variables & Statistical Analyses

Stability was quantified in terms of glenohumeral joint stiffness (N/mm) and joint dislocation (dislocation or no dislocation), while ROM was reported in degrees. For internal-external rotation, this value was taken as the rotation from the maximum internal to the maximal external rotation position, while horizontal extension ROM was quantified as the magnitude of humeral rotation about the scapula's superior axis posterior to the scapular plane**.** Two-way repeated-measures Analyses of Variance (RM-ANOVAs) were performed for each outcome variable to assess the main effects and any interaction effects of repair technique (Bristow vs. Latarjet) across the three defect levels (0, 15, 30% glenoid defect). In the case of any interactions, follow-up *post-hoc* tests were performed. The results from intact testing could not be included in the Two-way RM-ANOVAs as they were not a repeated measurement and thus a series of One-way RM-ANOVAs were performed in order to allow comparisons between the reconstructions and the intact state. These One-way RM-ANOVAs and associated pair-wise comparisons were carried out for all outcome variables at each tested shoulder configuration and defect level. Each analysis consisted of three conditions: intact, Bristow, and Latarjet. Significance was set to $p<0.05$. *A-Priori* power analyses were performed for each outcome variable. It was found that 8 specimens were sufficient to achieve a minimum power of 80% in detecting clinically relevant differences of approximately 10° for ROM and 30% for joint stiffness.

4.3 Results

4.3.1 Joint Stiffness and Stability

Comparing the Bristow and Latarjet procedures across the three defect levels using a Two-way RM-ANOVA demonstrated that there were no interaction effects between changes in reconstruction technique and defect size ($p \geq 0.189$) except with the arm in Add-NR ($p=0.014$). In this case, *post-hoc* tests demonstrated that the Bristow produced significantly less stiffness than the Latarjet for the 15 and 30% defects (4.7±1.1 N/mm, $p=0.004$ & 5.6±1.9 N/mm, $p=0.021$, respectively) but not the 0% defect (2.0±1.2 N/mm, $p=0.156$). The main effect of reconstruction type was found to be significant for all joint configurations, with the Latarjet resulting in significantly greater stiffness than the Bristow across all three glenoid defect levels (Add-NR:4.1±1.3 N/mm, $p=0.018$; Add-ER:4.9±1.3 N/mm, $p=0.007$; Abd-NR:1.8±0.5 N/mm, $p=0.012$; Abd-ER:1.9±0.4 N/mm, $p=0.003$).

Subsequent One-way RM-ANOVAs for each joint configuration at each of the three defect levels (Figure 4.3 & Figure 4.4) further illustrate the significance of the above trends. The Bristow reconstruction resulted in joint stiffness values that were consistently less than the intact and the Latarjet. Decreases in stiffness between the Bristow and intact shoulder were significant at all defect levels with the joint in adduction ($p \leq 0.040$) and for the 15 and 30% defects with the shoulder in Abd-ER ($p \leq 0.002$). In contrast, the Latarjet produced stiffness values similar to intact and only differed significantly in one case; with the shoulder in Add-NR, following reconstruction of a 0% defect, where stiffness was significantly less than intact (3.9±1.1 N/mm, $p \leq 0.026$).

One-way RM-ANOVAs also evaluated differences between the Bristow and Latarjet reconstructions and demonstrated that the greater joint stiffness seen following the Latarjet was significant for the 15% defect in Add-NR ($p=0.012$) and the 15 & 30% defects in Abd-ER ($p \leq 0.026$). Also, while not statistically significant, the Latarjet approached a statistically significant increase in stiffness for the 30% defect in Add-NR ($p \leq 0.062$) and the 15 & 30% defects in Add-ER ($p \leq 0.064$).

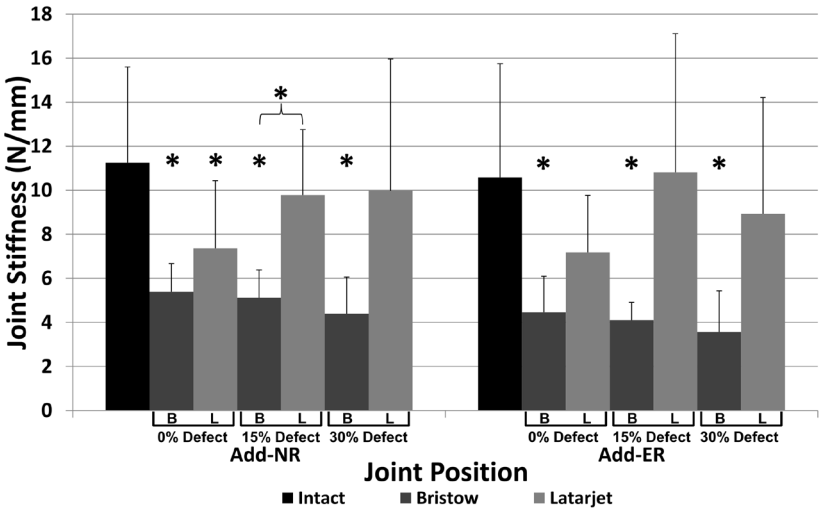

Figure 4.3: Adducted anterior glenohumeral joint stiffness.
*Data are presented for the arm in adduction (Add) and neutral (NR) or external (ER) rotation. Note that 'B' and 'L' denote Bristow and Latarjet reconstructions, respectively. Additionally, any testing state marked with a * symbol represents a significant difference to the intact state as found using One-way RM-ANOVA.*

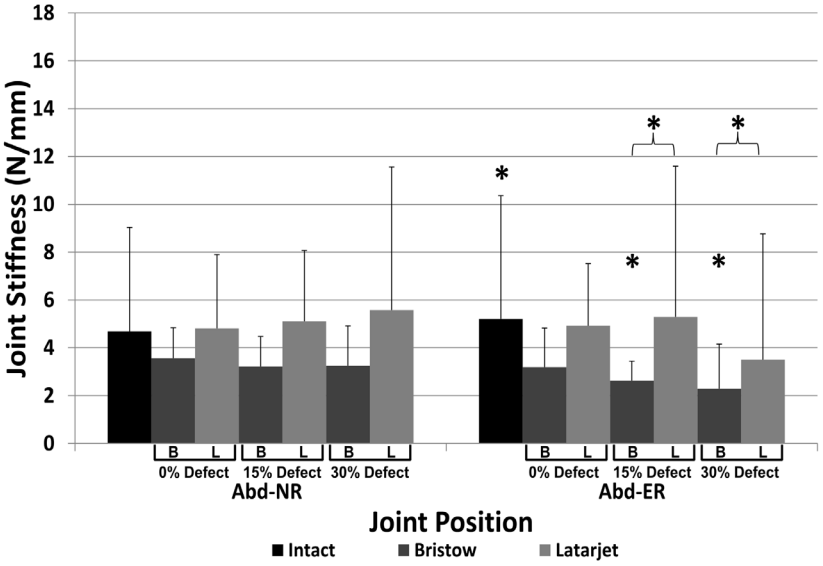

Figure 4.4: Abducted anterior glenohumeral joint stiffness.
*Data are presented for the arm in abduction (Abd) and neutral (NR) or external (ER) rotation. Note that 'B' and 'L' denote Bristow and Latarjet reconstructions, respectively. Additionally, any testing state marked with a * symbol represents a significant difference to the intact state.*

Glenohumeral joint stability, quantified in terms of incidents of dislocation as assessed during passive horizontal extension testing in the position of apprehension, resulted in 4 of 8 and 6 of 8 specimens dislocating with the Bristow procedure for the 15 and 30% defects, respectively. The Latarjet, however, allowed only one dislocation in either case (Table 4.1). Dislocations were also recorded during stiffness testing in abduction-external rotation. This assessment found that the Bristow resulted in dislocation in 6 of 8 specimens when treating a 15% glenoid defect and 4 of 8 specimens when treating a 30% defect, while the Latarjet allowed only one dislocation at each defect level.

4.3.2 Range of Motion

Two-way RM-ANOVA's for ROM in adduction and abduction indicated that there were no interaction effects between changes in repair technique and defect size ($p \geq 0.333$). No significant main effects existed in internal-external rotation ROM during adduction across either the reconstruction type or defect level ($p \geq 0.288$) (Figure 4.5). In abduction, there were also no significant main effects in internal-external rotation ROM across all testing conditions ($p \geq 0.452$). However, One-way RM-ANOVAs at each defect level demonstrated that there were statistical differences between the reconstructions, and when comparing the reconstructions to the intact state. Specifically, both the Bristow and Latarjet significantly reduced ROM compared to the intact condition with differences across the three defect levels ranging between 12.5-20.6° ($p \leq 0.045$) for the Bristow and 19.8-20.2° ($p \leq 0.033$) for the Latarjet. In contrast, the only difference between the two reconstructions was a significant reduction in ROM following the Latarjet compared to the Bristow for the 0% defect (7.7±2.2°, $p=0.033$).

During horizontal extension with the arm in Abd-ER, there was no significant interaction effect or main effect in ROM across reconstruction type or defect level ($p \geq 0.298$). There were also no trends from One-way RM-ANOVAs comparing the reconstructions to the intact state for the three defect levels (Figure 4.5).

	Drawer Test			Extension		
Defect Size	**0%**	**15%**	**30%**	**0%**	**15%**	**30%**
Bristow	0	6	4	0	4	6
Latarjet	0	1	1	0	1	1

Table 4.1: Incidents of Glenohumeral Dislocation for Two Stability Tests
Incidents of anterior glenohumeral joint dislocation during two stability tests. 'Drawer Test' indicates dislocations which occurred following reconstruction of a 0, 15, or 30% defect during the clinical drawer test. 'Extension' represents dislocations which occurred while passively extending the humerus from an initial position of abduction with external rotation in the scapular plane.

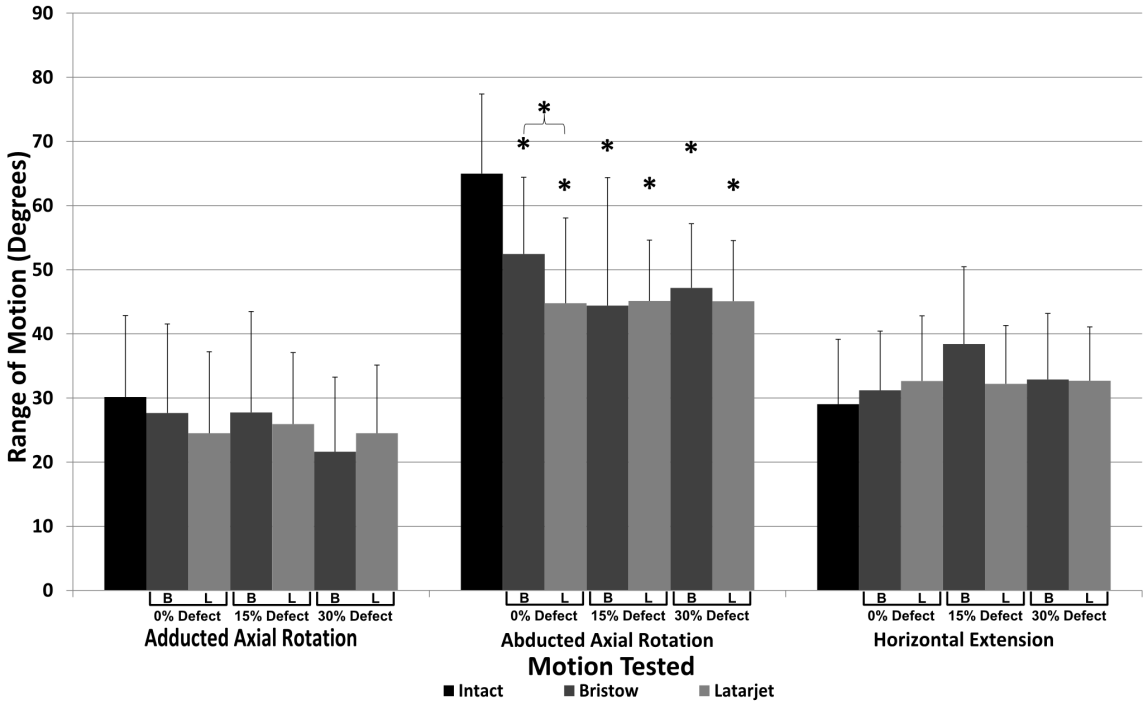

Figure 4.5: Glenohumeral joint ranges of motion.
*Range of motion is shown for 'Axial Rotation' with the arm in full adduction and 90° composite abduction, and during 'Horizontal Extension' with the arm beginning in abduction and 60° external rotation in the scapular plane. Note that 'B' and 'L' denote Bristow and Latarjet reconstructions, respectively. Additionally, any testing state marked with a * symbol represents a significant difference to the intact state.*

4.4 Discussion

The Bristow procedure and Latarjet procedure have long been labeled synonymously as the 'Bristow-Latarjet', under the assumption that the two procedures are equivalent; however, there is a lack of evidence to support this. Therefore, the purpose of this investigation was to clarify the biomechanical effects of the Bristow and Latarjet procedures and define which is optimal.

Glenohumeral joint stiffness was assessed similarly to the clinical drawer test which provided quantitative information about joint kinematics and the soft-tissues that resisted translation. In all joint configurations and with any glenoid defect, the Latarjet yielded greater stiffness than the Bristow, ranging from +30 to +90%. Additionally, the Bristow yielded stiffness markedly less than the intact condition (-27 to -99%), while the Latarjet was able to restore stiffness close to intact in most conditions (-16 to +17%). Comparing to intact, the Bristow's reduced stiffness was statistically significant in 8 of 12 joint conditions, while following the Latarjet, only 1 joint condition was significantly different. Comparing the two techniques, differences approached and surpassed significance in 6 of 12 comparisons with the Latarjet outperforming the Bristow in the 15 and 30% glenoid defect states. Abduction with neutral rotation was the only joint configuration where no difference was significant for any defect level. These findings indicate that the Latarjet consistently outperformed the Bristow in terms of restoring joint stiffness and that the disparity between the two techniques increases with increasing anterior glenoid bone deficiency. Finally, it was found that for all shoulder configurations, stiffness following Latarjet reconstruction actually increased between the 0 and 15% defect and in 2 of 4 joint configurations between the 15 and 30% defect, despite an increasingly larger glenoid defect. We believe that this somewhat unexpected result can be attributed to the progressive posterior positioning of the conjoint tendon origin on the coracoid tip as the graft is fixated to sequentially larger defects. This posterior translation of the tendon origin in turn causes the tendon to wrap under the humeral head more completely, strengthening the dynamic sling effect proposed by May (May, 1970) and biomechanically confirmed in previous literature (Giles et al., 2013; Wellmann et al.,

2009; Wellmann et al., 2012). This progressive stiffening effect, however, was not observed with the Bristow procedure.

In the condition of an isolated capsulolabral injury without glenoid bone loss, the Bristow and Latarjet procedures were equivalent in their ability to prevent dislocation. However, in conditions of glenoid bone loss, only one specimen dislocated following either instability test (Drawer Test and Horizontal Extension) at any defect level for the Latarjet reconstruction, while the Bristow permitted dislocation in 50-75% of specimens.

Shoulder ROM was assessed for multiple joint configurations and motions in order to determine what effect, if any, the two stabilization procedures produced. Internal-external rotation ROM was first assessed in adduction and it was found that the Bristow and Latarjet had variable effects between defect levels although no trends were observed and no differences were identified compared to the intact condition (-8 to -32%). In contrast, the effects of the two reconstructions were quite consistent across all conditions during abducted ROM testing, significantly reducing the internal-external rotation arc compared to the intact state (-31 to -37%, $0.001 \leq p \leq 0.045$) with the exception of the Bristow reconstruction with an isolated capsulolabral injury (-21%, $p=0.028$). In addition, the Latarjet has a significantly more restrictive effect than the Bristow for an isolated capsulolabral injury ($p=0.033$) but their effects are equivalent for the glenoid bone loss cases tested. The horizontal extension ROM consistently increased across all defects (+4.3±2.6°) but was not statistically different from intact. Therefore, neither reconstruction had an effect on the shoulder's horizontal extension ROM.

The results of this investigation should be considered in light of previous biomechanical investigations of coracoid transfer procedures. Comparing these results to those of Wellmann et al. demonstrates good agreement with regards to the stabilizing effect of the Latarjet procedure in both neutral and external rotation (Wellmann et al., 2012). However, Wellmann did not assess range of motion and thus comparison is not possible. The current results for the Latarjet reconstruction, including range of motion, are also in agreement with those previously published by our group in a comparison of two techniques of Latarjet coracoid orientation (Boons, Giles, Elkinson, Johnson, & Athwal,

2013). Previous literature on the biomechanical effect of the Bristow procedure was limited to a study by Wellmann et al. who assessed the effect of a coracoid tip transfer of similar size to the graft utilized in the Bristow procedure; however, their graft was oriented in the manner of the Latarjet procedure (Wellmann et al., 2012). With this pseudo-Bristow coracoid transfer, the authors found increased glenohumeral translations which also agrees with our finding of reduced glenohumeral stiffness. The agreement of these results with previous literature, especially with regards to the Latarjet, lends support to our findings for both procedures.

Limitations to this study include the use of cadaveric specimens, the need to utilize a donor coracoid for one repair, and the inability to test the unrepaired defect state prior to testing the reconstructions. The use of cadaveric specimens is an inherent limitation to this study and means that all results represent time-zero biomechanics without accounting for healing effects such as soft-tissue relaxation. Despite this limitation, this study provides a fair comparison of the two procedures. The use of a size matched coracoid donor with attached conjoint tendon is a limitation as it is possible that the donor graft may not have exactly matched the true coracoid; however, the use of the graft was randomized and balanced between specimens and thus any differences should affect both reconstructions equally. The use of successive glenoid defects precluded testing of the unrepaired state at each defect level as the specimen's coracoid was removed at the first defect level; however, the primary goal of the study was to make comparisons to intact and between reconstructions and thus collection of these data was not imperative. It is anticipated that had these data been measured, they would have demonstrated progressively greater instability as observed clinically due to the loss first of the anterior passive stabilizers and subsequently portions of the anterior glenoid bone.

This investigation has clarified the effects of the Bristow and Latarjet coracoid transfers and demonstrated that they are not equivalent, and should not be considered interchangeable when used to treat complex shoulder instability. Comparison has shown that the Latarjet coracoid transfer has a greater ability to restore glenohumeral joint stability. This restoration of stiffness will also help to normalize joint kinematics and kinetics by maintaining the joint in a well reduced configuration, preventing excessive

coracoid graft loading. Evaluation of the effects on ROM demonstrated that abducted axial rotation was significantly limited by both reconstructions. While this restriction is worrisome from a patient satisfaction point of view, it may prevent the joint from reaching the position of apprehension, which could subjectively cause proprioceptive feelings of instability despite improved stability. However, for the Bristow, motion was restricted without effectively restoring intact joint stiffness and thus it carries the disadvantages of the Latarjet—motion restriction—without its benefits—joint stabilization. Further studies are required to determine if this restriction is clinically significant, and whether it remains over time or decreases with soft-tissue attenuation.

In conclusion, through the use of the passive testing capability of the simulator, it was possible to clarify the effects of the two clinical procedures across a range of clinically meaningful injury levels and for various clinical assessments. Specifically, in the setting of anterior shoulder instability with an intact glenoid, the Bristow and Latarjet procedures are essentially equivalent in their ability to stabilize the shoulder. However, the Latarjet results in significantly greater restriction of rotational range of motion indicating that the Bristow may be the preferred coracoid transfer procedure for isolated capsulolabral injuries. In the setting of substantial glenoid deficiency, the Latarjet reconstruction is superior to the Bristow in its ability to restore joint stability and, therefore, in terms of its biomechanical efficacy, may represent a preferable treatment option among coracoid transfer procedures.

4.5 References

Boileau, P., Mercier, N., & Old, J. (2010). Arthroscopic bankart-bristow-latarjet (2B3) procedure: How to do it and tricks to make it easier and safe. *The Orthopedic Clinics of North America, 41*(3), 381-392. doi:10.1016/j.ocl.2010.03.005; 10.1016/j.ocl.2010.03.005

Boileau, P., Mercier, N., Roussanne, Y., Thelu, C. E., & Old, J. (2010). Arthroscopic bankart-bristow-latarjet procedure: The development and early results of a safe and reproducible technique. *Arthroscopy: The Journal of Arthroscopic & Related Surgery: Official Publication of the Arthroscopy Association of North America and the International Arthroscopy Association, 26*(11), 1434-1450. doi:10.1016/j.arthro.2010.07.011; 10.1016/j.arthro.2010.07.011

Boons, H. W., Giles, J. W., Elkinson, I., Johnson, J. A., & Athwal, G. S. (2013). Classic versus congruent coracoid positioning during the latarjet procedure: An in vitro biomechanical comparison. *Arthroscopy: The Journal of Arthroscopic & Related Surgery: Official Publication of the Arthroscopy Association of North America and the International Arthroscopy Association, 29*(2), 309-316. doi:10.1016/j.arthro.2012.09.007; 10.1016/j.arthro.2012.09.007

Burkhart, S. S., & De Beer, J. F. (2000). Traumatic glenohumeral bone defects and their relationship to failure of arthroscopic bankart repairs: Significance of the inverted-pear glenoid and the humeral engaging hill-sachs lesion. *Arthroscopy: The Journal of Arthroscopic & Related Surgery: Official Publication of the Arthroscopy Association of North America and the International Arthroscopy Association, 16*(7), 677-694.

Burkhart, S. S., De Beer, J. F., Barth, J. R., Cresswell, T., Roberts, C., & Richards, D. P. (2007). Results of modified latarjet reconstruction in patients with anteroinferior instability and significant bone loss. *Arthroscopy: The Journal of Arthroscopic & Related Surgery: Official Publication of the Arthroscopy Association of North America and the International Arthroscopy Association, 23*(10), 1033-1041. doi:10.1016/j.arthro.2007.08.009

Emami, M. J., Solooki, S., Meshksari, Z., & Vosoughi, A. R. (2011). The effect of open bristow-latarjet procedure for anterior shoulder instability: A 10-year study. *Musculoskeletal Surgery, 95*(3), 231-235. doi:10.1007/s12306-011-0149-0; 10.1007/s12306-011-0149-0

Giles, J. W., Boons, H. W., Elkinson, I., Faber, K. J., Ferreira, L. M., Johnson, J. A., & Athwal, G. S. (2013). Does the dynamic sling effect of the latarjet procedure improve shoulder stability? A biomechanical evaluation. *Journal of Shoulder and Elbow Surgery / American Shoulder and Elbow Surgeons ...[Et Al.], 22*(6), 821-827. doi:10.1016/j.jse.2012.08.002; 10.1016/j.jse.2012.08.002

Giles, J. W., Elkinson, I., Ferreira, L. M., Faber, K. J., Boons, H., Litchfield, R., . . . Athwal, G. S. (2011). Moderate to large engaging hill-sachs defects: An in vitro biomechanical comparison of the remplissage procedure, allograft humeral head reconstruction, and partial resurfacing arthroplasty. *Journal of Shoulder and Elbow Surgery / American Shoulder and Elbow Surgeons ...[Et Al.]*, doi:10.1016/j.jse.2011.07.017

Griesser, M. J., Harris, J. D., McCoy, B. W., Hussain, W. M., Jones, M. H., Bishop, J. Y., & Miniaci, A. (2013a). Complications and re-operations after bristow-latarjet shoulder stabilization: A systematic review. *Journal of Shoulder and Elbow Surgery / American Shoulder and Elbow Surgeons ...[Et Al.], 22*(2), 286-292. doi:10.1016/j.jse.2012.09.009; 10.1016/j.jse.2012.09.009

Griesser, M. J., Harris, J. D., McCoy, B. W., Hussain, W. M., Jones, M. H., Bishop, J. Y., & Miniaci, A. (2013b). Glenoid fracture after bristow-latarjet shoulder stabilization: A case report and review of the literature. *Journal of Shoulder and Elbow Surgery / American Shoulder and Elbow Surgeons ...[Et Al.], 22*(3), e17-20. doi:10.1016/j.jse.2012.11.003; 10.1016/j.jse.2012.11.003

Helfet, A. J. (1958). Coracoid transplantation for recurring dislocation of the shoulder. *The Journal of Bone and Joint Surgery. British Volume, 40-B*(2), 198-202.

Hovelius, L., Sandstrom, B., Olofsson, A., Svensson, O., & Rahme, H. (2012). The effect of capsular repair, bone block healing, and position on the results of the bristow-latarjet procedure (study III): Long-term follow-up in 319 shoulders. *Journal of Shoulder and Elbow Surgery / American Shoulder and Elbow Surgeons ...[Et Al.], 21*(5), 647-660. doi:10.1016/j.jse.2011.03.020; 10.1016/j.jse.2011.03.020

Hovelius, L., Vikerfors, O., Olofsson, A., Svensson, O., & Rahme, H. (2011). Bristow-latarjet and bankart: A comparative study of shoulder stabilization in 185 shoulders during a seventeen-year follow-up. *Journal of Shoulder and Elbow Surgery / American Shoulder and Elbow Surgeons ...[Et Al.], 20*(7), 1095-1101. doi:10.1016/j.jse.2011.02.005; 10.1016/j.jse.2011.02.005

Itoi, E., Lee, S. B., Berglund, L. J., Berge, L. L., & An, K. N. (2000). The effect of a glenoid defect on anteroinferior stability of the shoulder after bankart repair: A cadaveric study. *The Journal of Bone and Joint Surgery. American Volume, 82*(1), 35-46.

Latarjet, M. (1954). Treatment of recurrent dislocation of the shoulder. *Lyon Chirurgical, 49*(8), 994.

May, V. R.,Jr. (1970). A modified bristow operation for anterior recurrent dislocation of the shoulder. *The Journal of Bone and Joint Surgery. American Volume, 52*(5), 1010-1016.

Montgomery, W. H.,Jr, Wahl, M., Hettrich, C., Itoi, E., Lippitt, S. B., & Matsen, F. A.,3rd. (2005). Anteroinferior bone-grafting can restore stability in osseous glenoid defects. *The Journal of Bone and Joint Surgery. American Volume, 87*(9), 1972-1977. doi:10.2106/JBJS.D.02573

Omidi-Kashani, F., Sadri-Mahvelati, E., Mazlumi, S. M., & Makhmalbaf, H. (2008). Is bristow-latarjet operation effective for every recurrent anterior shoulder dislocation? *Archives of Iranian Medicine, 11*(3), 270-273. doi:08113/AIM.007; 08113/AIM.007

Paladini, P., Merolla, G., De Santis, E., Campi, F., & Porcellini, G. (2012). Long-term subscapularis strength assessment after bristow-latarjet procedure: Isometric study. *Journal of Shoulder and Elbow Surgery / American Shoulder and Elbow Surgeons ...[Et Al.], 21*(1), 42-47. doi:10.1016/j.jse.2011.03.027; 10.1016/j.jse.2011.03.027

Saito, H., Itoi, E., Sugaya, H., Minagawa, H., Yamamoto, N., & Tuoheti, Y. (2005). Location of the glenoid defect in shoulders with recurrent anterior dislocation. *The American Journal of Sports Medicine, 33*(6), 889-893. doi:10.1177/0363546504271521

Tauber, M., Resch, H., Forstner, R., Raffl, M., & Schauer, J. (2004). Reasons for failure after surgical repair of anterior shoulder instability. *Journal of Shoulder and Elbow Surgery / American Shoulder and Elbow Surgeons ...[Et Al.], 13*(3), 279-285. doi:10.1016/S1058274604000254

Walch, G., & Boileau, P. (2000). Latarjet-bristow procedure for recurrent anterior instability. *Techniques in Shoulder & Elbow Surgery, 1*(4) Retrieved from http://journals.lww.com/shoulderelbowsurgery/Fulltext/2000/01040/Latarjet_Bristow_Procedure_for_Recurrent_Anterior.8.aspx

Warner, J. J., Gill, T. J., O'hollerhan, J. D., Pathare, N., & Millett, P. J. (2006). Anatomical glenoid reconstruction for recurrent anterior glenohumeral instability with glenoid deficiency using an autogenous tricortical iliac crest bone graft. *The American Journal of Sports Medicine, 34*(2), 205-212. doi:10.1177/0363546505281798

Wellmann, M., de Ferrari, H., Smith, T., Petersen, W., Siebert, C. H., Agneskirchner, J. D., & Hurschler, C. (2012). Biomechanical investigation of the stabilization principle of the latarjet procedure. *Archives of Orthopaedic and Trauma Surgery, 132*(3), 377-386. doi:10.1007/s00402-011-1425-z

Wellmann, M., Petersen, W., Zantop, T., Herbort, M., Kobbe, P., Raschke, M. J., & Hurschler, C. (2009). Open shoulder repair of osseous glenoid defects: Biomechanical effectiveness of the latarjet procedure versus a contoured structural bone graft. *The American Journal of Sports Medicine, 37*(1), 87-94. doi:10.1177/0363546508326714

Wu, G., van der Helm, F. C., Veeger, H. E., Makhsous, M., Van Roy, P., Anglin, C., . . . International Society of Biomechanics. (2005). ISB recommendation on definitions of joint coordinate systems of various joints for the reporting of human joint motion--part II: Shoulder, elbow, wrist and hand. *Journal of Biomechanics, 38*(5), 981-992.

Yamamoto, N., Itoi, E., Abe, H., Kikuchi, K., Seki, N., Minagawa, H., & Tuoheti, Y. (2009). Effect of an anterior glenoid defect on anterior shoulder stability: A cadaveric study. *The American Journal of Sports Medicine, 37*(5), 949-954. doi:10.1177/0363546508330139

CHAPTER 5 – Development and Validation of a Multi-PID Muscle Loading Driven *In-Vitro* Active Motion Shoulder Simulator

OVERVIEW

In-vitro active shoulder motion simulation can provide improved understanding of shoulder biomechanics; however, accurate simulator systems using advanced control theory have not been developed. Therefore, in this chapter, the development and validation of a simulator which uses real-time kinematic feedback and closed-loop PID (Proportional, Integral, Differential) control to achieve active abduction and horizontal extension is presented. Motion control of cadaveric shoulder specimens was achieved by applying continuously variable loads to seven muscle groups. Muscle loads controlling each of the three rotational Degrees-of-Freedom (DOF) of the glenohumeral joint were modulated using three independent PID controllers running in parallel, each using Euler angle kinematic output corresponding to its DOF. The simulator achieved a mean error over repeated trials which was ≤1.7° across abduction and ≤2.2° across horizontal extension with Root Mean Squared Errors (RMSE) of 0.88° and 0.98°, respectively. The non-profiled DOF were maintained to within 5.0 degrees with RMSE <1.0 degrees. Repeatability was high, with Average Standard Deviations (ASDs) of <0.31 degrees. Therefore, this simulator is capable of accurately and repeatably controlling shoulder motion entirely through muscle loading which is critical to gaining a better understanding of shoulder function because glenohumeral kinematics are predominantly dictated by muscle loading[8].

---

[8] A version of this work has been submitted for journal publication: Giles, J.W., Ferreira, L.M., Athwal, G.S., & Johnson, J.A. (In Submission Feb 2014). Development of a Novel In-vitro Shoulder Simulator for Real-Time Control of Active Movements in Various Planes. Journal of Biomechanical Engineering.

5.1 Introduction

As discussed in Chapters 1 & 2, *in-vitro* simulators have been developed for a number of joints in the human body with the goal of accurately replicating *in-vivo* loading conditions and kinematics. Replicating the *in-vivo* condition has proven difficult, with simulators achieving varying levels of success. The accuracy of the replicated *in-vivo* condition can largely be related to the type of *in-vitro* testing being performed. While passive testing such as that described in Chapters 2-4 is a very important tool in assessing joint function it is incapable of quantifying the effects of differing joint conditions on shoulder kinematics and kinetics during muscle driven active motions. Additionally, the work of Kedgley et al. has shown that the implementation of a simulator which uses continually variable muscle forces to drive shoulder motion, as is the case *in-vivo*, can produce motions with higher repeatability than those performed passively (Kedgley, Mackenzie, Ferreira, Drosdowech, King, Faber, & Johnson, 2007a). This higher repeatability in turn increases the statistical power of the findings and their physiologic validity, as the kinetics of the joint are more closely replicated. A small number of systems have investigated the biomechanics of muscle loading driven, or 'active,' motion (Debski et al., 1995; Henninger et al., 2012; Kedgley, Mackenzie, Ferreira, Johnson, & Faber, 2007; Wuelker, Wirth, Plitz, & Roetman, 1995). It is these active motion systems that enable the evaluation of joint kinematics and kinetics continuously across a given motion.

To date, shoulder active motion systems have used constant middle deltoid velocity or linearly increasing middle deltoid force in conjunction with an open-loop controller, which apportions other muscle loads as a function of *a-priori* physiologic loading ratios. This control scheme has proven to produce repeatable motions in the primary degree of freedom (DOF) (*i.e.* abduction); however, their dependence on *a-priori* muscle loading ratios to maintain the desired elevation plane and level of axial rotation has precluded their ability to fully control all three rotational DOF. Control of these secondary DOF can be best achieved through the use of real-time kinematic feedback in a closed-loop control system. Additionally, implementation of this type of system would also enable simulation of motions such as horizontal extension that, unlike abduction, are not dictated by a one-to-one muscle force profile function. As well, a system of this type would enable

simulation of motions that simultaneously vary two DOF, such as cross body motion. The lack of more refined shoulder simulators based on control theory can primarily be attributed to the complex, unconstrained nature of the shoulder and the number of degrees of freedom with large ranges of motion (*e.g* plane of abduction, abduction angle, and axial rotation) that must be controlled.

Therefore, the objective of this chapter was to develop and test a new *in-vitro* shoulder motion simulator that uses real-time kinematic feedback and closed-loop PID (Proportional, Integral, Differential) control of all three rotational DOF simultaneously, to achieve active abduction and horizontal extension movements. These motions were selected as they represent the most common shoulder motion in daily life (Magermans, Chadwick, Veeger, & van der Helm, 2005) and the most unstable position for patients suffering from shoulder instability (Speer, Hannafin, Altchek, & Warren, 1994). A further objective was to refine the simulator's kinematic and kinetic outcomes in order to gain an improved understanding of the effects of surgical procedures and implant designs on shoulder function. Therefore, in this chapter the simulator's performance is evaluated based on its accuracy in following a predefined motion profile, its motion repeatability, its response to changes to the shoulder's size-to-weight ratio and adjustments to the optimal PID control parameters, and its ability to compensate for non-physiologic disturbances in scapular rotation.

5.2 Materials & Methods

5.2.1 Specimen Preparation

Two fresh frozen cadaveric shoulder specimens (81±0.7 years, both male) were transected mid-humerus and denuded of skin and sub-cutaneous tissue as described in Chapter 3. Prior to fixing the scapula to the active shoulder motion simulator (Figure 5.1), sutures were secured to the distal tendinous insertions of the Anterior, Middle, and Posterior Deltoid, as well as to the musculotendinous junctions of the Subscapular, Supraspinatus, and both the Infraspinatus and Teres Minor together. The instrumented intra-medullary humeral rod described in Chapter 2 was then cemented into the transected canal such that

a transverse reference bar was oriented parallel to the trans-epicondylar axis of the previously removed elbow (Balg, Boulianne, & Boileau, 2006). The instrumented rod served to provide real-time kinematic feedback regarding the humeral orientation as well as providing the ability to mount masses which simulated the weight and moment of inertia of the previously removed arm (Kedgley, Mackenzie, Ferreira, Drosdowech, King, Faber, & Johnson, 2007b).

An optical tracking marker was also placed on the scapula in order to provide real-time kinematics feedback and provide a reference for the data collected from the humeral markers. The scapula was then cemented into a pot mounted to the simulator in 10° forward inclination while maintaining the glenoid plane vertical (Forte, de Castro, de Toledo, Ribeiro, & Loss, 2009; McClure, Michener, & Karduna, 2006). The sutures placed in each muscle group were then transitioned to low friction, low stretch polymer braided lines that, in order to achieve physiological lines-of-action, were routed through the custom low friction guide system and connected to the computer controlled low friction pneumatic actuators discussed in Chapter 2 (Airpel E16, Airpot Co., Norwalk, CT). Tissues were kept moist throughout testing using normal saline solution.

In order to provide physiologically meaningful kinematic data for the control system, bone fixed local coordinate systems were created on the humerus and scapula using the International Society of Biomechanics (ISB) recommendations as described by Wu et al.

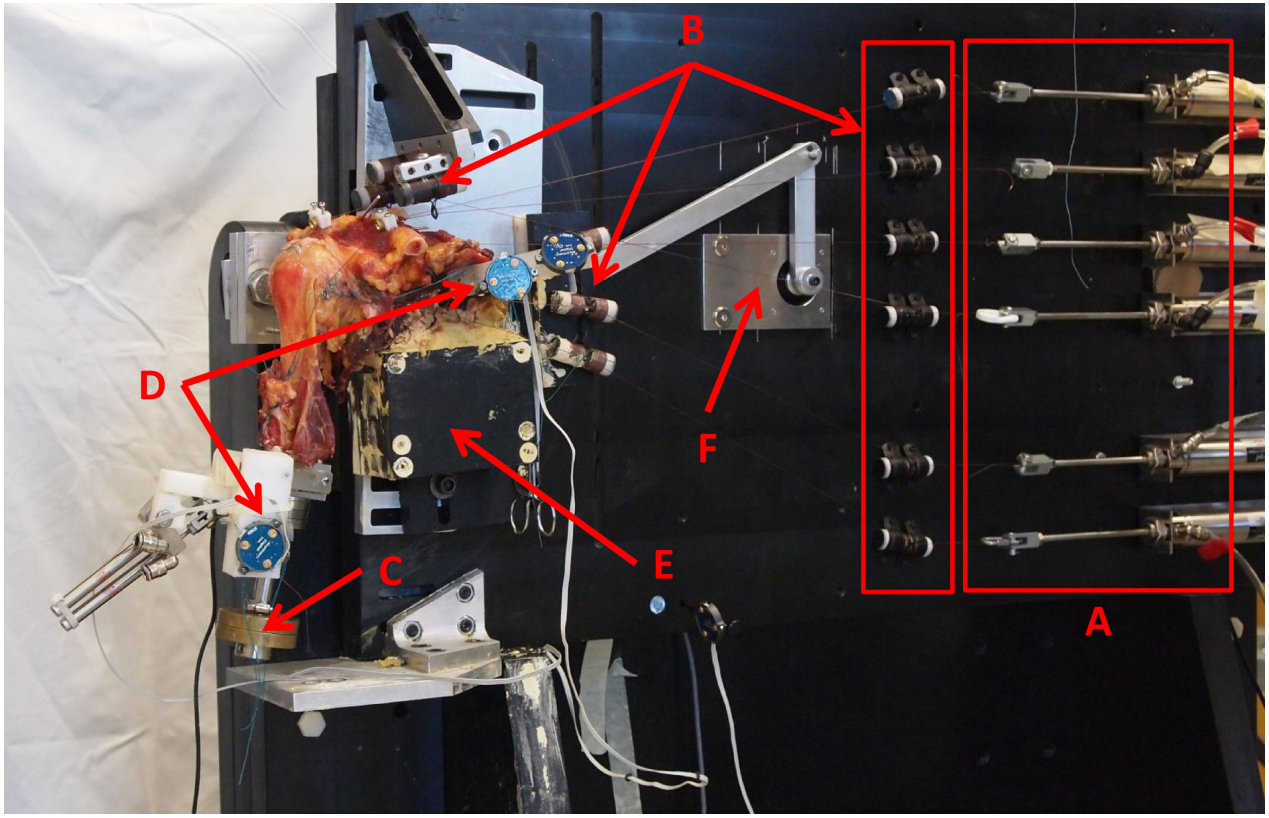

Figure 5.1: Shoulder Active Motion Simulator.
Photograph of the active motion simulator with a right shoulder mounted. Note the low friction pneumatic actuators (A), low friction cable guides (B), mass replacement system (C), optical trackers on the humerus and scapula (D), adjustable scapula pot which permits scapular elevation (E) and DC servomotor and linkage system which drives the scapula pot's rotation (F).

(Wu, van der Helm, Veeger, Makhsous, Van Roy, Anglin, Nagels, Karduna, McQuade, Wang, Werner, Buchholz, & International Society of Biomechanics, 2005a). Due to the previous transection of the humerus, the prescribed medial and lateral epicondylar digitizations were replaced with medial and lateral digitizations on the transverse bar, which was oriented parallel to the epicondylar axis. The required humeral head center digitization was determined using the algorithm of Woltring et al. applied to kinematic recordings of the humerus relative to the scapula with the glenohumeral joint intact (Woltring, 1990).

5.2.2 Glenohumeral Joint Control System

The present simulator's control system was predicated on the use of previously validated *in-vivo* muscle loading ratios as an *a-priori* set of data to be modulated by a series of Closed-Loop PID controllers running in parallel. This would achieve real-time control of the glenohumeral joint's three rotational DOF.

5.2.2.1 *A-Priori* Muscle Loading Ratios

A number of muscle loading ratio data sets exist in the literature. Some prescribe equal loads to all muscle groups (Apreleva et al., 1998; Debski et al., 1995), others consider the physiological cross-sectional area (pCSA) to apportion load based on muscle size (Halder et al., 2001; Itoi et al., 1994; Sharkey, Marder, & Hanson, 1994; Wuelker et al., 1995), and still others combine pCSA with electromyographic (EMG) activation data, averaged over a motion, to describe loading ratios based on the muscle's capacity and behaviour during motion (Hsu, Luo, Cofield, & An, 1997). However, the most physiologically accurate set of ratios has come from the evaluation of pCSA, and EMG while it varies throughout a motion, rather than averaged over a motion (Kedgley, Mackenzie, Ferreira, Drosdowech, King, Faber, & Johnson, 2007b). In the literature, these data were only recorded for abduction in the scapular plane with neutral axial rotation, and as such, PID controllers are required to modulate these ratios, thereby allowing control of motions in other planes of elevation and levels of axial rotation (Table 5.1) (Kedgley, Mackenzie, Ferreira, Drosdowech, King, Faber, & Johnson, 2007b).

Abduction Angle	Anterior Deltoid	Middle Deltoid	Posterior Deltoid	Infraspinatus	Subscapularis	Supraspinatus
2°	0.22	1.00	0.08	2.59	1.10	1.51
20°	0.35	1.00	0.20	1.22	0.53	0.68
40°	0.37	1.00	0.19	0.92	0.29	0.41
60°	0.43	1.00	0.17	0.78	0.22	0.30
90°	0.51	1.00	0.14	0.73	0.24	0.26

Table 5.1: Muscle Loading Ratios.
This table illustrates the physiologic muscle loading ratios, at various levels of humeral abduction, utilized by the simulator to achieve accurate joint loading. These ratios are modulated by the PID controllers based on real time kinematic feedback.

5.2.2.2 Nested-Parallel Closed-Loop PID Controllers

In designing the glenohumeral joint active motion control system, three inputs were identified: (1) the setpoints – target rotation angles for each of the three rotational DOF; (2) the process variables – the instantaneous joint angles taken from real-time kinematic data; and (3) the muscle loading ratios corresponding to the real-time abduction angle. The first input is defined as a desired motion profile or constant joint angle for the secondary DOF, and the third input is drawn from *a-priori* muscle loading ratio data. However, because the second input is drawn from real-time kinematic data, a custom LabView (National Instruments, Austin, TX) program was written to acquire humerus and scapula marker data from the Optotrak Certus and convert it to three joint rotations using the previously defined local bone coordinate systems and the ISB recommended YXY Euler angle rotation sequence (Wu, van der Helm, Veeger, Makhsous, Van Roy, Anglin, Nagels, Karduna, McQuade, Wang, Werner, Buchholz, & International Society of Biomechanics, 2005b). The output from this system is a load command for each muscle group.

The three inputs allowed the control of the glenohumeral joint's rotational DOF through independent PID controllers running in a combined cascade-parallel structure, each using one Euler angle rotation corresponding to its respective DOF (FGIURE). Each PID controller was configured to control the loading of an individual or set of muscles which, from previous *in-vivo* investigations, have been found to be primarily responsible for movement in the PID's respective DOF.

The three heads of the deltoid are the primary elevators of the shoulder *in-vivo*; therefore, the PID controlling abduction angle was configured to output the total deltoid force. This PID was considered the primary controller because its force output had to be sufficient to actively overcome the gravitational load of the arm during glenohumeral abduction, and to maintain the level of abduction during extension motions.

The other two DOF were each controlled by an independent PID. These controllers ran in parallel to each other but cascaded below the primary abduction PID controller. The total

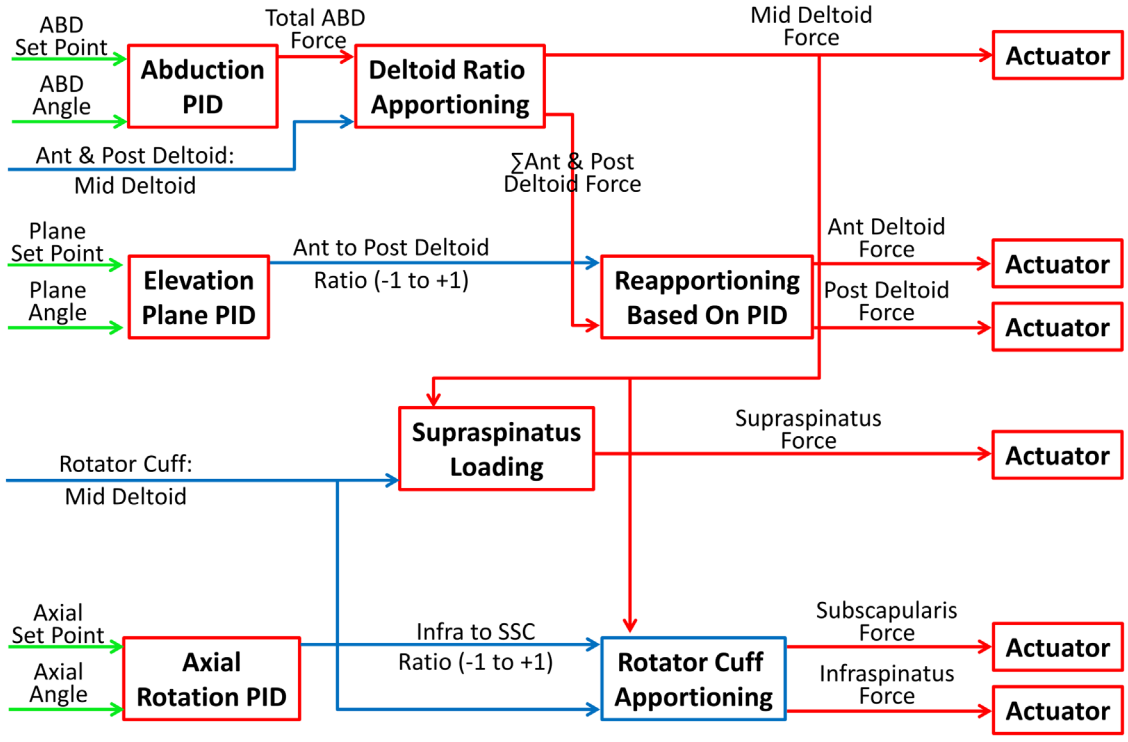

Figure 5.2: Block Diagram of Shoulder Active Motion Control System.
The above block diagram illustrates the control algorithm implemented including the inputs, outputs, and intermediate data within the controller. Green arrows represent setpoints and real-time feedback; blue arrows represent a-priori muscle ratio data or intermediate output from PID controllers; red arrows represent load commands to be sent to actuators and in some cases to other parts of the controller.

force applied to the muscles controlling each of these two DOF was dictated by the sum of the physiologic ratios of each muscle forming the force couple (Plane of Abduction DOF: ∑Anterior and Posterior Deltoid, Axial Rotation DOF: ∑Subscapularis and Infraspinatus/Teres Minor) relative to the middle deltoid at the instantaneous abduction angle (Table 5.1). This total force was then redistributed between the muscles forming the force couple for each DOF using the corresponding Euler angle kinematics as the process variable for the PID controllers. These PID controllers output a ratio ranging from -0.95 to +0.95 which was then multiplied by the total force determined earlier in order to redistribute the load between the muscles in the force couple. The output range was defined in this way to ensure that a minimum tone of 5% of the total load was maintained on both muscles. This method of using *a-priori* loading ratios ensured that the two secondary controllers did not apply non-physiologic forces while still leveraging the control provided by the PID algorithm to produce smooth accurate motion.

Finally, the supraspinatus was actuated based on the magnitude of middle deltoid load, and its physiologic loading ratio with respect to the middle deltoid. This ratio varies with abduction angle since the supraspinatus functions as a primary abductor in early motion, with a decreasing role later on. The supraspinatus was the only muscle not directly controlled by a PID algorithm because while its primary function is to abduct, its role is secondary to that of the middle deltoid (Kedgley, Mackenzie, Ferreira, Drosdowech, King, Faber, & Johnson, 2007a).

5.2.2.3 Control System Tuning

Following implementation of the control system, a tuning procedure was undertaken for each of the three PIDs controlling an individual DOF. Each PID was tuned for two distinct forms of operation: (1) to follow a smooth predefined motion profile; and (2) to maintain a constant rotation angle when a predefined motion profile is being followed in another DOF (*e.g.* maintaining an axial rotation angle during an abduction motion). The abduction PID – the primary controller – was tuned first, since its output cascades to the others. The secondary PIDs were then tuned, and a heuristic process was applied to the primary PID to account for any effect this secondary PID tuning had on its performance.

The initial tuning procedure undertaken for the primary and secondary DOF followed the Ziegler–Nichols method (Ziegler & Nichols, 1942); first, a proportional only controller is implemented, then its gain is increased until oscillation is initiated (K_u). 45% of this gain is then used to achieve a desirable Quarter Amplitude Decay Response (K_p). The estimated oscillation period (T_u) from the first step was then used to select an initial integral time value (inverse action of gain) (T_i) using the formula:

$$T_i = 0.83\frac{T_u}{K_p} \qquad \text{Eq. 5.1}$$

Equation 5.1: Ziegler-Nichols equations for determination of Integral Time PID parameter initial guess.

The derivative time (T_d) was then increased from zero in a heuristic manner until the resulting profile was sufficiently responsive. Through these tuning procedures, it was determined that the optimal PID gains required for following an abduction profile and for maintaining a constant abduction level were equal. This was also the case for the plane of elevation PID controller (Table 5.2). However, for controlling internal-external rotation, the tuning procedures produced two different sets of gains (Table 5.2). An example of the continuously variable muscle loads produced by this tuned control system can be seen in Figure 5.2.

5.2.3 Scapular Orientation Control

In order to accurately replicate *in-vivo* glenohumeral joint stability and kinematics, it is necessary to not only control the forces applied to the muscles crossing the joint, but also to mimic the glenohumeral-to-scapulothoracic rhythm by controlling the scapula's rotation. This rotation was calculated by applying McQuade et al.'s (McQuade & Smidt, 1998) rhythm to the instantaneous glenohumeral abduction angle. The scapula was then rotated to the required orientation by rotating its pot using a DC servo-motor and linkage system controlled using a custom Labview program designed to convert the scapular orientation into a motor position. This conversion was achieved by applying the results of an inverse kinematic analysis of the scapula pot and linkage system to the known motor and gearhead rotation ratios (Appendix B). As discussed in the description of the design of the physical scapula rotation mechanism in Chapter 2 (Section 2.2.3), scapular

Motion	Proportional Gain (K_p)	Integral Time (T_i)	Derivative Time (T_d)
Abduction Profiling/Constant	1.4	0.003	0.003
Plane of Elevation Profiling/Constant	0.13	0.08	0.00
Internal-External Rotation Profiling	0.30	0.01	0.00
Internal-External Rotation Constant	0.30	0.10	0.00

Table 5.2: PID Control Parameters.
This table provides the PID gains implemented for each of the DOFs when attempting to follow a desired motion profile or maintain a constant value. Note that only the Internal-External rotation DOF required distinct PID parameters for the two control cases.

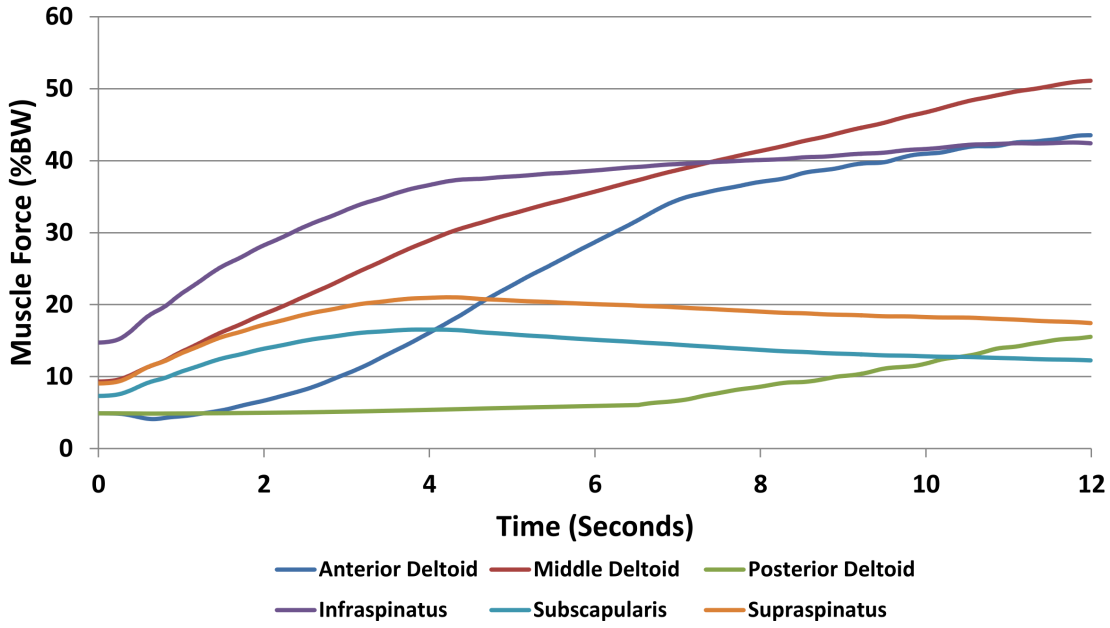

Figure 5.3: Example Muscle Loads Produced by Motion Controller.
This graph illustrates a set of example muscle loads produced by the tuned closed loop control system during abduction in the scapular plane for an intact shoulder specimen.

protraction/retraction was not controlled by this system as it does not affect glenohumeral joint stability, and scapular tilting was not adjusted because there is currently no clear definition of how this DOF changes with humeral motion.

5.2.4 Validation Outcome Variables

The efficacy and performance of the simulator were evaluated using a number of outcome variables. First, the accuracy in following a predefined motion profile was assessed for abduction in the scapular plane and for horizontal extension after the humerus was actively abducted to 60° of glenohumeral rotation, 30° of scapulothoracic rotation and externally rotated 60°. In this assessment, the accuracy of the resulting motion profile was evaluated as well as how well the non-profiled DOF (*e.g.* axial rotation and plane of elevation for an abduction motion) were maintained with respect to their predefined target. These assessments were quantified in terms of the Root Mean Squared Error (RMSE). Second, the repeatability of the system to follow these profiles was assessed by calculating the standard deviation over three repeated trials at each joint angle, and averaging these across the entire motion profile (average standard deviation, ASD).

Changes in arm mass replacement were made to simulate varying mass-to-anthropometric size characteristics among specimens. A third outcome was the assessment of the control system's characteristics in response to these changes. Specifically, arm mass replacement was tested at 60 and 140% of the physiologic mass replacement level for abduction in the scapular plane. Horizontal extension was not assessed as variations in mass were not expected to markedly affect horizontal extension. In order to assess the accuracy and repeatability of the controller for these varying mass levels, the RMS Error (RMSE) and average standard deviation (ASD) over three trials was determined.

The fourth outcome was an assessment of the controller's response to systematic changes in PID gain values and of how closely it replicates a classical closed loop control system. For abduction profiling, the systematic PID gain variation procedure first involved eliminating the integral time (inverse action of gain) and increasing proportional gain to the point of instability and oscillation. This was followed by restoration of the gains from the previously tuned (*i.e.* optimal) PID controller and subsequent systematic increases and

decreases in the integral time to the point of a slow overdamped response or an unstable underdamped response, respectively. This integral time variation procedure was performed for the controllers responsible for abduction and horizontal extension profiling. The procedure was performed for all three mass replacement levels; however, only the physiologic mass replacement level will be presented.

A final outcome was the system's ability to reject disturbances. This outcome was considered important due to the concurrent motion of the scapula which could affect control of glenohumeral motions. Disturbance rejection was assessed in terms of the size of disturbance in glenohumeral abduction and the time required to reject the disturbance when a non-physiologic scapular rotation was introduced. A disturbance of 23° of scapular rotation was applied while commanding the controller to maintain a constant glenohumeral rotation. The 23° disturbance was chosen since it would force the controller to compensate for large changes in the humeral gravity load. Changes in glenohumeral rotation were recorded throughout the test.

5.3 Results

5.3.1 Performance

Accuracy of the active motion simulator was found to be quite high with mean differences to the desired motion profile never greater than 1.7° for abduction and 2.2° for horizontal extension with Root Mean Squared (RMS) Error of 0.88° and 0.98°, respectively (Figure 5.3). Additionally, the non-profiled DOF were maintained to within 2.5° during abduction and 5.0° during horizontal extension each with an RMSE of <1.0°. Repeatability was found to be high with average standard deviations (ASDs) of 0.31° for abduction and 0.30° for horizontal extension while the maximum standard deviation at any instant in time during profiling never exceeded 0.84° for either motion over three trials (Figure 5.3). As well, repeatability for the non-profiled DOF averaged <0.5° across the entire motion.

5.3.2 Control System Characterization

There was little change in the control system's performance between any of the arm mass replacement levels (60, 100, 140 %BW). Specifically, with optimal PID parameters, it was found that for abduction, the RMSE and ASD for the three mass replacement levels were all similar (60%: 0.73° & 0.14°, 100%: 0.87° & 0.22°, 140%: 1.04° & 0.25°) (Figure 5.4).

The assessment of changes in proportional gain with no integral time value demonstrated that the abduction controller will yield a large steady state error of approximately 66% below the target value when using the gain value from the 'optimal' PID controller. This steady state error is decreased through increases in the proportional gain (Figure 5.5a); however, before the response reaches the target level, the system becomes unstable and oscillatory.

When increasing the integral time (*i.e.* decreasing integral gain) for abduction, the ability of the controller to follow the desired motion profile became progressively worse until the response was considered excessively slow and overdamped (integral time = 7x 'optimal' value) (Figure 5.5b). However, before this overdamped response was achieved, the system produced motions which lagged the setpoint profile, overshot the final target, and were slow to settle for integral times of 2-4x the 'optimal' value. During horizontal extension profiling, increasing the integral time value had little effect on the early stages of motion beyond slightly slowing the response; however, all of the attempted values of integration below the 'optimal' value resulted in unstable responses as the motion profile approached its completion (Figure 5.5c).

The effect of decreasing the integral time constant (*i.e.* increasing the integral gain) was characterized for abduction. The produced motion exhibited small increases in oscillation when integral time was decreased by 10 to 30%, but these oscillations remained small and centred on the setpoint profile (Figure 5.5d). However, when a 50% reduction in the integral time was applied, the prominence of oscillations increased markedly and these increased in amplitude as the motion progressed. Decreases in the integral time of the horizontal extension PID controller resulted in similar oscillatory behaviour to that of the

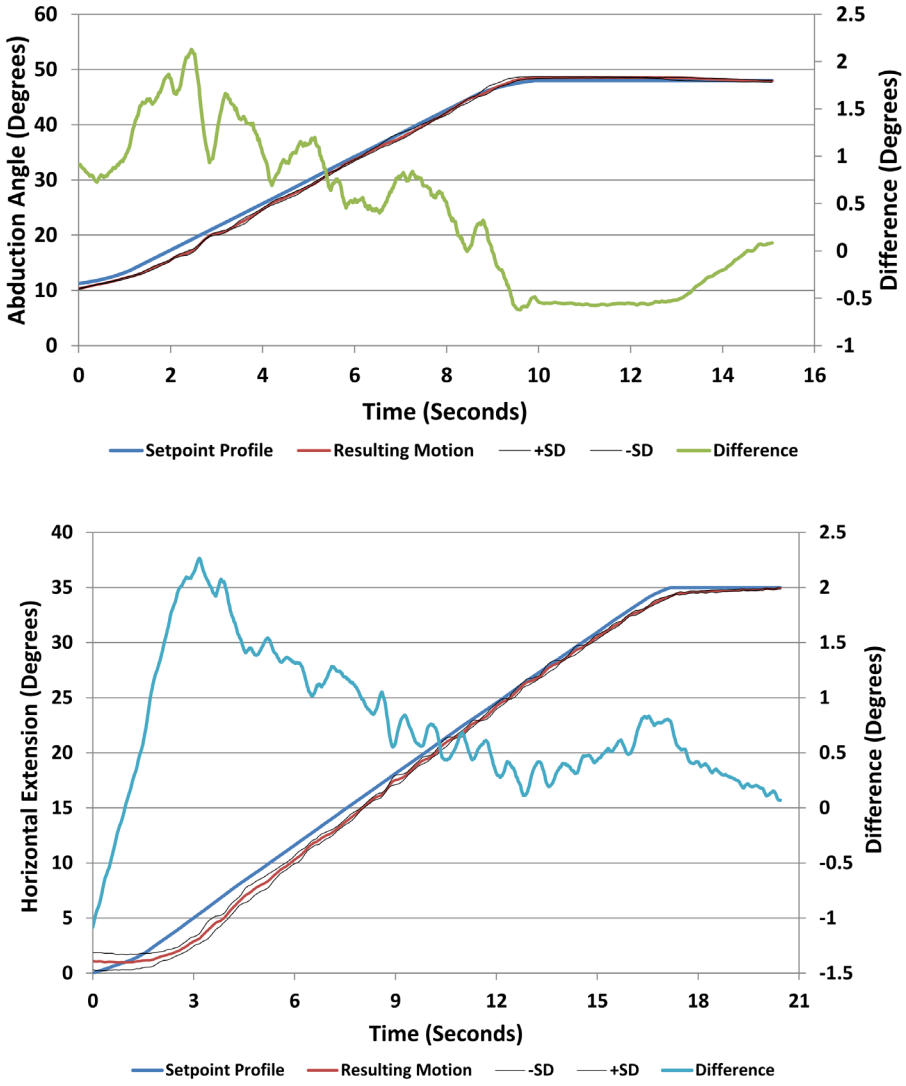

Figure 5.4: Abduction & Horizontal Extension Profiling Accuracy and Repeatability.

(Top) This graph illustrates the accuracy of the active motion simulator in following a predefined motion profile consisting of abduction in the scapular plane. The profile begins at the resting position (~10°) and ends with the arm parallel to the ground. (Bottom) This graph illustrates the accuracy of the active motion simulator in following a predefined motion profile consisting of horizontal extension with the arm parallel to the ground and externally rotated. The profile begins with the humerus in the scapular plane and ends 35° posterior to that plane. Note the 'Difference' series which is plotted on the secondary axis and is the difference between the profile and resulting motion. Also note the thin black standard deviation lines throughout the motion which demonstrate the high repeatability of the system.

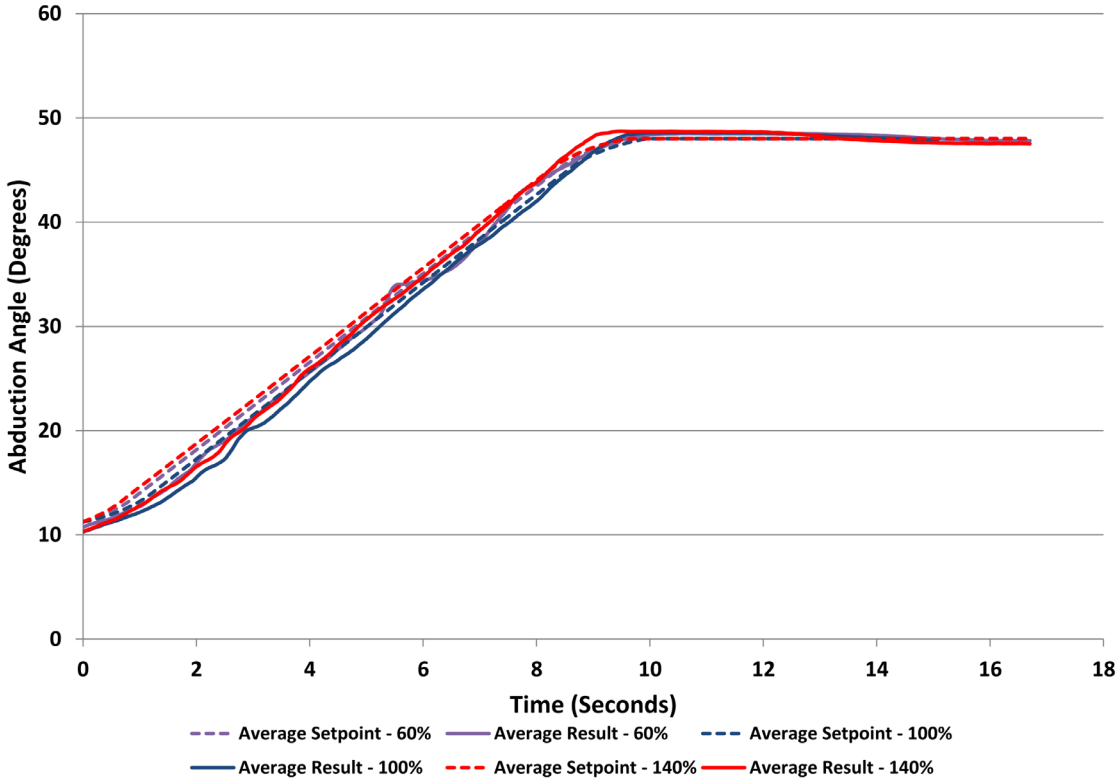

Figure 5.5: Effect of Variations in Specimen's Size-to-Mass Ratio.
This graph illustrates the simulator's response to a ±40% change in the specimen's mass which is used to replicate subjects with varying size-to-mass ratios. The dashed lines represent the respective setpoint profiles for this abduction motion while the solid lines are the resulting motions.

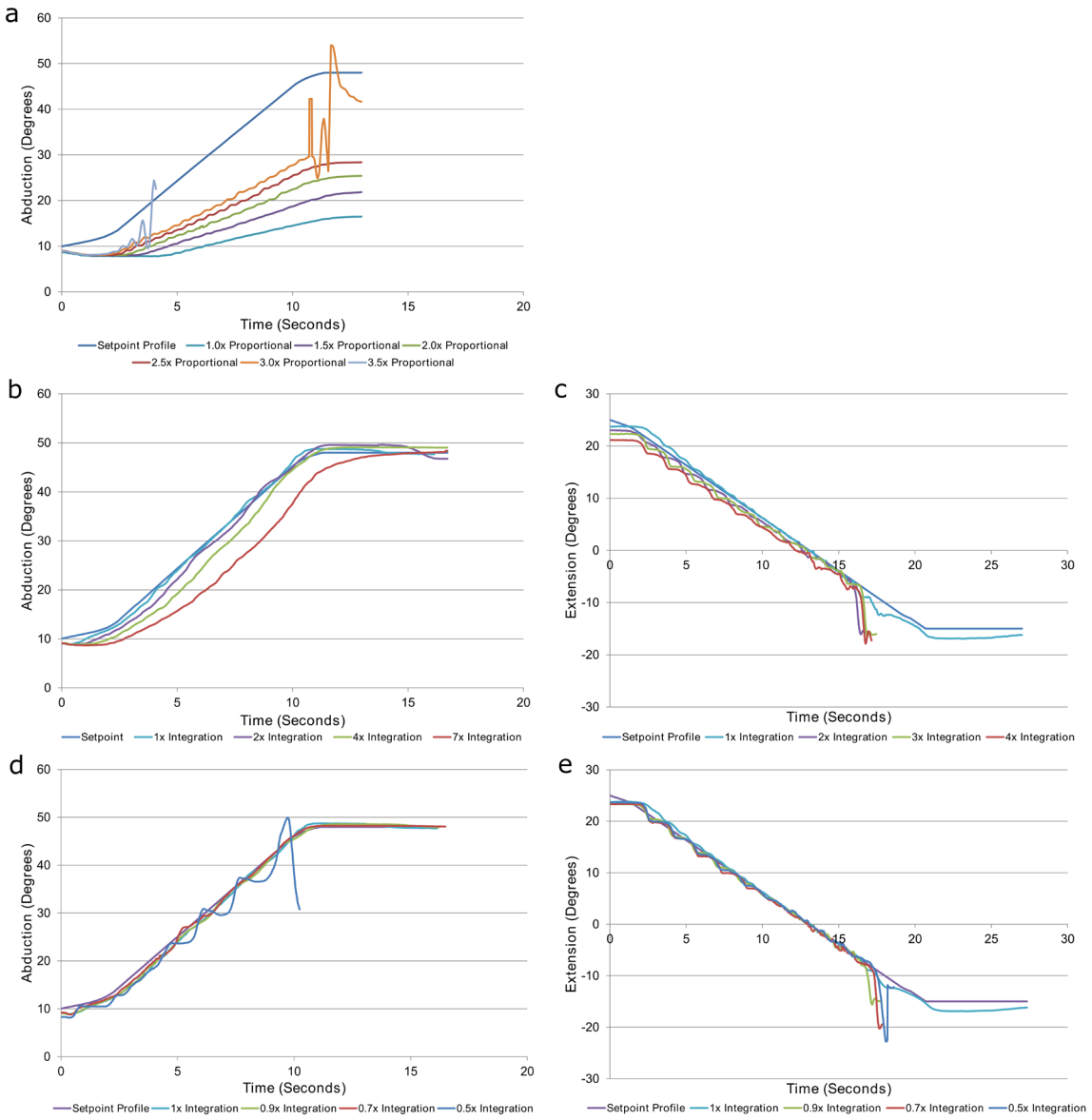

Figure 5.6: Effect of Varying Proportional and Integral Gains on Controller Characteristics.

(a) This graph demonstrates the response of a Proportional only controller and how this response varies with increasing gain values during abduction in the scapular plane. Graphs (b) and (c) demonstrate the effects of increasing the Integral time component of the 'optimal' PID controller during abduction in the scapular plane and horizontal extension, respectively. Similarly, graphs (d) and (e) demonstrate the effects of decreasing Integral time during abduction and horizontal extension, respectively.

abduction controller early in the motion profile, whereby oscillations were centred about the setpoint profile (Figure 5.5e). However, unlike the abduction controller, these oscillations were damped out for all decreases in integral time (10-50%) as the motion progressed. This dampening, however, was overcome near the end of the motion when all reductions in integral time resulted in instability that increased in magnitude as the effect of integration was increased.

The control system's ability to reject disturbances was assessed and it was found that the system was able to maintain the joint angle to within 4.8° of the desired level of abduction during the application of a non-physiologic scapular rotation (Figure 5.6). Additionally, the control system was capable of rejecting this disturbance and settle back to the desired abduction level within 3 seconds.

5.4 Discussion

In the past, *in-vitro* shoulder simulation has largely involved static assessments of shoulder stability and evaluation of motions passively applied by the experimenter while constant muscle loads were applied. However, the highly unconstrained nature of the glenohumeral joint is such that its kinematics are predominantly dictated by muscle loading and thus accurate replication of *in-vivo* muscle loading patterns is critical to the control of the shoulder's three rotational degrees of freedom. It is for this reason that we believe the implementation of real-time kinematic feedback and a closed-loop control system is critical to improving the physiological accuracy of simulated shoulder kinematics and kinetics. By refining these outcomes, we can gain an improved understanding of the effects of surgical procedures and implant designs on shoulder function. It was with this in mind that we developed and worked to validate the repeatability and physiologic accuracy of the simulator presented.

The primary measures of an active motion simulator's performance have traditionally been their accuracy in achieving a desired orientation and their repeatability in doing so. Our results indicate that this simulator, which is the first to use closed-loop control theory to produce smooth glenohumeral motion, is capable of accurately controlling abduction

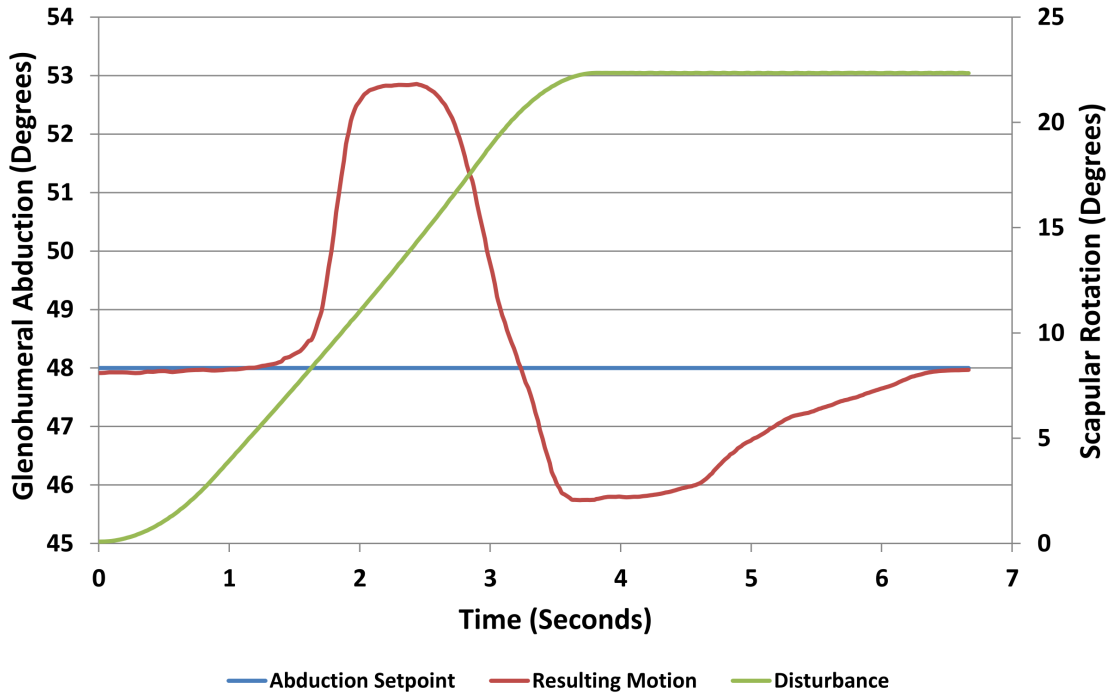

Figure 5.7: Simulator's Response to Scapular Disturbance.
This graph demonstrates the ability of the simulator's control system to minimize the effect of disturbances, in the form of a non-physiologic scapular rotation, and quickly reject any disturbance which does occur in the glenohumeral orientation. Note that the Disturbance series of data is plotted on the secondary axis.

and extension motions, with a high degree of repeatability, while maintaining predefined physiologic orientations in the two remaining degrees of freedom. The simulator's accuracy in following a desired motion profile can be characterized by an RMSE over the entire motion of 0.88° for abduction and 0.98° for horizontal extension. It is difficult to compare this accuracy to previous reports (Debski et al., 1995; Kedgley, Mackenzie, Ferreira, Drosdowech, King, Faber, & Johnson, 2007a) which only discussed an apparatus' ability to achieve a desired final orientation (mean error: 0.1-2.3°) but as demonstrated by Figure 5.3 A&B the PID action of our system ensures that all steady state error is eliminated at the final orientation. The accuracy of the system in controlling the non-profiled DOF was also excellent with an RMSE of <1.0°.

The system's repeatability was found to be very high with standard deviations averaged across the profile of ~0.3° for both motions. Again, comparisons of our repeatability across an entire motion to that of final orientation repeatability, which one would expect to be the highest possible throughout motion, are difficult; however, our results of ~0.3° compares well to that of Debski et al. who reported a repeatability of 1.0° (Debski et al., 1995). In terms of the repeatability of the non-profiled DOFs during a given motion profile, our result of average standard deviations of <0.5° compares well to the 2.0° report by Kedgley et al. who performed repeated trials using predefined load levels (Kedgley, Mackenzie, Ferreira, Drosdowech, King, Faber, & Johnson, 2007a).

In addition to traditional measures of performance, the simulator's characteristics were evaluated for various specimen conditions and variations in controller parameters in order to assess the effect on the closed loop control system's output. The first of these was determining the effect of variations in the ratio between the specimen's anthropometric size and the simulated weight, which was varied using masses attached to the intramedullary humeral rod. This was intended to evaluate the simulator's stability among specimens from donors of variable Body Mass Index (BMI). It was found that changes in the simulator's performance in response to adjustments of up to ±40% of the physiologic level of mass replacement were negligible (ΔRMSE=0.3°) but that performance did improve slightly with lower masses and declined with greater masses. Therefore, the

simulator's control system has been found to be sufficiently robust and stable as to not require adjustments to its parameters when specimens with varying anthropometric mass and size characteristics are tested using our current quasi-static motions. This robustness has been confirmed over the range of ±40% of the average adult male; however, it is conceivable that specimens exhibiting extreme size or mass characteristics may require adjustment to the control system's parameters. It has also been found that controller parameters do require adjustment when testing conditions in which the joint's geometry and/or function have been significantly altered such as the case of replacing native anatomy with a Reverse Total Shoulder Arthroplasty which inverts the glenohumeral ball and socket articulation.

From the assessment of the simulator's response to changes in the PID control parameters a number of conclusions can be drawn. First, when assessing the effect of a proportional controller with no integral effect, the proportional gain of the optimal controller was found to be insufficient to achieve the desired level of abduction and no increase in this gain would achieve the desired rotation at the rate of motion required without first causing unstable oscillations. Second, when assessing the effects of increasing the integral time (decreasing the integral gain) it was found that the response differed between abduction motions and horizontal extension motions. During abduction, it was found that it is possible to avoid any level of overshoot by increasing integral time; however, this requires a minimum 500% increase in integral time and slows the response by several seconds over the course of a full motion. As seen in Figure 5.5b, this overdamped motion in fact produced the smoothest and likely the most repeatable motion but at the expense of accurately following the desired profile. It can be argued that following the desired profile is of secondary importance to achieving optimal repeatability. However, this objective was not pursued as future work in simultaneously simulating multiple rotations would demand that the desired profile in each rotation be accurately followed, thus necessitating a controller tuned to minimize error.

During horizontal extension, attempts to create an overdamped response by increasing the integral time had little effect in the early stages of motion but initiated instability as the motion approached its end point. It is possible that this instability is related to the

decreased speed of the humerus, compared to that which occurs using the optimal parameters, which would cause error accumulation and rapid increases in load leading to oscillation. Third, when assessing the effects of decreasing the integral time (increasing the integral gain) it was found that two motions produced similar results in the early and late stages of motion whereby any decrease in the integral time ≥10% resulted in a motion pathway which oscillated about the setpoint as abduction progressed and eventually lead to unstable oscillations. However, in the case of horizontal extension, during the mid-range of motion these oscillations were dampened to the point of being nearly eliminated. It is possible that this dampening can be related to the greater effect of passive ligamentous restraint associated with the shoulder being positioned in 60° of humero-scapular abduction and most especially the effect of the Middle Glenohumeral Ligament which would tighten as the arm is extended. However, this dampening effect appears to be overcome as the shoulder reaches its most unstable position and the increased Integration effect becomes dominant.

Overall, the assessment of the simulator's response to changes in the closed loop control systems parameters has demonstrated that the system does largely replicate the characteristics of a classical control system whereby increases in proportional or integral gain cause an unstable underdamped response, while decreases cause a slow overdamped response and steady state errors. However, these expected responses are augmented by the variable effects of ligamentous tissues and bony impingement.

The simulator's ability to reject disturbances in scapular rotation was found to be quite robust in that the system only permitted a 4.8° change in glenohumeral orientation in response to a non-physiologic scapular rotation much larger than would be seen during testing. Additionally, the response to this disturbance was rejected within three seconds indicating that in the event that a disturbance is introduced, the resulting glenohumeral kinematics can be expected to closely replicate those produced during an undisturbed trial.

Despite the high levels of accuracy and repeatability, the simulator's physiologic accuracy has a number of limitations. First, the simulator is currently unable to accurately

replicate high velocity motions such as throwing due to the speed at which the controller would be required to react, and the added complexity of dynamic accelerations and inertia. However, we believe that the biomechanics associated with daily motions can largely be considered quasi-static. A second limitation of the simulator is its inability to actively control plane of elevation and axial rotation when the arm is below ~15° of abduction. This lack of control is an unavoidable result of using an Euler angle sequence which results in gimbal lock between these two rotations when the arm was adducted. As a result the error between the desired plane of elevation and axial rotation in these first 15° could be up to 5° as presented in the results. However, since these data were recorded, a shoulder joint decomposition algorithm, of the type described by Grood and Suntay for other joints, has been implemented as described by Amadi et al. (Amadi & Bull, 2010; Grood & Suntay, 1983). A description and validation of the use of this new decomposition method can be found in Appendix C. With this new method implemented, the lack of control during early abduction that was observed in this chapter and which led to large errors has now been eliminated. A third limitation relates to the single glenohumeral-to-scapulothoracic rhythm utilized in this investigation. Throughout this study a traditional 2:1 ratio was used despite more recent evidence that it may vary across abduction with the scapula producing a greater portion of the arm's overall rotation late in the arc of motion (McClure et al., 2001). Finally, although this evaluation was able to clarify the system's capabilities, an analytical model using concepts from Multiple Input Multiple Output control (for the multiple joint angle inputs and multiple muscles load outputs) and wire driven robots (Nazari & Notash, 2013) should be performed to ensure that the results of this chapter are in agreement with these widely validated methods.

In conclusion, the data presented in this chapter have demonstrated that the current simulator is capable of accurately replicating one of the most common motions of daily life – abduction – as well as the motion which commonly initiates instability – horizontal extension in abduction external rotation. The simulator has also demonstrated the ability to perform these motions with a repeatability as high as or higher than previously reported simulators. Additionally, the current simulator is the first to simultaneously control all three rotational degrees of freedom of the shoulder while also applying physiologically

accurate scapular rotations based on the instantaneous glenohumeral orientation. Finally, the simulator has moved away from heuristically defined muscle loading in favour of a closed loop PID control system, which we believe will more closely replicate *in-vivo* muscle loading and thus joint kinetics. With all of these factors in mind, the true strength of this control system, which uses three parallel PIDs, lies in its ability to perform motions that combine profiles in multiple DOF, such as cross body motions, where it would be extremely difficult to choose loads heuristically. As well, it is believed that this novel simulator produces an environment representative of physiological loading and is capable of providing new insight into shoulder biomechanics during normal and dysfunctional joint conditions.

5.5 Nomenclature

PID	Proportional, Integral, Differential controller
RMSE	Root Mean Square Error
ASD	Average Standard Deviation
K_u	Proportional gain causing oscillation in a proportional only controller
K_p	Proportional gain in proportional only controller causing a Quarter Amplitude Decay Response
T_u	Estimated oscillation period
T_i	Initial integral time value
T_d	Initial derivative time value

5.6 References

Amadi, H. O., & Bull, A. M. (2010). A motion-decomposition approach to address gimbal lock in the 3-cylinder open chain mechanism description of a joint coordinate system at the glenohumeral joint. *Journal of Biomechanics, 43*(16), 3232-3236. doi:10.1016/j.jbiomech.2010.07.034

Apreleva, M., Hasselman, C. T., Debski, R. E., Fu, F. H., Woo, S. L., & Warner, J. J. (1998). A dynamic analysis of glenohumeral motion after simulated capsulolabral injury. A cadaver model. *The Journal of Bone and Joint Surgery. American Volume, 80*(4), 474-480.

Balg, F., Boulianne, M., & Boileau, P. (2006). Bicipital groove orientation: Considerations for the retroversion of a prosthesis in fractures of the proximal humerus. *Journal of Shoulder and Elbow Surgery / American Shoulder and Elbow Surgeons ...[Et Al.], 15*(2), 195-198. doi:10.1016/j.jse.2005.08.014

Debski, R. E., McMahon, P. J., Thompson, W. O., Woo, S. L., Warner, J. J., & Fu, F. H. (1995). A new dynamic testing apparatus to study glenohumeral joint motion. *Journal of Biomechanics, 28*(7), 869-874.

Forte, F. C., de Castro, M. P., de Toledo, J. M., Ribeiro, D. C., & Loss, J. F. (2009). Scapular kinematics and scapulohumeral rhythm during resisted shoulder abduction--implications for clinical practice. *Physical Therapy in Sport: Official Journal of the Association of Chartered Physiotherapists in Sports Medicine, 10*(3), 105-111. doi:10.1016/j.ptsp.2009.05.005; 10.1016/j.ptsp.2009.05.005

Grood, E. S., & Suntay, W. J. (1983). A joint coordinate system for the clinical description of three-dimensional motions: Application to the knee. *Journal of Biomechanical Engineering, 105*(2), 136-144.

Halder, A. M., Halder, C. G., Zhao, K. D., O'Driscoll, S. W., Morrey, B. F., & An, K. N. (2001). Dynamic inferior stabilizers of the shoulder joint. *Clinical Biomechanics (Bristol, Avon), 16*(2), 138-143.

Henninger, H. B., Barg, A., Anderson, A. E., Bachus, K. N., Tashjian, R. Z., & Burks, R. T. (2012). Effect of deltoid tension and humeral version in reverse total shoulder arthroplasty: A biomechanical study. *Journal of Shoulder and Elbow Surgery / American Shoulder and Elbow Surgeons ...[Et Al.], 21*(4), 483-490. doi:10.1016/j.jse.2011.01.040; 10.1016/j.jse.2011.01.040

Hsu, H. C., Luo, Z. P., Cofield, R. H., & An, K. N. (1997). Influence of rotator cuff tearing on glenohumeral stability. *Journal of Shoulder and Elbow Surgery / American Shoulder and Elbow Surgeons ...[Et Al.], 6*(5), 413-422.

Itoi, E., Motzkin, N. E., Morrey, B. F., & An, K. N. (1994). Contribution of axial arm rotation to humeral head translation. *The American Journal of Sports Medicine, 22*(4), 499-503.

Kedgley, A. E., Mackenzie, G. A., Ferreira, L. M., Drosdowech, D. S., King, G. J., Faber, K. J., & Johnson, J. A. (2007a). The effect of muscle loading on the kinematics of in vitro glenohumeral abduction. *Journal of Biomechanics, 40*(13), 2953-2960. doi:10.1016/j.jbiomech.2007.02.008

Kedgley, A. E., Mackenzie, G. A., Ferreira, L. M., Drosdowech, D. S., King, G. J., Faber, K. J., & Johnson, J. A. (2007b). The effect of muscle loading on the kinematics of in vitro glenohumeral abduction. *Journal of Biomechanics, 40*(13), 2953-2960. doi:10.1016/j.jbiomech.2007.02.008

Kedgley, A. E., Mackenzie, G. A., Ferreira, L. M., Johnson, J. A., & Faber, K. J. (2007). In vitro kinematics of the shoulder following rotator cuff injury. *Clinical Biomechanics (Bristol, Avon), 22*(10), 1068-1073. doi:10.1016/j.clinbiomech.2007.06.005

Magermans, D. J., Chadwick, E. K., Veeger, H. E., & van der Helm, F. C. (2005). Requirements for upper extremity motions during activities of daily living. *Clinical Biomechanics (Bristol, Avon), 20*(6), 591-599. doi:10.1016/j.clinbiomech.2005.02.006

McClure, P. W., Michener, L. A., Sennett, B. J., & Karduna, A. R. (2001). Direct 3-dimensional measurement of scapular kinematics during dynamic movements in vivo. *Journal of Shoulder and Elbow Surgery, 10*(3), 269-277.

McClure, P. W., Michener, L. A., & Karduna, A. R. (2006). Shoulder function and 3-dimensional scapular kinematics in people with and without shoulder impingement syndrome. *Physical Therapy, 86*(8), 1075-1090.

McQuade, K. J., & Smidt, G. L. (1998). Dynamic scapulohumeral rhythm: The effects of external resistance during elevation of the arm in the scapular plane. *The Journal of Orthopaedic and Sports Physical Therapy, 27*(2), 125-133.

Nazari, V., & Notash, L. (2013). Workspace Of Wire-Actuated Parallel Manipulators And Variations In Design Parameters. *Transactions of the Canadian Society for Mechanical Engineering, 37*(2), 215.

Sharkey, N. A., Marder, R. A., & Hanson, P. B. (1994). The entire rotator cuff contributes to elevation of the arm. *Journal of Orthopaedic Research: Official Publication of the Orthopaedic Research Society, 12*(5), 699-708. doi:10.1002/jor.1100120513

Speer, K. P., Hannafin, J. A., Altchek, D. W., & Warren, R. F. (1994). An evaluation of the shoulder relocation test. *The American Journal of Sports Medicine, 22*(2), 177-183.

Woltring, H. (1990). Data processing and error analysis. In P. Berne, & A. Capozzo (Eds.), *Biomechanics of human movement, applications in rehabilitation, sport and ergonomics*. (pp. 203-237). Worthington, OH: Berlec Corporation.

Wu, G., van der Helm, F. C., Veeger, H. E., Makhsous, M., Van Roy, P., Anglin, C., . . . International Society of Biomechanics. (2005a). ISB recommendation on definitions of joint coordinate systems of various joints for the reporting of human

joint motion--part II: Shoulder, elbow, wrist and hand. *Journal of Biomechanics, 38*(5), 981-992.

Wu, G., van der Helm, F. C., Veeger, H. E., Makhsous, M., Van Roy, P., Anglin, C., . . . International Society of Biomechanics. (2005b). ISB recommendation on definitions of joint coordinate systems of various joints for the reporting of human joint motion--part II: Shoulder, elbow, wrist and hand. *Journal of Biomechanics, 38*(5), 981-992.

Wuelker, N., Wirth, C. J., Plitz, W., & Roetman, B. (1995). A dynamic shoulder model: Reliability testing and muscle force study. *Journal of Biomechanics, 28*(5), 489-499.

Ziegler, J., & Nichols, N. (1942). Optimum settings for automatic controllers. *Trans ASME,* , 759.

CHAPTER 6 – The Influence of Reverse Total Shoulder Arthroplasty Implant Geometric Variables on Muscle Activation, Joint Load and Shoulder Function

OVERVIEW

This chapter presents application of the newly developed passive and active simulator (as described in Chapters 2 & 5) functionality to the investigation of Reverse Total Shoulder Arthroplasty (RTSA). Use of these two sets of functionality enabled a more comprehensive assessment of the RTSA's effect. The configuration of RTSA implants is defined by a large number of parameters, but there is little information about the effects of each of these variables on post-operative shoulder function and loading. Therefore, we investigated the effects of three common parameters (humeral offset, humeral poly cup thickness, and glenoid offset) on active internal and external rotational range of motion, and on joint and deltoid muscle loading during active abduction. Humeral offset improved external rotation ($p=0.003$) and deltoid loading ($p=0.004$), and had no effect on joint loading. Humeral polyethylene cup thickness on the other hand, had no effect on external rotation but increased joint load and deltoid load ($p\leq0.012$). Glenosphere offset improved external rotation but worsened joint load and deltoid load ($p\leq0.002$). These results indicated that by using the methods developed in this thesis it has been possible to provide new insights into RTSA function; specifically, that humeral offset has the most positive effects on both shoulder function and loading.

6.1 Introduction

Reverse total shoulder arthroplasty (RTSA) has become an accepted option for the treatment of pseudoparalysis due to severe rotator cuff deficiency (Drake, 2010; Ek, Neukom, Catanzaro, & Gerber, 2013; Leung, Horodyski, Struk, & Wright, 2012; Nolan & Ankerson, 2011), as a salvage procedure following failed primary total shoulder arthroplasty (Castagna et al., 2013; Flury, Frey, Goldhahn, Schwyzer, & Simmen, 2011; Ortmaier et al., 2013; Werner, Boehm, & Gohlke, 2013), and as an alternative to hemi-arthroplasty in cases of severely comminuted proximal humeral fractures (Acevedo, VanBeek, Lazarus, Williams, & Abboud, 2014; Anakwenze, Zoller, Ahmad, & Levine, 2014; Bufquin, Hersan, Hubert, & Massin, 2007; Cuff & Pupello, 2013; Mata-Fink, Meinke, Jones, Kim, & Bell, 2013). Boguski et al. found in a review of 100 hospitals that RTSAs represented nearly 50% of all total shoulder arthroplasties performed in 2012 (Boguski, Miller, Carpenter, Mendenhall, & Hughes, 2013). Despite the widespread use of this procedure, there remains a paucity of information in the literature about the effects of specific RTSA implant parameters on biomechanical variables such as range of motion, joint and muscle loading, and strength.

Range of motion and strength have been investigated clinically by a number of authors (Boileau et al., 2006; Boileau, Watkinson, Hatzidakis, & Hovorka, 2006; Cuff, Pupello, Virani, Levy, & Frankle, 2008; Ek et al., 2013; Lenarz, Shishani, McCrum, Nowinski, & Gobezie, 2011). Results from these authors have all shown improvements in active abduction post-operatively, but only the results of Cuff et al. (2008) demonstrated a statistically significant improvement in active external rotation. The theoretical ranges of motion for various implant configurations have also been investigated using computer based solid models that use implant-bone impingement as the end points of motion (Gutierrez, Levy, Lee, Keller, & Maitland, 2007; Gutiérrez, ComiskeyIV, Luo, Pupello, & Frankle, 2008; Gutiérrez, Luo, Levy, & Frankle, 2009). However, these models have been unable to account for the effect of soft tissues and for the level of motion achievable through active muscle contraction. With respect to the muscle loads required to produce motion and the resulting joint loading, data in the literature are confined to computational models and a few *in-vitro* studies that investigate a small number of implant

configurations (Gutierrez, Walker, Willis, Pupello, & Frankle, 2011; H. B. Henninger, King, Tashjian, & Burks, 2013; H. B. Henninger et al., 2012; Kontaxis & Johnson, 2009; Nigro, Gutiérrez, & Frankle, 2013). Despite the information provided by these investigations, there remains a lack of comparisons between the effect of differing implant designs and more specifically, of the effect of the varying geometrical parameters underlying these components.

Therefore, the purpose of this investigation was to evaluate the effects of glenosphere and humeral component design parameters on shoulder ranges of motion, external rotation strength, resultant joint load, and total deltoid force required to achieve active abduction. The component parameters examined were glenosphere lateral offset, humeral polyethylene thickness, and lateral offset between the humeral cup and the humeral stem. To allow the assessment of levels of these variables beyond those currently achievable using commercially available systems, a custom adjustable implant system was designed. The glenoid components of this system were instrumented with a load sensing device to assess joint loading, and a custom active motion shoulder simulator was used to enable muscle loading driven assessments. For the above mentioned implant parameters, we hypothesized that glenosphere lateralization would increase the external rotation range of motion but would result in greater total deltoid force and increased joint loading. Conversely, we hypothesized that lateralizing the humerus would decrease the demands on the deltoid and reduce joint loads, whereas increasing the thickness of the humeral component would have little effect on deltoid and joint loading.

6.2 Materials & Methods

6.2.1 Custom Adjustable & Instrumented RTSA System

In order to assess a full range of RTSA geometric parameters beyond those achievable using the limited configuration options of any one commercial implant, custom humeral and scapular components were designed with multiple levels of adjustability for a number of variables (Figure 6.1). The custom scapular components were designed to accommodate a load sensor so that loads transmitted through the joint could be measured.

In this study, the implant variables of interest were glenosphere lateralization, humeral polyethylene cup thickness, and humeral cup medialization, which results in humeral lateralization; however, the custom implants were also designed for use with interchangeable glenosphere/humeral cup sizes, and allowed for the adjustability of glenosphere inferiorization, humeral head-neck angle, and humeral cup anteversion-retroversion. Glenosphere lateralization – also referred to as glenosphere offset – was evaluated at 0, 5, and 10mm, where 0mm represents a clinically neutral configuration when the base of the glenosphere is flush with the reamed glenoid surface. Humeral polyethylene cup thickness was tested at 0, 3, and 6mm, where 0mm corresponds to a clinically neutral configuration with the underside of the humeral cup's superior rim in line with the level of the anatomic neck. Humeral cup medialization, henceforth called 'humeral offset,' was assessed at 0, 5, and 10mm where, 0 mm corresponds to a clinically neutral configuration with the deepest point of the humeral cup being 12.5 mm medial to the long axis of the humeral shaft. Throughout this study, the remainder of the pertinent geometric parameters were held constant as follows: glenosphere/humeral cup size = 38mm, glenosphere inferiorization = 0 mm, humeral head-neck angle = 155°, humeral cup retroversion = 0° (note: see specimen preparation section for description of neutral implantation orientation).

6.2.1.1 Humeral Components

A commercially available polyethylene humeral cup (Delta XTEND, Depuy, Warsaw, IN) with a +3mm polyethylene cup thickness was used, and modified, in order to eliminate the possibility of our results being confounded by a custom component's differing material properties and surface finish. The humeral implant system (Figure 6.2) was also composed of a head-neck component, and humeral baseplate and stem that enabled offset and retroversion adjustments. The head-neck component (Figure 6.2C) could be interchanged to achieve differing head-neck angles and was also designed to permit the humeral cup (Figure 6.2A) to be threaded on with or without 3mm spacers interposed (Figure 6.2B). By interposing spacers, the polyethylene cup thickness could be effectively adjusted. In this study, zero, one, or two 3mm spacers were used. Prior to

Figure 6.1: Custom modular Reverse Total Shoulder Arthroplasty implants.
Photograph showing the humeral and scapular components including the six degree of freedom load cell interposed between the glenosphere and baseplate.

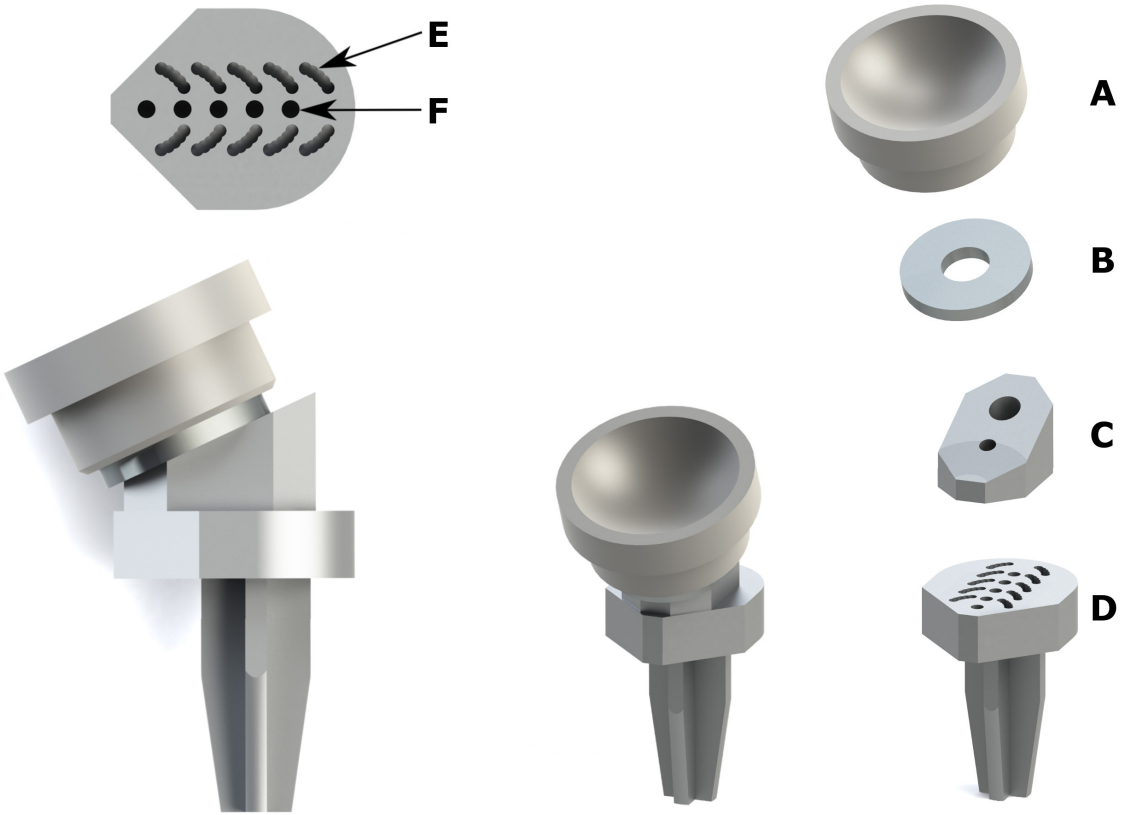

Figure 6.2: Custom modular humeral implant of our Reverse Total Shoulder Arthroplasty.
Top view of humeral stem and side view of assembled implant (left), isometric view of assembled implant (middle), and isometric exploded view (right). (A) Depuy Delta XTEND +3mm humeral cup, (B) 3mm humeral polyethylene cup thickness spacer (also 0 & 6mm), (C) 155° head-neck angle component (also 135° & 145°), (D) humeral stem and baseplate for cup adjustability, (E) retroversion dowel holes spaced at 5° (0-20°), and (F) threaded holes for medialization spaced at 5mm (-5 to +15mm).

attaching the humeral cup, the head-neck component could be fixed to humeral stem (Figure 6.2D) using a recessed bolt and locating pin. The bolt could be threaded into any of five holes spaced 5mm apart (Figure 6.2F) which corresponded to -5, 0, 5, 10, and 15mm of cup medialization (i.e humeral offset), where the 0mm hole is collinear with the implant stem. Additionally, at each of the five humeral offset levels, the locating pin could be placed into any of 9 holes spaced at 5° increments (Figure 6.2E) in order to achieve humeral retroversion of ±20° relative to the implant orientation. The humeral stem extended 35mm inferior to the humeral baseplate with a tapering cross-shaped cross-section to achieve maximum fixation stability. The full range of adjustability permitted by the custom modular implants is illustrated in Appendix D.

6.2.1.2 Scapular Components

Unlike the humeral cup, a corresponding commercially available glenosphere component was not used, as modifications to its fixation method were required. However, the custom glenosphere's articulating geometry mirrored the glenosphere component of the Depuy Delta XTEND humeral cup that was used. The articulating surface of the custom glenosphere was machined and polished to a finish equivalent to that of the commercial implant (Figure 6.3D). A commercially available six degrees of freedom (DOF) load cell (Nano 25, ATI-IA, Apex, NC) was interposed between the glenosphere and its underlying baseplate (Figure 6.3B) to measure loads passing through the RTSA (Appendix E). Use of this load cell permitted the full description of the joint loads and their transformation into any relevant coordinate system. The load cell's 22mm thickness precluded it from being interposed between the glenosphere and baseplate without affecting the component designs and surgical technique. Neutral glenosphere positioning was therefore achieved through modification of the glenosphere's undersurface and the implantation procedure. The base of the hemispherical glenosphere was machined to create a 10mm deep cylindrical pocket that would accommodate the load cell. The remaining 12mm load cell thickness and an additional 3mm of glenosphere baseplate thickness, which protruded beyond the glenosphere base, were accommodated by creating a 1" diameter, 15mm deep flat bottomed hole in the glenoid vault. The glenosphere baseplate (Figure 6.3A) was

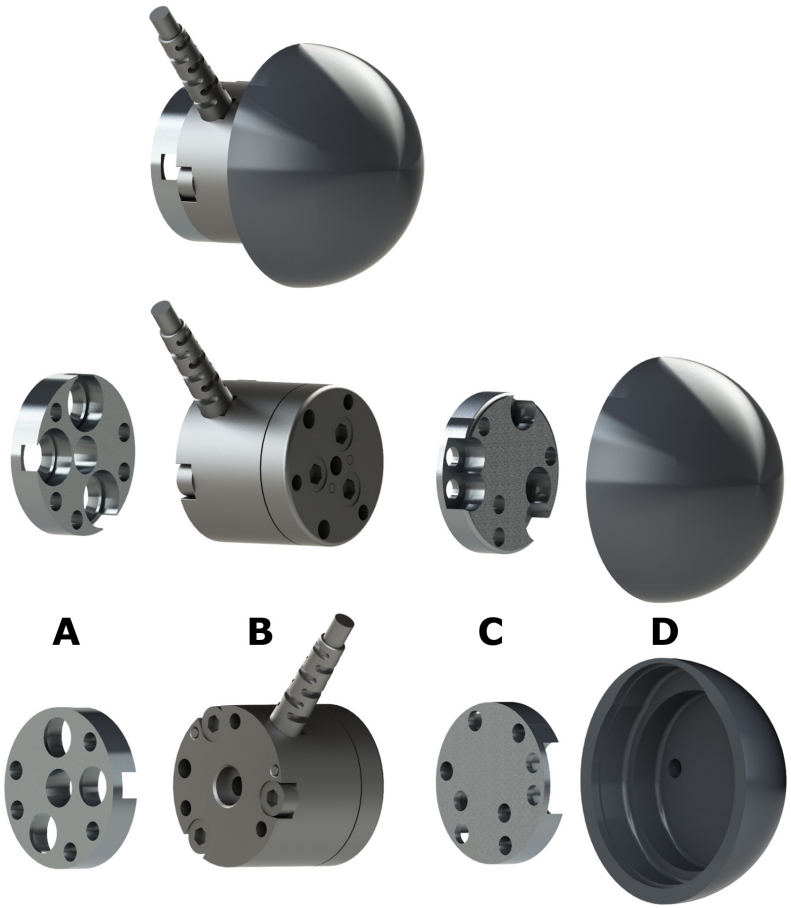

Figure 6.3: Custom modular scapular implant of our Reverse Total Shoulder Arthroplasty.
Isometric view of assembled glenosphere components (top), isometric exploded view (middle), and reverse angle of isometric exploded view (bottom). (A) glenosphere baseplate, (B) six DOF load cell, (C) 5mm (also 0 & 10mm) glenosphere lateralization spacer, and (D) custom glenosphere component with hollowed out base.

fixed in the glenoid vault using three 4.5mm screws and allowed the load cell to be mated using a tight push fit achieved using multiple locating pins. This allowed the sensor to be removed as required while maintaining rigid fixation during testing. This component setup – baseplate-load cell-glenosphere – corresponds to the 0mm glenosphere offset configuration while 5mm spacers could be further interposed between the load cell and glenosphere to achieve 5 and 10 mm offset configurations.

6.2.2 Specimen Preparation

Seven fresh-frozen cadaveric shoulders (71±10 years) free of rotator cuff deficiency, osteoarthritic changes, and prior surgery, were used in this study. The humerus was transected mid-shaft and minimally dissected to identify the deltoid insertion and rotator cuff muscles. The deltoid muscle was sharply resected from its humeral insertion to visualize the subacromial space. A full thickness tear was then created at the supraspinatus' insertion on the greater tuberosity. Next, the subscapularis was elevated from the subscapular fossa and reflected laterally in order to allow clear access to the glenohumeral joint both during implantation and implant configuration changes throughout testing.

Implantation of the custom RTSA was performed using the method described by the Depuy product manual with small modifications to accommodate the custom components. One modification that was required in some specimens was the removal of a small portion of the medial anatomic neck beyond the level of the traditional humeral head resection. This was done to permit full adjustability of the humeral implant. The humeral component, assembled in its neutral configuration, was then cemented in place as described in the implant design section. It was placed in the standard RTSA position of 0° humeral cup retroversion relative to the epicondyles and such that its superior rim was level with the superior anatomic neck (Figure 6.4). To implant the scapular components, the labrum was first resected from 3 to 9 o'clock and the glenoid face was lightly reamed. A guide pin was then placed in the glenoid so that the inferior edge of the glenosphere baseplate would coincide with the inferior glenoid (Figure 6.5). In order to accommodate

Figure 6.4: Photograph of implanted humeral component.
Photograph illustrating the positioning of the humeral implant relative to the intact humeral head anatomy.

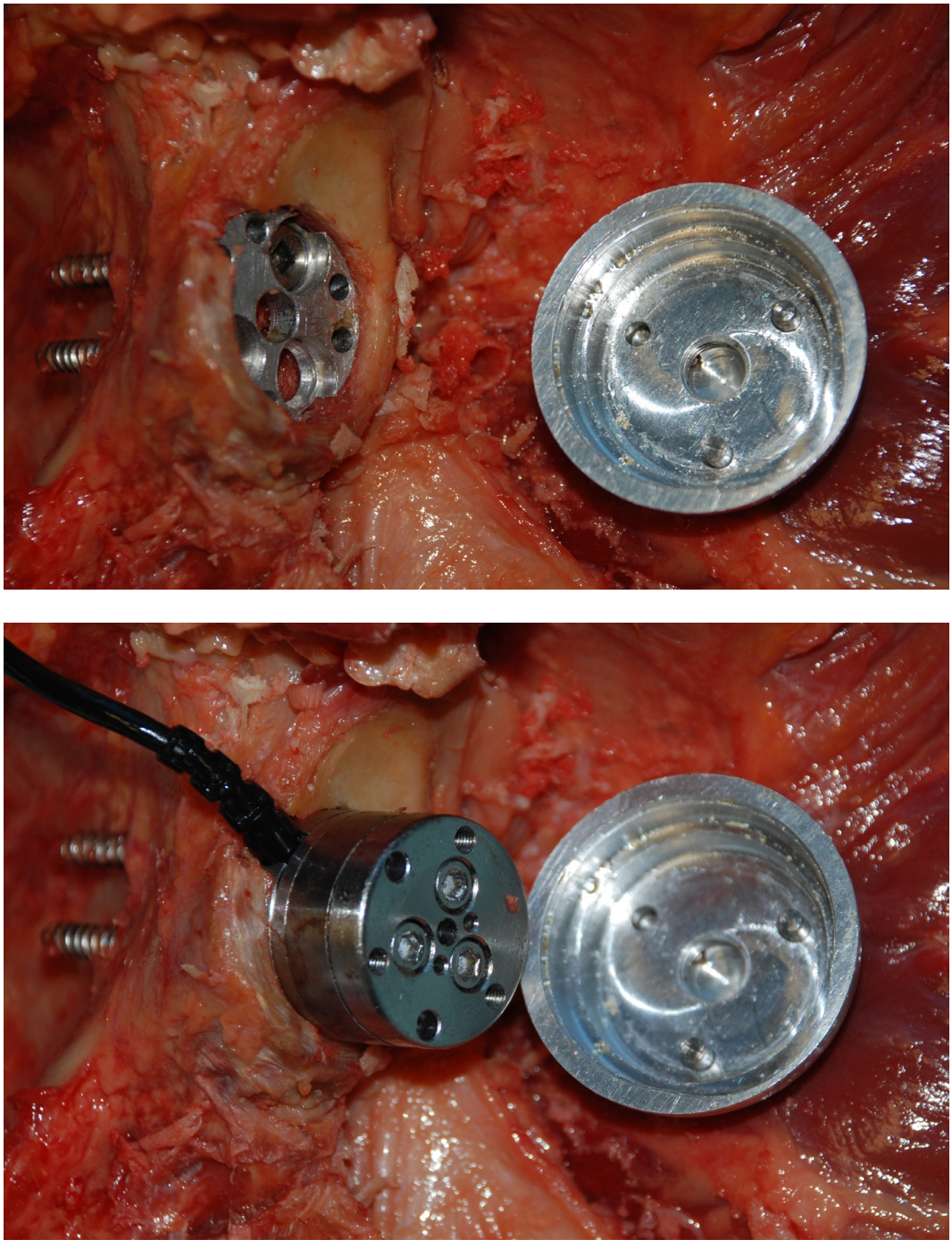

Figure 6.5: Photographs of glenosphere implantation.
Top, photograph taken during fixation of the glenosphere baseplate, demonstrating the flat bottomed hole created in the glenoid; bottom, photograph taken following attachment of the load cell and glenosphere showing the glenosphere in neutral lateralization with its inferior edge just lateral to the intact glenoid rim.

the interposed six DOF load cell, a 1" diameter flat bottomed, cannulated drill bit was then used to bore a 15mm deep hole in the glenoid using the previously placed pin as a guide. Using this hole depth ensured that when the glenosphere-load cell construct was placed on the baseplate, the glenosphere would be located in a neutral position. Once this hole was created, the custom baseplate was secured using three 4.5 mm screws. The glenosphere-load cell construct could then be attached and removed from the baseplate throughout testing as needed.

With implantation complete, the deltoid and rotator cuff tendons were sutured to permit loading during testing. The three heads of the deltoid were each sutured separately using a transosseous suture technique with holes located at the deltoid insertion. The subscapularis and infraspinatus were sutured at their musculotendinous junction using a running locking stitch that encompassed the inferosuperior breadth of the tissue. The remainder of specimen preparation was completed as described in Section 3.2, including the fixation of optical trackers (OptoTrak Certus, NDI, Waterloo, ON) to the scapula and the insertion of a load sensing and optically tracked intramedullary humeral rod.

6.2.3 Simulator Testing Apparatus

Following specimen preparation, humeral and scapular anatomic landmarks were digitized to create physiologically relevant coordinate systems for use in the real time control of joint motion and in *post-hoc* data analysis. The load sensor, glenosphere, and humeral cup were also digitized to facilitate the transformation of the recorded joint loads into meaningful coordinate systems. The scapula was cemented into the pot of the simulator as described in Chapter 3 (Section 3.2.1). This simulator enables loads to be independently applied to each of the rotator cuff groups and the three heads of the deltoid along physiologically accurate lines of action. It also has a guide system that facilitates the assessment of clinically relevant tests including passive and active range of motion, and strength. Additionally, as described in Chapter 5, the simulator is capable of producing accurate and repeatable muscle driven active motions through the use of real time kinematic data and a validated multi-PID control system. Before being passed to the control system, the raw kinematic data measured by the bone mounted optical trackers

was transformed into meaningful joint rotations using the joint motion decomposition method of Amadi et al. (Amadi & Bull, 2010). This method was implemented in place of the technique used in Chapter 5 (Section 5.2.2.2) because it allowed the control of all three rotational DOF even with the humerus in full adduction where traditional Euler angle methods would be unable to provide reliable measurements. The simulator system, in addition to producing glenohumeral motion, produced scapular rotations, which maintain the correct glenohumeral-to-scapulothoracic rhythm throughout active abduction.

6.2.4 Experimental Testing Protocol

Twenty-seven implant configurations were evaluated using a full factorial study design similar to that of Clouthier *et al.* (2013), corresponding to all of the possible combinations of the following three variables: (1) glenosphere lateralization – 0,5,10mm; (2) humeral polyethylene cup thickness – 0,3,6mm; (3) humeral lateralization – 0,5,10mm (Table 6.1). The testing order of these 27 configurations was randomized. It is important to note the 0, 3, 6 mm humeral polyethylene cup thicknesses would correspond to clinical thicknesses of 3, 6, and 9mm due to the +3mm Depuy polyethylene cup used in this study. Therefore, from this point forward the polyethylene cup thicknesses will be referred to as 3, 6, and 9 mm. Also, for each configuration, four distinct tests were performed: passive internal-external rotational ROM, active internal-external rotational (IR-ER) ROM, active external rotation (ER) strength, and active abduction. With the humeral rod held in adduction by the guide system described in Chapter 2 (Section 2.2.2), active IR-ER ROM was assessed by applying a combined 50 N load distributed between the subscapularis, infraspinatus, and three deltoid heads using the loading ratios described by Escamilla, Yamashiro, Paulos, and Andrews (2009), as outlined in Table 6.2. Loads were ramped over 10 seconds, and the final IR and ER orientations were recorded once the maximum load was held constant for three seconds. ER strength was assessed with the humerus held in adduction, neutral rotation, using the same loading protocol as for ER ROM. The torque produced by the joint was recorded by the load cell interposed between the two halves of the intramedullary humeral rod and was averaged over a two second period. Passive IR-ER ROM was assessed while constant loads were applied to the shoulder musculature as

described by Wellmann et al. (2009). In this test, the experimenter internally and externally rotated the arm until a predefined torque end point of 0.8 Nm was achieved, as previously described in Section 3.2.2. Active abduction was simulated from 0° (or as close as the RTSA configuration's adduction deficit would permit) to 90° of humerothoracic abduction at a rate of 1 degree/second. During this motion, scapular rotations were dictated by the 2:1 glenohumeral-to-scapulothoracic rhythm described by Inman and Abbott (1944). In the most extreme implant configurations, the mechanical advantage of the deltoid is severely diminished, and to facilitate smooth motion, active abduction was performed using 50% of the standard mass required to replace that of the removed distal arm.

6.2.5 Outcome Variables & Statistical Analyses

A number of outcome variables were used in this testing protocol to assess both the functional effects of the various configurations as well as their effects on muscle and joint loading during active motion. Active and passive IR ROM and ER ROM were each quantified as the magnitude of rotation from the neutral position with the humerus maintained in adduction using the humeral guide arc validated in Chapter 2 (Section 2.2.2). Active ER strength was quantified as the average torque measured by the humeral rod load cell. However, in the interest of brevity, this chapter will only present the active IR and ER ROMs from these functional outcomes.

In addition to the above-mentioned outcomes, the effects of implant configuration on active abduction were assessed using three outcome variables. First, resultant joint force was calculated by transforming the joint loads (Cartesian forces and torques) measured by the glenosphere load cell (using the previously recorded specimen, load cell, and implant digitizations) into a coordinate system oriented coincident with a standard glenoid coordinate system and located at the center of rotation of the glenosphere. It is important to note that movement of the center of the glenosphere due to lateralization was accounted for in this transformation. The accuracy of transforming these loads is assessed in Appendix A. The transformed Cartesian forces were then used to calculate the resultant joint force. Second, effects on total deltoid load were evaluated by measuring and

Implant Parameter	Adjustability Levels
Glenosphere Offset	*0, 5, 10 mm*
Humeral Poly Cup Thickness (including inherent +3mm component thickness)	*+3, +6, +9 mm*
Humeral Lateralization	*0, 5, 10 mm*

Table 6.1: Tested levels of RTSA implant parameters.

	Anterior Deltoid	Middle Deltoid	Posterior Deltoid	Infraspinatus	Subscapularis
Internal Rotation	0.16	0.00	0.00	0.16	1.00
External Rotation	0.00	0.22	0.30	1.00	0.32

Table 6.2: Muscle loading ratios used to achieve active internal and external rotation.

summing the force applied by the three heads throughout motion. The load recorded for joint load and deltoid load were transformed into percent body weight (%BW) by first accounting for the reduced level of mass replacement used during testing, and then dividing by the donor's total body weight. The third outcome – joint loading direction in the scapular plane – was calculated using the transformed y and z forces, which correspond to the superior and lateral directions, respectively. With this variable, 0° corresponds to a purely compressive force and positive angles to upwardly directed forces (Figure 6.6). Each of these three outcome variables were assessed at 5° increments between 15 and 50° of glenohumeral abduction – a range that all implant configurations were able to achieve.

A three-way (glenosphere lateralization, humeral polyethylene cup thickness, humeral lateralization) Repeated Measures ANOVA (RM-ANOVA) was performed for both the active IR and ER ROM outcome variables. A four-way (glenosphere lateralization, humeral polyethylene cup thickness, humeral lateralization, level of abduction) RM-ANOVA was performed for the three outcomes related to active abduction. Pairwise comparisons and analyses of interaction effects were performed for any cases demonstrating a significant trend effect ($p<0.05$). Power analyses were carried out for each outcome variable and it was found that seven specimens were sufficient to achieve at least 80% power for each outcome.

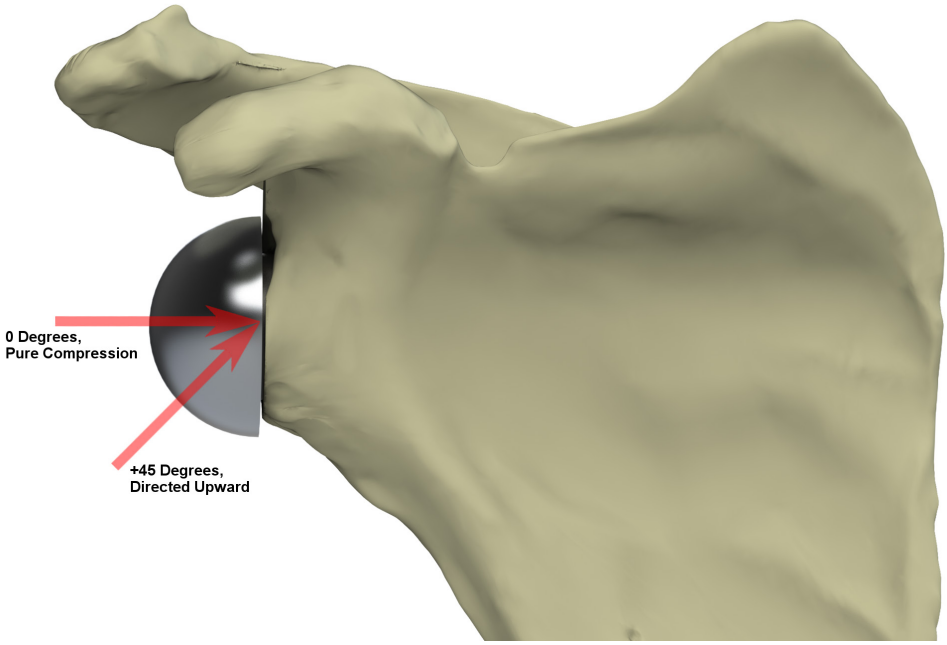

Figure 6.6: Definition of loading angle convention.
This figure illustrates the angular values which correspond to a purely compressive and upwardly directed joint load.

6.3 Results

6.3.1 Active IR & ER ROM

Results of the three way RM-ANOVA evaluating IR ROM demonstrated that humeral polyethylene cup thickness and glenosphere offset had a significant main effect on motion ($p=0.017$ & $p=0.04$, respectively). No statistically significant interaction effects were observed. Increases in humeral polyethylene cup thickness were found to decrease IR ROM while increases in glenosphere lateralization increased and then decreased motion (Figure 6.7). A similar analysis for ER ROM showed that humeral offset and glenosphere offset had significant main effects on motion ($p=0.003$ & $p=0.043$, respectively). In this case, increases in either variable resulted in increases in motion with glenosphere offset having a slightly stronger effect (Figure 6.7).

6.3.2 Joint Load

Results from the four way RM-ANOVA for resultant joint force demonstrated that humeral polyethylene cup thickness, glenosphere offset, and the level of abduction, produced significant main effects on loading ($p=0.007$, $p<0.001$, & $p=0.033$, respectively), but humeral offset did not (Table 6.3). Additionally, humeral offset and glenosphere offset each interacted significantly with abduction ($p=0.029$ & $p=0.003$, respectively) (Figure 6.8). Humeral polyethylene cup thickness and glenosphere offset both showed increases in joint load as the offsets were increased, while abduction showed increasing joint load as active motion progressed. The joint load produced by the +9mm humeral polyethylene cup thickness was significantly greater than that of the two lower levels (+3mm: 4.0±1.1%BW, $p=0.034$ & +6mm: 2.6±0.7%BW, $p=0.026$) while the joint loads associated with the varying glenosphere offsets were all significantly different from each other (at least 7.4%BW, $p\leq0.007$). Investigation of the pairwise comparisons for the two significant interactions showed that only one comparison, 0 vs 10mm at 30 abduction, was statistically significant (2.2±0.6%BW, $p=0.021$) for the humeral offset factor, while all but one

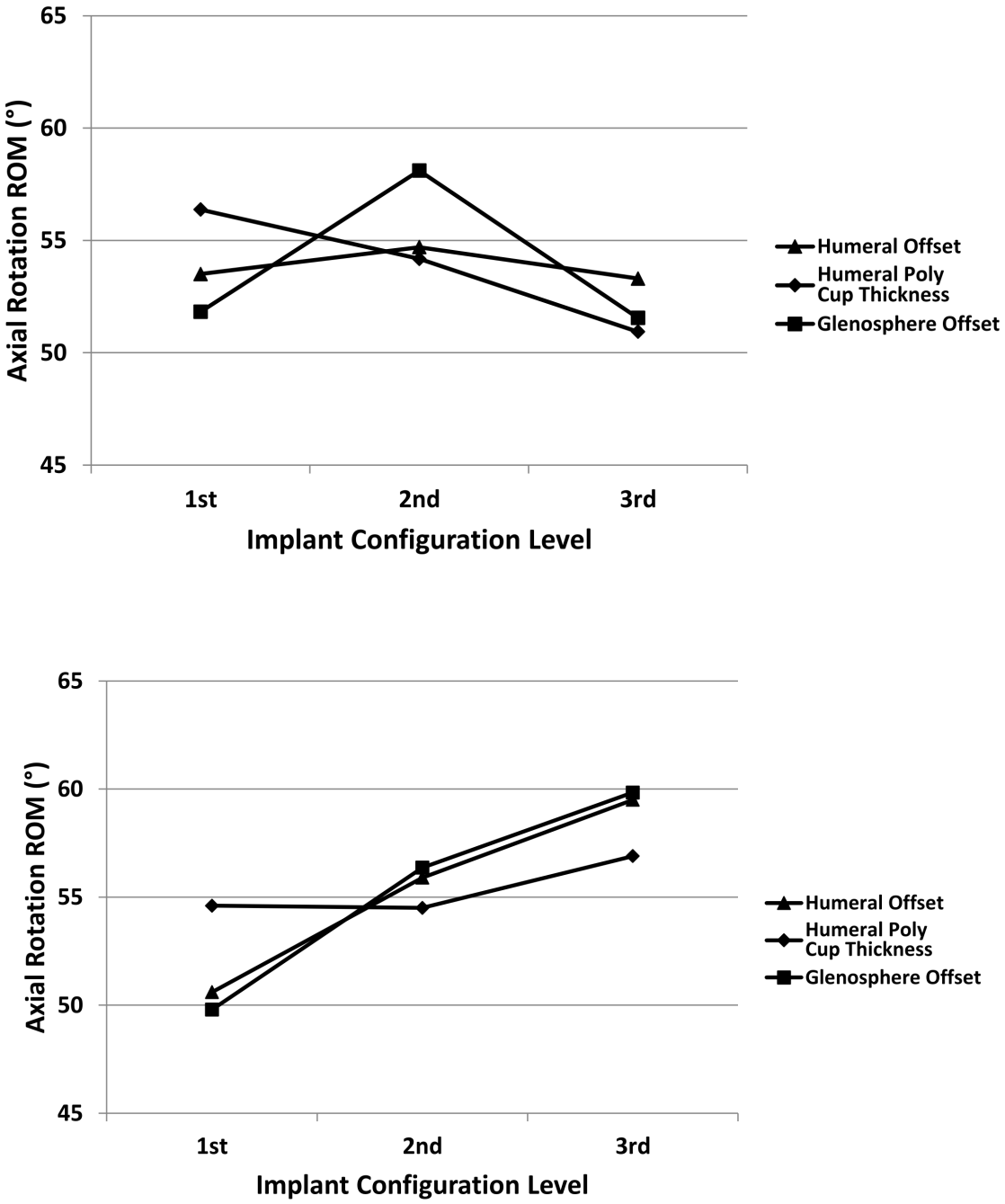

Figure 6.7: Implant variables with main effects on IR and ER ROM.
Graphs of mean (SDs omitted for clarity) IR (top) and ER (bottom) ROM for implant variables with a significant main effect. Note that levels on x-axis correspond to +3, +6 and +9 for the humeral polyethylene cup thickness variable and 0, 5, & 10mm for the humeral and glenosphere offset variables. Standard deviations from 9.1° to 16.0°.

	Joint Load (%BW)			Deltoid Load (%BW)			Joint Load Angle (°)
	Humeral Offset	Poly Cup Thickness	Glenosphere Offset	Humeral Offset	Poly Cup Thickness	Glenosphere Offset	Humeral Offset
	Main Effects						
	p=0.275	p=0.007	p<0.001	p=0.004	p=0.012	p=0.002	p<0.001
	Pairwise Comparisons						
1st Configuration Level	62.2±3.2 (346N)	60.0±2.8* (334N)	53.4±3.0*,† (298N)	67.8±3.3* (378N)	64.8±3.4* (361N)	61.4±2.8*,† (342N)	37.2±4.4*,†
2nd Configuration Level	62.0±3.2 (345N)	61.4±3.2† (342N)	62.3±2.8*,‡ (347N)	66.3±3.2 (369N)	66.5±3.0† (371N)	67.2±2.5* (374N)	34.6±4.2*,‡
3rd Configuration Level	61.3±2.8 (341N)	64.0±3.3*,† (357N)	69.7±3.7†,‡ (388N)	64.9±2.9* (362N)	67.7±2.9*,† (377N)	70.4±4.2† (392N)	31.2±4.1†,‡

Table 6.3: Summary of implant parameters with significant main effects for active motion outcome variables.
This table outlines the factors which produced significant main effects for each of the three outcome variables. Additionally, follow-up pairwise comparisons are shown (mean±SE) for these significant variables. As well, the Newton load values are provided in brackets. Note that the 1st, 2nd, and 3rd offsets correspond to 0, 5, and 10mm for the humeral offset and glenosphere offset factors but 0, 3, and 6mm for the humeral polyethylene cup thickness factor.

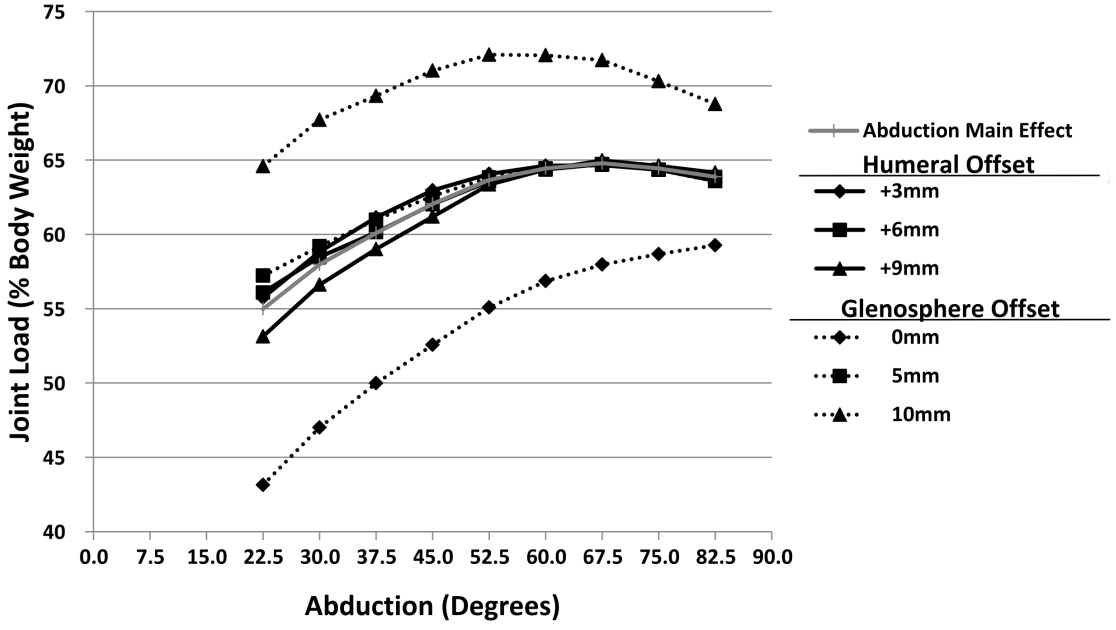

Figure 6.8: Implant variables whose effects on joint load varied across abduction. *Data represent the mean (SDs omitted for clarity) joint load averaged over all conditions and for differing levels of humeral and glenosphere offset (0, 5, 10mm). Standard deviations from 7.3 to 12.3 %BW.*

comparison in the glenosphere offset interaction were significant (≥4.3%BW, p≤0.023) (Figure 6.8).

6.3.3 Total Deltoid Load

All factors in this analysis were found to produce a significant main effect: humeral offset (p=0.004), humeral polyethylene cup thickness (p=0.012), glenosphere offset (p=0.002), and active abduction angle (p<0.001) (Table 6.3). The variations in deltoid load across active abduction, for the differing levels of humeral and glenosphere offset, are shown in Figure 6.9. Additionally, there was a significant interaction effect between the humeral offset and glenosphere offset factors (p=0.03). The humeral offset main effect demonstrated a trend of decreasing deltoid load with increasing offset while the remaining three main effects produced increases in force as their value increased. Pairwise comparisons for each of the implant factor main effects demonstrated that: 0 and 10mm humeral offsets significantly differed (3.0±0.7%BW, p=0.022); +9mm humeral polyethylene cup thickness significantly differed from +3 and +6mm (2.9±0.8%BW, p=0.03 & 1.1±0.2%BW, p=0.006, respectively); 0mm glenosphere offset significantly differed from 5 and 10mm (5.8±1.2%BW, p=0.01 & 9.1±1.8%BW, p=0.007, respectively). The interaction between humeral offset and glenosphere offset demonstrated that deltoid load decreased with increasing humeral offset for all levels of glenosphere offset; furthermore, the effect of humeral offset was strongest with the glenosphere in its 10mm position (Figure 6.10). Moreover, the stronger effect of humeral offset with the glenosphere in 10mm caused the comparisons at 5 and 10mm of humeral offset to not be significant between the 5 and 10mm glenosphere offsets (≤3.1 %BW, p≥0.878) when all other comparisons were (≥5.5%BW, p≤0.031).

6.3.4 Joint Load Angle

Only humeral offset and active abduction angle produced significant main effects (both p<0.001) for this outcome, while glenosphere offset significantly interacted with abduction (p=0.012) (Table 6.3) (Figure 6.11). Increases in humeral offset or abduction angle both produced decreases in the joint load angle (*i.e.* a more centrally directed load).

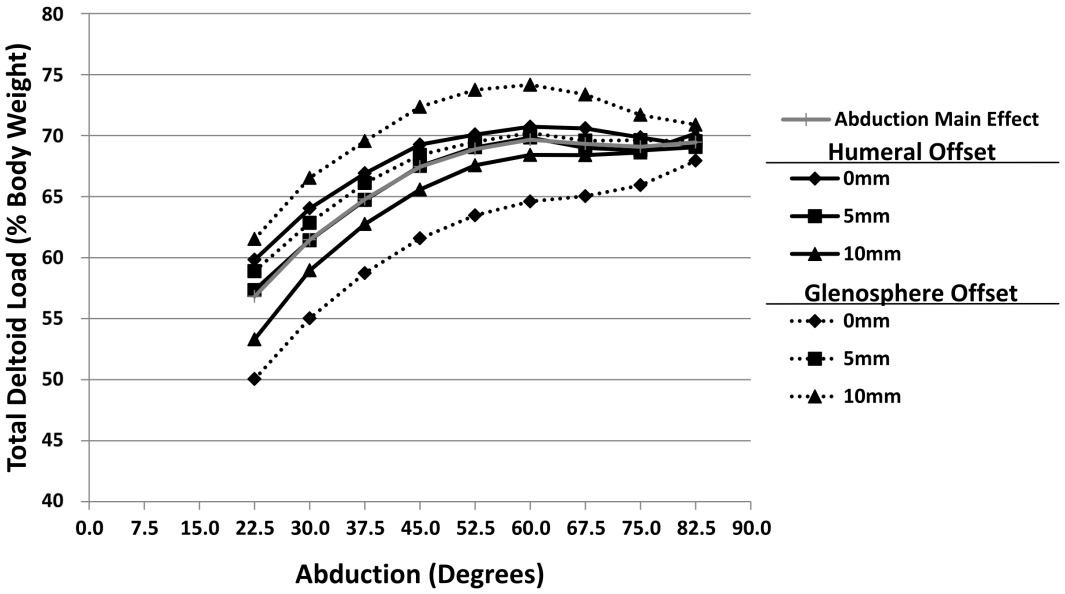

Figure 6.9: Total deltoid load across abduction.
Data represent mean (SDs omitted for clarity) of total deltoid force over all conditions and for differing levels of humeral and glenosphere offset (0, 5, 10mm). Note that humeral and glenosphere offset data sets are shown for interest sake but neither produced a significant interaction with abduction for this outcome. Standard deviations from 4.0 to 15.6 %BW.

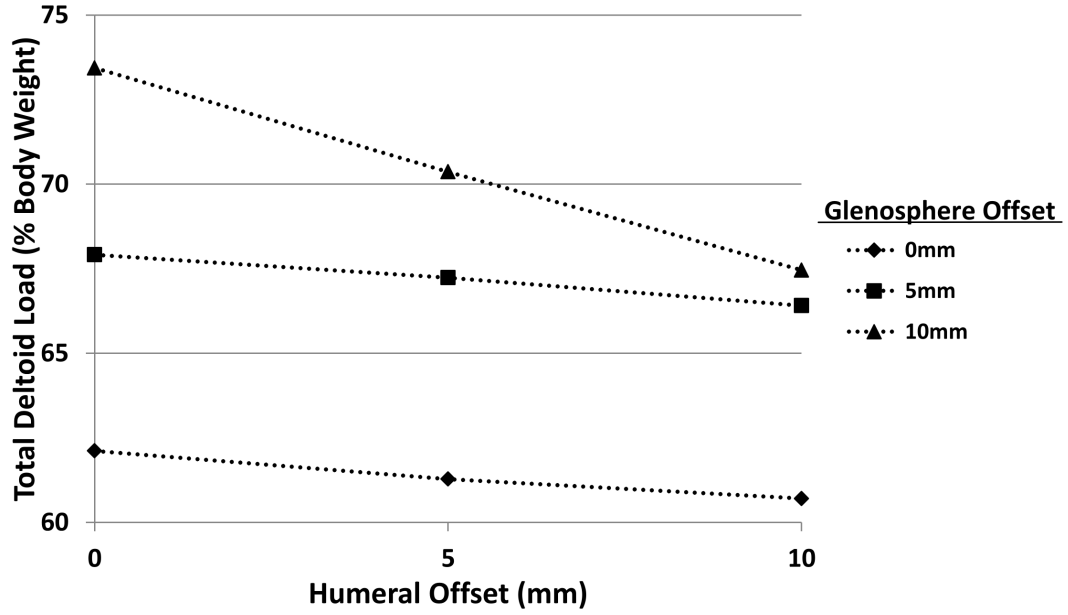

Figure 6.10: Total deltoid load interaction between humeral and glenosphere offset.
Data represent mean (SDs omitted for clarity) of total deltoid load across abduction for changes in humeral and glenosphere offset. Standard deviations from 5.8-12.3 %BW.

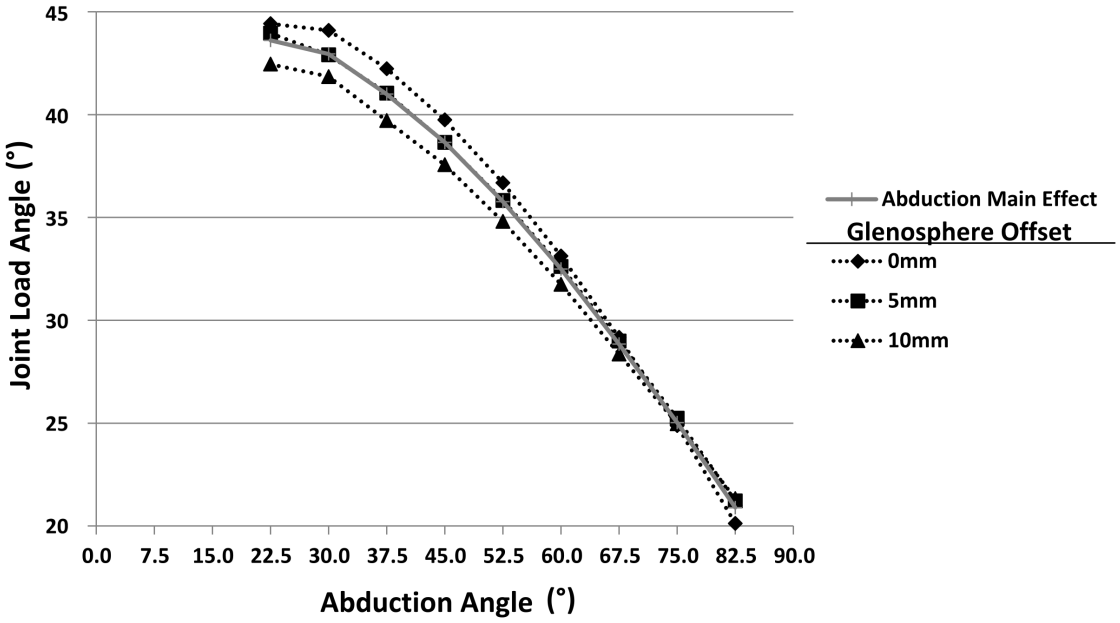

Figure 6.11: Joint load angle across abduction.
Data represent mean (SDs omitted for clarity) of joint load angle over all conditions and for differing levels of glenosphere offset (0, 5, 10mm) which produced a significant interaction with abduction. Standard deviations ranged from 9.5° to 13.5°.

All pairwise comparisons between the three humeral offset levels were significantly different (Mean at 0mm: 37.2±11.5°; Difference 0mm vs 5mm: 2.6±0.4°, $p=0.002$; Difference 0mm vs 10mm: 6.0±0.5°, $p<0.001$; Difference 5mm vs 10mm: 3.4±0.3°, $p<0.001$).

6.4 Discussion

Reverse Total Shoulder Arthroplasty has become a common procedure for an array of shoulder conditions; however, its primary indication is for the treatment of patients suffering from rotator cuff tear arthropathy that impair shoulder function. The purpose of this procedure, as described by Grammont and Baulot (1993), is to medialize the shoulder's center of rotation, thus increasing the mechanical advantage (*i.e.* effective strength) of the remaining muscles – primarily the deltoid. Since RTSA's original description, a number of implant parameters have been introduced to improve its efficacy with respect to increasing the deltoid muscle's mechanical advantage, and to address clinical problems, such as scapular notching. Three implant parameters that vary among current commercial RTSA systems are: humeral cup medialization, humeral polyethylene cup thickness, and glenosphere lateralization. However, the effects of these variables on important functional and biomechanical variables have not been fully investigated. Thus, this study aimed to clarify the implant variables' effects on: internal rotation range of motion, external rotation range of motion, the deltoid loading required to produce active shoulder abduction, and the joint loading resulting from this motion.

6.4.1 Active IR & ER ROM

Internal and external rotational ROMs were each evaluated. Humeral polyethylene cup thickness and glenosphere offset were each found to affect IR ROM. Although humeral polyethylene cup thickness produced a decrease in motion that totaled ~5° across its three levels, glenosphere offset increased rotation by ~6° when offset was increased by 5mm; however, this increase was reversed when the offset was further increased to 10mm. With respect to the effects of changing humeral polyethylene cup thickness, the decreases observed can perhaps be attributed to how the rotator cuff insertions are inferiorized when

humeral polyethylene cup thickness is increased. This inferiorization may decrease the overall effectiveness of the cuffs or the range across which they are effective. Despite these neutral or negative effects on IR ROM, all of these values fell just below or above (-5 to +11°) the average physiologic value (~46°) in the literature for native anatomy (Virani et al., 2013). In contrast, humeral offset had no effect at any level of lateralization.

The range of external rotation was significantly increased by both humeral and glenosphere offset with each producing approximately equivalent increases of 10° when their levels were increased from 0 to 10mm. These ER ROM exceeded the post-operative results reported by Cuff et al. (2008) but were still ~17° less than the average physiologic ER ROM presented in the literature for native anatomy (Virani et al., 2013). In the clinical setting, external rotation is typically limited following RTSA, but internal rotation is less affected; therefore, both humeral and glenosphere offsets represent a positive option for increasing ER without negatively affecting IR. Conversely, humeral polyethylene cup thickness has no effect on ER and decreases IR, and thus is not a favourable option for improving post-operative ROM.

6.4.2 Joint Load

The joint loading results obtained in this active motion study averaged over all conditions were much higher than those of Ackland et al.'s static simulation (65%BW vs 29%BW at 90° abduction) and somewhat higher than the computational results of Kontaxis et al. (50%BW at 100° abduction) both of whom did not simulate rotator cuff loading (Ackland, Roshan-Zamir, Richardson, & Pandy, 2011; Kontaxis & Johnson, 2009). Our results, however, were very similar to the finite element study by Terrier et al. (60%BW), who like us, simulated only a supraspinatus deficiency (Terrier, Reist, Merlini, & Farron, 2008). Joint load magnitude was not affected by changes in humeral offset, but did increase as a result of increases in humeral polyethylene cup thickness or glenosphere offset. However, humeral polyethylene cup thickness only increased joint load by 3%BW from its +3 to +9 configuration, which may not represent a clinically significant change. Glenosphere offset, on the other hand, increased joint load by ~16%BW from its 0 to 10mm configuration. The greatest effect of glenosphere lateralization on joint load was

seen at the initiation of active abduction and decreased as the arm approached 90°. Glenosphere lateralization is often advocated as a means to avoid scapular notching, which occurs when the humeral cup impinges on the lateral scapular border inferior to the glenoid; however, this adjustment reduces the effectiveness of the shoulder musculature and as a result, increases joint loading as observed in these data. These increases in joint loading may lead to increased wear of the polyethylene humeral cup and will increase the loads experienced at the glenosphere baseplate, which may negatively affect fixation.

6.4.3 Total Deltoid Load

In comparing our average total deltoid load results over all joint conditions to those of Ackland et al. and Kontaxis et al., our loads are larger (67%BW vs 37%BW & 45%BW, respectively)(Ackland, Roshan-Zamir, Richardson, & Pandy, 2011; Kontaxis & Johnson, 2009). However, the studies by Ackland *et al.* and Kontaxis *et al.* modeled RTSA with complete rotator cuff deficiency, whereas our model involved actively loading the infraspinatus/teres minor and the repaired subscapularis muscle. It is possible that the remaining rotator cuff muscles function as adductors, thus increasing demands on the deltoid during the initiation of active abduction. Detailed analysis of our data demonstrated that the total deltoid muscle load required from the three heads to achieve motion was significantly affected by all three implant variables. Increases in humeral offset were found to effectively decrease the required deltoid force, while increases in the other two parameters (glenoid offset and humeral polyethylene cup thickness) each increased the required deltoid load. Humeral offset and humeral polyethylene cup thickness produced equivalent changes in the magnitude of deltoid load, but the former decreased deltoid load while the latter increased it. Glenosphere lateralization produced a much more significant effect by increasing deltoid load by 7%BW when increased by 10mm. Although the clinical significance of these findings are difficult to determine, humeral offset is the only parameter in this model that decreased deltoid loading, whereas glenosphere offset produced a marked increase. Therefore, humeral offset and glenosphere offset should be important considerations when addressing the common clinical complications of deltoid fatigue and acromial fractures, which are both, associated with excessive increases in deltoid load. In most implant systems, the only

modifiable factor of the aforementioned three parameters is humeral polyethylene cup thickness. Therefore, during surgery the implant should not be over-stuffed with placement of an overly thick polyethylene insert, as this will likely have detrimental effects on deltoid muscle loading. Further studies are required to determine the optimum joint load and soft tissue tension to maximize stability and minimize deltoid muscle loads.

Results for total deltoid loading also showed that humeral and glenosphere offsets interacted significantly. This interaction indicated that increasing humeral offset can be used to counter the increasing deltoid load requirements associated with increased glenosphere lateralization, and that this countering effect is strongest when the glenosphere is offset by 10mm. However, this effect cannot fully reverse the deleterious effect of glenosphere lateralization on required deltoid load, and thus humeral offset should not be considered as a valid means to completely compensate for excessive glenosphere lateralization. This is especially important when considering the effect of glenosphere lateralization on baseplate loading. It is unlikely that the observed decreases in the deltoid load associated with humeral offset would be sufficient to eliminate the increases in baseplate moments produced by the increased distance between the baseplate and glenosphere rotation center.

6.4.4 Joint Load Angle

The joint loading angle in the scapular plane was found to be affected only by changes in humeral offset. Increases in humeral offset decreased average load angle from ~37° to ~31° over a 10mm change. Glenosphere offset interacted with abduction angle whereby increases in offset had a more pronounced effect of decreasing load angle with the arm in adduction than in abduction. These findings further support the use of humeral offset as a means to limit the negative effects of joint loading by producing a load vector which is more compressive, and thus less challenging to baseplate fixation.

6.4.5 Limitations and Strengths

This study had a number of associated limitations. First, the study used cadaveric specimens, which limits the precise replication of the physiologic condition. However,

because RTSA is used to treat massive rotator cuff tears, the articulating surface and a number of soft tissues, whose properties may be of concern in other cadaveric models, were removed as part of the implantation protocol. Second, the full mass of each specimen's arm was not simulated because pilot testing demonstrated that some RTSA configurations severely diminished the musculature's mechanical advantage, making motion simulation difficult. The presented %BW should, however, be physiologically accurate because joint and muscle forces are directly related to the arm mass. Although not necessarily a limitation, it should be noted that the muscle groups loading in this study are not representative of all patients treated with RTSA as some have only partial rotator cuff function post-operatively, while others have no function. Finally, stability of the joint during differing implant configurations was not investigated and this information may be important to fully understanding the positive and negative effects of these variables.

This model also had a number of strengths: (1) it is the first to evaluate a full range of possible implant configurations that encompass both commercially available configurations and those that were previously unconsidered; (2) it is the first to directly measure the six DOF joint loads occurring at the glenosphere; and (3) it combined assessments of both shoulder function and loading characteristics. Further to the second strength, the six DOF loads were quantified using a novel glenosphere-load cell construct which is a first in the investigation of shoulder joint loads. Prior studies that have investigated joint loading following arthroplasty have used load cells mounted beneath the potted scapula which is likely to result in loading artifacts related to contact of muscle cables on the scapula as well as the inability to quantify internal joint loads caused by passive soft tissues. These limitations are effectively eliminated in the construct described in this study.

6.4.6 Conclusion

By considering the results from each of these outcome variables, it is possible to draw a number of conclusions about the effects and potential implications of the three Reverse Total Shoulder Arthroplasty implant parameters investigated. First, medializing the humeral cup, and thus lateralizing the greater tuberosity, improves external rotation

without limiting internal rotation. This medialization also decreases the demands on the deltoid during abduction, and produces a more compressive joint load; however, it does not decrease the magnitude of joint load. Second, increasing the thickness of the humeral polyethylene cup negatively affects internal rotation without an associated improvement in external rotation. Additionally, these increases in thickness produce increases in joint load magnitude and required deltoid force without improving the joint load angle. It is thus important with this variable to balance between thinner components which may be more susceptible to failure due to wear and thicker components which induce greater joint load and thus the potential for wear. Third, increasing glenosphere lateralization improves external rotation and has neutral to positive effects on internal rotation depending on the amount of the offset used. However, this offset produces the largest increase in joint load and total deltoid force of any parameter tested without having a positive effect on joint loading direction.

Therefore, with respect to the assessed outcomes, humeral polyethylene cup thickness may not represent a useful option in optimizing RTSA implant design since it was not found to have any meaningful positive effect on shoulder function or loading. Glenosphere lateralization is often used to eliminate scapular notching, but caution is required when specifying its level of offset. This is because glenosphere lateralization produced marked negative effects on joint and muscle loading, which are two of the greatest long term concerns for the success of this procedure. If a large overall offset is required, consideration should be given to bone graft lateralization as this can decrease the offset between the implant and fixation locations thus decreasing loading. Lateralization of the humerus, through medialization of the humeral cup, may represent the most promising implant parameter to optimize the biomechanical aspects of Reverse Total Shoulder Arthroplasty design, since it had positive or neutral effects on all variables tested. Finally, humeral lateralization may be a useful tool in countering some of the negative effects of glenosphere lateralization but this must be cautiously considered.

In addition to their inherent clinical value, the data produced in this study has demonstrated the value of this simulator's functionality, especially the active motion capability validated in Chapter 5. The information provided about resultant joint loads,

total deltoid force, and joint loading angle, have not been previously described in the literature and could only be meaningfully assessed using a testing apparatus that produces motion entirely through muscle loading. Thus, the active motion simulator developed in this thesis is uniquely capable of assessing clinical questions such as those addressed here and brings a greater level of physiologic accuracy in comparison to other techniques such as computer modelling.

6.5 References

Ackland, D. C., Roshan-Zamir, S., Richardson, M., & Pandy, M. G. (2011). Muscle and joint-contact loading at the glenohumeral joint after reverse total shoulder arthroplasty. *Journal of Orthopaedic Research, 29*(12), 1850-1858.

Acevedo, D. C., VanBeek, C., Lazarus, M. D., Williams, G. R., & Abboud, J. A. (2014). Reverse shoulder arthroplasty for proximal humeral fractures: Update on indications, technique, and results. *Journal of Shoulder and Elbow Surgery, 23*(2), 279-289.

Amadi, H. O., & Bull, A. M. (2010). A motion-decomposition approach to address gimbal lock in the 3-cylinder open chain mechanism description of a joint coordinate system at the glenohumeral joint. *Journal of Biomechanics, 43*(16), 3232-3236. doi:10.1016/j.jbiomech.2010.07.034

Anakwenze, O. A., Zoller, S., Ahmad, C. S., & Levine, W. N. (2014). Reverse shoulder arthroplasty for acute proximal humerus fractures: A systematic review. *Journal of Shoulder and Elbow Surgery,*

Boguski, R. M., Miller, B. S., Carpenter, J. E., Mendenhall, S., & Hughes, R. E. (2013). Variation in use of reverse total shoulder arthroplasty across hospitals. *Journal of Shoulder and Elbow Surgery, 22*(12), 1633-1638.

Boileau, P., Watkinson, D., Hatzidakis, A. M., & Hovorka, I. (2006). Neer award 2005: The grammont reverse shoulder prosthesis: Results in cuff tear arthritis, fracture sequelae, and revision arthroplasty. *Journal of Shoulder and Elbow Surgery, 15*(5), 527-540.

Bufquin, T., Hersan, A., Hubert, L., & Massin, P. (2007). Reverse shoulder arthroplasty for the treatment of three-and four-part fractures of the proximal humerus in the elderly: A prospective review of 43 cases with a short-term follow-up . *Journal of Bone & Joint Surgery, British Volume, 89*(4), 516-520.

Castagna, A., Delcogliano, M., de Caro, F., Ziveri, G., Borroni, M., Gumina, S., . . . De Biase, C. F. (2013). Conversion of shoulder arthroplasty to reverse implants: Clinical and radiological results using a modular system. *International Orthopaedics,* , 1-9.

Clouthier, A. L., Hetzler, M. A., Fedorak, G., Bryant, J. T., Deluzio, K. J., & Bicknell, R. T. (2013). Factors affecting the stability of reverse shoulder arthroplasty: A biomechanical study. *Journal of Shoulder and Elbow Surgery, 22*(4), 439-444.

Cuff, D. J., & Pupello, D. R. (2013). Comparison of hemiarthroplasty and reverse shoulder arthroplasty for the treatment of proximal humeral fractures in elderly patients. *The Journal of Bone & Joint Surgery, 95*(22), 2050-2055.

Drake, G. N. (2010). Indications for reverse total shoulder arthroplasty in rotator cuff disease. *Clinical Orthopaedics and Related Research®, 468*(6), 1526-1533.

Ek, E. T., Neukom, L., Catanzaro, S., & Gerber, C. (2013). Reverse total shoulder arthroplasty for massive irreparable rotator cuff tears in patients younger than 65 years old: Results after five to fifteen years. *Journal of Shoulder and Elbow Surgery,*

Escamilla, R. F., Yamashiro, K., Paulos, L., & Andrews, J. R. (2009). Shoulder muscle activity and function in common shoulder rehabilitation exercises. *Sports Medicine, 39*(8), 663-685.

Flury, M. P., Frey, P., Goldhahn, J., Schwyzer, H., & Simmen, B. R. (2011). Reverse shoulder arthroplasty as a salvage procedure for failed conventional shoulder replacement due to cuff failure—midterm results. *International Orthopaedics, 35*(1), 53-60.

Giles, J. W., Boons, H. W., Elkinson, I., Faber, K. J., Ferreira, L. M., Johnson, J. A., & Athwal, G. S. (2013). Does the dynamic sling effect of the latarjet procedure improve shoulder stability? A biomechanical evaluation. *Journal of Shoulder and Elbow Surgery / American Shoulder and Elbow Surgeons ...[Et Al.], 22*(6), 821-827. doi:10.1016/j.jse.2012.08.002; 10.1016/j.jse.2012.08.002

Grammont, P., & Baulot, E. (1993). Shoulder update: Delta shoulder prosthesis for rotator cuff rupture. *Orthopedics, 16*(1)

Gutiérrez, S., ComiskeyIV, C. A., Luo, Z., Pupello, D. R., & Frankle, M. A. (2008). Range of impingement-free abduction and adduction deficit after reverse shoulder arthroplastyHierarchy of surgical and implant-design-related factors. *The Journal of Bone & Joint Surgery, 90*(12), 2606-2615.

Gutiérrez, S., Luo, Z., Levy, J., & Frankle, M. A. (2009). Arc of motion and socket depth in reverse shoulder implants. *Clinical Biomechanics, 24*(6), 473-479.

Gutierrez, S., Levy, J. C., Lee, W. E.,3rd, Keller, T. S., & Maitland, M. E. (2007). Center of rotation affects abduction range of motion of reverse shoulder arthroplasty. *Clinical Orthopaedics and Related Research, 458*, 78-82. doi:10.1097/BLO.0b013e31803d0f57

Gutierrez, S., Walker, M., Willis, M., Pupello, D. R., & Frankle, M. A. (2011). Effects of tilt and glenosphere eccentricity on baseplate/bone interface forces in a computational model, validated by a mechanical model, of reverse shoulder arthroplasty. *Journal of Shoulder and Elbow Surgery / American Shoulder and Elbow Surgeons ...[Et Al.], 20*(5), 732-739. doi:10.1016/j.jse.2010.10.035; 10.1016/j.jse.2010.10.035

Henninger, H. B., King, F. K., Tashjian, R. Z., & Burks, R. T. (2013). Biomechanical comparison of reverse total shoulder arthroplasty systems in soft tissue–constrained shoulders. *Journal of Shoulder and Elbow Surgery,*

Henninger, H. B., Barg, A., Anderson, A. E., Bachus, K. N., Tashjian, R. Z., & Burks, R. T. (2012). Effect of deltoid tension and humeral version in reverse total shoulder

arthroplasty: A biomechanical study. *Journal of Shoulder and Elbow Surgery / American Shoulder and Elbow Surgeons ...[Et Al.], 21*(4), 483-490. doi:10.1016/j.jse.2011.01.040; 10.1016/j.jse.2011.01.040

Inman, V. T., & Abbott, L. C. (1944). Observations on the function of the shoulder joint. *The Journal of Bone & Joint Surgery, 26*(1), 1-30.

Kontaxis, A., & Johnson, G. (2009). The biomechanics of reverse anatomy shoulder replacement–A modelling study. *Clinical Biomechanics, 24*(3), 254-260.

Leung, B., Horodyski, M., Struk, A. M., & Wright, T. W. (2012). Functional outcome of hemiarthroplasty compared with reverse total shoulder arthroplasty in the treatment of rotator cuff tear arthropathy. *Journal of Shoulder and Elbow Surgery, 21*(3), 319-323.

Mata-Fink, A., Meinke, M., Jones, C., Kim, B., & Bell, J. (2013). Reverse shoulder arthroplasty for treatment of proximal humeral fractures in older adults: A systematic review. *Journal of Shoulder and Elbow Surgery, 22*(12), 1737-1748.

Mattiassich, G., Marcovici, L. L., Krifter, R. M., Ortmaier, R., Wegerer, P., & Kroepfl, A. (2013). Delta III reverse shoulder arthroplasty in the treatment of complex 3-and 4-part fractures of the proximal humerus: 6 to 42 months of follow up. *BMC Musculoskeletal Disorders, 14*(1), 1-10.

Nigro, P. T., Gutiérrez, S., & Frankle, M. A. (2013). Improving glenoid-side load sharing in a virtual reverse shoulder arthroplasty model. *Journal of Shoulder and Elbow Surgery,*

Nolan, B. M., & Ankerson, E. (2011). Reverse total shoulder arthroplasty improves function in cuff tear arthropathy. *Clinical Orthopaedics and Related Research®, 469*(9), 2476-2482.

Ortmaier, R., Resch, H., Matis, N., Blocher, M., Auffarth, A., Mayer, M., . . . Tauber, M. (2013). Reverse shoulder arthroplasty in revision of failed shoulder arthroplasty—outcome and follow-up. *International Orthopaedics, 37*(1), 67-75.

Terrier, A., Reist, A., Merlini, F., & Farron, A. (2008). Simulated joint and muscle forces in reversed and anatomic shoulder prostheses. *The Journal of Bone and Joint Surgery.British Volume, 90*(6), 751-756. doi:10.1302/0301-620X.90B6.19708

Virani, N. A., Cabezas, A., Gutierrez, S., Santoni, B. G., Otto, R., & Frankle, M. (2013). Reverse shoulder arthroplasty components and surgical techniques that restore glenohumeral motion. *Journal of Shoulder and Elbow Surgery / American Shoulder and Elbow Surgeons ...[Et Al.], 22*(2), 179-187. doi:10.1016/j.jse.2012.02.004; 10.1016/j.jse.2012.02.004

Wellmann, M., Struck, M., Pastor, M. F., Gettmann, A., Windhagen, H., & Smith, T. (2013). Short and midterm results of reverse shoulder arthroplasty according to the preoperative etiology. *Archives of Orthopaedic and Trauma Surgery,* , 1-9.

Wellmann, M., Petersen, W., Zantop, T., Herbort, M., Kobbe, P., Raschke, M. J., & Hurschler, C. (2009). Open shoulder repair of osseous glenoid defects: Biomechanical effectiveness of the latarjet procedure versus a contoured structural bone graft. *The American Journal of Sports Medicine, 37*(1), 87-94. doi:10.1177/0363546508326714

Werner, B. S., Boehm, D., & Gohlke, F. (2013). Revision to reverse shoulder arthroplasty with retention of the humeral component: Good outcome in 14 patients followed for a mean of 2.5 years. *Acta Orthopaedica, 84*(5), 473-478.

CHAPTER 7 – General Discussion and Conclusions

OVERVIEW

This chapter briefly touches on each of the objectives and hypotheses defined in Chapter 1 (Section 1.9). The development work undertaken to achieve the stated objectives and the investigations employed to address the hypotheses are also discussed. The strengths and limitations are reviewed, as are the testing methods used to evaluate the apparatus' performance and to assess research questions of interest. Finally, an outline for potential future development and research with this simulator system is proposed.

7.1 Summary

In order to gain an improved and more holistic understanding of healthy and dysfunctional shoulder biomechanics, it is critical to study the joint's function, kinematics, and kinetics as they act together within the joint. Evaluation of these outcomes may be achieved using a number of different techniques; however, the balance between physiologic accuracy and assessment repeatability that can be achieved through *in-vitro* simulation makes this mode of testing especially powerful. Additionally, *in-vitro* simulation can enable the evaluation of multiple joint conditions and surgical procedures in a single specimen (which increases the statistical power of the findings), thus allowing direct comparisons to be performed. *In-vitro* simulation of the entire shoulder joint complex can be classified into three types of testing: static, passive and active. To date, static and passive testing have represented the vast majority of *in-vitro* testing in the shoulder (Ackland et al., 2008; Alexander et al., 2013; McGarry, Lee, Duong, & Lee, 2005). These types of systems can provide important data with respect to inherent joint parameters and joint function, but lack the ability to accurately replicate *in-vivo* kinematics and kinetics. Active motion systems have been developed intermittently over the past 25 years to investigate these outcomes, but none of these systems have persisted long enough to achieve the same level of development as those for other joints. Therefore,

due to the importance of all of these forms of testing and the value of using them concurrently on an individual specimen, this research was undertaken to develop a system which could perform static, passive, and active assessments. A number of studies were performed to aid in its development and validation.

The first phase of this research involved the design and evaluation of a system that would improve the physiologic accuracy of the simulations through a number of different developments (Objective 1), allow the repeatable orientation of the shoulder throughout its range of motion (Objective 2), and enable the manipulation of individual rotational degrees of freedom (DOF) (Objective 2). The goals of Objective 1 were achieved through the implementation of the apparatuses described in Sections 2.2.3-2.2.5. The new muscle guide system was shown to produce load losses that were always <4 N and which averaged only 2.2 N. Therefore, the new guide system was considered a valid means to accurately load the muscles of interest. Objective 2 was addressed through the development of the humeral guide system outlined in Section 2.2.2. Hypothesis 1 was confirmed; it was shown that the device was a valid method for improving the accuracy and repeatability of joint positioning—on average 3.9° more accurate and 1.3° more repeatable than freehand placement—and for isolating individual DOF – 6.8° less variation in abduction during rotation tests.

The second phase of this research (Objectives 3 & 4) used the new functionality to assess a basic biomechanical phenomenon (Chapter 3) and a relevant clinical question (Chapter 4). In the study of Chapter 3, the effect of loading the short head of the biceps and coracobrachialis on joint function and stability was assessed. From this investigation, it was possible to demonstrate that the studied muscle group does have an effect. Importantly, the data confirmed Hypothesis 2 – that the simulator could effectively explore a basic biomechanical phenomenon. Specifically, it was possible to statistically differentiate the small variation in the muscle's effect at different load levels, thus illustrating the importance of the high level of repeatability achieved by the system. In Chapter 4, we addressed a clinical question of ongoing interest– are the Bristow and Latarjet coracoid transfer procedures biomechanically equivalent, as suggested by the combined name 'Bristow-Latarjet,' which is commonly used. This question was of

interest because clinical reports on this procedure often fail to clearly define which technique was used despite a lack of evidence that they are in fact equivalent. Using the same functionality as in Chapter 3, we were able to clearly define the biomechanical effects of these two procedures and demonstrate that, in all but one injury state, they are not equivalent, and that the Latarjet technique provides superior joint stabilization. When comparing the findings for the three tested levels of bone loss, it was possible to observe clear yet subtle changes in the effects of the two procedures. This provides further evidence in support of Hypothesis 3 – that the simulator's capabilities help to clearly differentiate the biomechanical effects of varying injury conditions and reconstruction states.

Objective 5 was achieved in the third phase of this research through the development of the functionality required to produce active abduction in multiple planes of motion. Chapter 5 describes the design and development of the software and hardware systems required to achieve active motions in which all three rotational degrees of freedom of the shoulder are simultaneously controlled. Unlike previous active motion shoulder simulators, the design of the presented system uses real time kinematic feedback and multi-PID closed loop control. This control system employs three controllers – one for each rotational degree of freedom – that are structured in a cascade-parallel structure in which the PID controlling abduction generates muscle loading commands for the deltoids as a whole. This information is cascaded to the two other PIDs to enable control of the secondary rotational DOF while still maintaining physiologically appropriate muscle loading between the different groups. Chapter 5 and Appendix B also describe the design of a method to continuously orient the scapula, throughout glenohumeral abduction, such that the proper scapulothoracic rhythm is maintained.

Validation of the simulator's active motion capabilities in terms of accuracy, repeatability, and robustness was presented in Chapter 5. It was found that the simulator was capable of following a predefined motion pathway in its primary DOF (*e.g.* abduction or horizontal extension) to within an average of 1° for both motions. Additionally, repeatability was found to be very high, with averaged standard deviations across both motions to be ~0.3°. The system could also control the secondary, non-

profiled DOF with high repeatability (<0.5°). Finally, the simulator's controller was found to be robust; nearly identical accuracy and repeatability results were produced for a range of simulated specimen body mass indices, and, when the system was perturbed, there was only a small disturbance in glenohumeral position and the disturbance was quickly rejected. As a whole, these findings confirm Hypothesis 4 – that an active motion controller based on real time kinematic feedback and closed loop PID control will achieve active motions with improved accuracy and repeatability.

The final phase of this research (Objective 6) was the assessment of a clinically relevant question that required the evaluation of static, passive, and active biomechanics in order to provide a more holistic understanding of its effects. The questions addressed were: (1) what are the effects of various Reverse Total Shoulder Arthroplasty implant parameters on range of motion and total deltoid load required to produce active motion; and (2) what is the joint load and the joint loading angle that results from active motion? In order to assess the implant parameters of interest, a custom modular Reverse Total Shoulder Arthroplasty implant system was designed as outlined in Chapter 6 and Appendix D. A six DOF load cell was installed beneath the glenosphere component of the RTSA to record the loads passing through the joint.

Using this implant system and the static, passive, and active functionality of the simulator, data were recorded that previously would have been impossible to obtain. From this data, it was determined that the implant parameter that is most often adjusted clinically – humeral polyethylene cup thickness – negatively affects functional outcomes, such as range of motion, and also negatively affects active motion outcomes, such as joint load and deltoid load. Conversely, humeral polyethylene cup lateralization – which is currently not adjustable in any commercial implant – was the only parameter capable of increasing range of motion while also decreasing joint and deltoid load. Therefore, the results of this study confirm Hypothesis 5 – using the full range of functionality developed in this thesis would enable clinical questions to be more completely assessed and help to provide greater clarity with respect to the overall effects of the tested conditions.

7.2 Strength and Limitations

To our knowledge, this simulator is the first to combine the capabilities to assess static and passive outcomes in a well-controlled manner while also enabling the same specimen to undergo muscle driven active motion testing. As demonstrated in Chapter 6, by combining these capabilities, it is possible to gain a better understanding of the effects of different testing conditions on a wider range of outcomes, thus allowing investigators and the clinical community the opportunity to weigh the importance of positive and negative effects. In addition to the value of combining both passive and active testing, the simulator is further enhanced by the individual developments presented in this work. Static/passive simulators have been widely used to assess *in-vitro* shoulder biomechanics; however, as outlined in Chapter 2, previous systems have each suffered from limitations. Although not all of the limitations of previous simulators have been addressed by this system, the developments made herein have increased the physiologic accuracy of the simulated testing environment as well as the accuracy and repeatability of the testing procedures. Respectively, these improvements have enabled testing to more closely replicate the true *in-vivo* case and enabled the simulator to more precisely differentiate the effects of the tested conditions.

The strength of the active motion simulation functionality developed during this work lies in the improvements in control and the physiologic accuracy of the applied muscle loading. In comparison to previous systems, the active motion simulator is capable of producing motions which progress at a more consistent rate and more accurately along a prescribed pathway. As well, unlike previous systems, use of the described multi-PID controller allows all rotations to be controlled in real time rather than depending on heuristic loading changes between tests in order to achieve the desired joint configurations. Additionally, use of this control system improves the physiologic accuracy of the applied muscle loads by modulating muscle force until the desired configuration is achieved instead of relying entirely on EMG data which may not directly apply to the specific specimen or motion being tested. Finally, the system developed here is the first to integrate scapular rotation into an active motion simulator and thus should more closely replicate the joint kinematics and stability of the shoulder *in-vivo*.

The simulator system and investigations presented in this dissertation did have some limitations. First, as with all *in-vitro* biomechanical testing apparatuses and investigations, this work used cadaveric specimens which precluded the precise replication of the *in-vivo* environment of the shoulder. In many cases these cadaveric specimens were drawn from an elderly donor population meaning that the properties of the tissues may have been poorer than those of a younger donor. Additionally, the results may have been influenced by the fact that the patient population which experiences some of the clinical conditions evaluated – specifically, the instability conditions tested in Chapter 4 – is typically much younger than the specimens available. However, in many cases, the effects of specimen tissue quality were negated by the repeated measures testing procedures used during *in-vitro* simulation. Second, the scapular rotation mechanism developed during this work cannot currently control all three rotations of the scapula during arm motion and thus the simulated glenohumeral kinematics and stability may not precisely match the *in-vivo* environment. However, scapular abduction is thought to have the greatest effect on joint stability, and this rotation was simulated. Third, although it is believed that the present active motion system will produce muscle loading with greater physiologic accuracy in comparison to previous systems – due to its combined use of *a-priori* EMG data and PID control – it is unlikely that these muscle loads precisely reflect those which exist *in-vivo*. Fourth, the current system is only capable of achieving quasi-static active motions (~3°/sec) precluding the assessment of motions which may be affected by inertial loads. However, the types of research questions for which this system was developed do not involve rapid motions where inertial effects would be relevant.

7.3 Current and Future Directions

The current simulator system has fulfilled the objectives set out at the beginning of this work; however, a number of avenues exist to expand its functionality and improve its physiologic accuracy. The current active motion control system has been designed with the theoretical capability to control motion in any plane; however, its ability to perform active abduction in the frontal plane (*i.e.* 60° anterior to the scapular plane) has not been evaluated despite the importance of this motion in daily life. Therefore, evaluation of the

simulator's present ability to perform this motion and subsequent refinement should be a primary objective for the future. Although the current system is likely capable of achieving active forward flexion, the physiologic accuracy of the results, especially with respect to joint loading, may be compromised because the Pectoralis Major muscle group – which has a large role in producing this motion – is not presently simulated (Ackland & Pandy, 2011; Ackland et al., 2008). Thus, it would be important to configure the simulator to load this muscle group and develop a means to control its load using the existing closed loop control system.

A second area that should be pursued is the evaluation of the simulator's ability to control abduction motions above 90° (*i.e.* parallel to the ground). Abducting the arm beyond 90° has the potential to reduce the quality of the simulated motion because the external load due to gravity begins to decrease once the arm moves past horizontal. To date, no joint conditions have been tested whose primary orientation of importance is beyond 90 (e.g. reverse total shoulder arthroplasty is primarily intended to aid in the initiation of motion and recovery of some motion for patient's exhibiting pseudo-paralysis and not the achievement of overhead motion) and as a result, it has not been systematically evaluated. With that said, this motion was attempted for a small set of Reverse Total Shoulder Arthroplasty conditions during an ongoing testing protocol and the simulator was able to smoothly abduct the arm to 135°. However, if upon a more thorough evaluation, the simulator's performance is not acceptable, it may be necessary to pursue a more complex control system that, in addition to the current kinematic process variables, may also use actuator position feedback. This feedback will help overcome the effects of having decreased muscle load requirements (due to decreased resistance from the arm's mass after it passes 90° of abduction) while the actuator is still required to retract as discussed by Ferreira and colleagues (Ferreira, 2011; Ferreira, Johnson, & King, 2010).

Another area of future work is in the improvement of the physiologic accuracy of simulating scapular rotation. The first step in doing this would involve the reprograming of the current scapular rotation controller to replicate different glenohumeral-to-scapulothoracic rhythms that have been presented in the literature. By replicating these differing ratios it may be possible to determine what affect they have on glenohumeral

kinematics and this may allow the extrapolation of the importance of simulating the scapula's other rotations. As discussed previous, the current system was not developed with the capability to simulate scapular version or tilting. This was a conscious choice, as simulating scapular version would not affect glenohumeral joint stability and scapular titling is not well understood. Despite there being disagreement about the scapula's tilting pathway across glenohumeral abduction, development of a system capable of manipulating this degree of freedom may be warranted if the above mentioned investigations show that varying scapular elevation strongly influences glenohumeral kinematics. With the development of this new capability it would then be possible to perform basic biomechanical studies to assess the effects of different tilting pathways on glenohumeral joint stability.

A final area of future simulator development would be the evaluation and subsequent improvement of the simulator's ability to achieve complex rotational trajectories which involve simultaneous profiling of multiple glenohumeral degrees of freedom. As discussed in Chapter 5, the simulator is capable of controlling horizontal extension motion which is a first among shoulder simulators. Control of this rotation has demonstrated the simulator's ability to produce motion which is not simply against gravity as with abduction and thus is an important stepping stone to more complex trajectories which combine these two rotations. The current control system's design was structured such that it is fully capable of controlling these combined motion trajectories; however, it is anticipated that a new round of tuning would be required to produce satisfactory results.

With the simulator's current functionality and that which could be added as discussed above, a number of new areas of research could be pursued. First, the system could be used to investigate clinically relevant implant failure modes by evaluating specific aspects of implant design which have been shown to be prone to failure. An example would be directly measuring the loads passing through an implant at regions which have been identified as being vulnerable to over loading. A second new form of testing could involve the refinement of the standards which are used to design and evaluate medical devices.

7.4 Significance

In-vitro biomechanical simulation of the shoulder joint complex is an important method for investigating both basic biomechanical phenomena and questions of direct clinical relevance. Although *in-vitro* simulation cannot fully replicate the *in-vivo* condition, it can play an important role in improving our understanding of shoulder biomechanics, since it enables the assessment of outcomes which cannot be tested with a patient population and enables the evaluation of multiple injury/reconstructed joint conditions. Therefore, the overall goal of this research was to maximize the relevance of *in-vitro* simulation through improvement of its physiologic accuracy, refinement of static/passive simulation techniques, and the development of an active motion controller based on real time kinematic feedback rather than predefined loading protocols. As discussed above, each of the goals of this research has been achieved. As a result, the simulator is now capable of performing assessments that have not been possible with any previously reported system, such as addressing both the shoulder's functional (*e.g.* stability and ROM) and kinematic/kinetic (*e.g.* active motion) biomechanics. This has and will continue to enable researchers to consider all of the effects of a given joint condition on the shoulder's biomechanics, and thus provide greater insight to the medical community.

The specific advancements presented in this thesis that were made in each of the areas of *in-vitro* simulation are also significant. The refinements to the simulator's physiologic accuracy, and the improved methods for performing passive assessments and recording their results, have enabled the effects of both basic biomechanical and clinically relevant conditions to be clearly and accurately defined. The development of an active motion control system based on closed loop control theory – a first in shoulder simulation – is also significant, as the motions produced by this system have been shown to have greater accuracy and repeatability than previous systems. Additionally, and more importantly, previous research has shown that active muscle driven motion is more physiologically accurate than passive experimenter manipulation of the arm and will thus ensure that the results produced are of the greatest possible value to the research and clinical community.

Finally, the greatest significance of this work is that studies performed on this simulator can improve clinical practice, as well as patient outcomes and quality of life. This was demonstrated by the two clinical studies presented in this thesis, which were both able to clarify the effects of commonly used orthopaedic procedures/implants on shoulder biomechanics. This can in turn inform clinical decisions and guide the design and use of future implants. The new experimental developments presented in this dissertation and the improvements they can bring to patient care will only increase in value as the clinical and fiscal demands on the health care system continue to grow.

7.5 References

Ackland, D. C., & Pandy, M. G. (2011). Moment arms of the shoulder muscles during axial rotation. *Journal of Orthopaedic Research*, 29(5), 658-667.

Ackland, D. C., Pak, P., Richardson, M., & Pandy, M. G. (2008). Moment arms of the muscles crossing the anatomical shoulder. *Journal of Anatomy*, 213(4), 383-390. doi:10.1111/j.1469-7580.2008.00965.x

Alexander, S., Southgate, D. F., Bull, A. M., & Wallace, A. L. (2013). The role of negative intraarticular pressure and the long head of biceps tendon on passive stability of the glenohumeral joint. *Journal of Shoulder and Elbow Surgery, 22*(1), 94-101. doi:10.1016/j.jse.2012.01.007; 10.1016/j.jse.2012.01.007

Ferreira, L. M. (2011). *Development of an active elbow motion simulator and coordinate systems to evaluate kinematics in multiple positions*. (Doctoral dissertation, University of Western Ontario). Retrieved from http://ir.lib.uwo.ca/etd/84

Ferreira, L. M., Johnson, J. A., & King, G. J. (2010). Development of an active elbow flexion simulator to evaluate joint kinematics with the humerus in the horizontal position. *Journal of Biomechanics, 43*(11), 2114-2119. doi:10.1016/j.jbiomech.2010.04.007

Yu, J., McGarry, M. H., Lee, Y. S., Duong, L. V., & Lee, T. Q. (2005). Biomechanical effects of supraspinatus repair on the glenohumeral joint. *Journal of Shoulder and Elbow Surgery, 14*(1 Suppl S), 65S-71S. doi:10.1016/j.jse.2004.09.019

Appendix A – Index of Anatomical & Research Terminology

Abduction: To draw away from the median plane, specifically, in the plane of the scapula.

Adduction: To draw towards the median plane, specifically, in the plane of the scapula.

Acetabulum: The hemispherical cup of the hip joint.

Acromion: The lateral extension of the spine of the scapula, forming the highest point of the shoulder. Adj. acromio-

Acromioclavicular: Pertaining to the acromion and the clavicle.

Actuate or Actuation: The act of changing or affecting something (*e.g.* apply motion or force).

Actuator: A device that actuates; typically a pressure driven cylinder-piston device.

Alternative hypothesis: In statistics, the hypothesis that there is in fact a significant difference between two populations, or, more specific to biomechanics, two conditions.

Analysis of Variance (ANOVA): A statistical method for making simultaneous comparisons between two or more means; a statistical method that yields values that can be tested to determine whether a significant relation exists between variables.

Anatomical neck: The boundary between an articular surface and surrounding bone.

Anterior: Situated at or directed toward the front; opposite of posterior. Adj. antero-

Anteversion: Tipping forward.

Arthroplasty: Repair of a joint by implanting an artificial component.

Anthropometry: The science dealing with the measurement of the size, weight, and proportions of the human body. Adj. antropometric,

Articular: Pertaining to a joint.

Articular cartilage: A specialized, fibrous connective tissue present in adults lining the articular surface of synovial joints.

Articulate: To divide into or to unite so as to form a joint.

Articulation: A joint; the place of union or junction between two or more bones of the skeleton.

A-priori: Relating to or denoting reasoning or knowledge that proceeds from theoretical deduction rather than from observation or experience.

Axial plane: See ‘Transverse plane’.

Ball-in-socket joint: An articulation in which the two surfaces are perfectly conforming.

Bankart: An injury of the anterior glenoid caused by dislocation of the humeral head and which may include only soft tissue tearing or also involve a fracture of the glenoid bone.

Benchtop: Simple testing which utilizes prescribed external loads and motions.

Biarticular: Relating to a structure (*e.g.* a muscle group) which crosses to joints.

Biceps: Muscle which flexes and supinates the forearm.

Biceps or Bicipital Groove: The indentation between the greater and lesser tuberosity that the tendon of the long head of the biceps passes through as it exits the glenohumeral joint.

Biomechanics: The study of the mechanical laws relating to the movement or structure of living organisms.

Biplane radiography (x-ray): A form of medical imaging that records two simultaneous images of the body using x-ray to determine the 3D position of structures in the body. This is typically done at a high capture rate to produce stereoscopic videos.

Body Mass Index (BMI): A weight-to-height ratio, calculated by dividing one's weight in kilograms by the square of one's height in meters and used as an indicator of obesity and underweight.

Bone fixed coordinate system: See 'local coordinate system'.

Bursa: A fluid-filled sac or saclike cavity situated in placed in tissues where friction would otherwise occur.

Cadaveric: Pertaining to a human body preserved for anatomical study.

Cancellous: Of or denoting bone tissue with a mesh-like structure containing many pores, typical of the interior of mature bones.

Cannulated: A structure or tool with a cylindrical hole completely through it.

Capsuloligamentous: Relating to a structure where joint capsule and ligaments blend together.

Cartilage: A specialized, fibrous connective tissue present in adults, and forming the temporary skeleton in the embryo, providing a model in which the bones develop, and constituting a part of the organisms joint mechanism.

Cascading-Parallel: In this thesis, a control structure where multiple PID controllers run in parallel but cascaded below another.

Clavicle: Elongated slender, curved bone (collar bone) lying horizontally at the root of the neck, in upper part of thorax.

Closed-loop control: A type of control system that automatically changes the output based on the difference between the feedback signal to the input signal.

Conjoint or Conjoined Tendon: A tendon which acts as the terminus of more than one muscle; as with the tendon of the short head of the biceps and coracobrachialis.

Contact mechanics: The study of the deformation of solids that touch each other at one or more points.

Coracoid: A bone projection from the anterosuperior glenoid. Adj. coraco-

Coracoacromial: Relating to the coracoid and acromion.

Coracobrachialis: A muscle which originates on the coracoid and flexes/adducts the forearm.

Coronal plane: A vertical plane, at right angles to a sagittal plane, dividing the body into anterior and posterior portions.

DC servo-motor: An electronically controlled drive motor.

Degree of freedom (DOF): In kinematic and kinetic analysis, a manner in which a motion or force can occur. For two DOF to be independent, they must be defined about two perpendicular axes.

Deltoid: Muscle which abducts, flexes or extends the arm.

Diarthrodial joint: See synovial joint.

Digitization: In the context of this thesis, the process of digitally recording anatomical landmarks.

Distal: Remote, farther from any point of reference.

Distraction: Separation of joint surfaces without rupture of their binding ligaments and without displacement; surgical separation of the two parts of a bone after the bone is transected.

Disturbance Rejection: The ability and speed at which a control system eliminates error in its response due to an external disturbance.

Electromagnetic tracking: The use of the physics of electromagnetic fields to monitor the position of an object.

Electromyography (EMG): The recording and study of the electrical properties of skeletal muscle.

Elevation: To move away from the body.

Epicondyle: A projection or boss upon a bone, above its condyle. Adj. epicondylar

Euler Angle Sequence: A specific method used to decompose an objects orientation using a sequence dependent set of rotations.

Extension: The movement by which the two ends of any jointed part are drawn away from each other; the bringing of the members of a limb into or toward a straight condition. [Motion in the vertical plane perpendicular to the plane of the scapula (Wuelker et al., 1998)]

Extensor: Any muscle that extends a joint.

External rotation: Rotation about the longitudinal axis of the humerus laterally.

External validity: The extent to which the results of a study can be generalized to other situations.

Fibrocartilage: Cartilage of parallel, thick, compact collagenous bundles, separated by narrow clefts containing the typical cartilage cells. Fibrocartilaginous ajd.

Fiducial: (esp. of a point or line) assumed as a fixed basis of comparison. In biomechanics, a landmark that can serve as a means to compare results between to measurement teachniques.

Finite element analysis (FEA): A method which discretizes a continuous object into many small 'finite' pieces that can then be analyzed individually using traditional mechanics equations to determine the overall load and displacement of the object.

Flexion: Elevation in the sagittal plane of the body.

Flexor: Any muscle that flexes a joint.

Fluoroscopy: An imaging technique in which it is possible to record plane x-ray images at video capture rates (*i.e.* $\geq$60 Hz).

Force Couple: The synergistic action of muscles to produce stability or movement in a joint.

Forward flexion: Motion of the arm directly anterior away from the body.

Fossa or Fossae: In anatomy, a hollow or depressed area.

Gimbal lock: The loss of one degree of freedom in a three-dimensional space that occurs when the axes of two of the three gimbals are driven into a parallel configuration, "locking" the system into rotation in a degenerate two-dimensional space

Glenohumeral: Pertaining to the glenoid and humerus.

Glenohumeral ligaments: Bands, usually three on the inner surface of the articular capsule of the humerus, extending from the glenoid lip to the anatomical neck of the humerus.

Glenoid: A fossa located on the lateral scapula resembling a pit or socket. Adj. gleno-

Glenosphere: The hemispherical ball placed on the glenoid to reverse the anatomy of the shoulder during Reverse Total Shoulder Arthroplasty.

Global coordinate system: A coordinate system which is fixed and can be used to provide a constant reference for any other coordinate system.

Goniometer: An instrument for measuring angles.

Greater tuberosity: The large bone protuberance on the posterolateral humeral head.

Hemi-arthroplasty: The replacement of one surface of a joint with artificial material.

Heuristic: A method for proceeding to a solution using a loosely defined set of rules and through trial and error.

Horizontal flexion-extension: Motion of the arm in a plane parallel to the ground forward and backwards, respectively.

Humerothoracic: Relating to the humerus and thorax.

Humerus: Long bone of upper arm. Adj. humero-

Hyaline: Glassy and transparent or nearly so.

Impingement: When two bones contact each other in a pathological manner.

Inertia: A property of matter by which it continues in its existing state of rest or uniform motion in a straight line, unless that state is changed by an external force.

Inferior: Situated below, or directed downward; in anatomy, used in reference to the lower surface of a structure, or to the lower of two (or more) similar structures. Adj. infra- or infero-

Inferiorization: In Reverse Total Shoulder Arthroplasty, movement of the center of rotation of the shoulder joint in the inferior direction.

Infraspinatus: Muscle originating on the posterior scapula which rotates the arm laterally.

Instability: A pathologic condition in which there is an inability to maintain the normal relationship of the humeral head on the glenoid fossa.

Interaction effect: In the analysis of variance (ANOVA) statistical method, an interaction effect is the effect of at least two independent variables on a dependent variable. Changes in the levels of these two variables influence the dependent variable in ways which are not additive and may not be one-to-one as their values increase.

Internal rotation: Rotation about the longitudinal axis of the humerus medially.

Intra-articular: Of or related to the space between to contacting surfaces.

Intramedullary: Of or related to the cavity in the center of the long bones.

***In-silico*:** Performed on computer or via computer simulation

***In-vitro*:** In an artificial environment.

***In-vivo*:** Within the living body.

Isometric: Of, relating to, or denoting muscular action in which tension is developed without contraction of the muscle.

Joint capsule: The saclike envelope enclosing the cavity of a synovial joint.

Kinematics: Description of an objects motion without consideration for the forces causing it.

Kinetics: Of, or relating to, or resulting from motion; as in forces.

Labrum: An edge, rim or lip. In the shoulder this is located at the rim of the glenoid.

Lateral: Denoting a position farther from the median plane or midline of the body or a structure.

Lateralization: In Reverse Total Shoulder Arthroplasty, movement of the center of rotation of the shoulder joint or the humeral head in the lateral direction.

Length-tension curve: The relation between a muscle's length and the isometric force which it generates when fully activated. In this relationship, muscle tension decreases as its length moves away from an optimal value.

Lesion: Any pathological or traumatic discontinuity of tissue or loss of function of a part.

Lesser tuberosity: The small bone protuberance on the anterolateral humeral head.

Lines-of-action: The direction that a structure or force follows (*e.g.* a muscle).

Ligament: A band of fibrous tissue connecting bones or cartilages, serving to support and strengthen joints. Adj. ligamentous.

Load sensing: Of or relating to the measurement of the forces and moments applied to an object.

Local coordinate system: A coordinate system which is attached to and moves with an object and can be used to provide a description of the objects configuration with respect to another reference.

Magnetic resonance imaging: A form of medical imaging that measures the response of the atomic nuclei of body tissues to high-frequency radio waves when placed in a strong magnetic field.

Main effect: In the analysis of variance (ANOVA) statistical method, a main effect is the effect of an independent variable on a dependent variable averaged across the levels of any other independent variable.

Mechanical Advantage: Increasing the effectiveness of a force by applying it at a distance.

Mechatronics: Technology combining electronics and mechanical engineering.

Medial: Situated toward the midline of the body or a structure. Adj. medio-

Medialization: In Reverse Total Shoulder Arthroplasty, movement of the center of rotation of the shoulder joint in the medial direction.

Moment: The tendency of a force to rotate an object about an axis when that forces is applied at a distance (also known as Torque).

Moment arm: The perpendicular distance between a force and the axis it is causing a moment about.

Multi-articular: Of or relating to a structure which crosses more than two joints (*e.g.* a muscle).

Musculotendinous junctions: The transition in a muscle group between the muscular tissue and tendinous tissue.

Muscle: An organ which by contraction produces movement of an animal organism. Adj. muscular and musculo-.

Muscle loading ratios: Relationships between the various muscles crossing a joint which define the load on each relative to one primary muscle known as the 'prime mover'.

Non-profiled DOF: In this thesis, a shoulder rotation which is not currently commanded to follow a profile.

Null hypothesis: In statistics, the hypothesis that there is no significant difference between two populations, or, more specific to biomechanics, two conditions.

Off-axis loading: In pneumatic actuation, a load which is not applied collinear with the shaft of the piston.

Optical tracking: The use of the physics of light to monitor the position of an object.

Orthopaedics: That branch of surgery dealing with the preservation and restoration of the function of the skeletal system, its articulations, and associated structures.

Osseous: Relating to bones.

Output range: The minimum to maximum values a control system is allowed to output (*e.g.* muscle forces).

Pathological: Of or relating to pathology/injury.

Physiological: Normal, not pathologic.

Physiologic cross-section: The cross-section of the muscle fibres calculated by measuring the volume of the muscle and dividing by the fibre length.

PID (Proportional, Integral, Differential): A control algorithm that uses the error between input and output signals to achieve control by applying an adjustment Proportional to error,

by accumulating (Integrating) the error over time, and accounting for the rate of change (Derivative) of the error.

Plane of elevation: A rotation degree of freedom which defines the plane in which the arm will elevate in.

Plane radiography: An imaging technique in which an x-ray image is taken in a single direction.

Pneumatic: Containing or operated by air or gas under pressure

Posterior: Directed towards, or situated at the back; opposite of anterior. Adj. postero-

Post-hoc: Occurring or done after the event.

Power: In statistics, the power of a statistical test is the probability that the test will reject the null hypothesis when the alternative hypothesis is true (*i.e.* successfully reject the null hypothesis when in reality it should be rejected).

Primary DOF: See 'Profile DOF'.

Process: A prominence or projection, as from a bone.

Profiled DOF: The shoulder rotation which is currently commanded to follow a predefined profile.

Protraction: The act of moving an anatomical part forward.

Proximal: Nearest to the point of reference, as to a center or median line or to the point of attachment or origin.

Pseudoparalysis: The inability to move a part of the body owing to factors, as pain, other than those causing actual paralysis.

Quarter Amplitude Decay Response: The response of a control system which is balanced between speed of response and limitation of overshoot.

Quasi-static: A condition in which a body is moving but at a rate for which the effects of acceleration and inertia can be neglected.

Radiostereometric Analysis (RSA): An imaging technique in which two individual x-ray images from two planes are used to determine the 3D configuration of a structure.

Range of motion: The arc of motion that a joint possess.

Reduce: To restore to the normal place or relation of parts, as to reduce a fracture.

Reduction: The correction of a fracture, luxation, or hernia.

Retraction: The act of moving an anatomical part backward.

Retroversion: Tipping backward.

Rigid body: An idealization of a solid body in which deformation is neglected

Rotation Sequence Decomposition: The process of breaking an objects orientation down into discrete rotations which can be more readily interpreted. See Euler Angle Sequence.

Rotator cuff: Group of muscles surrounding the glenohumeral joint, consisting of the supraspinatus, subscapularis, infraspinatus and teres minor muscles.

Sagittal plane: A longitudinal vertical plane that divides the body into left and right segments.

Scapula: Wide, thin, triangular bone (shoulder blade) opposite second to seventh ribs in upper part of back. Adj. scapular or scapulo-

Scapulohumeral: Pertaining to the scapula and humerus.

Scapulothoracic: Pertaining to the scapula and thorax.

Secondary DOF: See 'Non-profiled DOF'.

Shear: A motion or force parallel to the face of an object.

Simulator: Any device or system that simulates specific conditions or the characteristics of a real process for the purpose of research or operator training. Types of shoulder simulator are static, passive and active. Static systems apply muscle and external loads but do not permit specimen movement. Passive systems apply the same loads but permit experimenter driven motions. Active systems use muscle loading to cause joint motion.

Spatial tracking: The process of monitoring an objects 3D position and orientation in space.

Spherical bearing: Permits angular rotation about a central point in two orthogonal directions.

Spinous fossa: The large, slightly concave area below the spinous process on the dorsal surface of the scapula.

Statistical shape modelling: Geometrical analysis from a set of shapes in which statistics are measured to describe geometrical properties from similar shapes or different groups.

Sternoclavicular: Pertaining to the sternum and the clavicle.

Sternum: Elongated flat bone, forming anterior wall of chest. Adj. sterno-

Subacromial: Relating to the articulation between the superior humeral head and the inferior side of the acromion.

Subluxation: Incomplete or partial dislocation.

Subscapularis: Muscle which rotates the arm medially.

Superior: Situated above, or directed upward. Adj. supra-

Supraspinatus: Muscle which originates at the supraspinatus fossa and abducts the arm.

Suture: A stitch or series of stitches made to secure apposition of the edges of a surgical or traumatic wound; to apply such stitches.

Synovial joint: An articulation permitting more of less free motion, the union of the bony elements being surrounded by an articular capsule enclosing a cavity lined by synovial membrane.

Tendon: A fibrous cord of connective tissue continuous with the fibres of a muscle and attaching the muscle to bone or cartilage. Adj. tendinous

Teres minor: Muscle which originates on lateral border of the scapular and rotates the arm laterally.

Tilting: In scapular motion, the rotation about a mediolateral axis which causes the glenoid to move tip anterior or posterior.

Tool plate: The surface of a load cell that is subject to direct external loading.

Thorax: The chest.

Torso: See Thorax.

Transected: Cut across or make a transverse section in something.

Transformation matrix: A 4x4 matrix which describes both the position and orientation of a coordinate system with respect to a reference system.

Transosseous: Through an osseous structure.

Transverse: Extending from side to side; at right angles to the long axis.

Transverse plane: Horizontal plane passing through the body at right angles to the frontal and sagittal planes, dividing the body into superior and inferior segments

Trapezius: Muscle which elevates the clavicle, adducts, elevates or depresses the scapula, and extends the head.

Trunk: The main part of the body, to which the head and limbs are attached.

Tuberosity or Tuberacle: An elevation or protuberance.

Vent: To open, or an opening or outlet.

Version: In scapular motion, the rotation about a superoinferior axis which causes the glenoid to face anterior (ante-) or posterior (retro-).

Appendix B – Inverse Kinematic Calculations for the Scapular Rotation Motor and Linkage System

In this appendix, the calculations used to calculate the motor position required to achieve a desired level of scapular abduction are presented. The calculations are based on an inverse kinematic analysis using the known linkage geometry. The result of this analysis is a set of equations which can be used to calculate the required drive link rotation for any desired scapular abduction angle. This angle is then converted into a motor position command based on knowledge of the motor and gearhead parameters. Presented below is a labelled rendering of the linkage (Figure B.1) and a hand solution (Figure B.2) illustrating the equations which describe the relationship of interest.

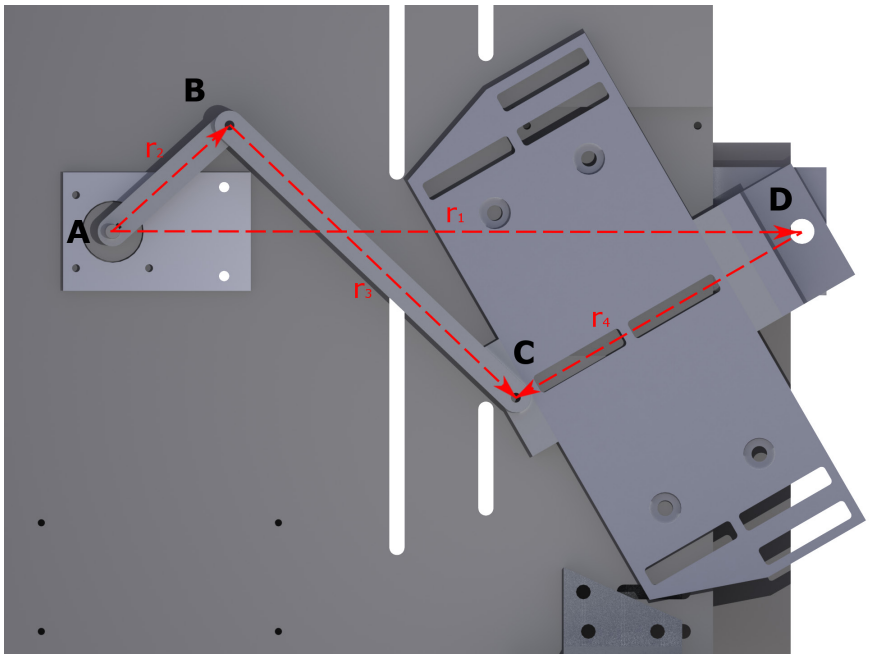

Figure B.1: Computer rendering of scapular rotation linkage.
Shown are the pins of the linkage and the letters corresponding to the equations presented below. (A) Axis of motor, (B) pin between drive link and connecting link, (C) pin between connecting link and scapula pot, (D) hinge of scapula pot. (r_1) Ground 'link', (r_2) drive link, (r_3) connecting link, (r_4) scapula pot.

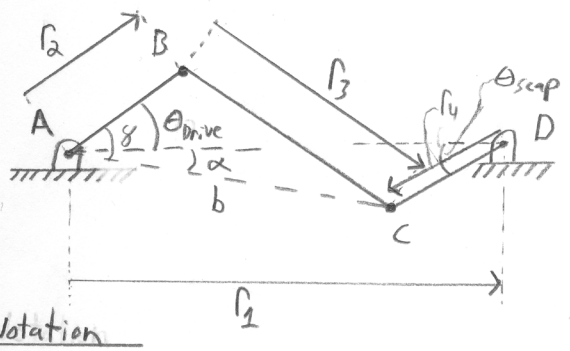

Notation

A = Axis of motor
B = Pin between Drive link & connecting link
C = Pin between connecting link & scapula pot
D = Hinge of scapula pot

r_1 = ground 'link'
r_2 = Drive link
r_3 = Connecting link
r_4 = Scapula pot

θ_{scap} = Desired angle of Scapula
= 20° = Scapula in adduction.

θ_{Drive} = angle required to obtain θ_{scap}
= 40° when $\theta_{scap} = 0°$

Knowns

$r_1 = 443.2mm$
$r_2 = 101.6mm$
$r_3 = 254.0mm$
$r_4 = 212.7mm$

Inverse Kinematic Solution of θ_{Drive} wrt θ_{scap} & r's

- Because $\theta_{Drive} = \gamma - \alpha$, we calculate α & γ from the known geometry.
- determine length of b using triangle ADC & cosine law

$$b^2 = r_4^2 + r_1^2 - 2 r_4 r_1 \cos\theta_{scap}$$

$$b = \sqrt{r_4^2 + r_1^2 - 2 r_4 r_1 \cos\theta_{scap}}$$

$$b = \sqrt{241671.4 - 188559.6 \cos\theta_{scap}}$$

- Knowing eqn for b, use triangle ACD & Sine law to find α

$$\frac{\sin\alpha}{\sin\theta_{scap}} = \frac{r_4}{b} \quad \therefore \quad \alpha = \sin^{-1}\left[\frac{r_4 \sin\theta_{scap}}{b}\right]$$

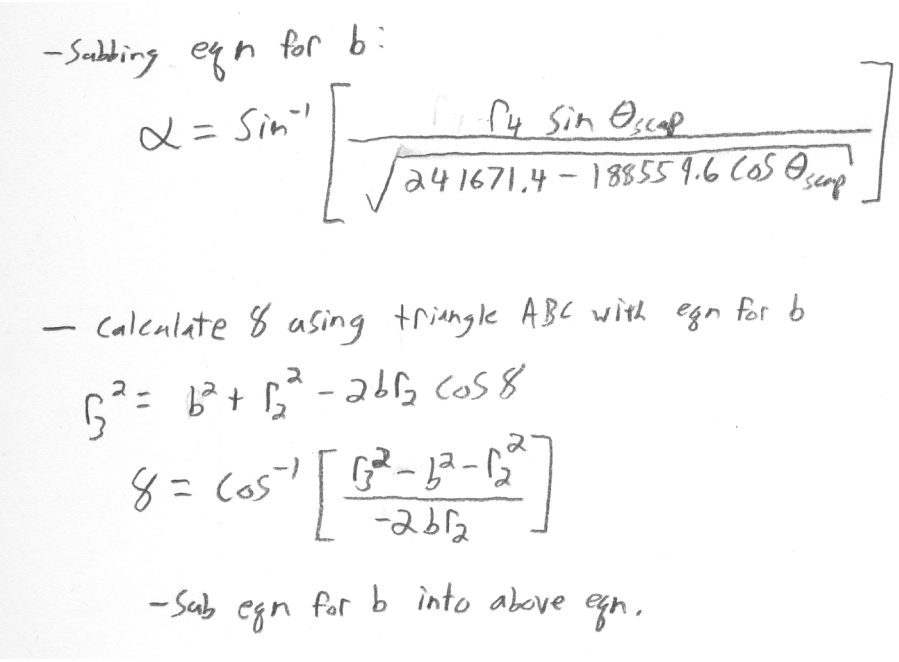

Figure B.2: Hand written solution for inverse kinematics of scapular rotation linkage.

With the equations to calculate α and γ now known, it is possible to subtract them to yield the desired angle, θ_{Drive}, relative to the horizontal. However, the design of the linkage also dictates that when θ_{Scap}= 0°, θ_{Drive} = 90°. Therefore, in order to calculate the angle the motor must travel, we calculate $\Delta\theta = 90° - \theta_{Drive}$. Δθ is then converted to motor encoder counts by dividing by 360°, multiplying by the number of motor counts in one revolution (in the current system configuration, 2000 counts/rev), and multiplying by the gear ratio (in the current system configuration, 100:1). This motor encoder position describes the motors level of rotation relative to its initialized position. Using these equations, a custom LabView program was written to convert the desired scapular abduction angle – which varies continuously as the humerus abducts during an active motion test – into a motor position command in real time.

Appendix C – Implementation of a Geometric Motion-Decomposition Technique for the Elimination of Gimbal Lock Artifacts in Real-Time Active Motion Kinematic Data

C.1 Introduction

As discussed in Chapter 5 (Section 5.1), previously reported simulators have primarily achieved abduction through the use of a prime mover that displaces at a predefined speed in order to 'control' the rate of abduction. These simulators have largely ignored the issue of actively controlling the two secondary degrees of freedom (DOF) (*i.e.* plane of abduction and internal-external rotation [IR-ER]) during abduction, and have instead taken a heuristic approach to achieving the desired level of rotation. In contrast, this dissertation aimed to achieve simultaneous active control over all three of the shoulder's rotational DOF. The method discussed in Chapter 5 (Section 5.2.2) allowed the achievement of this goal with a high level of accuracy, but only when the arm was oriented at more than ~15° of abduction.

This limitation was caused by using the Euler angle rotation sequence suggested by the International Society for Biomechanics (ISB) and used in previous simulator based investigations. Although Euler angle sequences are commonly used, they suffer from the mathematical phenomenon known as 'gimbal lock' in which the values for the first and third rotations in the sequence fluctuate greatly and unpredictably, because they are impossible to uniquely define. In the case of the shoulder, the effects of gimbal lock are most pronounced with the humerus in 0° abduction and slowly taper off as the arm is elevated to ~15°. Therefore, in the context of *in-vitro* shoulder simulation, it is not possible to clearly define the physiologic rotations required of the two secondary DOF when the arm is in this orientation. The ability of previous simulators was not affected by this complication as they did not rely on real time kinematic data to achieve motion. Once this phenomenon was recognized as the source of difficulty in controlling these two DOF, a new motion decomposition method, which avoided gimbal lock, was pursued.

C.2 Materials and Methods

A review of the literature identified a number of methods for eliminating the effects of gimbal lock. Kedgley (2004) describes how the limitation of the YXY shoulder Euler angle sequence can be overcome by assuming a value for one of the two secondary DOF. This method can be applied in protocols where one value is well known and readily assumed, such as in an axial rotation test in adduction, where it is known that the plane of abduction is effectively 0°; however, in the case of active unconstrained shoulder motion, it is impossible to make such an assumption. As an alternative, Ishida (1990) and Novotny, Beynnon, and Nichols (2001) each suggested integrating measured axial rotation angular velocities to calculate an accumulated rotation from a known starting orientation. Unfortunately, angular velocity data is often obtained by taking the derivative of position data, which is known to produce high levels of noise and thus large accumulated error. Masuda, Ishida, Cao, and Morita (2008) proposed the redefinition of humeral axial rotation using a term in the rotation matrix which is stable at the gimbal lock position; however, with this definition, when the arm is abducted from 0° to 90° while physically holding the level of axial rotation constant, the calculated value would change by 90°. Finally, using the general Joint Coordinate System (JCS) technique of Grood and Suntay (1983), Amadi and Bull (2010) proposed a geometric motion decomposition method for the shoulder (from this point forward referred to as GMD). This technique uses basic geometric analysis, rather than the interpretation of a rotation matrix, to discretize the three rotations of the shoulder. Amadi and Bull (2010) validated this GMD algorithm by applying it to raw data drawn from a paper by Fung et al. (2001) and comparing their determined rotations to those determined in the paper using the standard Euler angle sequence. The authors found that the results from their GMD method were in close agreement with those of the standard Euler sequence and only noticeably differed during forward flexion motions in the sagittal plane. The primary limitation of this method lies in that the solution technique differs for motions that are primarily composed of abduction versus those primarily involving flexion. However, the authors proposed a simple test to determine which of these two types of motion the shoulder is currently oriented in, making it possible to switch between the two solution techniques if/when the motion changes.

After considering each of these techniques, the constraints related to the technologies currently used on the simulator, and the types of testing to be performed, it was decided that the GMD method of Amadi and Bull (2010) would be capable of producing the most robust and readily achievable solution. As detailed in their paper, the glenohumeral joint's motion is uncoupled by determining and then removing each rotation in a stepwise manner as follows:

1) Identify the primary motion (abduction vs flexion) by comparing the magnitude x and y components of humeral x-axis
    a. If y>x, primary motion is abduction, otherwise, it is flexion
2) Coupled rotation of non-primary motion is determined, reported and then decomposed from primary before quantifying the magnitude of the primary's rotation (*i.e.* remove flexion when abduction is primary)
    a. This angle is quantified as the magnitude of the rotation about an axis perpendicular to the superior humeral and anterior scapular axis required to bring the humerus into the coronal plane of the scapula
    b. Once this angle is determined, the relevant humeral axes can be rotated in the opposite direction, to subtract this rotation, using the Rodrigues equation for rotation of a vector about another vector
3) Primary rotation is then determined, reported, and subtracted from new joint orientation resulting from step 2
    a. This angle is quantified as the magnitude of the rotation between the new humeral superior axis and the unchanged scapular superior axis
    b. The superior humeral axis is then brought into alignment with the superior scapular axis by rotating the relevant humeral axis about the anterior scapular axis in the opposite direction to the determined angle.
4) Internal-external rotation is then determined, reported, and subtracted from the new joint orientation resulting from step 3
    a. This angle is quantified as the magnitude of the rotation between the current humeral lateral axis and the unchanged scapular lateral axis

b. The humeral coordinate system is then brought into full alignment with the scapular system by rotating the relevant humeral axis about the superior scapular axis in the opposite direction to the determined angle.

5) The success of this decomposition process can then be assessed by viewing the final rotation matrix relationship between the two coordinate systems which should correspond to the identity matrix.

This GMD technique was implemented through a custom LabView program that enabled the five steps outlined above to be carried out on real time kinematic data output with respect to the humeral and scapular coordinate systems as described in Chapter 5 (Section 5.2.1).

There is no information in the literature demonstrating the use of this GMD technique with real time data derived from a 6 DOF tracking system. Therefore, once implemented, the program was evaluated to ensure the calculated results were valid. Three motions were assessed: internal-external rotation with the humerus in 0° of abduction and abduction from 0° to 90° with the humerus held in a relatively constant plane of abduction and level of axial rotation (both affected by gimbal lock), and horizontal flexion and extension in 90° of abduction (unaffected by gimbal lock). Each of the motions was manually applied by the experimenter. Kinematic data were recorded throughout each motion using an Optotrak Certus (Northern Digital Inc, Waterloo, ON) marker attached to each bone, and using standard scapular and humeral coordinate systems as described in Chapter 3 (Section 3.2.1). To ensure the results were not influenced by joint translations, a shoulder phantom whose glenohumeral joint was substituted by a universal joint was used (Figure C.1).

Rotations were computed using the raw kinematic data recorded for each motion using the GMD method and the standard shoulder Euler angle sequence method. These rotations were then compared to assess overall agreement. Additionally, the linear algebraic Trace function was calculated for each rotation matrix that resulted from the decomposition, and these were then averaged over all frames of motion. The ideal value

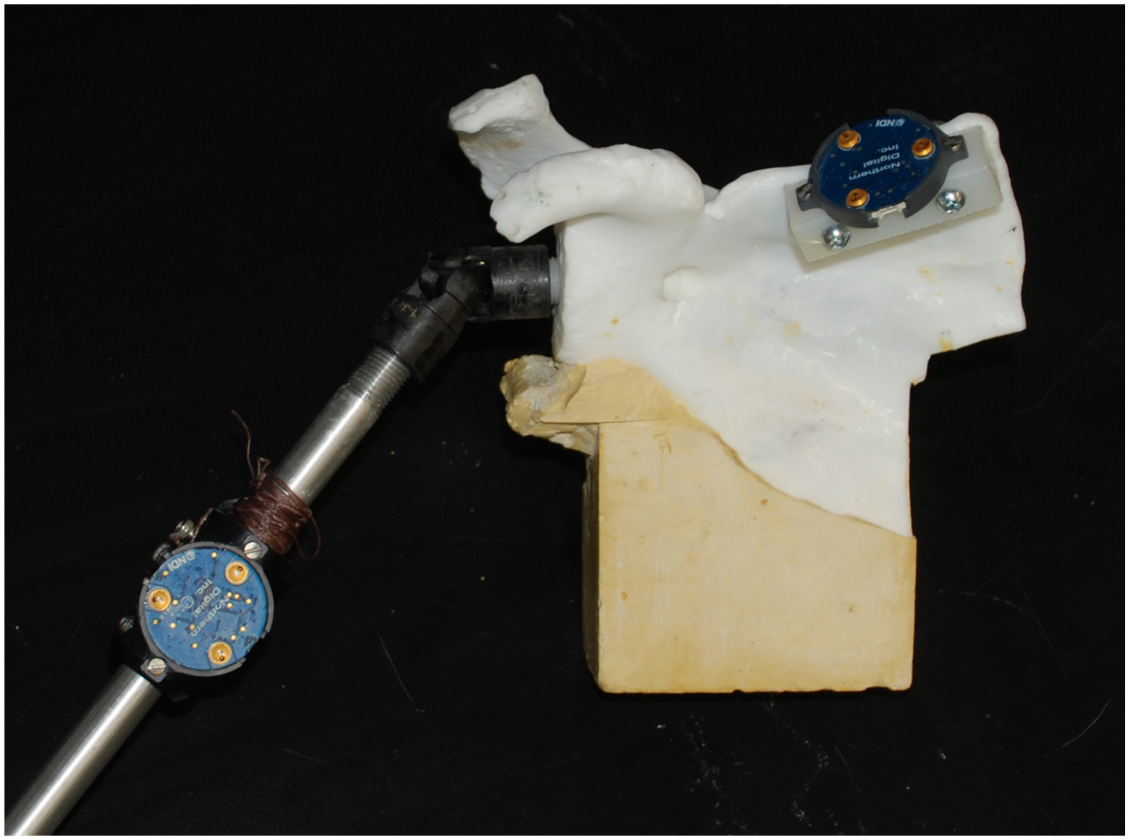

Figure C.1: Shoulder phantom used in assessment of kinematic analysis techniques. *The shoulder phantom was composed of a plastic scapula model and aluminum rod representing the humerus, connected by a universal joint. The scapula and humerus were each equipped with an optical tracking marker to monitor their motion during testing. A coordinate system was defined for each bone using anatomical point digitizations as outlined in Chapter 3 (Section 3.2.1). Note that in the case of the humerus, the rod was specifically designed to accommodate the attachment of an anatomically correct distal humerus model in order to facilitate the acquisition of accurate landmark digitizations.*

of this outcome is a mean value of 3, with deviations from this value representing mathematical errors in the algorithm's estimate of the three rotations.

C.3 Results

As expected, for all motions tested, the average difference between the angles calculated for the abduction DOF by the two techniques was small (0.79±0.63°).

During the flexion-extension motion test, the angles calculated for the plane of abduction DOF by the two techniques were nearly equal (0.29±0.23°). The average difference between the angles calculated for the IR-ER DOF by the two techniques was 3.67±2.28°; however, this value was only this small because the calculated differences were equally spread between positive and negative. In reality, despite the phantom being locked in this DOF, the values calculated by the Euler sequence actually varied by ~12°, while the results of the GMD technique only varied by ~2° (Figure C.2).

For the IR-ER motion test in 0° of abduction, as anticipated, the angles calculated for the plane of abduction and IR-ER DOF using the Euler sequence were unrepresentative of the true joint orientation and varied widely across the motion. The angles calculated for the plane of abduction DOF using the GMD method were constant across the motion, while the angles calculated for the IR-ER DOF varied by ~50° across the motion, which was in agreement with what was observed during testing (Figure C.3).

For the abduction motion test, the angles calculated for the plane of abduction and IR-ER DOF using the Euler sequence were also unrepresentative early in the trial, but these reached meaningful values when the arm was in >15° of abduction (Figure C.4). On the other hand, the angles calculated for these DOF using the GMD method were stable and exhibited variations of <15°.

The average Trace for the decomposition of each of these three motions was 2.995-3.00 (SD: 0.00-0.0068), indicating that the final decomposed humeral coordinate system was in close alignment with the scapula's coordinate system.

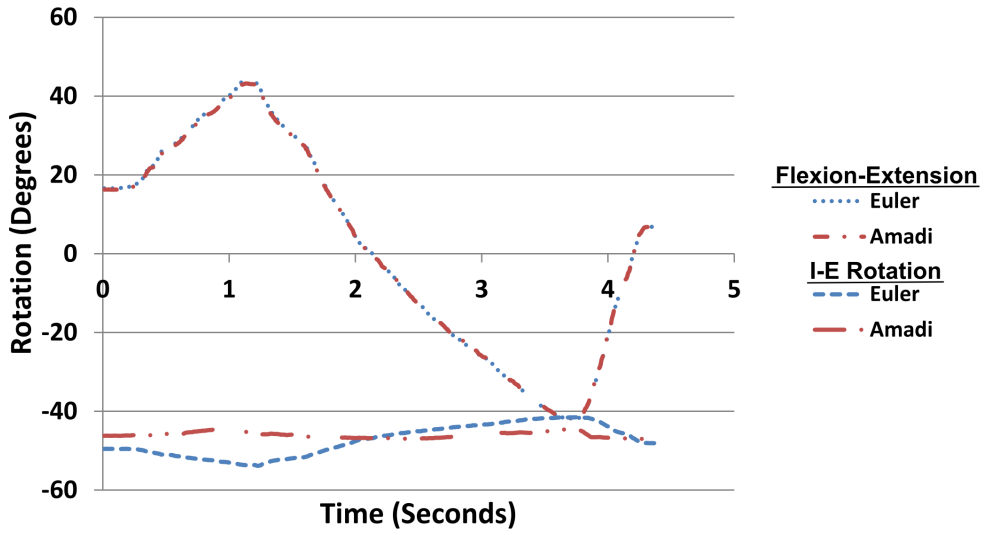

Figure C.2: Flexion-extension motion with arm held in 90° of glenohumeral abduction.

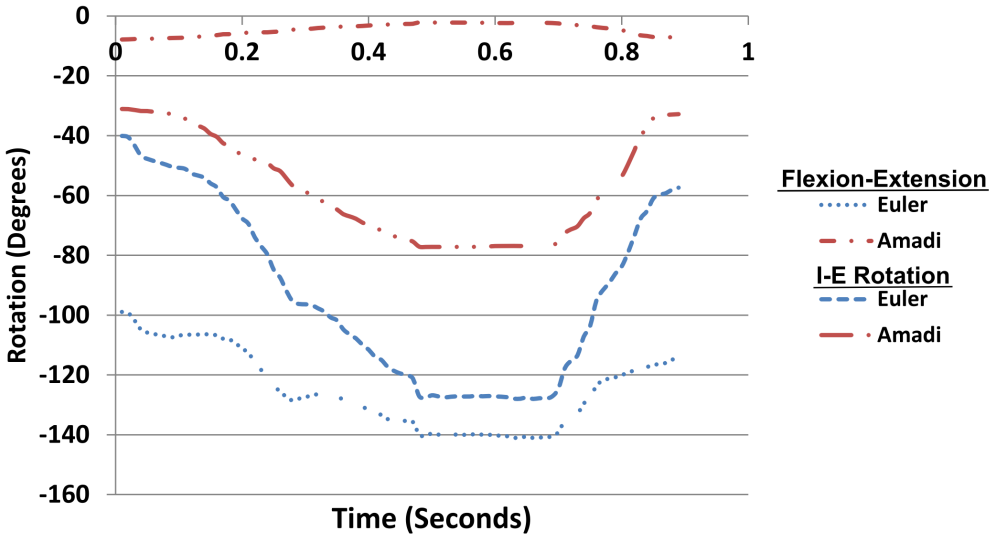

Figure C.3: Internal-external rotation motion with arm held in 0° of glenohumeral abduction.

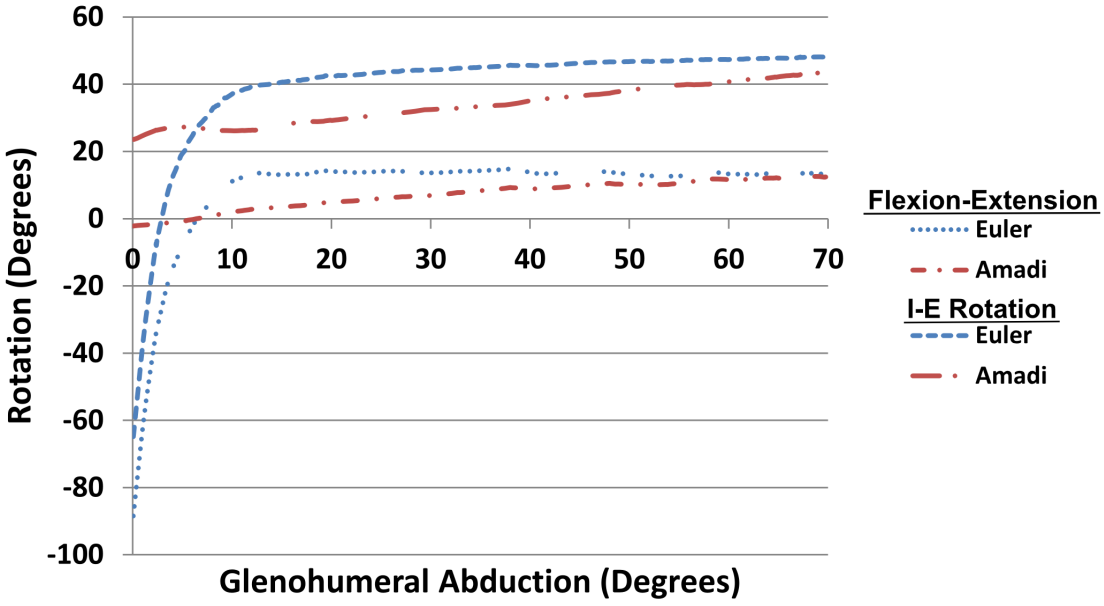

Figure C.4: Abduction motion in scapular plane. Note that the plane of abduction and axial rotation DOF were held constant.

C.4 Discussion

Implementing a method to overcome the limitations of standard Euler angle analysis is an important step in improving the validity of the current *in-vitro* shoulder simulator, and was precipitated by the desire to not only control abduction but also the plane of abduction and axial rotation. The GMD method of Amadi and Bull (2010) was chosen ahead of all other alternatives presented above because it appeared to provide a robust solution to the problem of gimbal lock without requiring the implementation of new motion tracking technologies or changing the current clinical definitions of shoulder rotation.

Results for the abduction DOF are equivalent to those of the ISB recommended YXY Euler rotation sequence across the range of motion tested and the remaining DOF show strong agreement to the Euler results when the arm is manipulated in higher levels of abduction. Additionally, gimbal lock – the unpredictable, non-physiologic rotations which characterize the results of the Euler angle sequence when the arm is below 15° of abduction – was successfully avoided using this GMD technique. Although it was not possible to compare the results of the GMD technique to a gold standard when the arm was in adduction, the results were in agreement with the ranges of internal and external rotation observed during testing.

For the tests assessed in this appendix, the average Trace value demonstrated that the final humeral rotation matrix was extremely well aligned with the scapular coordinate system. This finding indicates that the accuracy of the results of the GMD technique does not degrade at any orientation throughout the large range of motion assessed. The value of the Trace was observed to decrease when approaching the transition between a primarily abduction vs flexion motion. However, since there is no intention to test multi-DOF motions that purposefully switch between the two primary rotations (*e.g.* cross body motions) using this simulator, this finding was considered insignificant.

The geometric motion decomposition (GMD) technique originally described by Amadi and Bull (2010) and presented here is therefore a valid and robust method for the

transformation of glenohumeral kinematics into clinically meaningful rotations. It produces similar results to the commonly used Euler analysis method, but avoids the mathematical ambiguity of gimbal lock. Therefore, this technique will serve as an important means to further enhance the experimental validity of the simulator by enabling the system to control all rotational DOF of the shoulder in any orientation, including those previously precluded by the use of Euler analysis.

C.5 References

Amadi, H., Hansen, U., & Bull, A. (2009). A numerical tool for the reconstruction of the physiological kinematics of the glenohumeral joint. *Proceedings of the Institution of Mechanical Engineers, Part H: Journal of Engineering in Medicine, 223*(7), 833-837.

Amadi, H. O., & Bull, A. M. (2010). A motion-decomposition approach to address gimbal lock in the 3-cylinder open chain mechanism description of a joint coordinate system at the glenohumeral joint. *Journal of Biomechanics, 43*(16), 3232-3236. doi:10.1016/j.jbiomech.2010.07.034

Fung, M., Kato, S., Barrance, P. J., Elias, J. J., McFarland, E. G., Nobuhara, K., & Chao, E. Y. (2001). Scapular and clavicular kinematics during humeral elevation: A study with cadavers. *Journal of Shoulder and Elbow Surgery, 10*(3), 278-285.

Grood, E. S., & Suntay, W. J. (1983). A joint coordinate system for the clinical description of three-dimensional motions: Application to the knee. *Journal of Biomechanical Engineering, 105*(2), 136-144.

Ishida, A. (1990). Definition of axial rotation of anatomical joints. *Frontiers of Medical and Biological Engineering : The International Journal of the Japan Society of Medical Electronics and Biological Engineering, 2*(1), 65-68.

Kedgley, A., E. (2004). *Design and development of a shoulder testing simulator*. London, Ont.: Faculty of Graduate Studies, University of Western Ontario.

Masuda, T., Ishida, A., Cao, L., & Morita, S. (2008). A proposal for a new definition of the axial rotation angle of the shoulder joint. *Journal of Electromyography and Kinesiology, 18*(1), 154-159.

Novotny, J. E., Beynnon, B. D., & Nichols Iii, C. E. (2001). A numerical solution to calculate internal–external rotation at the glenohumeral joint. *Clinical Biomechanics, 16*(5), 395-400.

Appendix D – Full Range of Adjustability of Custom Modular Reverse Total Shoulder Arthroplasty Components

In this appendix, photographs and computer renderings (Figure D.1 to Figure D.5) – in addition to those in Figure 6.2 and Figure 6.3 – are presented to illustrate the full range of adjustability permitted by the custom modular Reverse Total Shoulder Arthroplasty described in Chapter 6 (Section 6.2.1). Note that the 38mm glenosphere and polyethylene humeral cup are shown in all renderings except when size is the variable being demonstrated. However, all adjustability shown with 38mm components can also be achieved with the 42mm implants.

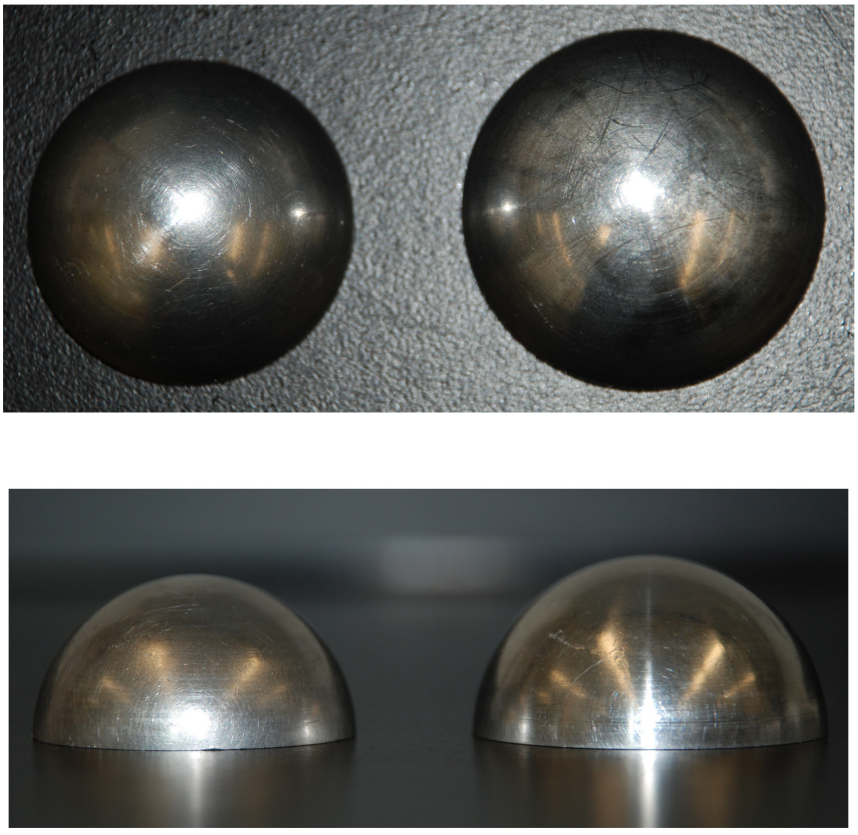

Figure D.1: Glenosphere sizes for custom modular implant.
This photograph shows the two glenosphere sizes (38 and 42mm) currently used with our custom modular implant system. (Top) Top view of the two glenosphere sizes, (Bottom) side view of the two glenosphere sizes.

Figure D.2: Available humeral polyethylene cup retention levels.
These photographs show the level of retention provided by each of three polyethylene humeral cups in the 38 and 42mm curvature sizes. The top two rows show the top view of the 38 and 42mm cups, respectively. The bottom two rows show the side view of the 38 and 42mm cups, respectively, with the corresponding glenosphere articulated. The three columns correspond to the levels of retention which are: highly mobile, standard, and retentive.

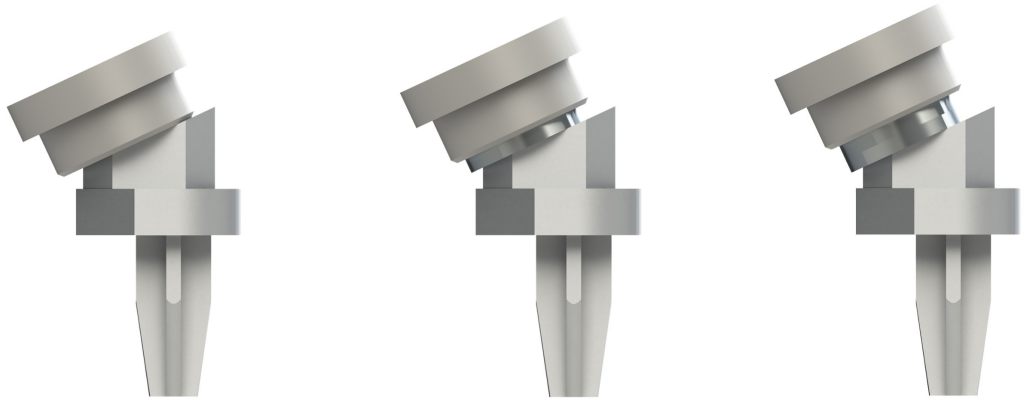

Humeral Poly Cup Thickness (3, 6, 9mm)

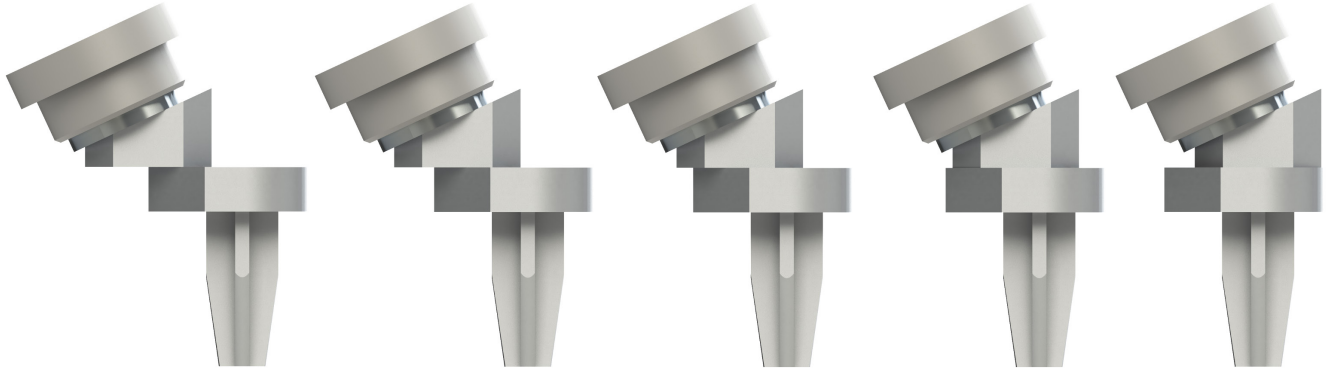

Humeral Lateral Offset (15, 10, 5, 0, -5mm)

Figure D.3: Adjustability of humeral polyethylene cup thickness, and humeral lateralization.

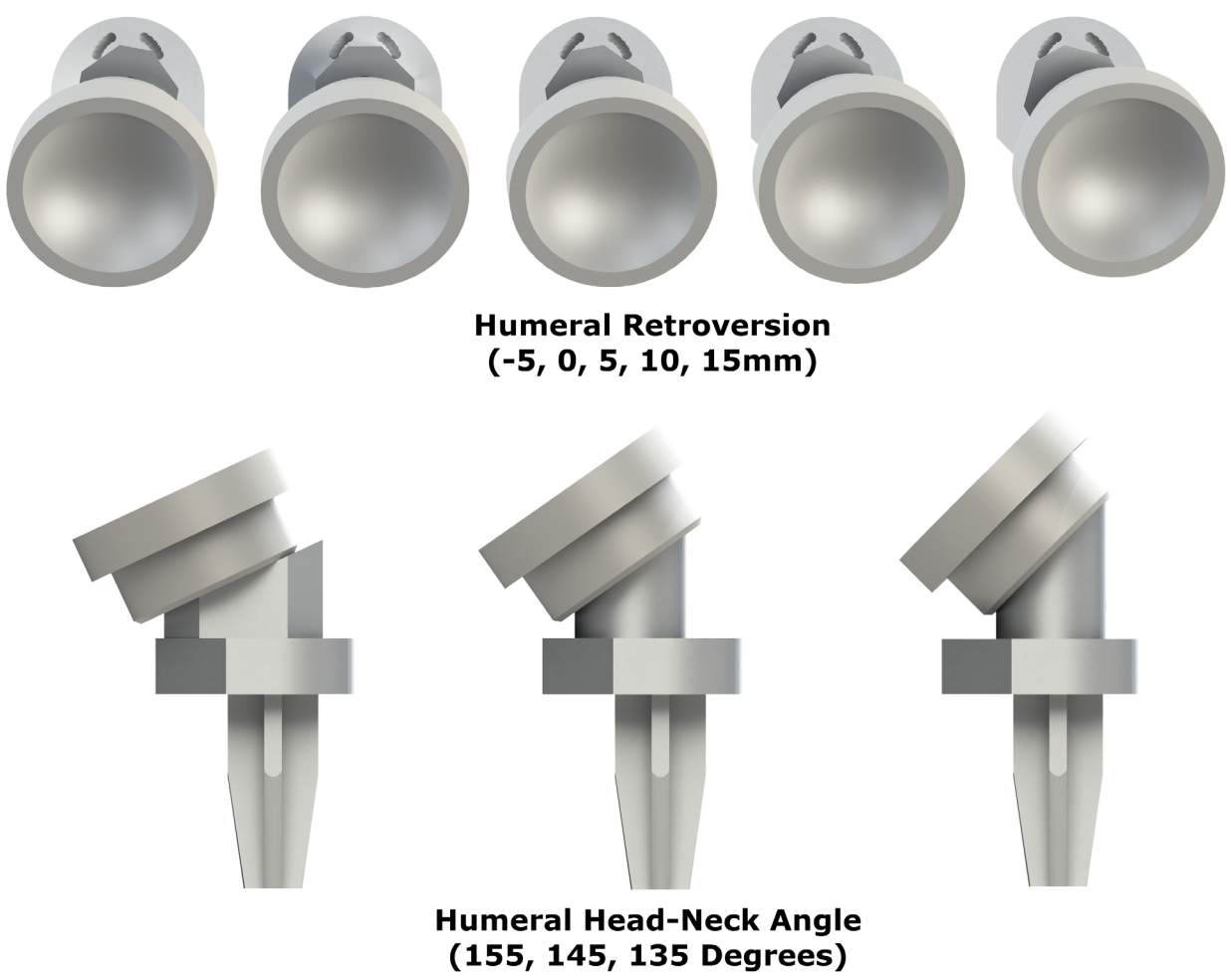

Figure D.4: Adjustability of humeral retroversion, and humeral head-neck angle.

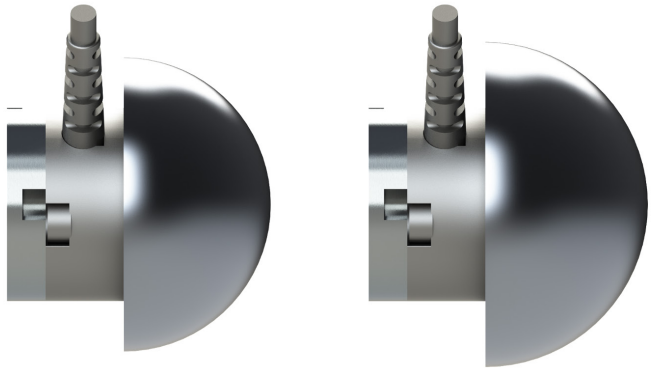

Glenosphere Size (38 & 42 mm)

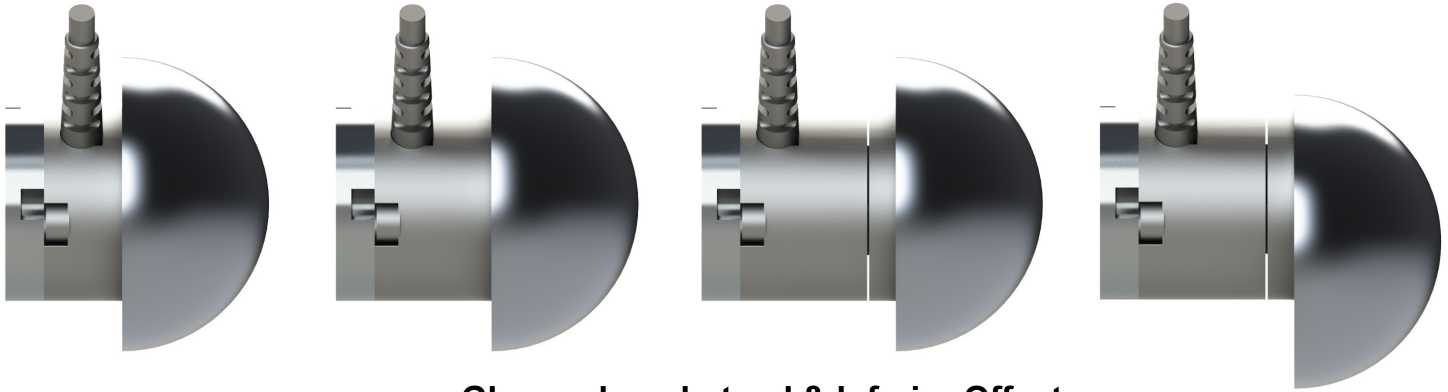

Glenosphere Lateral & Inferior Offset
(0, 5, 10mm & 5mm)

Figure D.5: Adjustability of glenosphere size, and glenosphere lateral and inferior offset.

Appendix E – Evaluation of the Accuracy of Transformed Six DOF Load Measurements Made Using a Glenosphere Embedded Load Cell

E.1 Introduction

Accurately measuring and providing a full description of the loads passing through the articulation of a Reverse Total Shoulder Arthroplasty (RTSA) is of primary importance when evaluating the effects of this implant, and can be achieved through the use of a six degree of freedom (DOF) load cell. Currently, however, no commercially available six DOF load cell has an appropriate sensing range and is small enough to be implanted in such a way that its sensing origin coincides with the joint center, and its sensing coordinate system (CS) is aligned with a physiologically relevant CS. As described in Chapter 6 (Section 6.2.1.2), this obstacle was overcome by designing a custom glenosphere component in which a load cell (Nano 25, ATI-IA, Apex, NC) could be nested. The loads measured by this sensor were then transformed from the load cell's CS into a desired physiologic CS of interest (*e.g.* a CS at the joint center, a CS coincident with the clinical baseplate fixation location, etc…). In order to ensure that the measured loads could be accurately transformed, a validation process was undertaken.

E.2 Methods

The transformation of forces and moments from one coordinate system to another can be performed using first principles and basic knowledge of the load magnitudes and directions, as well as the spatial configuration of the system of interest; however, the use of first principles becomes difficult and cumbersome when attempting to analyze a complex system or a system which must be analyzed in three dimensions. Particularly useful in these cases, are standard kinematic transformation matrix techniques that have been adapted for the transformation of forces and moments.

The following equations can be used to transform forces and moments, respectively, from one CS, namely the load cell measurement frame (LC), to another (*e.g.* a joint CS, JCS):

$$\begin{Bmatrix} F_x^{JCS} \\ F_y^{JCS} \\ F_z^{JCS} \end{Bmatrix} = \left[{}^{JCS}_{LC}R \right] * \begin{Bmatrix} F_x^{LC} \\ F_y^{LC} \\ F_z^{LC} \end{Bmatrix} \quad \text{Eq. E.1}$$

Eq. E.1: Coordinate system transformation of measured forces using spatial math.

$$\begin{Bmatrix} M_x^{JCS} \\ M_y^{JCS} \\ M_z^{JCS} \end{Bmatrix} = \left[{}^{JCS}_{LC}R \right] * \begin{Bmatrix} M_x^{LC} \\ M_y^{LC} \\ M_z^{LC} \end{Bmatrix} + \vec{P}_{LC}^{JCS} \begin{Bmatrix} F_x^{JCS} \\ F_y^{JCS} \\ F_z^{JCS} \end{Bmatrix} \quad \text{Eq. E.2}$$

Eq. E.2: Coordinate system transformation of measured moments using spatial math.

where $F_{x,y,z}^{JCS}$ & $M_{x,y,z}^{JCS}$ are the x, y, and z components of the measured forces & moments, respectively, transformed into the joint coordinate system; ${}^{JCS}_{LC}R$ is the rotation matrix describing the orientation of the load cell CS with respect to the JCS; $F_{x,y,z}^{LC}$ & $M_{x,y,z}^{LC}$ are the x, y, and z components of the measured forces & moments, respectively, in the load cell CS; and $\vec{P}_{LC}^{JCS}$ is the position vector describing the location of the load cell CS with respect to the joint CS (Bertec Corporation, 2012). As demonstrated by equations Eq. E.1 & Eq. E.2, these transformations depend on a clear understanding of the spatial relationship between the two coordinate systems. This relationship can be obtained through a series of digitizations; however, this introduces additional errors to the load values beyond those inherent in load cell measurements. Therefore, a testing apparatus and protocol was developed to evaluate the accuracy of the transformed loads.

The testing apparatus was composed of six main components: a method of load application, the RTSA implants, the embedded primary load cell, an implant positioning system, a secondary load cell, and a six DOF tracking system (Figure E.1). Loads were applied using a pneumatic actuator that was fixed to a rigid frame. Attached to the actuator was a small pot in which the polyethylene humeral cup was cemented in place such that the face of the cup was perpendicular to the actuator shaft. An adjustable x-y stage was placed on the base of the rigid frame and on top of it, an arc positioning device that allows a slider to be positioned between 0° (facing vertically) and 90°. The secondary six DOF load cell (Mini 45 ATI-IA, Apex, NC) was attached to the slider, and, via an adapter plate, it was attached to the primary six DOF load cell embedded in the RTSA

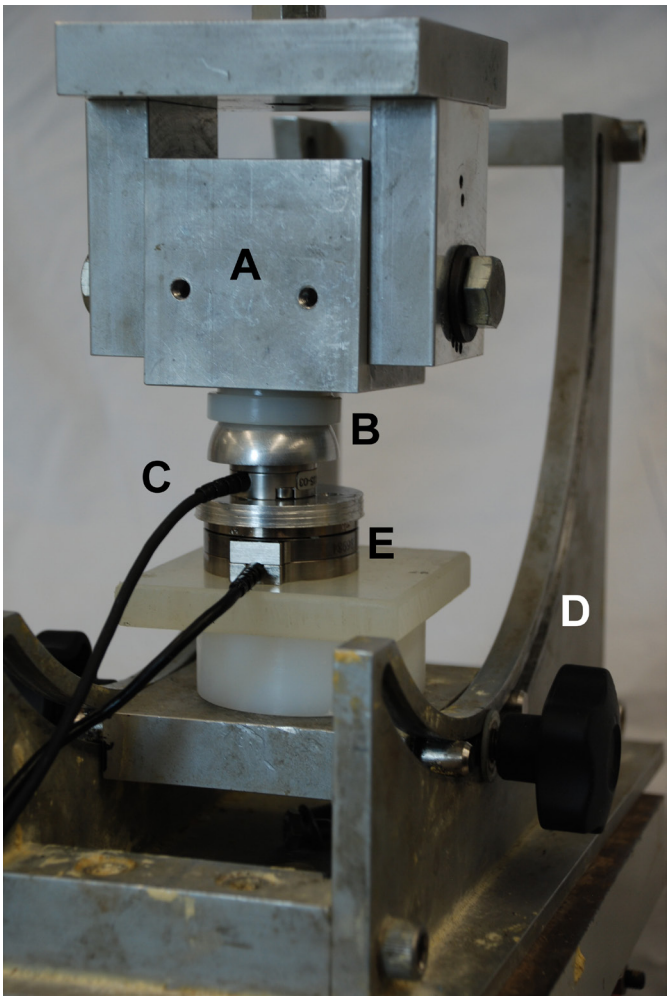

Figure E.1: Load transformation validation testing setup.
Shown is the testing setup used to evaluate the transformation of six DOF loads recorded by the implant embedded load cell to another arbitrary coordinate system. (A) Pot used to hold polyethylene cup (attached to pneumatic actuator-not shown), (B) Reverse Total Shoulder Arthroplasty *implant components, (C) implant embedded primary load cell, (D) implant positioning apparatus (shown is the arc and slider, used to change glenosphere orientation, which is mounted to an x-y stage), (E) secondary load cell. Note that the six DOF tracking system used in this testing setup is not shown.*

glenosphere component. The slider mechanism enabled the glenosphere and attached load cells to be rotated from 0°, aligned with the actuator for a purely compressive load, to 90°, a purely shear load. As well, the x-y stage enabled the glenosphere to be translated until it properly articulated the actuator mounted humeral cup. Finally, the six DOF tracking system (Optotrak Certus, NDI, Waterloo, ON) was implemented by placing a reference marker on the slider mechanism so that it was rigid relative to the two load cells.

This apparatus allowed the comparison of the loads measured by the secondary load cell to the forces and moments measured by the glenosphere-embedded load cell after transforming them to the secondary load cell's CS. The accuracy of transforming the six DOF loads measured by the primary load cell could then be assessed. For the purposes of this evaluation, the variables LC and JCS in equations Eq. E.1 & Eq. E.2 correspond to the primary load cell and the secondary load cell, respectively. Using an optically tracked stylus and the rigid reference described above, landmark digitizations were recorded for both load cells at well-defined markings on each sensor. These markings corresponded to each sensor's load measurement axes and their digitization therefore enabled the construction of optically tracked coordinate systems coincident with each of the sensor's load sensing frame.

A number of different loading configurations and levels encompassing a range of physiologically relevant joint angles and loading magnitudes were examined. Specifically, loads were applied at 0° (purely compressive), 30, 45, and 50° (full adduction when implant head-neck angle is accounted for). Sixty degrees was to be tested originally, but the humeral cup impinged on the load cell at this angle and thus 50° was tested instead. At each of these angles, five load magnitudes (0, 25, 50, 75, 100 N) were applied. These loads were applied as a ramp over the course of five seconds and were held for three seconds once the maximum was achieved.

For each of the 20 loading cases, the average value over the three second hold was calculated for each of the six loading components for both load cells. The values for the primary load cell were then transformed using equations Eq. E.1 & Eq. E.2 with the

coordinate transformations drawn from the landmark digitizations. The difference between each of the six transformed load values and the six loads measured by the secondary load cell were then subtracted to find the absolute difference. The average percent difference between the two values was calculated for each degree of freedom using the total force or moment measured by the secondary load cell as the true value. Instead of using each individual load measured by the secondary load cell, the sum of the three force/moment components were used for the force and moment percent differences, respectively, because some of the individual load components were so small that percent differences were unrealistically large. These values were then averaged over all 20 cases in order to give an overall estimate of the transformation accuracy. Repeatability was calculated for a subset of cases (all load levels at 0° & 50° load configurations) in which three repeated trials were performed. The average of all of these cases was then calculated.

E.3 Results

Comparison of the transformed results to those measured using the secondary load cell demonstrated that differences ranged from <0.5 N for all joint configurations with 0 N loading, to 2.6 N in the 50° configuration with 100 N loading applied. With the exception of this maximum value, all differences in force were ≤2 N (Figure E.2). The value of the moments from the two load cells for 0, 30 & 45° configurations at all load levels were nearly equal and never exceeded 0.04 Nm. However, in the 50° configuration, the differences in moment values between the transformed and secondary measurements increased more rapidly as load increased, and reached a maximum of 0.1 Nm at 100 N (Figure E.3). The percent difference of all test cases together was found to be ≤2.9±1.7% for the x & y forces and 1.2±1.4% for z, while the differences in moments were ~12.4±11.7% in the x & y and 3.4±4.1% for z. Finally, the average repeatability in the transformed forces and moments was ±0.1 N and ±0.01 Nm, respectively.

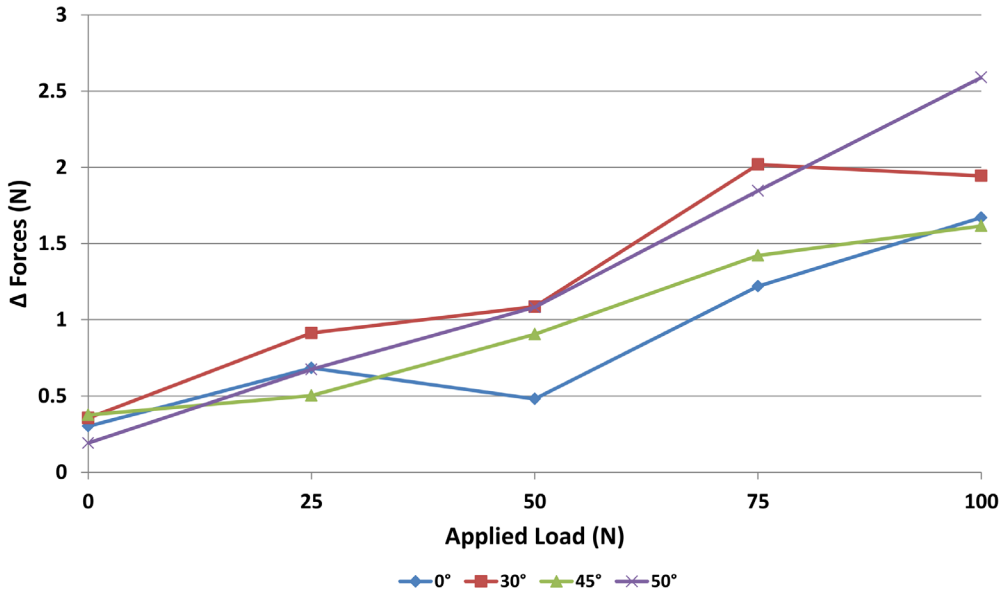

Figure E.2: Force difference between transformed primary readings and secondary load cell measurements.
Note that the data are the average of the three axes and presented for the four joint orientations.

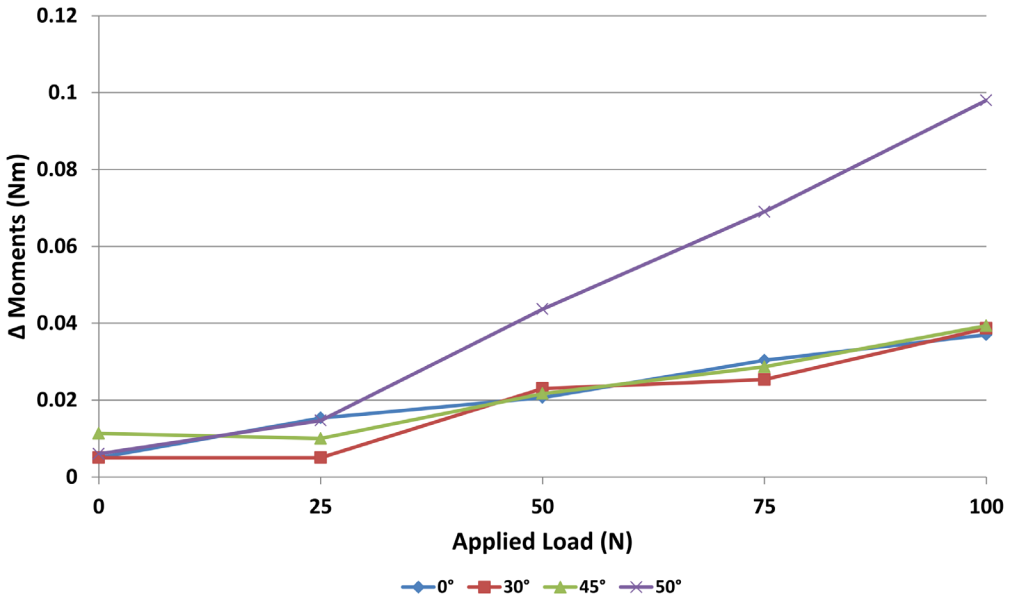

Figure E.3: Moment difference between transformed primary readings and secondary load cell measurements.
Note that the data are the average of the three axes and presented for the four joint orientations.

E.4 Discussion

Measurement of the joint loads passing through the RTSA and description of these loads with respect to any number of clinically relevant coordinate systems (*e.g.* joint center, fixation location etc.) were critical criteria when developing the custom components described in Chapter 6. In this Appendix, the accuracy of transforming the measured loads to another coordinate system – in this case, the coordinate system of a secondary load cell – is assessed. This evaluation demonstrates that the difference between the transformed loads and those measured by the secondary load cell increased linearly with applied load for both the forces and moments. Differences in the forces were seen to slightly increase with increasing joint angulation, but in the case of the moments, the differences were nearly identical at all load levels with the joint in 0, 35, and 45°. However, in the most angulated case (*i.e.* 50°), the differences in moments markedly increased. It is unsurprising that the differences in the moments would become greater with higher levels of angulation, since higher levels of angulation increase the effective moment arm and thus the applied moments, but is surprising that an abrupt rather than progressive increase was observed. A possible explanation is that the 50° configuration may have resulted in a portion of the applied load bypassing the primary load cell since this configuration represents an arm in adduction which, in the case of RTSA, can sometimes cause impingement between the humeral cup and underlying bone (or in this case, the underlying base).

The average percent differences across all configurations were small (≤2.9%), well within acceptable ranges for a system that includes load measurement errors and transformation errors related to optical tracking. In the case of the z axis, which was expected to experience the greatest portion of the transmitted load, differences averaged only 1.2%. The percent differences in moments were found to be markedly higher than observed in the forces (3.4-12.4%). These differences can be attributed to a number of factors including load cell measurement error, transformation error, error in the experimental setup, and the small magnitude of the moment values. The load cells used in this evaluation are both rated to ~2% error of their full scale moment readings for each axis, and thus, the higher percent differences in the moments may be explained by the fact that

their measurements represent a much smaller percent of the sensor's maximum range than is the case in the force measurements. A 2% load cell error would therefore have a more significant effect on the readings. Transformation error may also play an important part in the differences observed in the moments because, as demonstrated in equation Eq. E.2, the transformed moments are subject to error from transformation of the measured moments into the new coordinate system as well as error from the portion of the transformed moments produced by the transformed forces. In other words, the transformations of these forces possess inherent error which is compounded by error in the determination of the moment arms these forces act at.

In an effort to further explain the large differences seen in the 50° orientation, Figure E.4 was created to compare the differences in the resultant force measured by the two load cells. The data in this graph demonstrate that the magnitude of the resultant of all three force components are in close agreement for the first three joint orientations but diverge in the 50° angulation. This divergence in the resultant forces indicates that some phenomenon is preventing the entire load from being measured by both sensors. As a result, the differences in moments appear to be more a function of differences in the measured forces than in the transformation process. It is possible to attribute these differences to error in the load cells, but since the differences for the other orientations never approach this level, it is more likely that some form of error in the experimental setup is responsible.

An important consideration when assessing the percent differences presented here is that the 'true value' readings from the secondary load cell are themselves subject to a rated error of 2% of full scale per axis. However, the full scale range of the secondary load cell is much greater than that of the primary (2.3 times greater force and moment range in both the x & y axes), and therefore, it is likely that a large portion of the observed differences can be attributed to the markedly larger errors associated with the secondary load cell.

It is important to note a limitation associated with this evaluation of the errors in transforming the loads measured by the glenosphere load cell. Specifically, the loads

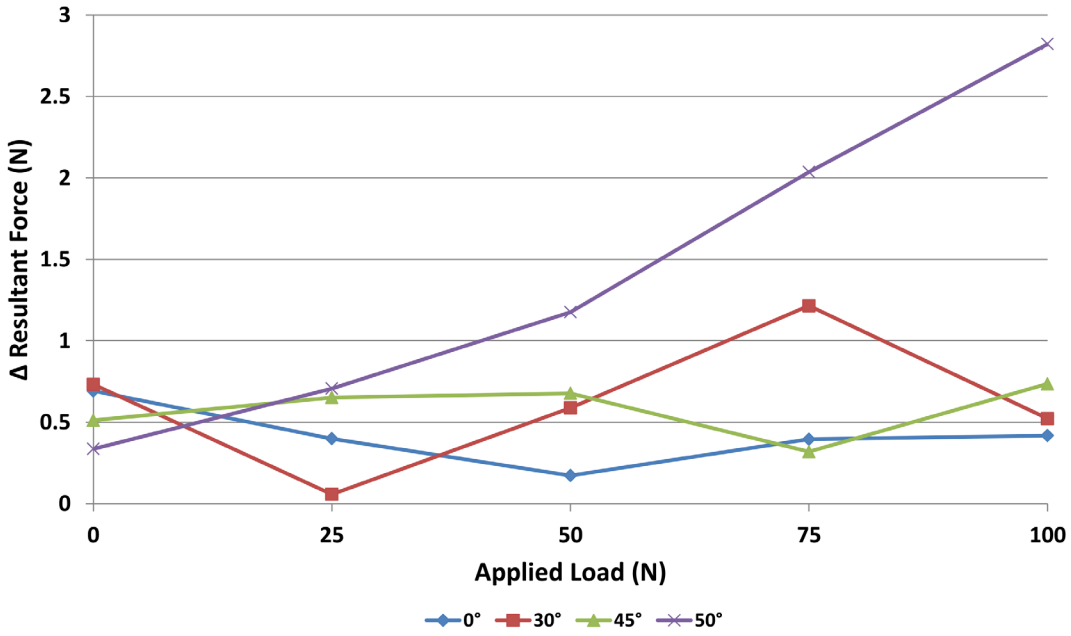

Figure E.4: Differences between resultant forces measured by each load cell.
Note that the data are the differences between the two load cells for the resultant forces of the three force components taken together.

applied to the glenosphere in this protocol did not reach the magnitude experienced during active motion testing due to the maximum load which could be applied by the actuator used in this testing setup. As a result, it is possible that the level of error observed in this study does not reflect the error which is present during active motion simulation. However, the percent error was not observed to increase markedly across the five load levels and thus it can be suggested that the percent error during active motion would be similar.

The results presented here have demonstrated that the load cell and transformation methodology used in Chapter 6 can be considered accurate and repeatable with respect to the transformation of the measured forces. The transformed moments were also very repeatable. The percent differences observed between the measured and transformed moments were markedly higher than those observed for the forces; however, due to the factors discussed above, it is believed that these differences may be heavily influenced by the secondary load cell. Also, the relatively small magnitude of the measurements may have resulted in misleadingly large percent differences, and thus the effect that these difference may have on the clinical interpretation of the moments may be minimal.

E.5 References

Bertec Corporation. (2012). Change of coordinate system. *Bertec force Plates Version 1.0.0* () Retrieved from http://bertec.com/uploads/pdfs/manuals/Force%20Plate%20Manual.pdf

Joshua William Giles

BESc (Mech)
PhD Candidate

Curriculum Vitae

Affiliation: Roth|McFarlene Hand and Upper Limb Centre
St. Joseph's Health Centre

EDUCATION

Fall 2013 **International Research Fellowship**
Development of a Biplane Fluoroscopic Technique for the Physiologic Description of Scapulothoracic Motion
Bone & Joint Research Center - Motion Analysis Laboratory
Henry Ford Hospital, Detroit, Michigan, USA
Supervisor: Dr. Michael J. Bey
Expected Completion Date: December 2013

2010- **Ph.D. Candidate, Biomechanics**
Design and Development of a Shoulder Simulator for the Assessment of Stability and Unconstrained Motion
Graduate Program in Biomedical Engineering
The University of Western Ontario, London, Canada
Supervisor: Dr. James A. Johnson
Expected Graduation Date: March 2014

2009-2010 **Master's Candidate, Biomechanics (Transferred)**
Graduate Program in Biomedical Engineering
The University of Western Ontario, London, Canada

2005-2009 **Bachelor of Engineering Science**
Mechanical and Materials Engineering with Distinction
The University of Western Ontario, London, Canada

EMPLOYMENT HISTORY

2009- **Engineering Research Associate, Orthopaedic Research**
Hand and Upper Limb Centre
St. Joseph's Health Centre
London, Ontario
Supervisor: James A. Johnson

2007-2009 **Engineering Research Assistant, Orthopaedic Research**
University of Western Ontario
London, Ontario
Supervisor: James A. Johnson

PROFESSIONAL MEMBERSHIPS

2013- **Engineering Intern Program (EIT)**
Professional Engineers Ontario

2013- **American Society of Mechanical Engineers**
Bioengineering Division

ACADEMIC HONOURS AND AWARDS

Awards and Scholarships (primary recipient)

2011-2014 NSERC Alexander Graham Bell Canada Graduate Scholarship (CGS-D), Competitive, National, $35,000/year

2013 NSERC Michael Smith Foreign Study Supplement (MSFSS), Henry Ford Hospital Bone & Joint Center, Competitive, National, $6,000

2013 Nellie Farthing Fellowship for Excellence in Research, University of Western Ontario, Competitive, Institutional, $3,000

2013 Fourth place, Three Minute Thesis (3MT) competition, University of Western Ontario, Institutional

2009-2013 Western Graduate Research Scholarship, University of Western Ontario, Institutional, $7,500/year

2012 Western Graduate Thesis Research Award, University of Western Ontario, Competitive, Institutional, $1,500/year

2011 Ontario Graduate Scholarship, Ontario Ministry of Training, Colleges and Universities (Declined), Competitive, Provincial, $15,000/year

2010 Ontario Graduate Scholarship, Ontario Ministry of Training, Colleges and Universities, Competitive, Provincial, $15,000/year

2009-2010 NSERC Alexander Graham Bell Canada Graduate Scholarship (CGS-M), Competitive, National, $17,500/year

2009 Ontario Graduate Scholarship, Ontario Ministry of Training, Colleges and Universities (Declined), Competitive, Provincial, $15,000/year

2009 Graduated with Distinction, Mechanical and Materials Engineering, University of Western Ontario

2009 Gold Medal, Canadian Society for Mechanical Engineering (CSME), Competitive, Institutional

2008 Faculty Association Award, University of Western Ontario, Competitive, Institutional, $900

2007 & 2008 NSERC Undergraduate Summer Research Award (USRA), Competitive, National, $11,250/summer

2005-2009 Engineering Dean's Honour List, University of Western Ontario

2005-2009 Continuing Scholarship**,** University of Western Ontario, Competitive, Institutional, $2,500/year

2005-2009 Queen Elizabeth Aiming for the Top Scholarship, Competitive, Provincial, $500/year

Awards and Scholarships (co-author)

2013 First Place Basic Science Research Paper, 41st Annual Orthopaedic Surgery Research Day, University of Western Ontario, Competitive, Institutional, $1000

2012 Awarded Opening Talk, Annual American Shoulder and Elbow Society Closed Meeting

2012 First Place Basic Science Research Paper, 40th Annual Orthopaedic Surgery Research Day, University of Western Ontario, Competitive, Institutional, $1000

PUBLICATIONS IN PEER-REVIEWED JOURNALS AND BOOK CHAPTERS

1. **Giles, J.W.**, Degen, R.M., Johnson, J.A., & Athwal, G.S. (Accepted Feb 2014). The Bristow-Latarjet: Why these techniques should not be considered synonymous. *Journal of Bone and Joint Surgery.*

2. Degen, R.M., **Giles, J.W.**, Thompson, S., Litchfield, R.B., & Athwal, G.S. (Oct 2013). Biomechanics of complex shoulder instability. Invited chapter in Clinics in Sports Medicine, *Shoulder Instability in the Athlete* (pp. 625-636).

3. Shannon, H.L., Deluce, S.R., Lalone, E.A., **Giles, J. W.**, Johnson, J.A., & King, G.J. (In Press). Effect of radial head implant shape on joint contact area and location during static loading: A biomechanical study. *Journal of Hand Surgery.*

4. Degen, R.M., **Giles, J.W.**, Johnson, J.A., & Athwal, G.S. (Jan 2014). Remplissage Versus Latarjet for Engaging Hill-Sachs Defects Without Substantial Glenoid Bone Loss: A Biomechanical Comparison. Invited publication in *Clinical Orthopaedics and Related Research.* Advanced online publication.

5. Puskas, G.J., **Giles, J.W.**, Degen, R.M., Johnson, J.A., & Athwal, G.S. (Jan 2014). Humeral head reconstruction for Hill-Sachs defects: A biomechanical comparison of two fixation techniques for bone grafting. *Arthroscopy: The Journal of Arthroscopic & Related Surgery*. 30(1):22-28.

6. **Giles, J.W.**, Puskas, G.J., Welsh, M.F., Johnson, J.A., & Athwal, G.S. (Nov 2013). Suture anchor fixation of bony Bankart fractures: Comparison of single-point with double-point "suture bridge" technique. *The American Journal of Sports Medicine.* 41(11):2624-31.

7. Degen, R.M., **Giles, J.W.**, Thompson, S.R., Litchfield, R.B., & Athwal, G.S. (Oct 2013). The biomechanics of complex shoulder instability. Invited publication in *Clinics in Sports Medicine.* 32(4): 625-636.

8. Burkhart, S.S., deBeer, J.F., **Giles, J.W.**, Johnson, J.A., & Athwal, G.S. (Jul 2013). Traditional and modified latarjet techniques: Letter to the editor. *The American Journal of Sports Medicine*. 41(7):NP31-2.

9. Elkinson, I., **Giles, J.W.**, Boons, H.W., Faber, K.J., Ferreira, L.M., Johnson, J.A., & Athwal, G.S. (Jun 2013). The shoulder remplissage procedure for Hill-Sachs defects: Does technique matter? *Journal of Shoulder and Elbow Surgery.* 22(6):835-41.

10. **Giles, J.W.**, Boons, H.W., Elkinson, I., Faber, K.J., Ferreira, L.M., Johnson, J.A., & Athwal, G.S. (Jun 2013). Does the dynamic sling effect of the Latarjet procedure improve shoulder stability? A biomechanical evaluation. *Journal of Shoulder and Elbow Surgery.* 22(6):821-7.

11. Boons, H.W., **Giles, J.W.**, Elkinson, I., Johnson, J.A., & Athwal, G.S. (Feb 2013). Classic versus congruent coracoid positioning during the Latarjet procedure: An *in-vitro* biomechanical comparison. *Arthroscopy: The Journal of Arthroscopic & Related Surgery.* 29(2):309-16.

12. Lalone, E.A., **Giles, J.W.**, Alolabi, B., Peters, T.M., Johnson, J.A., & King, G.J. (Feb 2013). Utility of an image-based technique to detect changes in joint congruency following simulated joint injury and repair: An *in-vitro* study of the elbow. *Journal of Biomechanics*. 46(4):677-82.

13. Degen, R.M., **Giles, J.W.,** Boons, H.W., Ferreira, L.M., Johnson, J.A., & Athwal, G.S. (Jan 2013). A biomechanical assessment of superior shoulder translation after reconstruction of anterior glenoid bone defects: The Latarjet procedure versus allograft reconstruction. *International Journal of Shoulder Surgery*. 7(1):7-13.

14. **Giles, J.W.**, Puskas, G.J., Welsh, M.F., Johnson, J.A., & Athwal, G.S. (Dec 2012). Do the traditional and modified Latarjet techniques produce equivalent reconstruction stability and strength? *The American Journal of Sports Medicine.* 40(12):2801-07.

15. **Giles, J.W.**, Elkinson, I., Ferreira, L.M., Faber, K.J., Boons, H., Litchfield, R., Johnson, J.A., & Athwal, G.S. (Sep 2012). Moderate to large engaging Hill-Sachs defects: An *in-vitro* biomechanical comparison of the remplissage procedure, allograft humeral head reconstruction, and partial resurfacing arthroplasty. *Journal of Shoulder and Elbow Surgery*. 21(9):1142-51.

16. Elkinson, I., **Giles, J.W.**, Faber, K.J., Boons, H.W., Ferreira, L.M., Johnson, J.A., & Athwal, G.S. (Jun 2012). The effect of the remplissage procedure on shoulder stability and range of motion: An *in-vitro* biomechanical assessment. *The Journal of Bone and Joint Surgery. American Volume.* 94(11):1003-12.

17. Armitage, M.S., Elkinson, I., **Giles, J.W.**, & Athwal, G.S. (Nov 2011). An anatomic, computed tomographic assessment of the coracoid process with special reference to the congruent-arc Latarjet procedure. *Arthroscopy: The Journal of Arthroscopic & Related Surgery*. 27(11):1485-89.

18. **Giles, J.W.**, Boons, H.W., Ferreira, L.M., Johnson, J.A., & Athwal, G.S. (Apr 2011). The effect of the conjoined tendon of the short head of the biceps and coracobrachialis on shoulder stability and kinematics during *in-vitro* simulation. *Journal of Biomechanics*. 44(6):1192-95.

SUBMITTED MANUSCRIPTS UNDER REVIEW

1. **Giles, J.W.**, Ferreira, L.M., Johnson, J.A., & Athwal, G.S. (Nov 2013). Validation of a novel *in-vitro* simulator for real-time control of active shoulder movements in various planes of motion. *Journal of Biomechanical Engineering.*

2. Shannon, H.L., Deluce, S.R., **Giles, J.W.**, Johnson, J.A., & King, G.J. (Under Review Jul 2013). The effect of radial head implant shape on radiocapitellar kinematics during *in-vitro* forearm rotation. *Journal of Shoulder and Elbow Surgery.*

MANUSCRIPTS IN PREPARATION

1. Welsh, M.F., Willing, R., **Giles, J.W.**, Johnson, J.A., & Athwal, G.S. Hill-Sachs defect engagement: the influence of size, range of motion and joint translation.
2. **Giles, J.W.**, Owens, B.D., & Athwal, G.S. A formula for predicting anterior glenoid bone loss due to instability.

3. **Giles, J.W.**, Langohr, G.D., Johnson, J.A., Athwal, G.S. The Influence of Reverse Total Shoulder Arthroplasty Implant Geometric Variables on Muscle Activation, Joint Load and Shoulder Function. *Journal of Bone and Joint Surgery.*

4. **Giles, J.W.**, Haladik, J., & Bey, M.J. Assessment of scapular motion relative to a physiologic thoracic coordinate system using biplane high speed x-ray. *Journal of Biomechanics.*

5. **Giles, J.W.**, Peltz, C.D., & Bey, M.J. Evaluation of the relationship between superior humeral head migration and acromiohumeral distance using biplane x-ray. *Journal of Shoulder and Elbow Surgery.*

ABSTRACTS AND PRESENTATIONS AT PROFESSIONAL MEETINGS

1. **Giles, J.W.**, Ferreira, L.M., Johnson, J.A., & Athwal, G.S. (June 2014). Development of a Novel *In-vitro* Shoulder Simulator for Active Control of Glenohumeral and Scapulothoracic Movements in Various Planes. Annual Meeting of the Canadian Orthopaedic Research Society. (National) (Podium) (PhD).

2. **Giles, J.W.**, Welsh, M.F., Willing, R.T., Johnson, J.A., Athwal, G.S. (June 2014) Hill-Sachs Defect Engagement: The Influence of Size, Range of Motion and Joint Translation. (National) (Podium) (Research Associate).

3. **Giles, J.W.**, Degen, R.M., Johnson, J.A., & Athwal, G.S. (Mar 2014). The Bristow-Latarjet: Why These Techniques Should Not Be Considered Synonymous. American Academy of Orthopedic Surgeons Annual Meeting (International) (Podium) (PhD).

4. Welsh, M.F., Willing, R., **Giles, J.W.**, Johnson, J.A., & Athwal, G.S. (Mar 2014). A Computational Assessment of Hill-Sachs Defect Size As It Relates To Glenohumeral Stability. American Academy of Orthopedic Surgeons Annual Meeting (International) (Podium) (PhD).

5. **Giles, J.W.**, Ferreira, L.M., Johnson, J.A., & Athwal, G.S. (Mar 2014). Development of a Novel *In-vitro* Shoulder Simulator for Active Control of Glenohumeral and Scapulothoracic Movements in Various Planes. 60th Annual Meeting of the Orthopaedic Research Society. (International) (Podium) (PhD).

6. Shannon, H.L., Deluce, S.R., **Giles, J.W.**, Johnson, J.A., & King, G.J. (Mar 2014). Effect of Radial Head Implant Shape on Radiocapitellar using an Image-Based Tool to Examine Joint Congruency. 60th Annual Meeting of the Orthopaedic Research Society. (International) (Podium) (Research Associate).

7. **Giles, J.W.**, Puskas, G., Welsh, M.F., Johnson, J.A., & Athwal, G.S. (Mar 2014). Humeral Head Allograft Fixation for Reconstruction of Hill-Sachs Defects: Antegrade versus Retrograde Fixation? 60th Annual Meeting of the Orthopaedic Research Society. (International) (Poster) (PhD).

8. **Giles, J.W.**, Degen, R.M., Johnson, J.A., & Athwal, G.S. (Mar 2014). Comparing Remplissage with Latarjet Coracoid Transfer for Recurrent Shoulder Instability with a Hill-Sachs Defect: An Engaging Topic. 60th Annual Meeting of the Orthopaedic Research Society. (International) (Poster) (PhD).

9. Welsh, M.F., Willing, R., **Giles, J.W.**, Johnson, J.A., & Athwal, G.S. (Oct 2013). Hill-Sachs Defect Engagement: The Influence of Size, Range of Motion and Joint Translation. American Shoulder and Elbow Society Annual Closed Meeting (International) (Podium) (PhD).

10. **Giles, J.W.**, Ferreira, L.M., Johnson, J.A., & Athwal, G.S. (Jun 2013). Validation of a Novel *In-Vitro* Simulator for Real-Time Control of Active Shoulder Movements in Various Planes of Motion. American Society of Mechanical Engineers Summer Bioengineering Conference (International) (Podium) (PhD).

11. **Giles, J.W.**, Degen, R.M., Desjardins, J., Johnson, J.A., & Athwal, G.S. (Jun 2013). The Bristow-Latarjet: Why These Techniques Should Not Be Considered Synonymous. Canadian Orthopaedic Association Annual Meeting (National) (Podium) (PhD).

12. Shannon, H.L., Deluce, S.R., **Giles, J.W.**, Johnson, J.A., & King, G.J. (Jun 2013). Radial Head Implant Shape Does Not Affect Radiocapitellar Kinematics During *In-Vitro* Forearm Rotation. Canadian Orthopaedic Research Society Annual Meeting (National) (Podium) (Research Associate).

13. **Giles, J.W.**, Puskas, G.J., Welsh, M.F., Johnson, J.A., & Athwal, G.S. (Jun 2013). Suture Anchor Fixation of Bony Bankart Fractures: A Comparison of Single Row versus Suture Bridge Techniques. Canadian Orthopaedic Association Annual Meeting (National) (Poster) (PhD).

14. **Giles, J.W.**, Puskas, G., Welsh, M.F., Johnson, J.A., & Athwal, G.S. (Jun 2013). Humeral Head Allograft Fixation for Reconstruction of Hill-Sachs Defects: Antegrade versus Retrograde Fixation? Canadian Orthopaedic Association Annual Meeting (National) (Poster) (PhD).

15. **Giles, J.W.**, Owens, B.D., & Athwal, G.S. (Jun 2013). A Formula for Predicting Anterior Glenoid Bone Loss Due to Instability. Canadian Orthopaedic Association Annual Meeting (National) (Poster) (PhD).

16. Degen, R.M., **Giles, J.W.**, Johnson, J.A., & Athwal, G.S. (Jun 2013). A Biomechanical Assessment of Superior Shoulder Translation after Reconstruction of Anterior Glenoid Bone Defects: The Latarjet Procedure versus Allograft Reconstruction. Canadian Orthopaedic Association Annual Meeting (National) (Poster) (PhD).

17. Degen, R.M., **Giles, J.W.**, Johnson, J.A., & Athwal, G.S (Jun 2013). Comparing Remplissage with Latarjet Coracoid Transfer for Recurrent Shoulder Instability with a Hill-Sachs Defect: An Engaging Topic. Canadian Orthopaedic Association Annual Meeting (National) (Poster) (PhD).

18. Puskas, G.J., **Giles, J.W.**, Welsh, M.F., Johnson, J.A., & Athwal, G.S. (Jun 2013). Suture Anchor Fixation of Bony Bankart Fractures: A Comparison of Single-Row Versus Suture Bridge Techniques. 73rd Annual Congress of the Swiss Society of Orthopaedics and Traumatology (International) (Podium) (PhD).

19. Puskas, G.J., **Giles, J.W.**, Welsh, M.F., Johnson, J.A., & Athwal, G.S. (Jun 2013). Strength of Hill-Sachs Allograft Reconstruction: A Biomechanical Comparison of Two Screw Fixation Techniques. 14th Annual Meeting of the European Federation National Associations of Orthopaedics and Traumatology (International) (Poster) (PhD).

20. Puskas, G.J., **Giles, J.W.**, Welsh, M.F., Johnson, J.A., & Athwal, G.S. (Jun 2013). The Biomechanical Strength and Load Transfer of Classic and Congruent Arc Latarjet Procedures. 14th Annual Meeting of the European Federation National Associations of Orthopaedics and Traumatology (International) (Podium) (PhD).

21. **Giles, J.W.**, Puskas, G.J., Welsh, M.F., Johnson, J.A., & Athwal, G.S. (Apr 2013). Stability of Hill-Sachs Allograft Reconstruction: A Biomechanical Study Comparing Two Screw Fixation Techniques. 12th International Congress of Shoulder and Elbow Surgery (International) (E-Poster) (PhD).

22. **Giles, J.W.**, Elkinson, I., Boons, HW, Faber, K.J., Ferreira, L.M., Johnson, J.A., & Athwal, G.S. (Mar 2013). Does Suture and Anchor Placement Technique Matter When Performing Remplissage for Hill-Sachs Lesions? American Academy of Orthopedic Surgeons Annual Meeting (International) (Podium) (PhD).

23. Shannon, H.L., Deluce, S.R., **Giles, J.W.**, Johnson, J.A., & King, G.J. (Mar 2013). Radial Head Implant Shape Does Not Affect Radiocapitellar Kinematics During *In-Vitro* Forearm Rotation. American Academy of Orthopedic Surgeons Annual Meeting (International) (Podium) (Research Associate).

24. Shannon, H.L., Deluce, S.R., **Giles, J.W.**, Johnson, J.A., & King, G.J. (Mar 2013). Radial Head Implant Shape Does Not Affect Radiocapitellar Kinematics During *In-Vitro* Forearm Rotation. Annual Speciality Day Meeting of the Society of American Shoulder and Elbow Surgeons (International) (Podium) (Research Associate).

25. Shannon, H.L., Deluce, S., **Giles, J.W.**, Johnson, J.A., & King, G.J. (Mar 2013). Radial Head Implant Shape Does Not Affect Radiocapitellar Kinematics During *In-Vitro* Forearm Rotation. Annual Speciality Day Meeting of the Society of American Shoulder and Elbow Surgeons (International) (Podium) (Research Associate).

26. **Giles, J.W.**, Degen, R., Desjardins, J., Johnson, J.A., & Athwal, G.S. (Mar 2013). Comparison of Two Competing Reconstructive Procedures for Complex Shoulder

Instability using a Novel *In-Vitro* Testing Apparatus. London Health Research Day. (Regional) (Poster) (PhD).

27. **Giles, J.W.**, Degen, R., Desjardins, J., Johnson, J.A., & Athwal, G.S. (Feb 2013). The Bristow-Latarjet: Why These Techniques Should Not Be Considered Synonymous. 59th Annual Meeting of the Orthopaedic Research Society. (International) (Poster) (PhD).

28. **Giles, J.W.**, Puskas, G., Welsh, M.F., Johnson, J.A., & Athwal, G.S. (Feb 2013). Suture Anchor Fixation of Bony Bankart Fractures: A Comparison of Single Row versus Suture Bridge Techniques. 59th Annual Meeting of the Orthopaedic Research Society. (International) (Poster) (PhD).

29. **Giles, J.W.**, Owens, B., Johnson, J.A., & Athwal, G.S. (Feb 2013). A Formula for Predicting Anterior Glenoid Bone Loss Due to Instability. 59th Annual Meeting of the Orthopaedic Research Society. (International) (Podium) (PhD).

30. **Giles, J.W.**, Puskas, G., Welsh, M.F., Johnson, J.A., & *Athwal, G.S. (Oct 2012). Do the Traditional and Modified Latarjet Techniques Produce Equivalent Reconstruction Stability and Strength? American Shoulder and Elbow Society Annual Closed Meeting (International) (Podium) (PhD). **Presenter*

31. **Giles, J.W.**, Elkinson, I., Boons, H.W, *Faber, K.J., Ferreira, L.M., Johnson, J.A., & Athwal, G.S. (Oct 2012). Does the Dynamic Sling Effect of the Latarjet Procedure Improve Shoulder Stability? A Biomechanical Evaluation. American Shoulder and Elbow Society Annual Closed Meeting (International) (Podium) (PhD). **Presenter*

32. Puskas, G.J., **Giles, J.W.**, Welsh, M.F., Athwal, G.S. & Johnson, J.A. (Jul 2012). The Biomechanical Effectiveness of Classic and Congruent Arc Latarjet Procedures. 72nd Annual Meeting of the Swiss Society for Orthopaedics and Traumatology (International) (Podium) (PhD).

33. **Giles, J.W.**, Boons, H.W., Elkinson, I., Ferreira, L.M., Faber, K.J., Litchfield, R.B., Johnson, J.A., & Athwal. G.S. (Jun 2012). A Biomechanical Evaluation of the Dynamic Sling Effect of the Latarjet Procedure: Does It Improve Shoulder Stability? Canadian Orthopaedic Association Annual Meeting (National) (Podium) (PhD).

34. **Giles, J.W.**, Boons, H.W., Elkinson, I., Kaber, K.J., Ferreira, L.M., Athwal, G.S., & Johnson, J.A. (Jun 2012). An *In-Vitro* Biomechanical Comparison of the Classic and Congruent Arc Latarjet Procedures. Canadian Orthopaedic Association Annual Meeting (National) (Podium) (PhD).

35. **Giles, J.W.**, Puskas, G.J., Welsh, M.F., Athwal, G.S., & Johnson, J.A. (Jun 2012). The Biomechanical Strength of Classic and Congruent Arc Latarjet Constructs. Canadian Orthopaedic Association Annual Meeting (National) (Podium) (PhD).

36. **Giles, J.W.**, Boons, H.W., Elkinson, I., Faber, K.J., Ferreira, L.M., Athwal, G.S., & Johnson, J.A. (Feb 2012). Classic and Congruent Latarjet Techniques: An *In-Vitro* Biomechanical Comparison. 58th Annual Meeting of the Orthopaedic Research Society (International) (Podium) (PhD).

37. **Giles, J.W.**, Boons, H.W., Elkinson, I., Ferreira, L.M., Faber, K.J., Litchfield, R.B., Johnson, J.A., & Athwal, G.S. (Feb 2012). Does the Dynamic Sling Effect of the Latarjet Procedure Improve Shoulder Stability? A Biomechanical Evaluation. American Academy of Orthopedic Surgeons Annual Meeting. (International) (Podium) (PhD).

38. **Giles, J.W.**, Puskas, G.J., Welsh, M.F., Athwal, G.S., & Johnson, J.A. (Feb 2012). The Biomechanical Effectiveness of Classic and Congruent Arc Latarjet Procedures. 58th Annual Meeting of the Orthopaedic Research Society (International) (Poster) (PhD).

39. **Giles, J.W.**, Elkinson, I., Boons, H.W., Faber, K.J., Ferreira, L.M., Athwal, G.S., & Johnson, J.A. (Feb 2012). The Shoulder Remplissage Procedure for Hill-Sachs Lesions: Does Technique Matter? 58th Annual Meeting of the Orthopaedic Research Society (International) (Poster) (PhD).

40. **Giles, J.W.**, Boons, H.W., Elkinson, I., Ferreira, L.M., Faber, K.J., Litchfield, R.B., Johnson, J.A., & Athwal, G.S. (Feb 2012). Does the Dynamic Sling Effect of the Latarjet Procedure Improve Shoulder Stability? A Biomechanical Evaluation. 58th Annual Meeting of the Orthopaedic Research Society (International) (Poster) (PhD).

41. **Giles, J.W.**, Elkinson, I., Ferreira, L.M., Faber, K.J., Boons, H.W., Litchfield, R.B, Johnson, J.A., & Athwal, G.S. (Oct 2011). Moderate to Large Engaging Hill-Sachs Defects: An *In-Vitro* Biomechanical Comparison of the Remplissage Procedure, Allograft Humeral Head Reconstruction and Partial Resurfacing Arthroplasty. American Shoulder and Elbow Surgeons Annual Closed Meeting. (International) (Podium) (PhD).

42. Elkinson, I., **Giles, J.W.**, Faber, K.J., Boons, H.W., Ferreira, L.M., Johnson, J.A., & Athwal, G.S. (Oct 2011). The Effect of the Remplissage Procedure on Shoulder Stability and Range of Motion: An *In-Vitro* Biomechanical Assessment. American Shoulder and Elbow Surgeons Annual Closed Meeting. (International) (Podium) (PhD).

43. **Giles, J.W.**, Elkinson, I., Faber, K.J., Ferreira, L.M., Boons, H.W., Litchfield, R.B., Johnson, J.A., & Athwal, G.S. (Jul 2011). Moderate to Large Hill-Sachs Defects: An *In-Vitro* Biomechanical Comparison of Remplissage, Allograft and Partial Resurfacing Arthroplasty. Canadian Orthopaedic Research Society Annual Meeting (National) (Podium) (PhD).

44. Elkinson, I., ***Giles, J.W.**, Faber, K.J., Ferreira, L.M., Litchfield, R.B., Johnson, J.A., & Athwal, G.S. (Jul 2011). The Effect of the Remplissage Procedure on

Shoulder Stability and Range of Motion: An *In-Vitro* Biomechanical Assessment. Canadian Orthopaedic Association Annual Meeting (National) (Podium) (PhD). **Presenter*

45. Elkinson, I., **Giles, J.W.**, Faber, K.J., Ferreira, L.M., Litchfield, R.B., Johnson, J.A., & Athwal, G.S. (Jul 2011). The Shoulder Remplissage Procedure for Hill-Sachs Lesions: Does Technique Matter? Canadian Orthopaedic Association Annual Meeting (National) (Podium) (PhD).

46. **Giles, J.W.**, Boons, H.W., Ferreira, L.M., Athwal, G.S., & Johnson, J.A. (Jul 2011). The Effect of the Conjoined Tendon of the Short Head of the Biceps and Coracobrachialis on Shoulder Stability & Kinematics during *In-Vitro* Simulation. Canadian Orthopaedic Research Society Annual Meeting (National) (Poster) (MESc).

47. Glennie, A., **Giles, J.W.**, Faber, K.J., & Johnson, J.A. (Jul 2011). The Effect of Cement Technique on Load Transfer and Fixation of the Glenoid Component in Total Shoulder Arthroplasty. Canadian Orthopaedic Association Annual Meeting (National) (Podium) (Research Associate).

48. Armitage, M.S., Elkinson, I., **Giles, J.W.**, & Athwal, G.S. (Jul 2011). An Anatomic Assessment of the Coracoid Process with Special Reference to the Congruent Arc Laterjet. Canadian Orthopaedic Association Annual Meeting (National) (Podium) (Research Associate).

49. Lalone, E.A., **Giles, J.W.**, Deluce, S.R., Peters, T.M., King, G.J., & Johnson, J.A. (Jul 2011). The Effect of Collateral Ligament Repair on Ulnohumeral Joint Congruency. Canadian Orthopaedic Research Society Annual Meeting (National) (Poster) (Research Associate).

50. **Giles, J.W.**, Boons, H.W., Ferreira, L.M., Athwal, G.S., & Johnson, J.A. (Mar 2011). The Effect of the Conjoined Tendon of the Short Head of the Biceps and Coracobrachialis on Shoulder Stability & Kinematics during *In-Vitro* Simulation. 22nd Annual Lawson Health Research Institute Annual Research Day (Institutional) (Poster) (MESc).

51. **Giles, J.W.**, Boons, H.W., Ferreira, L.M., Athwal, G.S., & Johnson, J.A. (Jan 2011). The Effect of the Conjoined Tendon of the Short Head of the Biceps and Coracobrachialis on Shoulder Stability & Kinematics during *In-Vitro* Simulation. 57th Annual Meeting of the Orthopaedic Research Society (International) (Poster) (MESc).

52. **Giles, J.W.**, Elkinson, I., Faber, K.J., Ferreira, L.M., Johnson, J.A., & Athwal, G.S. (Feb 2011). Moderate to Large Hill-Sachs Defects: A Comparison of Remplissage, Allograft and Partial Resurfacing. American Academy of Orthopedic Surgeons Annual Meeting (International) (Poster) (PhD).

53. Elkinson, I., **Giles, J.W.**, Faber, K.J., Boons, H.W., Litchfield, R.B., Ferreira, L.M., Johnson, J.A., & Athwal, G.S. (Feb 2011). Does the Remplissage

Procedure Decrease Shoulder Range of Motion? American Academy of Orthopedic Surgeons Annual Meeting (International) (Podium) (PhD).

54. Desai, S., Sanders, D., Ferreira, L.M., **Giles, J.W.**, & Johnson, J.A. (Oct 2010). The Mechanical Effect of Targeted Blocking Screws in Distal Femur Fractures. Orthopaedic Trauma Association Annual Meeting (International) (Podium) (Research Associate).

55. **Giles, J.W.**, Glennie, A., Ferreira, L.M., Athwal, G.S., Johnson, J.A., & Faber, K.J. (Jun 2010). Interface Distraction and Loosening of the Polyethylene Glenoid Implant for Various Joint Loading Modalities: Implications for Failure in Total Shoulder Arthroplasty. Canadian Orthopaedic Research Society Annual Meeting (National) (Podium) (MESc).

56. Glennie, A., **Giles, J.W.**, Ferreira, L.M., Athwal, G.S., Johnson, J.A., & Faber, K.J. (Jun 2010). Measuring Tensile and Compressive Forces on Underlying Glenoid Bone in Total Shoulder Arthroplasty. Canadian Orthopaedic Association Annual Meeting (National) (Podium) (MESc).

57. Desai, S., Sanders, D., Ferreira, L.M., **Giles, J.W.**, & Johnson, J.A. (Jun 2010). The Mechanical Effect of Locking and Blocking Screws in Distal Femur Fractures. Canadian Orthopaedic Association Annual Meeting (National) (Podium) (Research Associate).

58. **Giles, J.W.**, Glennie, A., Ferreira, L.M., Athwal, G.S., Faber, K.J., & Johnson, J.A. (Mar 2010). Mechanisms of Load Transfer Between a Polyethylene Glenoid Implant and Bone: Implications for Loosening in Total Shoulder Arthroplasty. 21st Annual Lawson Research Day (Institutional) (Poster) (BESc).

59. **Giles, J.W.**, Glennie, A., Ferreira, L.M., Athwal, G.S., Faber, K.J., & Johnson, J.A. (Mar 2010). Mechanisms of Load Transfer Between a Polyethylene Glenoid Implant and Bone: Implications for Loosening in Total Shoulder Arthroplasty. 56th Annual Meeting of the Orthopaedic Research Society (International) (Poster) (BESc).

INVITED PRESENTATIONS

1. **Giles, J.W.** (Oct 2013). From Benchtop Testing to Whole Joint Motion Simulation: *In-Vitro* Biomechanical Experimentation. Seminar Series of the Henry Ford Hospital Bone & Joint Research Center, Detroit, MI (Institutional) (PhD).

2. Degen, R., **Giles, J.W.**, Johnson, J.A., & Athwal, G.S. (Oct 2013). A biomechanical comparison of Remplissage versus the Latarjet Transfer for Hill-Sachs defects: An engaging topic. 41st Annual Orthopaedic Surgery Residents' Research Day (Institutional) (PhD).

3. **Giles, J.W.** (Apr 2013). Engineering in Orthopaedics: Guiding Clinical Practice Through Biomechanical Experimentation. University of Western Ontario's Three Minute Thesis (3MT) competition campus-wide final (Institutional) (PhD).

4. **Giles, J.W.**, *Degen, R., Johnson, J.A., & Athwal, G.S. (Oct 2012). The Bristow-Latarjet: Why These Procedures Should Not Be Considered Synonymous. 40th Annual Orthopaedic Surgery Residents' Research Day (Institutional) (PhD) **Presenter*

5. Glennie, A., **Giles, J.W.**, Ferreira, L.M., Athwal, G.S., Johnson, J.A., & Faber, K.J. (Oct 2011). The Effect of Cement Technique on Load Transfer of the Glenoid Component in Shoulder Arthroplasty. Orthopaedic Surgery Residents' Research Day (Institutional) (Podium) (MESc).

6. Glennie, A., **Giles, J.W.**, Ferreira, L.M., Athwal, G.S., Johnson, J.A., & Faber, K.J. (Oct 2010). Measuring Tensile and Compressive Forces on Underlying Glenoid Bone in Total Shoulder Arthroplasty. Orthopaedic Surgery Residents' Research Day (Institutional) (MESc).

7. Desai, S., Sanders, D., Ferreira, L.M., **Giles, J.W.**, & Johnson, J.A. (Oct 2012). The Effects of Targeted Blocking Screws on the Mechanical Stability of Distal Femur Fractures. Orthopaedic Surgery Residents' Research Day (Institutional) (Research Associate).

8. **Giles, J.W.** (Jan 2010). Re-Engineering the Shoulder: A Look at Implant Design and Computer Assisted Surgery. Lawson Health Research Institute's Talks On Fridays (Institutional) (MESc).

9. **Giles, J.W.** (Feb 2010). Interface Distraction and Loosening of the Polyethylene Glenoid Implant for Various Joint Loading Modalities: Implications for Failure in Total Shoulder Arthroplasty. The University of Western Ontario Department of Biomedical Engineering Seminar Series (Institutional) (MESc).

ARTICLES REVIEWED FOR ACADEMIC JOURNALS

1. Iliac Bone Grafting of the Intact Glenoid Improves Shoulder Stability with Optimal Graft Positioning. *Journal of Bone & Joint Surgery (Am)*, Paper # JBJS-D-13-01318

2. The Effects of Shoulder Remplissage on Glenohumeral Translation and Range of Motion. *Journal of Clinical Orthopaedics and Related Research*, Paper # CORR-D-13-00897

3. The Passive Effect of the Deltoid on Glenohumeral Translation in a Cadaveric Model of the Throwing Shoulder Using Intact Torsos. *Journal of Orthopaedic Research*, Paper #: JOR-13-0087

4. Joint Conformity Affects Direction of Glenohumeral Translation after Total Shoulder Replacement. *Journal of Biomechanics*, Paper #: BM-D-12-01233

5. Initial Fixation of a Cementless Glenoid Implant. *Journal of Biomechanical Engineering*, Paper #: BIO-11-1456

INDUSTRIAL COLLABORATIONS

May 2013- Depuy Synthes - *Investigation of the Effect of Reverse Total Shoulder Replacement Implant Parameters on Glenohumeral Kinematics and Kinetics*

May 2012 Wright Medical - *Validation Testing and Data Analysis for InBone Ankle Replacement*

Aug 2010 Wright Medical - *Contact Mapping Investigation and Data Analysis for Infinity Ankle Replacement*

Sep 2009 Arthrex - *Investigation of the Ability of a Partial Humeral Head Resurfacing Implant to Re-Establish Normal Joint Kinematics in the Setting of a Hill-Sachs Defect*